

Safety Regulation Group



CAA PAPER 2004/03

**Helicopter Turbulence Criteria for Operations to
Offshore Platforms**

www.caa.co.uk

CAA PAPER 2004/03

Helicopter Turbulence Criteria for Operations to Offshore Platforms

© Civil Aviation Authority 2004

ISBN 0 86039 962 1

Enquiries regarding the content of this publication should be addressed to:
Research Management Department, Safety Regulation Group, Civil Aviation Authority, Aviation House,
Gatwick Airport South, West Sussex, RH6 0YR.

The latest version of this document is available in electronic format at www.caa.co.uk, where you may also register for e-mail notification of amendments.

Printed copies and amendment services are available from: Documedia Solutions Ltd., 37 Windsor Street, Cheltenham, Glos., GL52 2DG.

List of Pages

Section	Page	Date	Section	Page	Date
	iii	September 2004	Section 7	3	September 2004
	iv	September 2004	Section 7	4	September 2004
	v	September 2004	Section 8	1	September 2004
	vi	September 2004	Section 8	2	September 2004
	vii	September 2004	Section 8	3	September 2004
	viii	September 2004	Section 8	4	September 2004
	ix	September 2004	Section 8	5	September 2004
Section 1	1	September 2004	Section 8	6	September 2004
Section 1	2	September 2004	Section 8	7	September 2004
Section 1	3	September 2004	Section 9	1	September 2004
Section 2	1	September 2004	Section 9	2	September 2004
Section 2	2	September 2004	Section 9	3	September 2004
Section 3	1	September 2004	Section 10	1	September 2004
Section 3	2	September 2004	Section 11	1	September 2004
Section 3	3	September 2004	Section 12	1	September 2004
Section 3	4	September 2004	Section 13	1	September 2004
Section 3	5	September 2004	Appendix A	1	September 2004
Section 3	6	September 2004	Appendix A	2	September 2004
Section 3	7	September 2004	Appendix A	3	September 2004
Section 3	8	September 2004	Appendix A	4	September 2004
Section 4	1	September 2004	Appendix A	5	September 2004
Section 4	2	September 2004	Appendix A	6	September 2004
Section 4	3	September 2004	Appendix A	7	September 2004
Section 4	4	September 2004	Appendix A	8	September 2004
Section 4	5	September 2004	Appendix A	9	September 2004
Section 4	6	September 2004	Appendix A	10	September 2004
Section 4	7	September 2004	Appendix A	11	September 2004
Section 4	8	September 2004	Appendix A	12	September 2004
Section 4	9	September 2004	Appendix B	1	September 2004
Section 4	10	September 2004	Appendix B	2	September 2004
Section 4	11	September 2004	Appendix B	3	September 2004
Section 4	12	September 2004	Appendix B	4	September 2004
Section 4	13	September 2004	Appendix B	5	September 2004
Section 4	14	September 2004	Appendix B	6	September 2004
Section 4	15	September 2004	Appendix B	7	September 2004
Section 5	1	September 2004	Appendix B	8	September 2004
Section 5	2	September 2004	Appendix B	9	September 2004
Section 5	3	September 2004	Appendix B	10	September 2004
Section 5	4	September 2004	Appendix B	11	September 2004
Section 5	5	September 2004	Appendix B	12	September 2004
Section 6	1	September 2004	Appendix B	13	September 2004
Section 6	2	September 2004	Appendix B	14	September 2004
Section 6	3	September 2004	Appendix B	15	September 2004
Section 6	4	September 2004	Appendix C	1	September 2004
Section 7	1	September 2004	Appendix C	2	September 2004
Section 7	2	September 2004	Appendix C	3	September 2004

Section	Page	Date	Section	Page	Date
Appendix D	1	September 2004	Appendix O	3	September 2004
Appendix D	2	September 2004	Appendix O	4	September 2004
Appendix D	3	September 2004	Appendix P	1	September 2004
Appendix E	1	September 2004	Appendix P	2	September 2004
Appendix E	2	September 2004	Appendix P	3	September 2004
Appendix E	3	September 2004	Appendix P	4	September 2004
Appendix E	4	September 2004	Appendix Q	1	September 2004
Appendix E	5	September 2004	Appendix Q	2	September 2004
Appendix F	1	September 2004	Appendix Q	3	September 2004
Appendix F	2	September 2004	Appendix Q	4	September 2004
Appendix G	1	September 2004	Appendix Q	5	September 2004
Appendix G	2	September 2004	Appendix R	1	September 2004
Appendix H	1	September 2004	Appendix R	2	September 2004
Appendix H	2	September 2004	Appendix R	3	September 2004
Appendix H	3	September 2004	Appendix R	4	September 2004
Appendix H	4	September 2004	Appendix R	5	September 2004
Appendix H	5	September 2004	Appendix R	6	September 2004
Appendix I	1	September 2004	Appendix R	7	September 2004
Appendix I	2	September 2004	Appendix R	8	September 2004
Appendix I	3	September 2004	Appendix R	9	September 2004
Appendix I	4	September 2004	Appendix R	10	September 2004
Appendix I	5	September 2004	Appendix R	11	September 2004
Appendix I	6	September 2004	Appendix R	12	September 2004
Appendix I	7	September 2004	Appendix R	13	September 2004
Appendix I	8	September 2004	Appendix R	14	September 2004
Appendix I	9	September 2004	Appendix R	15	September 2004
Appendix J	1	September 2004	Appendix S	1	September 2004
Appendix J	2	September 2004	Appendix S	2	September 2004
Appendix J	3	September 2004	Appendix S	3	September 2004
Appendix J	4	September 2004	Appendix S	4	September 2004
Appendix K	1	September 2004	Appendix S	5	September 2004
Appendix K	2	September 2004	Appendix S	6	September 2004
Appendix L	1	September 2004	Appendix S	7	September 2004
Appendix L	2	September 2004	Appendix T	1	September 2004
Appendix L	3	September 2004	Appendix T	2	September 2004
Appendix L	4	September 2004	Appendix T	3	September 2004
Appendix M	1	September 2004	Appendix T	4	September 2004
Appendix M	2	September 2004	Appendix T	5	September 2004
Appendix M	3	September 2004	Appendix T	6	September 2004
Appendix N	1	September 2004			
Appendix N	2	September 2004			
Appendix N	3	September 2004			
Appendix N	4	September 2004			
Appendix N	5	September 2004			
Appendix N	6	September 2004			
Appendix N	7	September 2004			
Appendix O	1	September 2004			
Appendix O	2	September 2004			

Contents

	List of Pages	iii
	Foreword	viii
	Executive Summary	ix
Section 1	Introduction and Background	
	Objectives	1
	Overview of Scope of Work	1
Section 2	Review of IVLL and Existing Wind Tunnel Data	
	Wind Tunnel Data Archive	1
	Installation/Vessel Limitation List Entries	1
	Selection of Candidate Installations	2
Section 3	A Turbulence Criterion Using Wind Tunnel Turbulence Data and Desktop Simulation	
	Method Overview	1
	Part 1 Wind Tunnel Tests	2
	Desktop Simulation	3
	Simulation Methodology	3
	Helicopter Model	4
	Wind Tunnel Test Matrix	4
	Interfacing with the Wind Tunnel Data	5
	Pilot Modelling	6
	Workload Correlation	7
Section 4	Calibration and Validation Using Pilot-in-the-Loop Simulation	
	Method Overview	1
	Flight Simulator Trials	2
	Method and Preparation	2
	Test Matrix	3
	Lessons Learnt from Trial BRAE01	4
	Part 2 Wind Tunnel Tests	5
	Results	5
	Revisions to the Desktop Simulation	8
	Correlation of Desktop and Simulation Results	8
	The Bristow HOMP Turbulence Parameter	10

	Discussion	10
	Test Pilot Task Performance	10
	SyCoS Workload Predictions	11
	Mapping HQR around Brae A	11
	Variation between Test Pilots	13
	Acceptable Levels of HQR	13
	Torque and Power Margins	14
	Effect of Degraded Visual Conditions on HQR	14
	Improving the Workload Predictor	15
	Application of the Workload Predictor to HOMP Data	15
	Offshore Platform Operational Envelopes	15
	Routine Workload Analysis within HOMP	15
Section 5	Extending the Method to Other Helicopter Types	
	Modelling Approach	1
	Discussion	4
Section 6	Turbulence Criterion for Safe Helicopter Operations	
	The Need for a Simple Turbulence Criterion	1
	Prediction of Workload from Turbulence	1
Section 7	Workload Predictions for Other Platforms	
Section 8	Summary and Discussion	
	Wind Tunnel Data and Desktop Modelling	1
	Piloted Flight Simulation	1
	Turbulence Criterion	1
	Application to Different Helicopter Types	2
	Validation	2
	Further Possibilities for Validation	6
	Further Analysis of Existing Platform Wind Tunnel Data	6
	Comparisons with Operational FDR Data	6
Section 9	Conclusions	
	Turbulence Criterion	1
	Main Conclusions	1
	Caveats	1
	Pilot Workload Prediction Method	1
	General	1
	Extension to Other Helicopter Types	2
	Other Conclusions	3
	Applicability of Results to Other Offshore Platforms	3
	Turbulence Generated by Offshore Platforms	3
	Calibration of Bristow Helicopters HOMP Turbulence Parameter	3

Section 10	Recommendations
Section 11	Abbreviations
Section 12	Acknowledgements
Section 13	References
Appendix A	Existing Wind Tunnel Data and the IVLL
Appendix B	Wind Tunnel Tests – Part 1
Appendix C	Exceedances and the Discrete Gust Model
Appendix D	Configuration Data for the S-76 Main Rotor
Appendix E	Review of General Applicability of Turbulence Data
Appendix F	Transformation of Turbulence
Appendix G	Fully Compensated Crossover Model
Appendix H	Workload Prediction: Wavelets, Spectra and Variances
Appendix I	Wind Tunnel Tests – Part 2 (Brae A)
Appendix J	Derivation of HQR Predictors from BRAE01 Trial
Appendix K	Simulator Test Schedule
Appendix L	Wind Tunnel Measurement Grid
Appendix M	Simulator Trial Results – BRAE01 and BRAE02
Appendix N	Analysis of Task Performance in Trial BRAE02
Appendix O	Results from the BRAE02 Trial
Appendix P	Results from Validation of Desktop Simulation
Appendix Q	Statistical Analysis of HQRs
Appendix R	Calibration of the Bristow HOMP Turbulence Parameter
Appendix S	Simulation of other Configurations
Appendix T	Analysis of Turbulence Standard Deviations and HQRs

Foreword

The research reported in this paper was funded by the Safety Regulation Group of the UK Civil Aviation Authority, and was performed by BMT Fluid Mechanics Limited and, under subcontract to BMT, QinetiQ (Bedford) and Glasgow Caledonian University. The work was commissioned in response to a recommendation (10.2 (i)) that resulted from earlier research into offshore helideck environmental issues, reported in CAA Paper 99004.

Turbulence around offshore platforms can represent a significant safety hazard and source of high cockpit workload. This was illustrated in the results of a questionnaire survey of offshore helicopter pilots, reported in CAA Paper 97009, where turbulence around platforms was ranked as the greatest of the fifteen factors contributing to workload and safety hazards that were considered. The absence of a turbulence criterion in CAA's associated guidance material (CAP 437 - Offshore Helicopter Landing Areas - Guidance on Standards) is therefore regarded as anomalous. Although the existing vertical wind speed criterion in CAP 437 in combination with a system of operational feedback (turbulence report forms) has served to contain the situation, the addition of a specific turbulence criterion which is calibrated to maximum safe pilot workload is viewed as a significant enhancement.

Work on validating the turbulence criterion using data from Bristow Helicopter's helicopter operations monitoring programme (HOMP) is already underway. Once satisfactorily completed, the turbulence criterion will be added to CAP 437 and incorporated in the Offshore Helideck Design Guidelines document which the HSE commissioned with the support of the CAA, and is endorsed by the Offshore Industry Advisory Committee's Helicopter Liaison Group (OIAC HLG).

A useful spin-off from the validation exercise will be the addition of an offshore helideck turbulence mapping capability to HOMP. This will enable helicopter operators with HOMP to better establish operating restrictions, and to monitor the turbulence environment around offshore platforms on a continuous basis with minimal effort. With this facility in place, any unannounced modifications to platform topsides adversely affecting the airflow over and around the helideck should be rapidly detected and appropriate changes to operating restrictions made.

Safety Regulation Group
September 2004

Executive Summary

This report describes work undertaken to develop a quantitative turbulence criterion for safe helicopter operations to helidecks on offshore platforms. The work arose as a result of a wide-ranging research project into the aerodynamic environment around helidecks, and a key recommendation from that research that a criterion for turbulence should be developed to complement existing criteria for downdraft and temperature rise.

The Safety Regulation Group of the Civil Aviation Authority commissioned the report, and the research was performed by BMT Fluid Mechanics (BMT), the prime contractor, QinetiQ (Bedford) and Glasgow Caledonian University (GCU). The QinetiQ large motion Advanced Flight Simulator (AFS) at Bedford was utilised for the piloted trials.

The work was accomplished in two main phases.

- a) In the initial phase existing evidence for turbulence problems around offshore helidecks as documented in the Installation/Vessel Limitation List (IVLL), and in previous measurements of turbulence made in wind tunnel tests on various offshore installations was explored. Wind tunnel tests were then performed on four example installations, and computer simulations of helicopter and pilot response to the turbulence performed. The results were interpreted in terms of established measures of pilot workload.
- b) The second phase concentrated on calibrating and validating the simulation techniques, making use of piloted flight simulation, and arrived at a measure of the vertical component of turbulence which corresponds to the safe upper limit of pilot workload.

The modelling and simulation techniques developed are believed to be the most comprehensive representation of helicopter flight in turbulence carried out to-date, using 3-axis spatially correlated time histories measured in the wind tunnel as input to the flight simulator blade element aerodynamics model.

The workload ratings awarded by the test pilots in the flight simulator were correlated with the input wind turbulence to arrive directly at the turbulence criterion.

The desktop simulation method was quantitatively validated in terms of the relationships between pilot control activity and pilot workload.

Qualitatively the whole simulation process has been validated through test pilot comments that the simulations were a realistic representation of flight in turbulence in close proximity to offshore platform helidecks.

A number of recommendations are made regarding further validation, and additional work required to quantify increased pilot workload in degraded visual conditions, and variations of pilot workload across different helicopter types in the offshore fleet.

Further validation of the new criterion, and the complete modelling process, is now possible through correlation with data collected by the Helicopter Operations Monitoring Programme (HOMP) trial, and to be collected in the future by the anticipated implementation of HOMP on the entire North Sea helicopter fleet.

Section 1 Introduction and Background

This report describes work undertaken to develop a quantitative turbulence criterion for safe helicopter operations to helidecks on offshore platforms. The work arose as a result of a wide-ranging research project into the environment around helidecks [1]¹, and a key recommendation from that research that a criterion for turbulence should be developed to complement existing criteria for downdraft and temperature rise.

The report was commissioned by the Safety Regulation Group of the Civil Aviation Authority (CAA²) under contract [2] in response to BMT Fluid Mechanics proposals [3] and [4]. The research was performed by BMT Fluid Mechanics (BMT), the prime contractor, QinetiQ (Bedford) and Glasgow Caledonian University (GCU). The QinetiQ large motion Advanced Flight Simulator (AFS) at Bedford was utilised for the piloted trials.

The work was accomplished in two main phases:

- a) In the initial phase the existing evidence for turbulence problems around offshore helidecks as documented in the IVLL [5], and in previous measurements of turbulence made in wind tunnel tests on various offshore installations was explored. Wind tunnel tests were then performed on four example installations, and computer simulations of helicopter and pilot response to the turbulence performed. The results were interpreted in terms of established measures of pilot workload.
- b) The second phase concentrated on calibrating and validating the simulation techniques, making use of piloted flight simulation, and arrived at a measure of the vertical component of turbulence which corresponds to the safe upper limit of pilot workload.

1.1 Objectives

The objectives of the research can be paraphrased from [3] and [4] as follows.

The overall objective of the work was:

- a) to develop an easy-to-use maximum safe turbulence criterion for all helicopter operations to offshore helidecks. The criterion is to be inserted into CAP 437 [6] and the Helideck Design, Modification and Verification Manual [7], as one of the means of determining the acceptability of helideck designs in given environmental conditions. (Designs/conditions, which do not meet the criteria, would be subject to some form of reporting and potential operational restrictions.)

At a more detailed level the objectives were:

- b) to develop and validate a helicopter pilot workload prediction method intended to establish a turbulence criterion for safe helicopter operations to offshore helidecks;
- c) to extend the applicability of the method so that it can be used for a number of different helicopter types;
- d) to document the method so that it can be referenced in CAP 437 [6] and/or the Helideck Design, Modification and Verification Manual [7].

1.2 Overview of Scope of Work

The work was performed and is reported in a number of stages as follows:

- a) Existing information on the effects of turbulence on helideck operations were sought from two sources; wind tunnel tests performed previously by BMT on offshore installations, and the operational experience of pilots flying in the North

1. References used in the main body of the text are listed in Section 13. References used in the appendices are listed at the end of each appendix.
2. A list of abbreviations used in this report is given in Section 11.

Sea as documented in the IVLL [5]. As well as providing some general conclusions on the occurrence and effect of turbulence, this information was used to help determine which offshore installations should be made the subject of more detailed investigation. Four offshore installations were identified, selected to include both high and low levels of turbulence, as well as different offshore installation configurations. This part of the work is described in Section 2.

- b) Wind tunnel tests were performed on the four selected installations in order to obtain more detailed information on the nature of the turbulence than was available from the historic sources. Computer simulations of the helicopter and pilot response to this turbulence were then performed. These simulations required validation before they could be used to help determine a turbulence criterion, but they provided an initial estimate of the pilot workload which was compared with the contents of the IVLL and found to be broadly in agreement. This part of the work is described in Section 3.
- c) Validation and calibration of the helicopter/pilot modelling and pilot workload estimates were performed by means of piloted trials in the QinetiQ Bedford Advanced Flight Simulator (AFS). Three different test pilots were used in order to obtain an indication of variability between pilots. The flight simulator trials were performed for only one installation (Brae A) and for one helicopter type (S-76X¹). Additional wind tunnel tests were performed prior to the trials in order to define the turbulent wake over a larger field, and to provide a 3-axis turbulent environment with realistic spatial variation in order that complete approaches could be flown in the simulator. The pilots all commented that this was the most realistic simulation of flight in turbulence in close proximity to an offshore platform that they had experienced. The data from the flight simulator trials was used to refine the workload estimate method, and was used to correlate the pilot workload against the aerodynamic turbulence. This phase of the work is described in Section 4. The simulator trials focussed on assessing the workload resulting from time-varying turbulence as opposed to potential operating limits imposed by lack of power or torque margin. Such limits are typically caused by an aircraft with low torque/power margins or significant downdraft in the vicinity of the helideck. Downdraft here is considered to be distinct from time-varying turbulence, although typically increased turbulence would accompany a large downdraft. Limitations on downdraft are currently expressed in CAP 437 [6] by way of the downdraft criterion². This criterion needs to be reviewed in the light of the new criterion for turbulence.
- d) With the calibration and validation of the helicopter/pilot computer simulation complete, the computer simulation was used to investigate the variability of predicted pilot workload for a range of helicopter parameters. The parameters varied were; size (represented by weight class), weight, blade loading and rotor hinge offset. These variations were not intended to correspond exactly to specific helicopter types, but rather to give an overall picture. This aspect of the work is described in Section 5.
- e) All the results from the foregoing work were then used to define and describe a turbulence criterion for safe helicopter operations. The turbulence criterion was required to be simple and accessible to the offshore community in general. In particular it needed to be useable by offshore platform designers to provide

1. The X designation here is used to indicate that this was *not* intended to be an exact representation of a Sikorsky S-76.

2. Whilst commonly referred to as a downdraft criterion, CAP 437 actually refers to a limiting vertical component of velocity rather than downdraft. It is generally assumed that a downward component represents a more severe risk to the helicopter than an upward component.

guidance for early assessment of platforms in terms of the impact of turbulence on operational limitations. The development of a simple criterion is described in Section 6, and the applicability of this criterion to the broad population of offshore platforms is discussed in Section 7. A summary and discussion are contained in Section 8, whilst the overall conclusions and recommendations from the work are given in Sections 9 and 10 respectively.

Section 2 Review of IVLL and Existing Wind Tunnel Data

A review was performed of existing offshore platform wind tunnel data in BMT's archives, and of the Installation/Vessel Limitation List (IVLL) [5], which effectively summarises the operational experience of pilots, in order to determine what conclusions could be drawn from this material. The apparent consistency of the two sources of turbulence information was of particular interest. The material was also used to help select candidate installations for subsequent phases of the work.

This phase of the work was reported in [8] but salient results and conclusions are also presented below and in Appendix A.

2.1 Wind Tunnel Data Archive

The principal objective of this part of the work was to assess data available from previous wind tunnel tests in terms of its usefulness to the project. In addition, the analysis considered the nature and magnitude of the turbulence experienced in the vicinity of offshore helidecks, and the variation of the key turbulence properties with platform or vessel type and wind direction.

The following conclusions were drawn:

- a) Turbulence levels vary greatly with wind direction.
- b) Highest turbulence levels are associated with the helideck being downstream of major items of superstructure such as the drilling derrick and gas turbine exhaust stacks.
- c) Maximum rms turbulence levels vary significantly from installation to installation.
- d) There does not appear to be a significant variation in maximum rms turbulence levels between different types of offshore installation.¹

2.2 Installation/Vessel Limitation List Entries

A review of existing IVLL entries for a range of installations was undertaken. Where possible the data from the IVLL were compared with the turbulence measurements from the existing wind tunnel data. This review also assisted the selection of installations to be modelled in the wind tunnel to provide specific turbulence data for the helicopter handling analysis.

It was concluded that in a number of cases, high levels of turbulence measured in the wind tunnel correlated with warnings of high turbulence in the IVLL. There were some instances where high values were measured in the wind tunnel but there was no corresponding reference to high levels of turbulence in the IVLL. In the original report (reproduced in Appendix A) it is postulated that these conditions are not being encountered by helicopters because of operational or meteorological factors. Further analysis of the wind tunnel data for sample platforms has shown that there are most likely two key factors:

- a) Firstly, the wind tunnel turbulence measurements are single point maximum values. As such, there is no recognition of the physical extent of the turbulent region. An example of this is Dunbar, which gave a high turbulence reading of 5.4 (Table A-1), but examination of detailed results for the platform showed that the high turbulence was confined to a relatively narrow region. Consequently Dunbar is likely to have a less significant impact on a helicopter than would be the case for

1. The differences in turbulence properties between different platforms were also investigated later in the work – see sub-section 3.3.3 and Appendix E.

a broad region of turbulence such as experienced on East Brae, even though peak turbulence values are similar for the two platforms.

- b) The second factor concerns local wind climate. In the case of Janice for example, which experienced high turbulence measurements in the wind tunnel like Dunbar, the wind speeds required to generate high rms values occur for less than 1.5% of the year. It is therefore a relatively rare occurrence, and may not have been experienced by a helicopter to cause an entry in the IVLL.

2.3 **Selection of Candidate Installations**

It was recommended that the following offshore installations be selected for wind tunnel testing and further study:

- a) Brae A fixed platform, selected for its expected high turbulence levels over the helideck.
- b) Beatrice A fixed platform, selected for its expected low turbulence levels over the helideck.
- c) Schiehallion FPSO, selected as a different type of installation to be tested and expected to produce a medium level of turbulence.
- d) Claymore fixed platforms, selected to represent a combined operations scenario.

Section 3 A Turbulence Criterion Using Wind Tunnel Turbulence Data and Desktop Simulation

3.1 Method Overview

Mathematical modelling has been used at Glasgow Caledonian University (GCU) to develop methods that take measured turbulence time histories from wind tunnel tests as input, and calculate the expected level of pilot workload required to deal with the effects. Initially, the favoured model made use of the Statistical Discrete Gust method (reviewed briefly in sub-section 3.3.1). However, early problems with the analysis of some of the available wind tunnel data precluded the full development of this method. Instead, a pilot model was configured alongside a non-linear model of the helicopter to estimate the control actions required to hold a particular flight path in the presence of the measured turbulence. In all cases where desktop simulation has been used for this study, the desired flight path was a ground-referenced hover.

The fundamental source of data was the turbulence measurements from wind tunnel experiments carried out in the BMT Boundary Layer Wind Tunnel [9]. Scale models of several platforms were mounted in the wind tunnel and instrumented to measure the time-varying components of wind velocity at the helideck position for a range of applied wind speeds. In addition, the orientation of the models was varied to represent a variety of wind directions. The directions were chosen so that the flow was sampled when the helideck was unobstructed, and also when it was downwind of identifiable obstructions such as derricks, or exhaust or flare stacks.

The turbulence data for the cases studied were supplied to a helicopter simulation configured to represent the principal features of the Sikorsky S-76, a type that operates to North Sea platforms. In early desktop simulations the time histories of wind velocity were fed into the rotor model directly, and were assumed to act equally at all points on the rotor disc.

Following further wind tunnel testing, an enhanced method for representing the wind velocity field was used. By defining time histories of both velocity and velocity gradients at the rotor hub, the distribution of vertical flows over the rotor disc was allowed to vary linearly in both longitudinal and lateral directions thereby more accurately representing the true character of the flow.

The helicopter simulation is 'flown' by a numerical pilot model designed to keep the helicopter on a given flight path. This pilot model is summarised later in sub-section 3.3.5, but its important features are that it adapts to the characteristics of the helicopter type being flown, and that it is designed to produce corrective control actions in response to external stimuli. Such stimuli may be atmospheric turbulence or system non-linearities such as control limits. The output from the simulation is the control activities for the cyclic stick, collective lever and tail rotor pedals.

The final stage is to use this control activity (or control responses) to predict the level of workload experienced by the pilot. Several potentially viable techniques for producing such predictions have been demonstrated, but a method based on the variance of the signal and the signal rate has been selected. The method requires a database of pre-existing flight measurements to provide a 'training set' from which to produce the 'predictors'; the set of coefficients or parameters that define the prediction model. As described in Section 4, these data were obtained using ground-based, pilot-in-the-loop flight simulation.

A key assumption in this work is that pilot workload can be used as an inverse measure of safety (i.e. the higher the workload, the lower the margin of safety), and the fundamental hypothesis upon which the workload predictions are based is that

the pilot's control activity is a reliable indicator of his perceived workload. However, it is recognised in this approach that many other factors impinge on the pilot's assessment of workload, some of which cannot satisfactorily be addressed in the type of simulation used for this part of the project. One example is the visual environment which, if degraded, can lead to a significant increase in workload as the pilot loses the visual cues on which to base his control strategy. Visual cues are also affected by the vehicle orientation which, during aggressive manoeuvring or unfavourable environmental conditions, can limit the pilot's view out of the cockpit. Some of these factors, it is believed, are reflected in increased stick activity, but there is no reliable quantified evidence of this to date. Therefore, the assumption for this study is that the visual environment is good and hence does not affect workload.

In order to quantify workload the Cooper-Harper [10] handling qualities rating (HQR) scale was employed, which uses structured debriefing of the pilot to arrive at a rating on a scale of 1 - 10. Figure 3.1 illustrates the scale and relates workload rating to levels of handling and task performance. For the remainder of the report the term workload rating will be used to indicate a rating equivalent to HQR, but produced through desktop simulation.

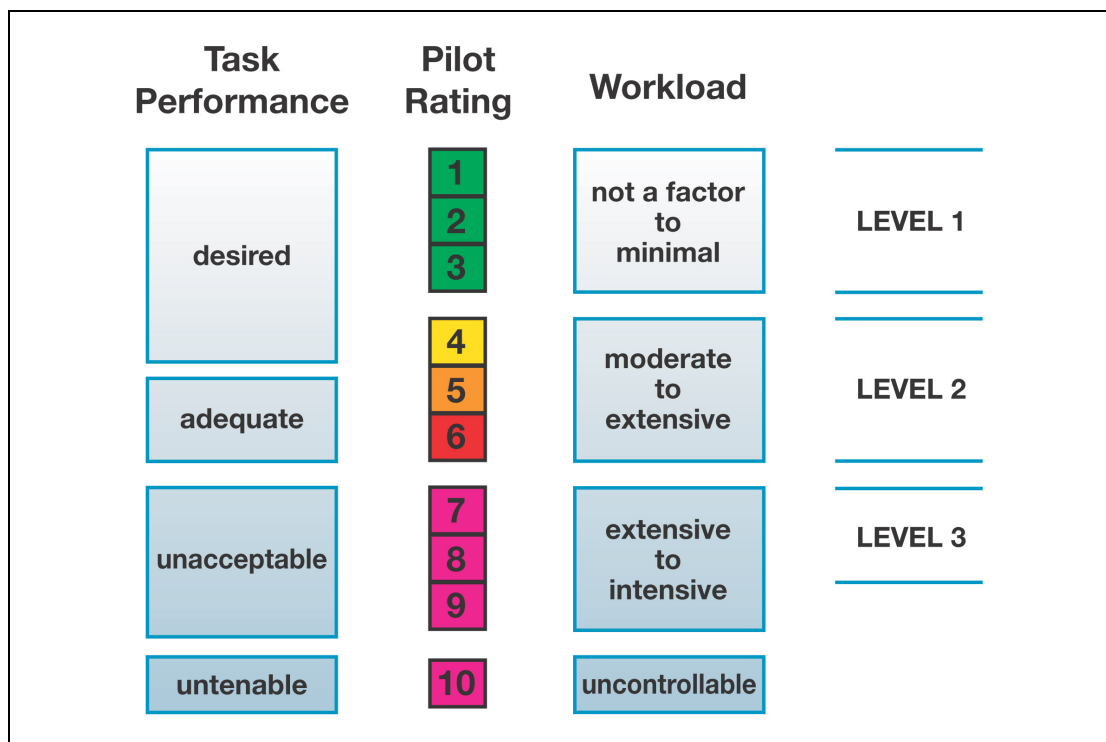


Figure 3.1 Workload Rating Scale

3.2 Part 1 Wind Tunnel Tests

Four offshore platform models, representative of the population of offshore structures were selected (see sub-section 2.3), and tested in the large BMT Atmospheric Boundary Layer Wind Tunnel at Teddington. The selected platform models were:

- Beatrice (1:100 scale);
- Brae A (1:100 scale);
- Claymore CAP (1:100 scale);
- Schiehallion FPSO (1:125 scale).

As noted in sub-section 2.3, these were selected to include examples of fixed offshore platforms with good and poor helideck environmental properties (Beatrice and Brae A respectively), and one representative of the new generation of Floating Production Systems (Schiehallion FPSO). The Claymore CAP was also included as an example of a 'combined operations' scenario, and because of the helicopter accident that occurred there in 1995 [11].

The wind tunnel tests are fully described in Appendix B, and were performed on the above four platforms with a range of different wind speeds and headings. A representative marine atmospheric boundary layer was created in the wind tunnel.

Three hot wire anemometers were positioned across the location of the helicopter rotor disc, one at the centre and the other two at the upwind and downwind edges of the disc. These were used to measure the wind flow velocity time history in two axes (along wind u and vertical w components) at a number of locations in the vicinity of the helideck. Different wind directions were selected for each installation to enable measurements to be taken with different obstructions upwind of the helideck. A wind direction was also selected to represent relatively unobstructed free-stream conditions to cover the full range of possible turbulence conditions.

In order to gain as complete a picture as possible of turbulence experienced by the helicopter during take-off and landing, measurements were also taken at equivalent full-scale heights of 10 and 20 m above the helideck, and at a distance of 15 m to the port side of the helideck.

These data were used in the earlier phases of the work for model development, including the first of the simulator trials BRAE01 described in Section 4. However, it should be noted that a further set of data was collected for the Brae A platform in support of the BRAE02 validation exercise; the Part 2 wind tunnel tests. Several enhancements were made to the wind tunnel measurements in this second phase and these are described later in sub-section 4.2.4 and Appendix I.

3.3 Desktop Simulation

3.3.1 Simulation Methodology

In the initial phase of the work it was intended to use a Statistical Discrete Gust (SDG) method to analyse turbulence measurements obtained from the wind tunnel data. The SDG method decomposes the turbulence time history into a number of discrete features (or individual gusts) of varying scale and amplitude until the entire signal can be represented by the aggregate of these features. Typically, such a feature would be a sharp linear ramp following by an exponentially decaying tail, but the exact form can be modified to best suit the particular signal being analysed. Once the decomposition has been achieved, a model is fitted to provide the distribution of scales and amplitude using a single function, details of which may be found in Appendix C.

The real benefit of using the SDG method comes when the system to which the turbulence is input (in this case the combined helicopter and pilot model) can be adequately represented by linear equations. Under these conditions the response of the system can also be expressed statistically by a single function, and therefore the characteristics of the discrete control actions that compensate for the turbulence can be found. Other works detailed in Appendix C have established the relationship between discrete control inputs and workload and therefore the overall method promised to deliver an efficient way of deriving the predicted pilot workload directly from wind tunnel data. However, the structure of the SDG model was not able to adequately represent a number of the turbulence signals obtained from wind tunnel testing because their spectra did not correspond to one of the standard atmospheric spectra such as Von Karman or Dryden, for which the SDG was developed. The

technique was therefore abandoned in favour of a more robust technique described below.

The components that make up the method used are a non-linear representation of the helicopter (described in sub-section 3.3.2), the wind tunnel data (summarised in sub-section 3.3.3 and Appendix B), the pilot model (reviewed in sub-section 3.3.5) and finally the workload predictor for obtaining a workload rating from the derived control activity (summarised in sub-section 3.3.6). Given wind tunnel measurements of the turbulence around the offshore platform of interest and configuration data to adequately represent the helicopter being considered, the method can produce workload predictions over the entire matrix for which wind measurements are available.

As will be described in Section 4, the method has been calibrated and validated using data collected from ground-based, pilot-in-the-loop simulation. The calibration exercise refers to the training of the workload predictor based on the measured control activity from the simulator trial with associated subjective workload ratings awarded by the pilots. The validation exercise entailed both assessment of the workload predictor using data independent from that used for calibration, and comparison of the estimated workload ratings from the integrated desktop simulation with those awarded by the pilots in the simulator. Once validated, it is not believed that further simulation trials will be required to apply the method to other offshore platforms or helicopters.

3.3.2 Helicopter Model

The flight simulations utilised a commercial off-the-shelf package, *FLIGHTLAB* (from Advanced Rotorcraft Technology, Inc.) that provides a user-friendly modelling environment containing libraries of all the major model components required for a high fidelity helicopter simulation. The model components are generic and therefore need to be configured with suitable design data to represent the particular aircraft being simulated.

The helicopter type selected for the *FLIGHTLAB* simulations was the Sikorsky S-76. This was due, in part, to the volume of North Sea operations flown by this particular helicopter. As sufficient design data were not available in this instance, a model with S-76-like features was developed (and referred to as S-76X). The S-76X model was based on the *FLIGHTLAB* model of the Westland Lynx Mark 3. This aircraft is of a similar weight and size to the S-76 but employs a hingeless main rotor. The rationale was, therefore, to use the existing Lynx model and replace the hingeless main rotor with an articulated main rotor of appropriate stiffness. The fuselage, control system and tail rotor of the Lynx remained unaltered apart from minor modifications to the weight of the vehicle. Configuration data, together with appropriate values for *FLIGHTLAB* variables, are contained in Appendix D. It should be noted that no engine model was included in the helicopter model, with the result that some features relating to pilot workload (such as prevention of rotor under/over-speed, respecting torque limits etc.) were not represented.

3.3.3 Wind Tunnel Test Matrix

The initial wind tunnel tests, described earlier in sub-section 3.2, provided all the required data for the development of the desktop simulation. Data was collected for the Brae A platform with wind from four directions given by 088°, 001°, 050° and 272° representing conditions where exhaust stacks, derricks, cranes and clear air, respectively, were positioned upwind. In each case the data were scaled to wind speeds of 15 kt, 25 kt, 35 kt, 50 kt and 60 kt at full scale. The total of 20 wind

conditions provided all the data needed for both desktop and pilot-in-the-loop simulations.

Data from the platforms other than Brae A listed in sub-section 3.2 were used in earlier development work, but were not re-used during the validation process. It was more economic to restrict the flight simulator validation to one visual/aerodynamic data set, and it was considered that the different turbulence conditions experienced for the different wind directions for Brae A adequately encompassed all conditions experienced for the other three installations. This point is discussed in more detail in Appendix E.

3.3.4 Interfacing with the Wind Tunnel Data

Before the wind tunnel data could be applied to the helicopter model, all measurements needed to be scaled up to full-scale. Details of the functions to perform this transformation are given in Appendix F. The scaling involves changes to both the amplitude and frequency of the wind measurements depending on the wind speed at which full-scale data are required.

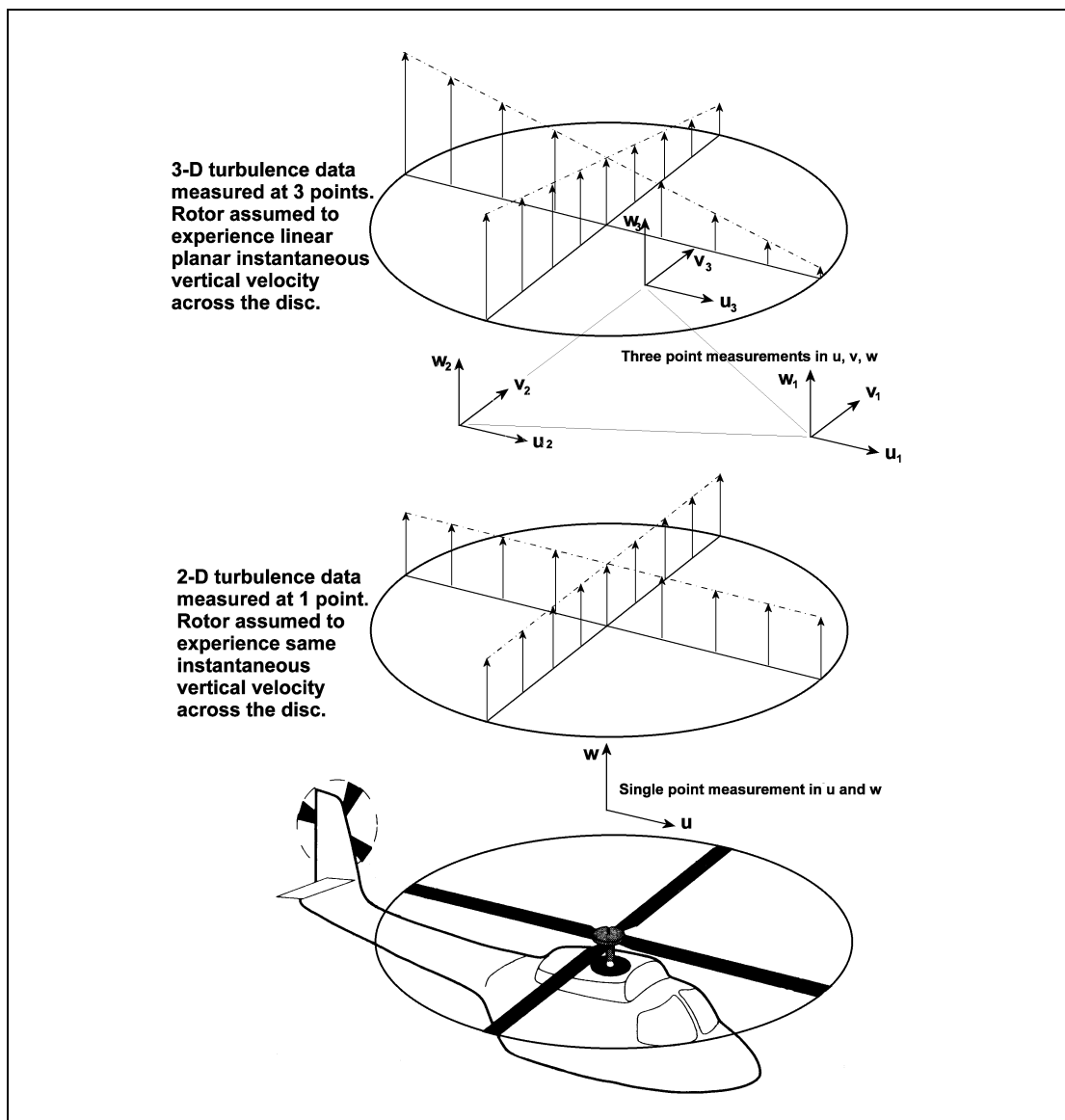


Figure 3.2 Different Representations of the Wind Tunnel Turbulence used in the Simulations

For the desktop simulation study the turbulence was fed into the main rotor model only. Turbulence effects on the tail rotor and fuselage were ignored. The data were fed into the main rotor in one of two ways:

- The initial (Part 1) wind tunnel data (Appendix B) comprised time histories of the longitudinal (u) and vertical (w) wind velocities at relatively few points above the helideck. For the simulation, time histories from a single measurement point were assumed to act simultaneously over the entire rotor disc (see Figure 3.2). Using data from a single point provided a convenient way of assessing the ability to hover in turbulence where the exact form of the turbulence encountered was known. Ignoring any change to aircraft position, which due to the nature of the flying task was likely to be small, avoided the need to interpolate between measurement points.
- Secondly, when the Part 2 enhanced wind tunnel data (Appendix I) were used, turbulence time histories were available for all three components of velocity (u , v , w) at three locations on the corners of an equilateral triangle (see Figure 3.2). These could be interpreted as a 3-axis u , v , w flow, and gradients for each of these velocities in the longitudinal and lateral directions at the centroid. Due to constraints on the amount of memory available in the simulation model host computer, the gradients of only one component could be used. The vertical component was chosen as this was expected to have a dominant effect compared with the longitudinal and lateral components. The longitudinal and lateral flows at any point on the disc were assumed to be equal to those at the rotor hub, whereas the vertical velocity was the sum of the flow at the rotor hub, and flow gradients multiplied by the appropriate lateral and longitudinal displacements.

The former method was used during the development of the desktop simulation. The latter method was employed for comparing the results of the BRAE02 piloted simulation trials with those produced by the SyCoS pilot using the desktop simulation (see sub-section 4.4).

A further method of implementing the turbulence was employed for the piloted simulation trials only, where the changing properties of the turbulence in the region surrounding the helideck were required (see Section 4). The velocities across the rotor disc were calculated as above, but the velocity and gradient time histories at the hub were formed by a weighted interpolation of all the time histories on the measurement grid directly surrounding the point of interest.

3.3.5 Pilot Modelling

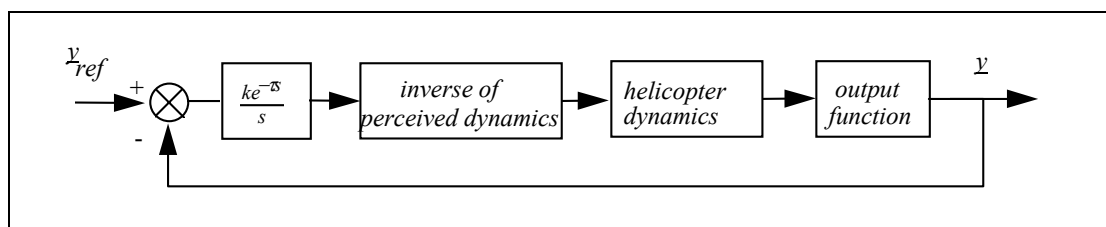


Figure 3.3 The SyCoS Pilot

The pilot model is one of a family of models collectively referred to as SyCoS (Synthesis through Constrained Simulation). The SyCoS pilot is a corrective pilot model developed to overcome some of the deficiencies of inverse simulation. Inverse simulation, in its exact implementation, generates the precise control actions required to fly a helicopter along a specified flight path. It therefore experiences difficulties with external inputs, such as turbulence, or system constraints such as control limits, where the method attempts to calculate unrealistic, or even unattainable, control

actions. A more practical approach is to systematically reduce the errors in following the flight path rather than eliminate them entirely and that is what a corrective pilot model does. That is, a pilot model is said to be corrective when it generates control actions that tend to correct an error between the observed output and a given reference value. The SyCoS pilot is a corrective pilot model that has the particular form shown in Figure 3.3, it is made up of two components:

- a) The crossover function made up of a gain, k , a delay τ , and an integration, expressed in terms of the Laplace transform variable, s .
- b) An approximate inverse of the helicopter model being controlled.

The values: delay, $\tau = 0.2$, and gain, $k = 2.0$, are typical values found by McRuer and Krendel [12] during the studies of pilot behaviour, and are those adopted in this work.

As there are four controls on the helicopter, the general situation is that four references can be specified for four outputs. In the present study, the four references are the three earth referenced components of velocity and the angular rate of heading - all of which are held at zero. In this form the SyCoS model is called the Fully Compensating Crossover Model (FCCM). The essential feature of the crossover model is that the pilot adapts to the dynamics of the system being controlled and, in the SyCoS model, that adaptation is captured by the component containing the approximate inverse. It includes, for example, compensation for any cross-couplings in the control axes. In many applications, a simple inverse of a linear representation of the helicopter's dynamics and output is all that is necessary for a successful implementation. The linear model initially has a large number of states but is reduced to nine states with six degrees of freedom. The nine state variables are 3 components of flow velocity, 3 components of angular velocity and 3 attitude angles.

Note that this simplification is applied to the pilot model only - the helicopter model remains a fully non-linear, individual blade, state of the art simulation. A fuller description of the FCCM implementation of the SyCoS pilot model may be found in Appendix F.

3.3.6 Workload Correlation

Having fully integrated the aircraft and pilot models with the wind tunnel test data, the outputs from this integrated system were the control responses for cyclic stick, collective lever and tail rotor pedals. These control responses are those required to compensate for the presence of the turbulence to maintain a stable hover in various wind states. Following this integration, the next step was to estimate the level of workload evident in the control activity.

In the course of the study there have been three candidate methods considered for prediction of workload ratings. All three methods: wavelet analysis, cut-off frequency and variance are described in Appendix H, and are summarised in the following paragraphs.

Wavelet analysis is a generalised form of the SDG model described earlier in sub-section 3.3.1, but applied directly to the control responses from either pilot-in-the-loop simulation or SyCoS. The method allows for a detailed analysis of the amplitude and timescale of all the discrete control inputs (or wavelets) that make up the entire control signal. From other work referenced in Appendix H, the relationship between the statistics of the wavelets and workload rating can be defined. The drawback of the method is the computational effort, and the level of expertise required to apply it to a large amount of data.

The cut-off frequency method is based on a spectral analysis of the control signals and the determination of the frequency below which 50% of the energy lies. The

basis for employing the cut-off frequency is the belief, or hypothesis, that increasing workload is reflected in stick movements that become more frequent. The higher the workload, the higher the frequencies at which inputs of significant amplitude are made.

Finally, the variance method uses a linear combination of workload metrics derived from the standard deviation of both stick position and stick rate in each control axis. Each metric is multiplied by a coefficient before being summed to produce an estimate of the overall workload rating. Coefficients are obtained through a data fitting exercise using a set of training data that comprise control responses with associated pilot workload ratings. The training data could be obtained from either flight test or pilot-in-the-loop simulation. In this study the latter source was used. Details of the data fitting exercise are given in Appendix J but any further discussion is deferred until Section 4, where the simulator trial that provided the training data is fully described.

A comparison of the methods is reported in [13] and concluded that there was no overwhelming evidence of superiority for any one of the methods. The choice was made, therefore, to adopt the variance method for the workload predictions on the basis that it is very convenient to calculate and, in the context of the current work, is at least as good as the other metrics.

When assessing the quality of the fits to the training data it must be borne in mind that the workload data from piloted tests is integer valued so that an error ± 0.5 in the predictions is acceptable. Furthermore, discussion with handling qualities and flight simulation experts has revealed that the precision expected in even test pilot's rating ability is limited, and that a 10% error rate would be considered remarkably good. That is, from a sample of ten data sets, the norm might be 1 or 2 predictions outside the ± 1 rating error and the rest in the ± 0.5 error bounds.

Section 4 Calibration and Validation Using Pilot-in-the-Loop Simulation

4.1 Method Overview

Having developed models that estimate the workload required to compensate for platform turbulence, the next step in validating the methodology requires suitable 'truth data' to assess the accuracy of these predictions. A suitable form of truth data is human pilot control responses with associated subjective workload ratings under various conditions of wind and turbulence. Although much data existed within QinetiQ giving both control responses and pilot workload ratings, none involved hovering for an extended period in turbulence. It was therefore necessary to design experiments specifically for this application in support of the validation exercise. Ground based simulation offered a safe and cost-effective way of generating such data.

In support of the validation exercise, data were collected to satisfy the following objectives:

- a) Replicate those runs conducted using desktop simulation by hovering over the helideck in turbulence with constant properties.
- b) Confirm that the effects of manoeuvring through turbulence can be adequately represented by the hover task in a) using a full approach and landing task.
- c) Quantify pilot variability by repeating item a) above for a total of three pilots.

The facility used to generate the data was the Advanced Flight Simulator (AFS) at the QinetiQ site in Bedford. The simulation models for the real-time work were identical to those assembled for the desktop analysis described in sub-section 3.3, with the obvious exception of the SyCoS pilot model, which was not required. For the purposes of the work a visual database representing the Brae A platform was produced with sufficient photo texturing to allow the pilot, as closely as possible, to use the same control strategies as at full scale. Figure 4.1 shows a typical view from the visual database.

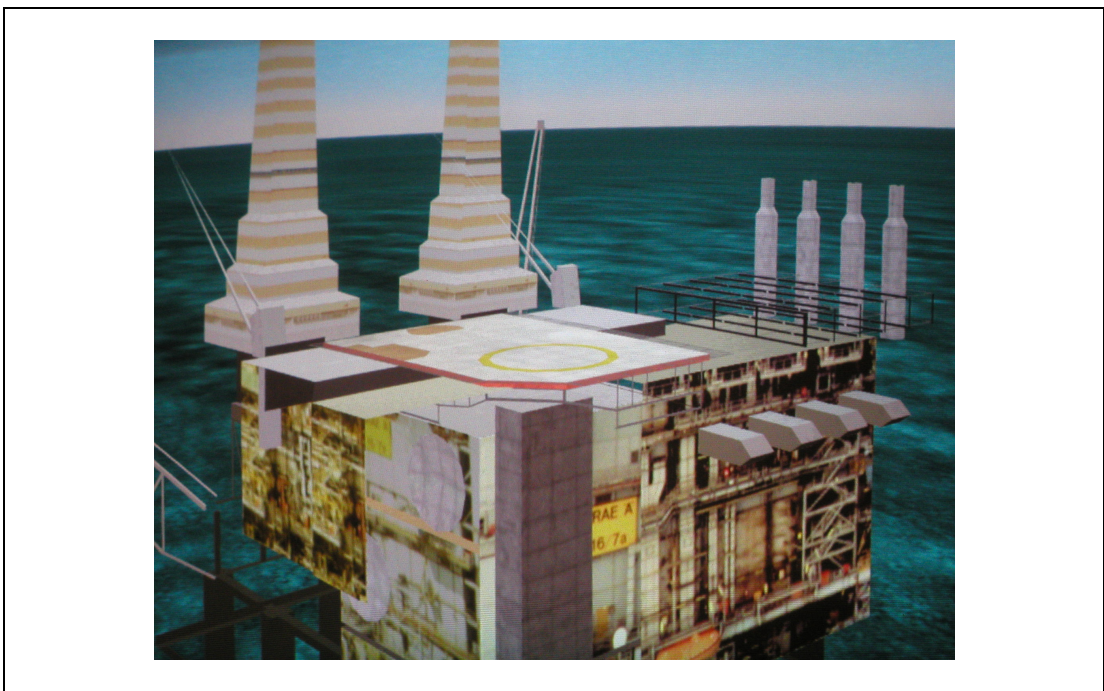


Figure 4.1 Example View from the Simulation Visual Representation of Brae A

4.2 Flight Simulator Trials

4.2.1 Method and Preparation

The simulator trials were conducted in two parts, designated trials BRAE01 and BRAE02.

BRAE01 was used for initial collection of data and demonstration of the suitability of the simulator for delivering the required validation data. An early sortie was used for assessing the platform visual database and modifications were made as required. This was followed by an evaluation sortie to capture the desired control responses and subjective workload ratings. The wind tunnel data used were those from the Part 1 wind tunnel tests described in sub-section 3.2 involving measurements of longitudinal and vertical components of velocity at a small number of points over the helideck. The time histories from a single measurement point at a full-scale height of 10 m above the centre of the landing circle were assumed to act over the entire rotor.

The BRAE02 trial involved assessments by three pilots to establish the variability in workload ratings due to individual pilot strategies. The pilots, referred to hereafter as pilots A, B and C, were all experienced and qualified test pilots who had flown recently to offshore platforms, although not necessarily the Brae A platform modelled for this study. BRAE02 used the measurements from the enhanced Part 2 wind tunnel tests described later in sub-section 4.2.4, and delivered the bulk of the data subsequently used for validation.

Three separate tasks were used during the BRAE01 and BRAE02 trials as follows:

- a) **Hover task** – establish a stable into-wind hover at a nominal height of 10 ft above the helideck, and maintain for a period of 60 seconds. (BRAE01 and BRAE02).
- b) **Hover task with sideslip** - establish a stable hover at the specified, out-of-wind heading at a nominal height of 10 ft above the helideck, and maintain for a period of 60 seconds. (BRAE01 and BRAE02).
- c) **Full approach** – starting from a point 1 km from the helideck on an into-wind heading, fly an approach to the helideck and land. (BRAE02 – pilot A only).

The hover and hover-with-sideslip tasks were flown by all three pilots and formed the bulk of the data generated during the trial, whereas the full approach was flown by pilot A only. All runs were immediately followed by award of a Cooper-Harper Handling Qualities Rating (HQR) using the decision tree given in Figure 4.2.

The task performance limits that form a crucial part of the HQR decision tree were generated during trial BRAE01 based on the judgement and experience of pilot A and were kept constant for all subsequent sorties. For the hover and hover-with-sideslip tasks the basic aim of the manoeuvre was to hold position in the presence of turbulence and therefore the performance limits related to the allowable deviations from the perfect hover. The limits used are given in Table 4.1.

Table 4.1 Task Performance Limits – Hover and Hover with Sideslip Tasks

Parameter	Desired	Adequate
Position relative to fore/aft reference	± 3 ft	± 5 ft
Position relative to lateral reference	± 2 ft	± 4 ft
Height relative to nominal hover height	± 3 ft	± 5 ft
Heading relative to reference	± 5°	± 10°

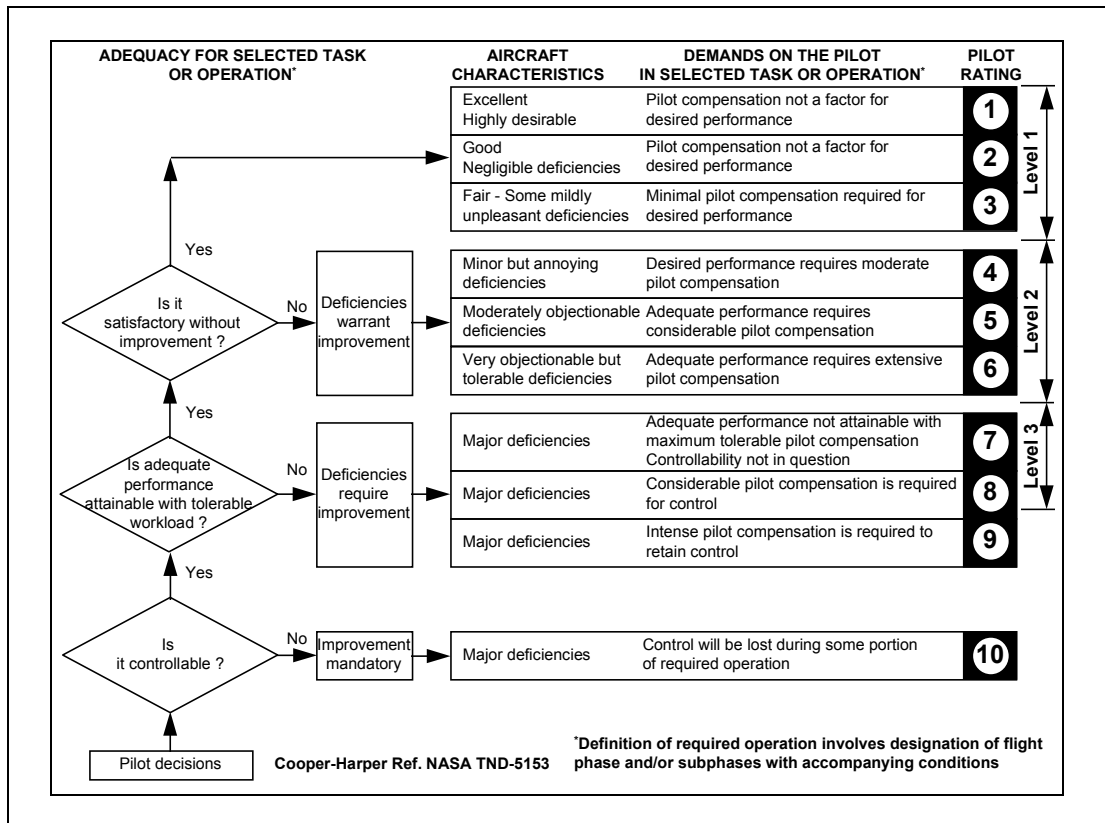


Figure 4.2 Decision Tree for HQR Rating

Definition of desired and adequate levels of task performance for the approach task was difficult as it was considered inappropriate to prescribe an exact flight path against which position accuracy could be judged. Not only would this have probably altered the pilot normal planning and flying strategy during the approach, but also would have required the addition of extra visual cues to allow the pilot to monitor his accuracy within the specified flight corridor, thus detracting from the realism of the task. However, during the approach a pilot will have a number of goals against which a general impression of desired or adequate performance may be awarded. A summary of such goals may include the following:

- a) Initial approach – decide and set an appropriate track towards the platform and establish a steady descent and deceleration.
- b) Mid-approach – remain clear of excessive turbulence and continue to descend and decelerate to set the aircraft up for final approach and landing. Judgement and smooth adjustment of closure rate will be important issues.
- c) Final-approach – transition smoothly across deck to establish a steady hover over landing spot whilst compensating for turbulence. If the control of flight path degrades to the point of feeling unsafe, then adequate performance cannot be awarded.

Using the goals in a) to c) to guide his decision, the pilot awarded task performance and an HQR for all full approaches flown.

4.2.2 Test Matrix

A full list of test points for the hover and hover with sideslip tasks is given in Appendix K. This matrix was used for both BRAE01 and BRAE02, although the number of test points actually completed varied from pilot to pilot. The test points

included three aircraft weights given by 9,510 lb, 9,910 lb or 10,510 lb. Wind speeds were set to 15 kt, 25 kt, 35 kt, 50 kt or 60 kt from one of four directions as dictated by the available wind tunnel test data. These were as follows:

- a) 088°, exhaust stacks upwind.
- b) 001°, derricks upwind.
- c) 272°, unobstructed.
- d) 050°, cranes upwind.

For each case the pilot was informed of wind direction and the required heading but not the wind speed. The order of the test points did not correspond to that given in Appendix K, but was randomised so as to avoid the possibility of the pilot anticipating any trend and perhaps colouring his award of an HQR. To enable a common set of test points from all pilots a certain number of the flight conditions were prioritised to ensure they were achieved within the allotted simulator time.

The approach task was flown by pilot A only, and concentrated on the condition with the derricks upwind and an into wind heading of 001°. The reason for choosing a single wind direction was due to constraints on time, and the turbulence field in the lee of the derricks was known to include some significant disturbances. Wind speeds were set across the complete range 15-60 kt and in all cases the weight was 10,510 lb.

4.2.3 **Lessons Learnt from Trial BRAE01**

Although the final sortie of BRAE01 was intended to provide the first set of validation data a number of issues arose that lead to modifications being made to the simulation and a full assessment being repeated as part of BRAE02. A summary of the lessons learnt prior to BRAE02 follows.

In scaling the turbulence from the wind tunnel test data during its integration with the helicopter model, the levels of turbulence were inadvertently set low by about 70%. For this reason, the BRAE01 results were of little use for comparison with desktop simulation predictions. However, they did provide a valuable data set for use as independent training data from which to configure the workload predictor (through correlating the pilot control activity against the awarded HQR value), because the data provided matched pilot control responses and subjective ratings (irrespective of the turbulence used) from which to characterise this relationship. The scaling of the wind tunnel data was corrected for trial BRAE02.

The method for injecting turbulence to the main rotor model (as described in sub-section 3.3.4) assumed the turbulence from a single measurement point to act over the entire rotor disc simultaneously. This implementation of the model was thought to be causing the heave response of the helicopter to be somewhat over-stated, and was not producing quite the expected levels of excitation in pitch and roll. This led to a different probe configuration being used for the latter wind tunnel tests (described in sub-section 4.2.4) that produced data for the velocity gradients at each measurement point, as well as the velocities themselves. The modifications required to integrate these data with the rotor model produced a simulation that is considered state-of-the-art in the simulation of response to turbulence.

The response of the aircraft to lateral turbulence was thought to be deficient. The cause of this was not clear, but the absence of any measurement for the lateral velocity in the wind tunnel was an obvious candidate. The measurement of this component was included in the specification for the Part 2 wind tunnel tests (see sub-section 4.2.4).

The responses of the aircraft model to control inputs in clear air were judged to be representative of the S-76 and needed no modification. A few minor adjustments were required for the visual database such as the colouring of the helideck and the removal of the depiction of the gas flare, as it had insufficient realism and was considered to be an unhelpful distraction.

4.2.4 **Part 2 Wind Tunnel Tests**

In support of the validation exercise, a further set of wind tunnel tests were conducted for the Brae A platform. The tests were an enhancement of those conducted previously, albeit limited to measurements on the Brae A. The tests and the analysis performed on the data are described in Appendix I. As before, a number of wind directions were considered relating to flows from an unobstructed sector and those from behind the derricks, cranes and exhaust stacks. The new data were enhanced in the following respects:

- a) The 2-axis hot-wire anemometers used in the earlier tests were replaced with 3-axis hot-wire anemometers allowing all three components of wind to be measured simultaneously. Previously, flow in the lateral direction had been omitted.
- b) Three such probes were arranged at the vertices of an equilateral triangle in order to capture the wind velocities at these points simultaneously. The spacing of the probes was set to correspond approximately to the scaled diameter of the main rotor on the S-76. From these data, estimates of the total flow and flow gradients were obtained at the centroid of the probe assembly.
- c) The test matrix was expanded to capture the flow time histories over a grid of points covering the region occupied by the helicopter and its rotor during the final approach and positioning to land. The exact grid used was modified according to the wind direction being considered in order to match the changes to the likely approach flown by the helicopter as it adapted to the layout of platform structure and the pilots' visual cues in each case. A table of measurement point locations is given in Appendix L, and these locations are shown diagrammatically in Appendix I, Figures I-3 to I-6.

4.2.5 **Results**

A full listing of the workload ratings awarded by the pilots in the form of Cooper-Harper HQRs is given in Appendix M. Table M-1 gives the results from BRAE01, Table M-2 the hover task results from BRAE02, and finally Table M-3 the approach and landing results from BRAE02.

The number of test points covered by each pilot varied according to the amount of time spent in the simulator and the time taken to familiarise with the simulator, task and rating scale. Pilot A conducted 29 hover test points in BRAE01, a further 26 hover and 5 approach test points in BRAE02. Pilots B and C took part in BRAE02 only and conducted 18 and 23 test points respectively.

In general, all the pilots were satisfied that the simulator and its models were adequate to produce valid workload assessments for the flying task. From the many comments received over the course of the trials, a number of important findings emerged. The aircraft model was considered reasonably representative of the S-76 although the roll axis was too well damped and responsive, and the attitude hold function was too efficient. The response to turbulence was felt to be somewhere between favourable and impressive, both in terms of the nature of the disturbances, the general intermittency, and impact on the vehicle and its motion. However, all pilots remarked on the lack of yaw disturbance and the associated required pedal activity, although this was not expected to have a large impact on the overall workload

ratings. This lack of yaw disturbance was not surprising because, as indicated in sub-section 3.3.4, the tail rotor and fuselage were not made subject to the turbulence.

The maintenance of good visual cues whilst hovering over the helideck was more difficult than in reality, due at least in part to the lack of texture on the surface of the helideck. The motion cues were generally adequate but the heave cues were thought by all pilots to be good, allowing a realistic strategy to be applied to compensate for vertical disturbances. Although only pilot A was exposed to both implementations of turbulence (with and without velocity gradients across the disc), the benefits of including the velocity gradients were considered to be more realistic turbulence and helicopter response to the disturbances.

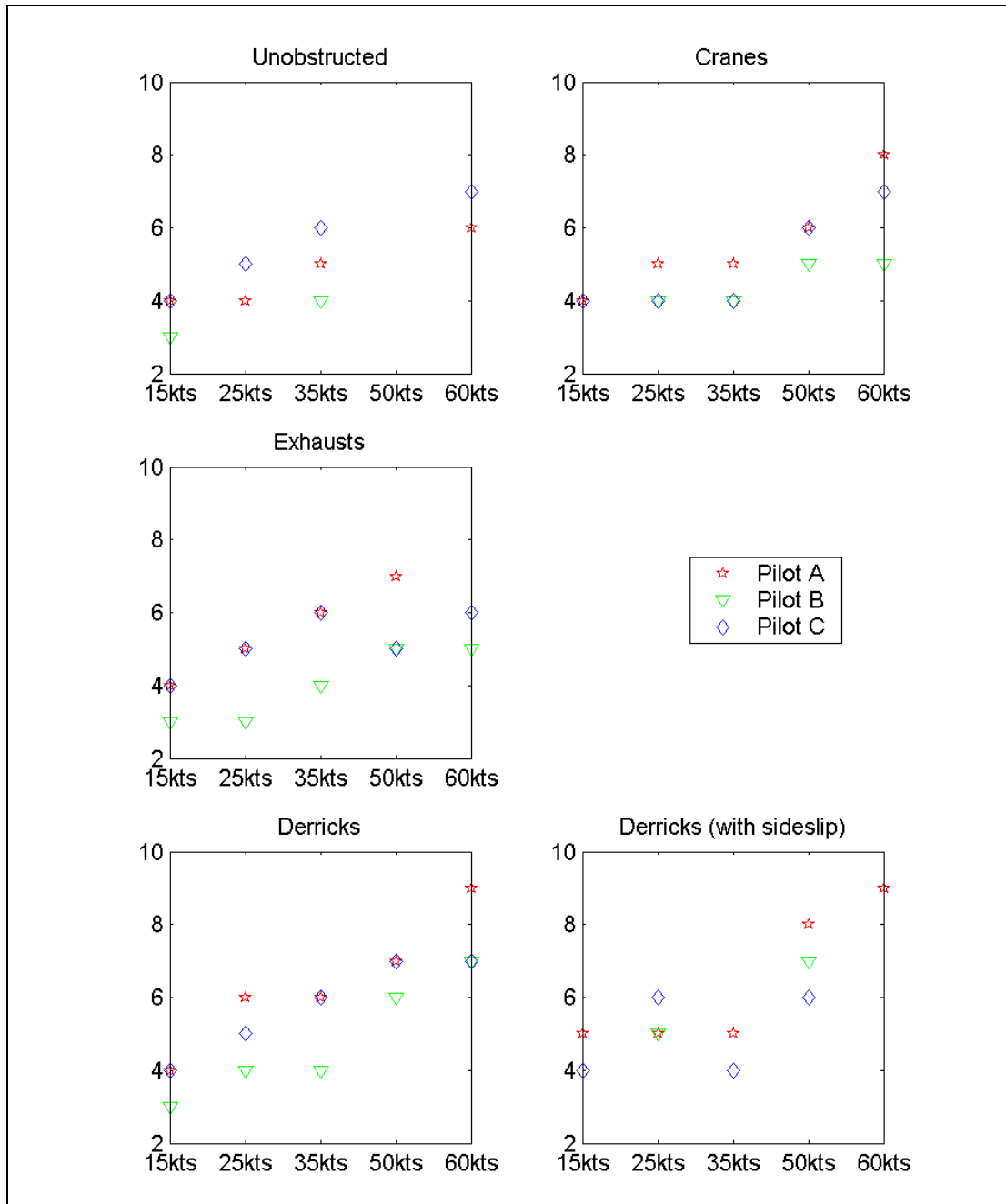


Figure 4.3 Comparison of Pilot HQR Ratings from Trial BRAE02.

A comparison of the trends in workload rating with wind condition is given in Figure 4.3. The increase in ratings with wind speed for each wind direction has shown similar trends in the results from each pilot, although the ratings from pilot B are often lower. In general the spread of ratings for a particular test point spans 2 HQR points with the exception of the case in the lee of the crane at 60 kt where a spread of 3 points was seen. It would normally be acceptable in such experiments for pilots to disagree by up to 1 HQR point only, and therefore the scatter seen here is larger than desired. The reason for this is most likely the difficulty experienced by all the pilots in judging the task performance against the criteria supplied. A discussion of this important issue is provided below in sub-section 4.6.

A presentation of the actual task performance achieved by each pilot is given in Appendix N on a case-by-case basis. From this analysis there are three main conclusions that emerge.

- a) Firstly, the boundaries between desired, adequate and less than adequate performance do not present themselves clearly in the data, giving quantitative evidence of the difficulty in making an accurate judgement.
- b) Secondly, the accuracy actually achieved for a given task performance rating in most cases violated the stated performance limits, suggesting that the values of these limits were too low.
- c) Thirdly, despite the apparent differences in the ability of each pilot to judge the task performance, the accuracy actually achieved was generally similar in the majority of cases.

The purpose of including the full approach task in BRAE02 was to assess whether the strategy of using the hover task to estimate the severity of turbulence, in terms of workload, was a reasonable simplification of looking at the entire approach and landing task. During the approach the amount of turbulence experienced by the pilot coming down the glide slope was found to be less than expected¹. However, until the helicopter enters the immediate vicinity of the helideck then the pilot has a certain amount of freedom in his flight path and typically, this freedom would be used to avoid any significant turbulence effects. Once in the vicinity of the helideck, the turbulence would be less avoidable and it was in this region where the model was fully functioning.

Given the experimental set-up, the approach task was essentially a test of the adequacy of the hover task to represent an approach to and landing on the helideck. Table 4.2 below shows a comparison of the workload rating for the approach task compared to that of the hover task in equivalent wind conditions. The table shows the ratings to be the same for all but the 25 kt case where there is a difference of just 1 HQR point. These results suggest that the hover task is a valid simplification and was appropriate for use in the desktop simulation.

Table 4.2 Comparison of Ratings from Hover and Approach Tasks

Obstruction	Wind	Hover Task Rating	Approach Task Rating
Derricks	001°/15 kt	4	4
Derricks	001°/25 kt	6	5
Derricks	001°/35 kt	6	6
Derricks	001°/50 kt	7	7
Derricks	001°/60 kt	9	9

1. This was consistent with the simulations since, due to constraints on simulation computer memory, the turbulence representation was limited to a box spanning the last 35 m of the approach.

4.3 Revisions to the Desktop Simulation

Although the results from trial BRAE01 could not be used directly for validation of the desktop simulation, the control responses and workload ratings recorded during this work proved to be useful. The results were used to provide an independent data set from which the coefficients for the workload predictor were derived. The details of this data fitting exercise are included in Appendix J. This was successful in defining the workload predictor subsequently used for prediction of workload ratings for comparison with the BRAE02 subjective ratings based on the BRAE02 control responses.

All other models remained as described in sub-section 3.3 but included the upgraded representation of turbulence to account for the gradients of vertical velocity across the rotor disc as previously described in sub-section 3.3.4.

4.4 Correlation of Desktop and Simulation Results

The workload ratings from the three BRAE02 pilots were used in three complementary ways:

- Firstly, they were compared with workload ratings predicted using BRAE02 pilot control activity and the workload predictor previously calculated from the BRAE01 data in order to demonstrate the validity of this predictor applied to an independent data set (see Appendix O).
- Secondly, they were used to validate workload ratings produced by the integrated desktop simulation (see Appendix P).
- Finally, they were analysed to examine the variability of workload ratings from each pilot and estimate some of the statistical properties of the data set as a whole (see Appendix Q).

The results of the validation of the BRAE01 workload predictor are plotted in Figure 4.4 showing a comparison between the subjective workload ratings from all pilots during BRAE02 with those estimated using the BRAE01 predictor and the measured control activities from BRAE02. A general observation is that the predictions are higher than those awarded by the pilots by approximately 0.5 to 1.0 HQR, suggesting that for a given level of turbulence the predictor would overestimate the difficulty of the task. In the context of the overall programme this is taken to be an acceptable variation.

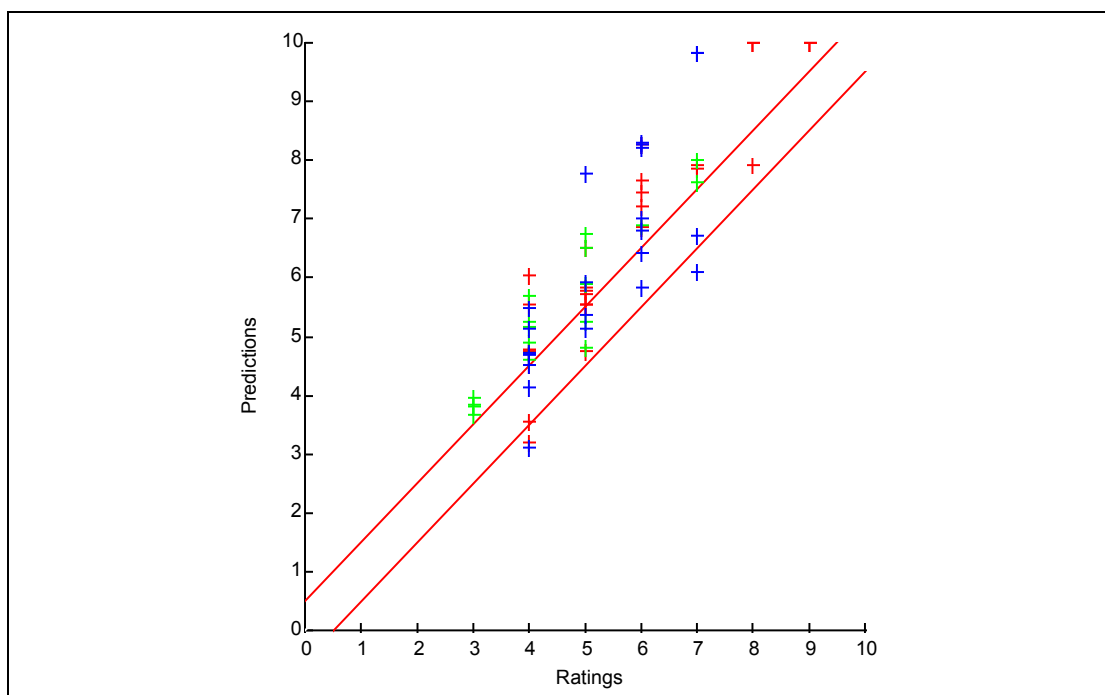


Figure 4.4 Validation of BRAE01 Predictor using BRAE02 Control Responses and HQRs

The results given in Appendix P can be plotted for each pilot in turn to show a comparison between the pilot subjective workload rating and that obtained by flying the SyCoS pilot in the same conditions of wind, turbulence and aircraft weight. The comparisons for pilots A, B and C are shown in Figures 4.5 to 4.7.

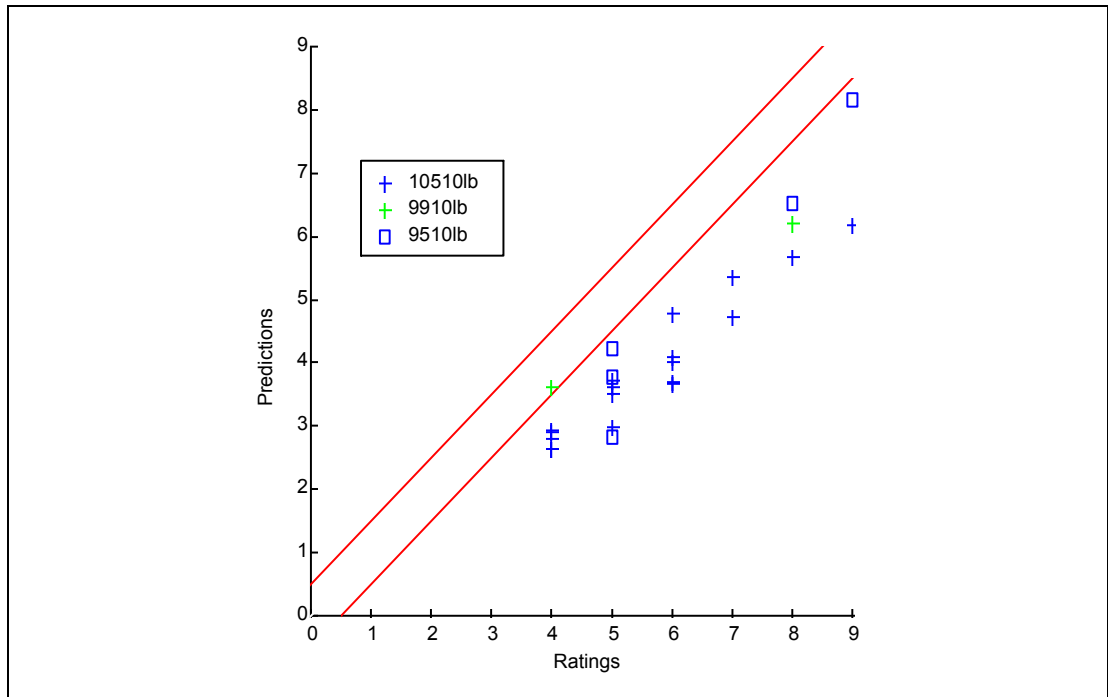


Figure 4.5 Comparison of SyCoS-based Workload Predictions with HQRs from Pilot A.

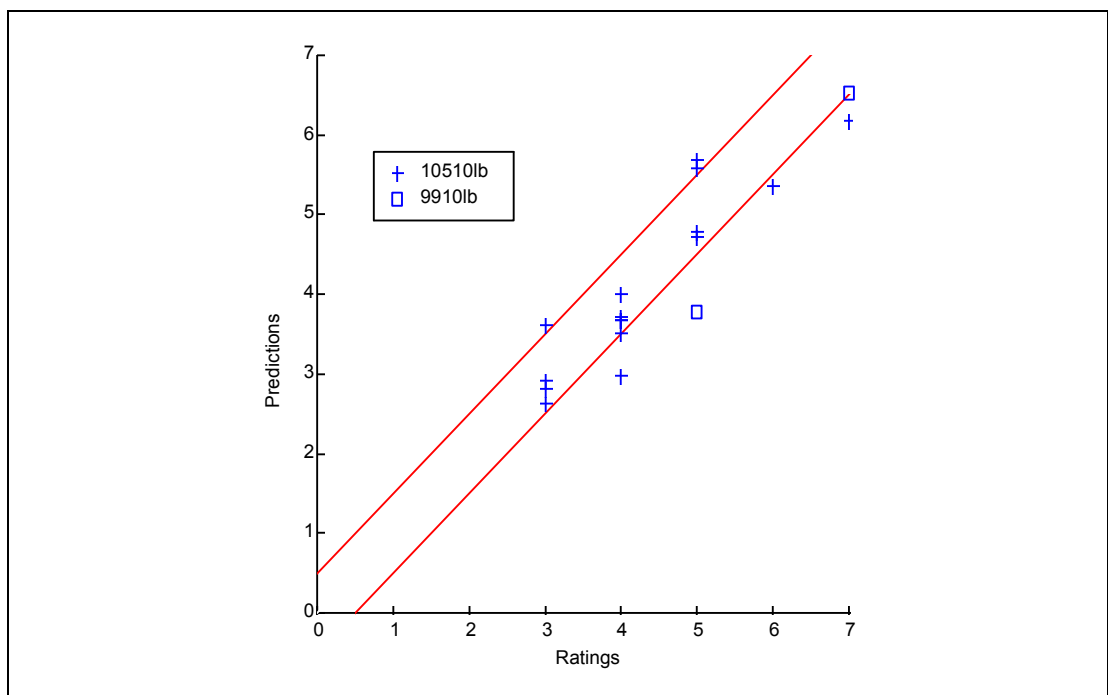


Figure 4.6 Comparison of SyCoS-based Workload Predictions with HQRs from Pilot B.

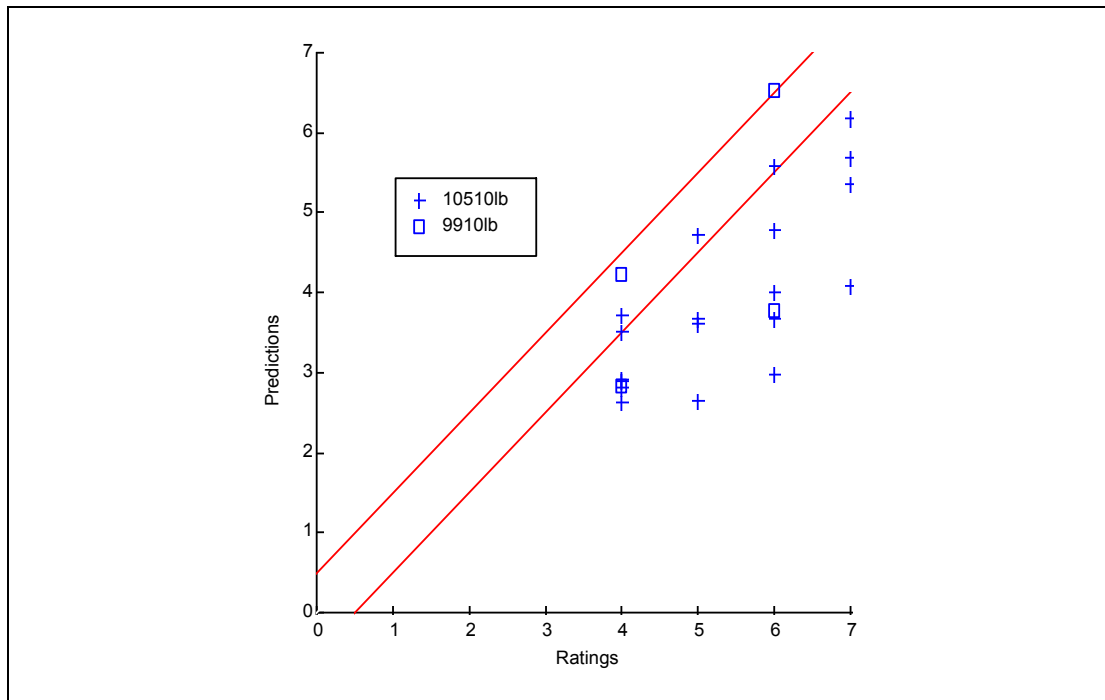


Figure 4.7 Comparison of SyCoS-based Workload Predictions with HQRs from Pilot C.

4.5 The Bristow HOMP Turbulence Parameter

Although not part of the main thrust of the work, the test piloted trials performed in the Advanced Flight Simulator BRAE01 and BRAE02 offered the opportunity to 'calibrate' the turbulence parameter that had been developed by Bristow Helicopters as part of the Helicopter Operations Monitoring Programme (HOMP) trial [14]. This parameter has been used to help identify 'turbulence events' in the HOMP data analysis, and has been used to start to map areas of turbulence around specific platforms.

The Bristow HOMP Turbulence Parameter was programmed, and the test pilot control records from trials BRAE01 and BRAE02 passed through the analysis. The resulting maximum values of the parameter were then compared with the test pilot subjective HQRs. The analysis and the results are presented and discussed in Appendix R.

4.6 Discussion

4.6.1 Test Pilot Task Performance

During the trials it became clear that judgement of task performance against the criteria given in Table 4.1 was difficult, due mainly to the lack of visual details on and around the helideck. Each pilot claimed to be able to rate the task performance with different levels of accuracy.

Pilot A was reasonably confident in rating the task performance, but did make reference to the difficulties involved. Pilot B did not feel able to estimate the hover accuracy at all in terms of the task performance limits supplied, but instead produced ratings based on an overall impression of the accuracy of the hover in terms of preparing to make a landing. Pilot C was often able to distinguish between a rating based on the criteria supplied (which he thought to be slightly too tight), and his general impression of the ability to maintain a stable hover from an operational standpoint.

The occurrence of such issues was no great surprise, and a solution would have been to ensure an abundance of visual cues in the database to allow pilots ample opportunity to make accurate judgements. However, much care would be needed in order to achieve this effect without compromising the realism of the simulation in terms of assessing the workload of the task. In the interests of realism, no artificial visual cues were introduced for either BRAE01 or BRAE02. For any future work, the addition of more detail to the helideck surface would offer the best way of increasing visual cueing without compromising realism, however, the computational limitations of the image generator might become an issue.

4.6.2 **SyCoS Workload Predictions**

The comparison of pilot subjective ratings with workload ratings estimated via desktop simulation shows that a reasonable set of predictions have been made. However, the predictions are low by 1-2 HQR points in comparison to pilots A and C, but very similar compared to pilot B (see Figures 4.5, 4.6 and 4.7). This suggests that, in comparison to pilots A and C, the desktop simulation predicts the task to be easier than it was actually found to be. At this point the observations of the previous paragraph are recalled. Interestingly, the ratings from pilot B were, in general, lower than those from pilots A and C, perhaps reflecting the more generous limits employed by pilot B when awarding ratings. Pilot C gave a greater scatter of ratings than either pilots A or B, perhaps suggesting that the distinction between the task performance limits and operational requirements were not always recognised when ratings were awarded. These observations are consistent with the differing levels of accuracy of the desktop simulation and suggest that SyCoS under-predicts the workload by 1-2 HQR points.

4.6.3 **Mapping HQR around Brae A**

Figures 4.8 and 4.9 show a graphical representation of the results from SyCoS and subjective pilot ratings respectively for an aircraft weight of 10,510 lbs. The workload ratings are placed on a compass rose where the bearing represents the direction of the wind and the distance from the centre of the rose represents the magnitude of the wind speed. The workload ratings are colour-coded as indicated on the key. The arc of the coloured segment represents the angle projected by the width of the obstruction. An approximate plan form of the Brae A platform at deck level is provided as a backdrop to indicate the orientation of the wind conditions in relation to obstacles around the helideck. The SyCoS results have been taken from Table O-1 although a bias of 1.5 HQR points has been added to all results to allow for the expected underestimate of 1-2 HQR points.

The subjective ratings in Figure 4.9 are an average rating calculated from the individual ratings provided by all three pilots. The results are reasonably similar with the majority of predicted ratings being no more than 1 HQR point different from the subjective rating, with the one exception being for turbulence from the cranes at 35 kt where the subjective rating is lower than the predicted rating by 2 HQR points.

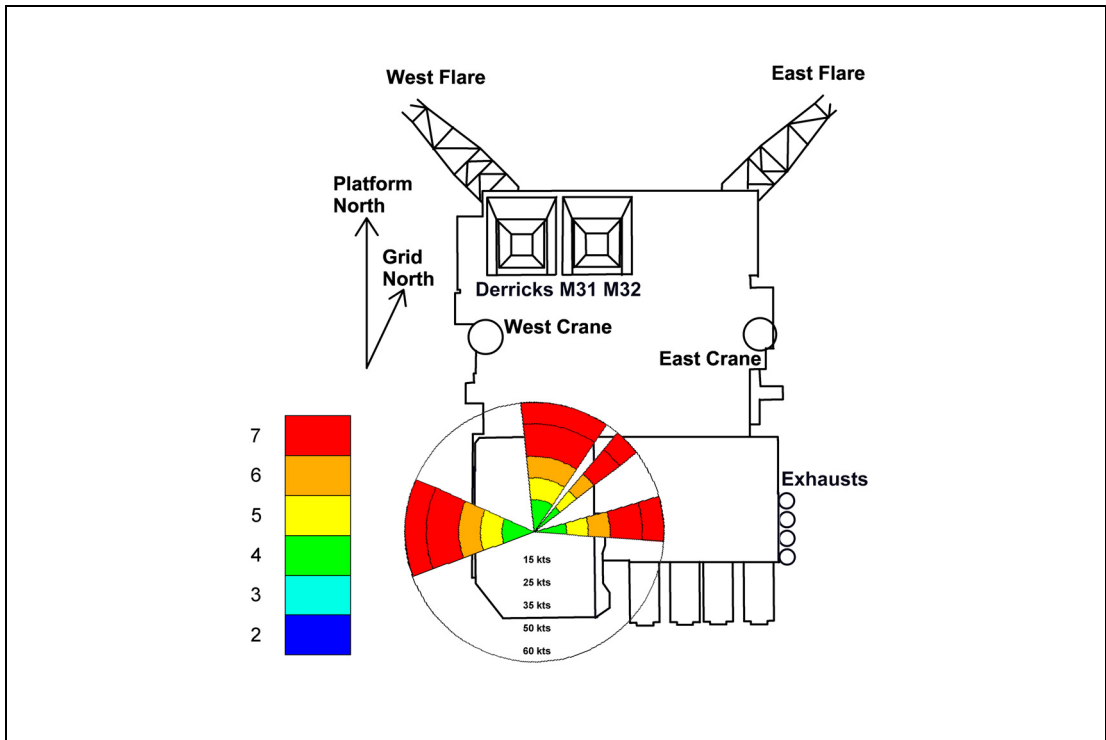


Figure 4.8 SyCoS Predicted Workload Ratings for Brae A (1.5 HQR added to compensate for bias)

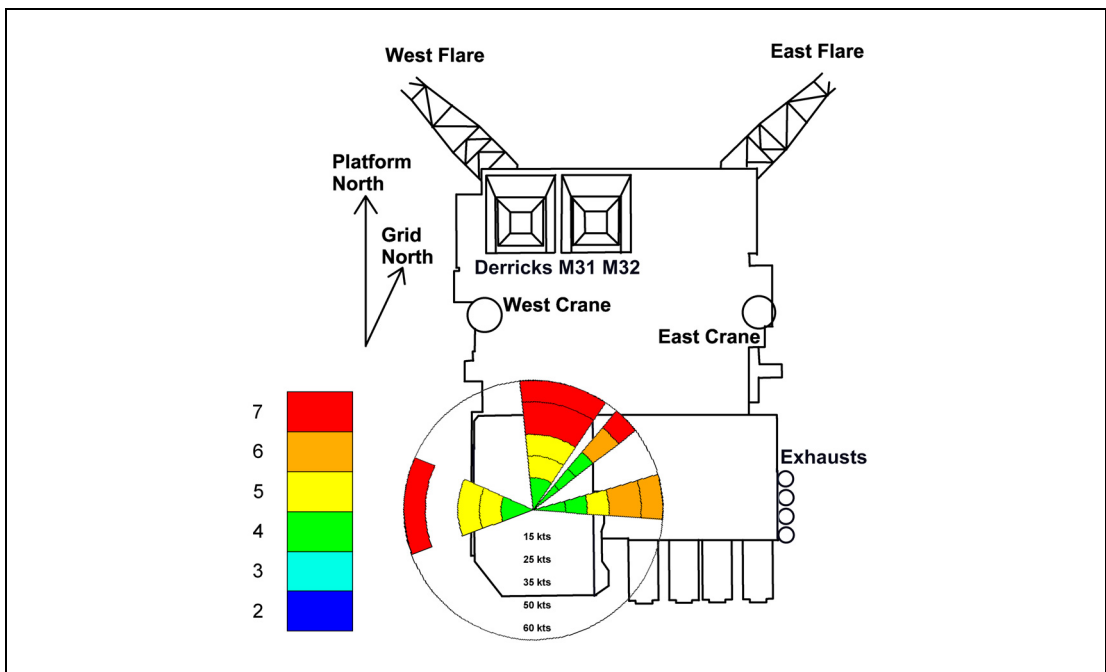


Figure 4.9 Average Test Pilot Subjective Workload Ratings from BRAE02 Trial

4.6.4 **Variation between Test Pilots**

The statistical analysis summarised in Appendix Q has used a method called Ordinal Logistic Regression to construct a model of the probability of a certain HQR occurring based on so called explanatory variables, namely, wind speed, pilot and wind direction - the last-mentioned variable referring to platform obstructions.

The model fitting strategy progressively identifies the most significant explanatory variables by using sub-models of the complete model. As might be expected, the best fit to the data using only one variable is achieved by using wind speed. More surprising is that the best fit using only two explanatory variables involves wind speed and pilot. That is, in determining the ratings, the pilot is a more significant factor than wind direction. However all three variables **are** significant in the final model which was subsequently verified by standard goodness of fit tests. In addition, the model provides predictions of the most probable ratings, and inspection of these predictions shows that the agreement with pilot subjective ratings is very good. One may have some confidence, therefore, that conclusions drawn from the model are valid.

In addition the technique can also show up less obvious trends in the data that may not be visible using other analyses. For example, for a given pilot and wind direction, the ratings are most strongly affected by changes of wind speed from 15 to 25 kt and from 35 to 50 kt. Further, for a given pilot and wind speed, the change in direction from 272° (no obstruction) to 001° (derricks) increased the ratings significantly but changes from 272° to 050° (cranes) and to 088° (exhaust stacks) caused no significant increase.

The same procedure was also applied, as a separate exercise, to the ratings from the SyCoS pilot model with the conclusion that the difference between the ratings awarded by the pilot model are not significantly different from those from Pilot B – that is, the SyCoS pilot produces ratings that are not untypical of human pilots.

In summary, the investigation has shown that data of the type collected in the BRAE02 trial is well suited to analysis by this technique. It has identified that although the wind speed is the dominant variable in the data, there is a systematic difference in the ratings awarded by each pilot. The reasons for the variations are considered to be as detailed in sub-section 4.6.1.

4.6.5 **Acceptable Levels of HQR**

This report has so far provided a description of the process of predicting workload ratings through desktop simulation, and the assessment of tasks in terms of HQRs in the simulator. However, for the application of the method it is important to establish where on the HQR scale a task is acceptable, and where it should be deemed unsafe. In this sense a two-point rating scale would suffice provided it defined the boundary between acceptable and unacceptable workload, although this would have been impractical from a validation standpoint. In the simulator exercise the outer boundary of adequate performance was defined as the point at which the flight path of the aircraft was insufficiently controllable to ensure continued safe flight. By reference to the descriptive text in the Cooper-Harper decision tree, Figure 4.2, the point at which adequate performance cannot be achieved even with extensive pilot compensation lies on the HQR 6/7 boundary. Therefore, workload ratings of greater than 6 represent conditions where turbulence levels are too high to ensure continued safe flight. In view of the fact that the SyCoS predictions give HQR estimates 1-2 points below those collected from real pilots, a suitable level (to be applied to SyCoS predictions only) is between HQR 4 and 5.

4.6.6 **Torque and Power Margins**

It is emphasised that no attempt has been made to predict where departure from the safe flight envelope would occur due to lack of torque and power margins. This would require a higher fidelity model of the S-76 (or any other aircraft of interest) and, as will be seen below, a number of improvements to the SyCoS pilot model. However, as turbulence is primarily a problem in high winds when the helicopter has a high margin of lift, it is considered that torque and power limits are unlikely to influence workload due to turbulence. This assumption may not be valid in cases where there is either a large downdraft impinging on the helicopter, or the rotor is shielded from the free stream flow by superstructure and thus operating in a low air speed regime. In either scenario, the amount of power in hand will be reduced and may become an issue depending on the power margins of the helicopter being considered. In terms of applying appropriate criteria to measurements of the expected airwake, the combination of the existing downdraft criterion and the proposed new turbulence criterion described in Section 6, may suffice for those cases involving downdraft.

Examination of the control responses from human and SyCoS pilots shows that there are significant differences in the control strategy used. The SyCoS pilot used a large number of small inputs to continually correct any deviations from the desired flight path whereas the human pilots would generally ride out the majority of the smaller disturbances and make relatively infrequent, but large, corrective inputs. This behaviour has been observed before in application of SyCoS to the manoeuvring of helicopters in the disturbed airwake of aviation compatible ships, and described by Turner and Bradley [15]. A number of additions were made to the pilot model that were successful in making the control responses more representative in heave and yaw axes. The enhancement of the cyclic, however, remained an area for further work. As one of the main differences is to make larger inputs (less frequently), these enhancements would be necessary if any accuracy were to be achieved in the prediction of torque exceedances.

4.6.7 **Effect of Degraded Visual Conditions on HQR**

The original proposal for the work described in this report included an option to capture validation data for night time operations as well as daytime. This part of the work was deferred, pending results from the daytime sorties. From a pilot's perspective, it is generally accepted that the workload increases in night approaches due to the difficulties in judging the approach angle and closure rate towards the structure. Any turbulence encountered during this more difficult approach would clearly increase workload. In addition, it may become more difficult to choose a flight path avoiding turbulence, thereby increasing the probability of turbulence encounters. Furthermore, there are other factors that can lead to similar levels of degradation to visual cues such as rain, sleet, snow or fog.

For the SyCoS pilot simulation model, there is currently no mechanism through which to represent the decrease in visual cues, and so no way of predicting the increase in workload needed to achieve controlled flight in turbulence under such circumstances. The benefit of performing further trials (for night time or otherwise) would be to quantify the change in workload expected when going from a good to a degraded visual environment, whilst encountering the same turbulence. Armed with this information the workload predictions arising from desktop simulations could subsequently be related to operations in degraded visual environments by applying an appropriate penalty. From discussions with aircrew, it would seem that making allowance for the increased workload at night is a matter for pilot judgement.¹

1. Night operations only attract additional restrictions in the Installation/Vessel Limitation List (IVLL) with respect to wave motion limits for operations to helidecks on smaller ships.

4.6.8 **Improving the Workload Predictor**

As has been described, the data from trial BRAE01 was used to produce the workload predictor subsequently used to produce predictions from the BRAE02 control activity. In this way, validation of the BRAE01 workload was performed against the independent data set obtained from trial BRAE02. As the workload predictor has been shown to produce reasonable estimates of the workload there has been no further attempt to modify the workload predictor using the BRAE02 data.

However, in order to provide a slightly more reliable workload predictor for future use, there would be a benefit in recalculating the workload predictor coefficients using the larger BRAE02 test pilot database.

4.6.9 **Application of the Workload Predictor to HOMP Data**

The workload predictor should have wider applicability in producing estimates of HQR for landings carried out in actual operations in the North Sea, where flight data can be made available via the Helicopter Operations Monitoring Programme (HOMP) [14]. Extracts from the available data could be analysed using the workload predictor to give estimates of workload rating for comparison with any pilot comments that accompanied the logged control responses.

4.6.10 **Offshore Platform Operational Envelopes**

Using the validated workload predictor in combination with wind tunnel data and the assembled desktop simulation tools can produce estimates of workload over a range of wind conditions. These data define the expected operational envelope in terms of allowable wind speed and direction and can be displayed in a format similar to the SHOL (Ship Helicopter Operating Limits) used by the UK Royal Navy. Some examples of estimated operational envelopes have been presented in Figures 4.8 and 4.9.

4.6.11 **Routine Workload Analysis within HOMP**

Clearly the application of the workload predictor to the HOMP data offers the opportunity to routinely update offshore platform operational envelopes (and the IVLL) using HQRs mapped around the offshore helidecks. This might be used to continuously improve the quality of the IVLL, and also to help to identify any changes in the operating environment (e.g. due to platform topsides modifications).

The workload predictor derived during this project was designed to operate on stationary records (i.e. steady state hover), and would require some adaptation before it could be applied to flight data records.

Section 5 Extending the Method to Other Helicopter Types

5.1 Modelling Approach

The Sikorsky S-76 was chosen as the baseline aircraft for this study partly because of its widespread use for offshore operations but also because a model of a similar weight class already existed and was relatively easily adapted to represent the S-76.

To make the results of the study more widely applicable it was necessary to establish the sensitivity of the workload predictions to changes in helicopter type. Ideally, this would involve configuring the *FLIGHTLAB* model with suitable aircraft configuration data to fully model particular types. However, the requirements for such data are extensive and involve requests to aircraft manufacturers for information that might be commercially sensitive and not freely available.

It was proposed, instead, that parameters in the S-76X model be modified in order to represent changes to key parameters of the aircraft design. Four case studies were made to look at the effects of flapping hinge offset, blade loading, vehicle weight (within the operating range of S-76) and overall size (large changes to the weight parameter to look at aircraft in three different weight classes). Details of each model are given in Appendix S, and the results are summarised below.

Figures 5.1 to 5.4 show the variation with flap hinge offset, blade loading, aircraft weight (over the S-76 operating range) and aircraft size (in three weight classes).

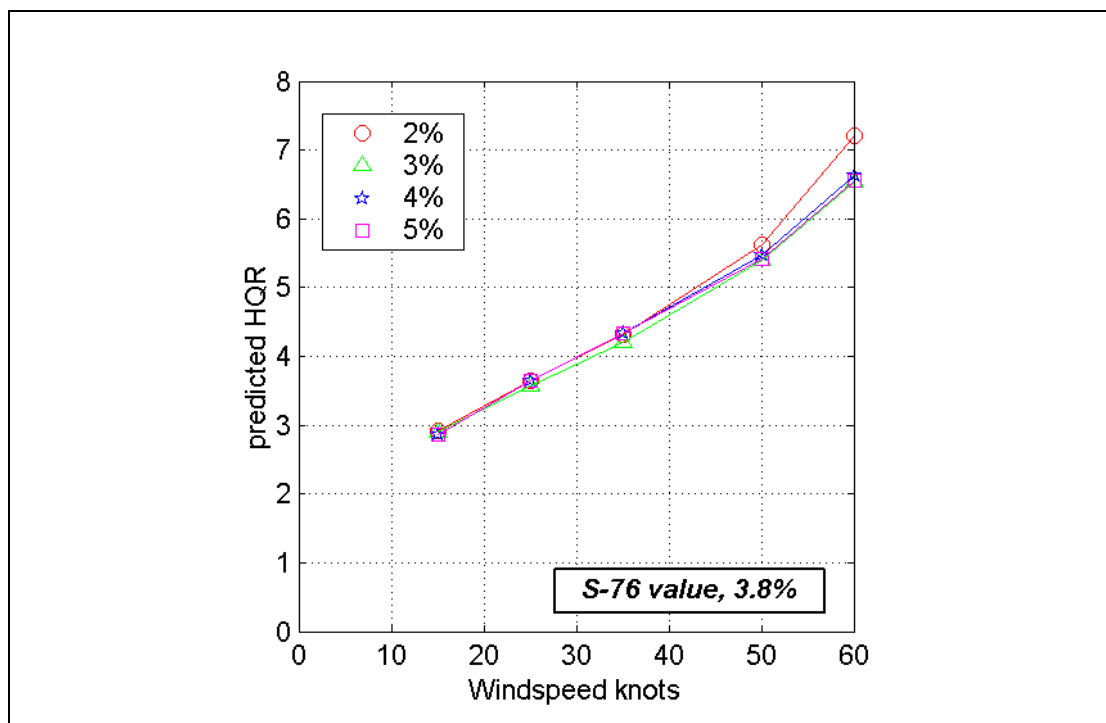


Figure 5.1 Workload Ratings for Various Hinge Offsets

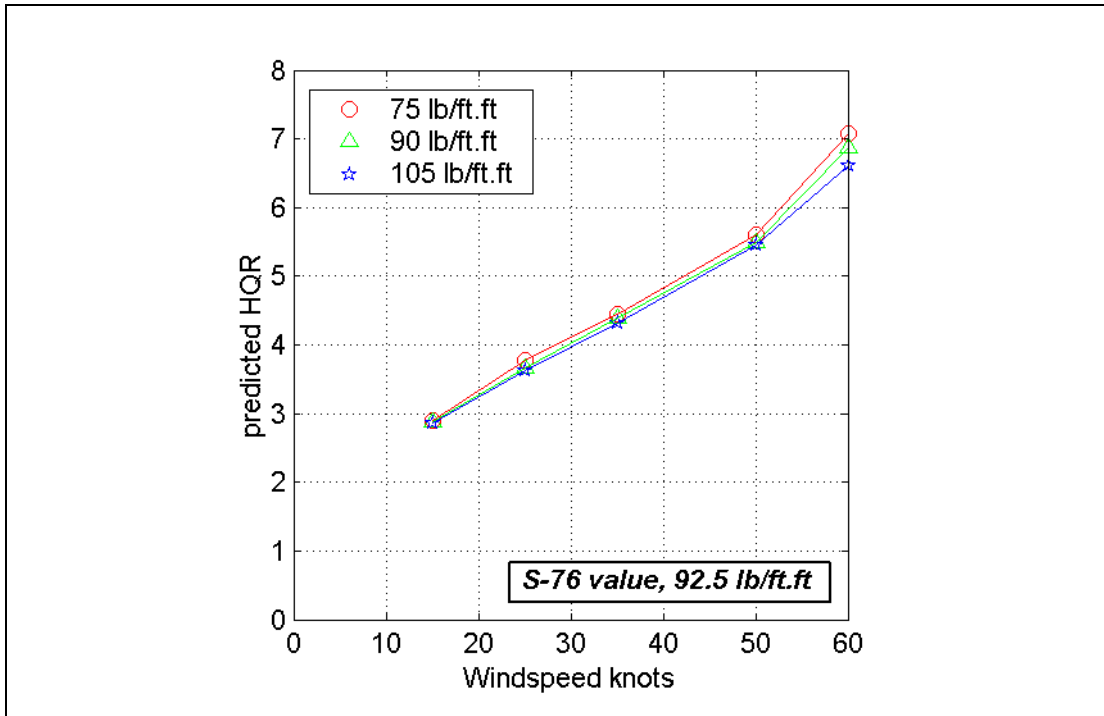


Figure 5.2 Workload Ratings for Various Blade Loadings

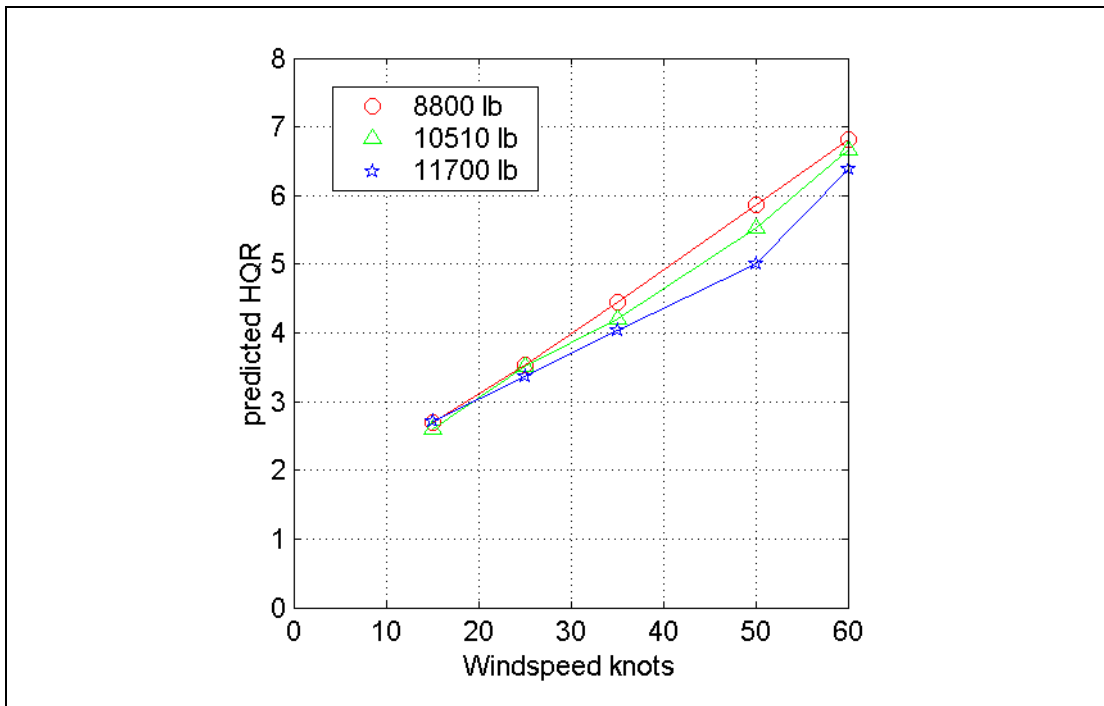


Figure 5.3 Workload Parameters Varying Aircraft Weight

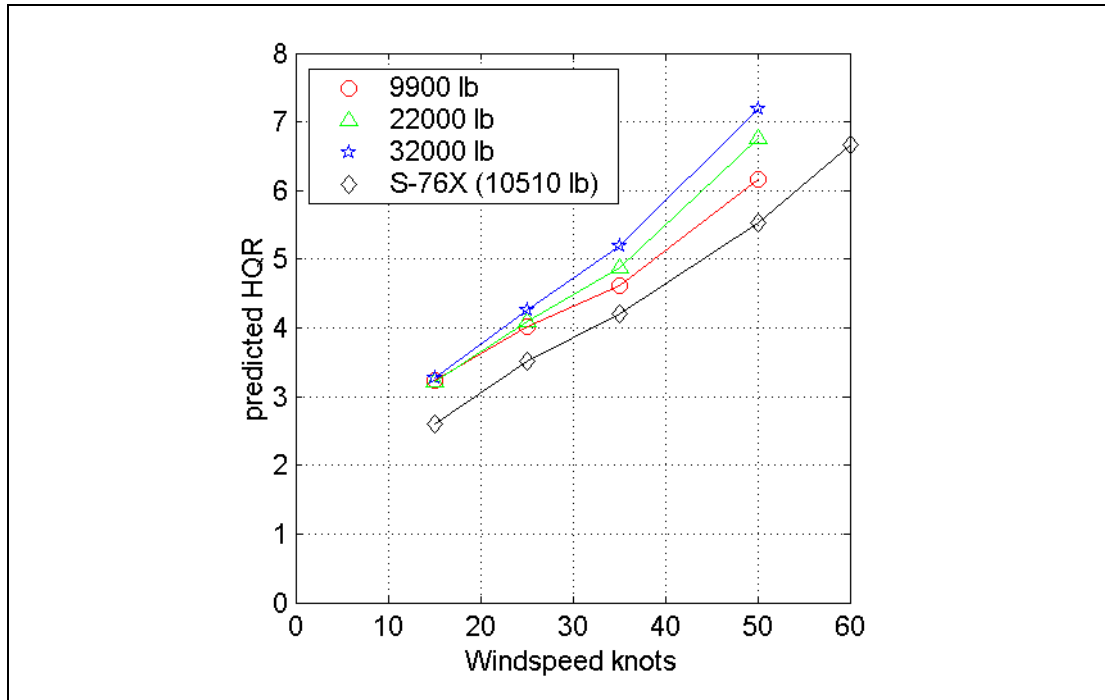


Figure 5.4 Workload Parameters for Various Aircraft Weight Classes

Both flap hinge offset and blade loading were considered over ranges that encompass the vast majority of types currently operating in the North Sea. Flap hinge offset is the distance from the rotor hub centre to the blade flap hinge and is quoted as a percentage of the rotor radius. Typical values for an articulated hub such as on the Sikorsky S-61 would be around 2% whereas the spheriflex hub on the Super Puma and the EC225 LP would have a value around 4-5%.

Blade loading is the ratio of the aircraft weight to the blade area (not to be confused with the disc loading which uses the total area of the rotor disc). Values range from 75 to 105 lb/ft².

The weight was first varied over the maximum expected range for S-76 operations, which was taken to be 8,800 lbs to 11,700 lbs. All other model parameters remained the same in these cases.

The weight was then varied more broadly to represent aircraft of varying size categorised into three different weight classes. The weights used were 9,900 lbs (approximately equivalent to S-76), 22,000 lbs and 32,000 lbs, referred to in the following as light, medium and heavy weight classes.

The differences in workload between configurations appears to be minimal in all but the study of varying aircraft weight and size. In the studies of flap hinge offset and blade loading, the summation of two effects produces a net change that is small. Firstly, an increase in flap hinge offset or decrease in blade loading would cause an increase in response to wind disturbances but secondly, and conversely, the control sensitivity would also increase such that the size of input required to compensate for the turbulence would be similar to the baseline case.

In both the case where weight has been varied over the S-76 operating range (Figure 5.3), and more widely to represent different helicopter sizes (weight classes) (Figure 5.4), there is a difference in workload of almost 1 HQR point. This maximum change is seen when the wind speed is near 50 kt. In the weight class variation of Figure 5.4 it is the lighter aircraft that appears the easier to fly. The reverse trend is

seen with the variation of S-76 weight in Figure 5.3. This latter trend is contrary to what would generally be expected in the IVLL where in highly turbulent conditions the maximum allowable aircraft weight would be decreased to allow a landing to proceed.

However, the assessment made here is based purely on workload related to aircraft handling whereas the IVLL will also be influenced by the amount of spare power available, a parameter that would be expected to increase as the aircraft weight is reduced. Neither the aircraft nor pilot models being used in the study are currently of sufficient fidelity to take account of limited power margins and this may be the reason for the discrepancy. Taken in the context of the overall accuracy with which the prediction of workload ratings has been demonstrated, the changes due to weight are not considered to be particularly significant.

5.2 Discussion

As a method for predicting the overall severity of turbulence the current desktop simulation was adequate. However, on the basis of the results above, the current level of fidelity would appear to be insufficient to make clear distinctions between the configurations modelled. Although the intention was to represent a broad range of designs it is clear that, in conducting the case studies, each of the modifications have been considered separately and that the combined effect of several modifications may result in a larger change in workload than has been demonstrated. Furthermore, actual designs may possess design parameters that do not correspond closely to the design rules of thumb used to configure the model for the different weight classes. The automatic flight control system used throughout was that of the Lynx Mk3 and the representation of the gust rejection properties of other types has not been feasible within the scope of work. If an aircraft is identified as being clearly outside the design range considered here, then attempts could be made to model that type in order to identify any specific issues with the handling of that vehicle in turbulence.

The combined experiences of the three simulator assessment pilots in offshore flying provided an opportunity to test the validity of the case studies relating to the handling of different aircraft. The general consensus was that there isn't a single helicopter type, currently used in European offshore operations, that stands out as being particularly poor for handling in turbulence.¹ However, the feel of various types is almost certainly different. For instance, a relatively large helicopter with a sluggish response will tend to smooth out many of the gust disturbances such that the pilot is less aware of the turbulence, and may tend to drift further from his intended flight path before it becomes apparent that compensatory inputs are required. The longer a disturbance is left unchecked then the larger the input required to correct for drift and the harder the task is to re-establish on the desired flight path. Conversely, for a relatively light and lively aircraft the majority of disturbances are felt immediately as sharp-edged gusts, and the pilot will make a large number of smaller inputs to compensate. Most disturbances are compensated for before any significant drift is allowed to build, however the overall impression is of a less comfortable ride.

Overall the evidence from pilots, and the results of the simulation case studies, would both suggest that the aircraft type is not a key parameter in determining workload required in turbulence.

However, a general limitation of the modelling used in this work is that the effects of power and torque limits have not been included, and this is often an important issue in deciding which aircraft types can and cannot operate in adverse environmental conditions. It will often be the case that shear and downdraft are experienced simultaneously with turbulence, and it is the presence of downdraft, and the

1. Though neither the simulations nor the test pilot comment encompassed teetering rotor types (i.e. blade offset = 0.0)

availability of sufficient power and torque margins to overcome it, that may often be the determining factor in limiting operations, or in requiring payload to be reduced in order to increase the margins. The pilots commented that, in terms of the problems experienced, the split is roughly 50/50 between insufficient power and difficulty in stabilising the helicopter.

In view of the rather inconclusive results from this part of the study, it is recommended that evidence be sought from helicopter operational experience to help determine whether different types vary significantly in their handling qualities in turbulence, perhaps through analysis of the data now available through the Helicopter Operations Monitoring Programme (HOMP). A recommendation to this effect is made in Section 10.

Section 6 Turbulence Criterion for Safe Helicopter Operations

6.1 The Need for a Simple Turbulence Criterion

The preceding Sections of this report have described the development and validation of a desktop simulation for predicting workload due to turbulence. The method has been used in Section 5 to examine the effects of changing aircraft parameters on the workload and, given appropriate data, could be used to look at specific aircraft types.

However, to be of general use the effects of turbulence on workload must be encapsulated in a simple form that is accessible to the broader offshore community, especially those responsible for offshore platform design. In support of this requirement, the simulator data collected for the purposes of validation have been analysed to identify a suitable relationship. Full details of the analysis are given in Appendix T and the results are summarised below.

6.2 Prediction of Workload from Turbulence

Appendix T includes a table showing the standard deviations for all the samples of turbulence used in the simulator trial BRAE02. It can be seen in the appendix that all the standard deviations for a given parameter increase linearly with speed and, indeed, this is no surprise as it is due to the linear scaling from the original wind tunnel data. However, further to this it would seem that from the four wind directions where data were available, the ratios of standard deviation for different parameters at the same wind speed are generally constant.

The consequence of this characteristic is that for the purposes of identifying a relationship between the standard deviations of turbulence and workload, any parameter could be used as a metric to capture the effects of increasing wind speed. In fact, if a curve fitting exercise were conducted with more than one parameter then the algorithm used would not be able to distinguish between changes to the weighting of either parameter.

It was therefore decided to pick a single parameter as the overall metric of the turbulence level. The standard deviation of vertical component of velocity was chosen, as it seemed to maintain a constant ratio with the other parameters to the greatest degree. Figure 6.1 shows a plot of the standard deviation of vertical velocity against the HQR awarded by pilots A, B and C in the corresponding runs of trial BRAE02. Also shown on the plot is the best fit line that is given by the following relationship:

$$\text{HQR} = 2.77 + 1.571 * (\text{standard deviation of vertical velocity}).$$

Using this formula to obtain a prediction of each HQR and comparing it with that awarded by all three pilots leads to Figure 6.2. The accuracy is generally within ± 1 HQR, which corresponds to the scatter of the original experimental data. However, it is stressed that this is not a validation of the formula but merely reflects the quality of the curve fitting.

As discussed in sub-section 4.6.5, and without any allowance for degraded visual cues, it is assumed that the workload has become excessive when the rating crosses the HQR 6/7 boundary. In experimentation an HQR should only ever take an integer value, however, the prediction of HQR produced by the formula above will produce non-integer values. If each HQR prediction is rounded to the nearest integer (i.e. 6.49 becomes 6 and 6.50 becomes 7) then the value describing the boundary between safe and unsafe flight becomes an HQR of 6.5. Given the criterion for unsafe flight of $\text{HQR} > 6.5$, the relationship above can be used to derive a turbulence criterion for flight in turbulence as follows :

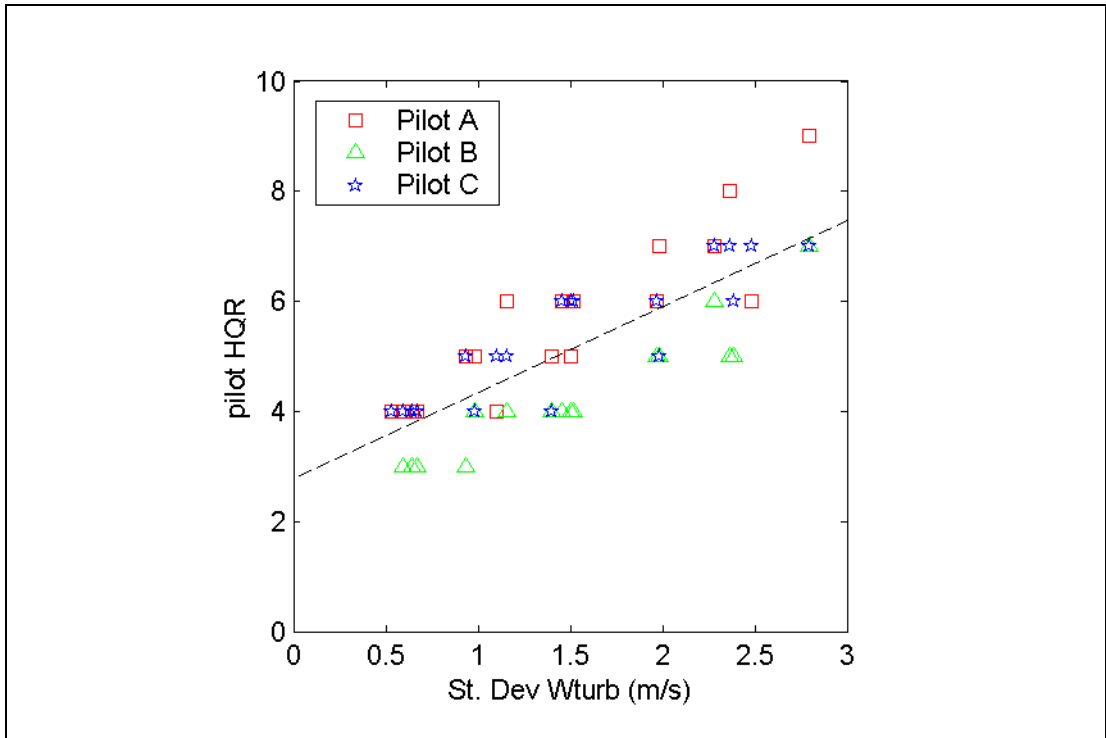


Figure 6.1 Pilot HQR Plotted against Standard Deviation of Vertical Flow

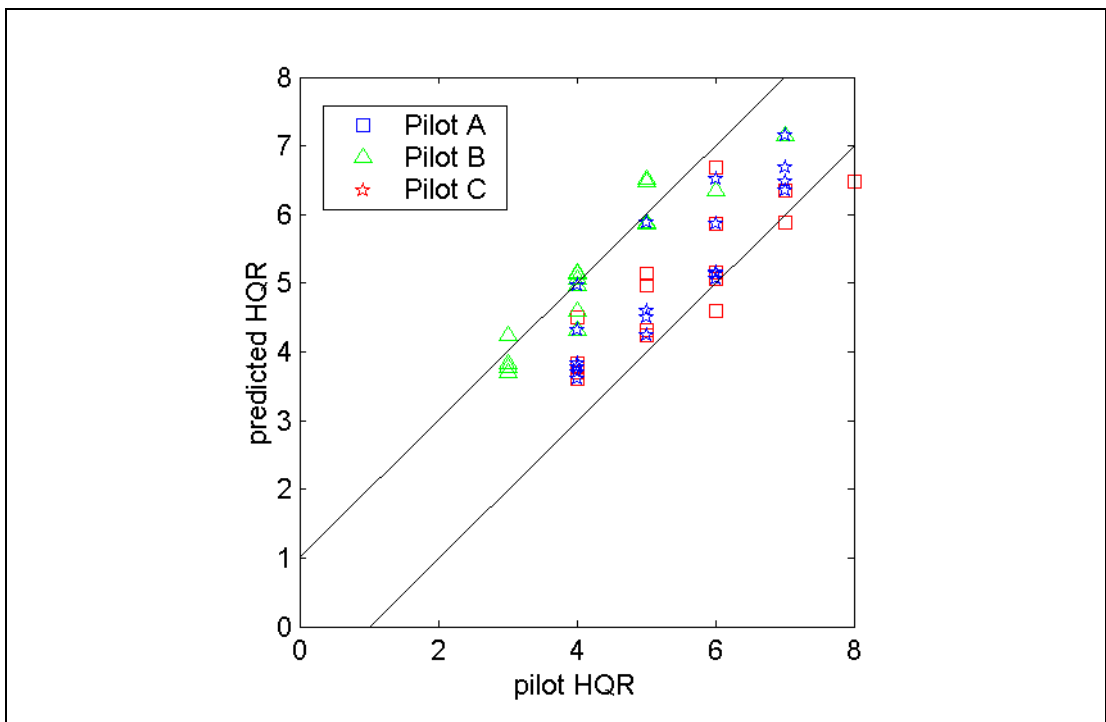


Figure 6.2 Test Pilot Subjective HQR Versus Prediction Based on Turbulence

Standard deviation of vertical velocity > 2.37 m/s, workload excessive.

However, slightly different relationships are found by taking the data from each pilot separately, and these are given in the appendix. If these are also combined with the $HQR > 6.5$ criterion then the limit on the standard deviation of vertical velocity becomes 1.94 m/s, 2.96 m/s and 2.31 m/s for pilots A, B and C respectively.

The (rounded) value of 2.4 m/s (from the combined datasets) is proposed as the working value for the turbulence criterion, however, the variation in the results from individual data sets serve to emphasise the need for validation of the criterion via an independent data source before it can be incorporated in CAP 437 or the Helideck Design, Modification and Verification Manual. The primary use of the criterion is to assist the interpretation of wind tunnel data and not to establish operational limits. However, as seen below the latter may offer a convenient format for further validation.

Figure 6.3 shows the workload prediction obtained by applying the turbulence criterion to the wind tunnel data, displayed in the same format as Figures 4.8 and 4.9 discussed in sub-section 4.6.3. The predictions compare well with those obtained from SyCoS (Figure 4.8) and the subjective ratings recorded in Trial BRAE02 (Figure 4.9).

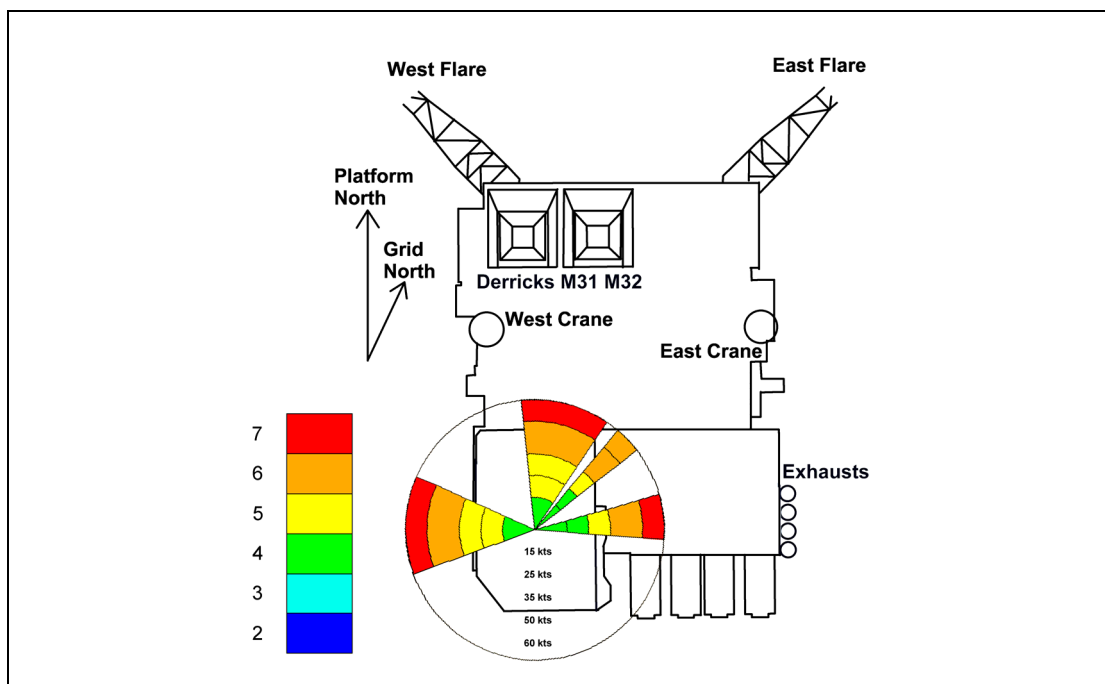


Figure 6.3 Workload Prediction Obtained by Applying Turbulence Criterion to Wind Tunnel Data

There are three possible sources of data for validation of the turbulence criteria:

- a) The first involves conducting further simulator trials in daylight conditions but using turbulence measurements from a platform other than Brae A. This would produce matched turbulence and workload ratings for a completely different set of wind tunnel data and ensure a wider applicability of the validation. It would not, however, validate the wind tunnel model, the implementation of the wind tunnel data in the *FLIGHTLAB* model, and the veracity of the *FLIGHTLAB* representation of the S-76 - see Section 8. See also Section 7 for further discussion on the applicability of the turbulence criterion to other offshore platforms.

- b) Secondly, the measurements of vertical velocity from as large a database of wind tunnel data as is available, could be analysed to estimate where the high turbulence sectors occur, and these data compared with the Installation/Vessel Limitation List (IVLL) for the platforms concerned. The importance of torque and power margins in the placement of limits in the IVLL must first be clarified, as the turbulence criterion only relates to those cases where workload becomes excessive.
- c) Finally, the data from the HOMP project has already been cited as a potentially valuable source of validation data for the workload predictor. If the workload ratings from this exercise could be referenced to the expected airwake at the time of the HOMP measurement (as measured in the wind tunnel), the results could also be used to validate the turbulence criterion.

The possibilities and justification for such further validation are discussed in Section 8.

Section 7 Workload Predictions for Other Platforms

The validation of the workload prediction technique has concentrated on modelling the Brae-A platform in order to limit the work necessary for conducting piloted simulations. However, as described in sub-sections 2.3 and 3.2 there is a larger body of wind tunnel and SyCoS response data available for other platforms, namely Beatrice, Claymore and Schiehallion. SyCoS responses were calculated as part of an earlier phase of work and fully reported in reference [13]. The current phase of work has introduced two main results that can now be retrospectively applied to these earlier data. Firstly, the validated workload predictor discussed in Appendix J can be applied to SyCoS control responses, and secondly the turbulence criterion discussed in Section 6 can be applied to the original wind tunnel measurements.

The format for displaying results is similar to that used earlier in Figures 4.8, 4.9 and 6.3 whereby a chart is drawn in the form of a compass rose with the compass bearing representing the wind direction and the distance from the centre of the compass representing the magnitude of the wind speed. A segment of the arc is then coloured according to the predicted workload rating for that particular wind speed and direction. In the following figures there are four compass roses representing the workload at four fixed positions at heights of 10m and 20m over the helideck centreline, and at similar heights but 15m to the left of centreline.

Figures 7.1, 7.3 and 7.5 show the results from analysis of the SyCoS control responses, using the workload predictor generated in Appendix J for Beatrice, Claymore and Schiehallion platforms respectively. In order to allow for the expected underestimation of 1-2 HQR points discussed in sub-section 4.6, all the workload predictions have been increased by 1.5 HQR points. Figures 7.2, 7.4 and 7.6 show the corresponding plots from analysis of the wind tunnel data and application of the turbulence criterion of 2.4 m/s applied to the standard deviation of the vertical turbulence. It is noted that only a limited number of cases were computed using SyCoS whereas a full set was considered when applying the turbulence criterion.

It is seen that there is good correspondence between the predictions from the two methods in so far as there is not a single wind speed/direction where the workload ratings differs by more than 1 HQR point. In this way the SyCoS predictions can be used to add credence to the turbulence criteria results (and vice versa) for platforms other than the Brae-A platform that was used for the validation exercise.

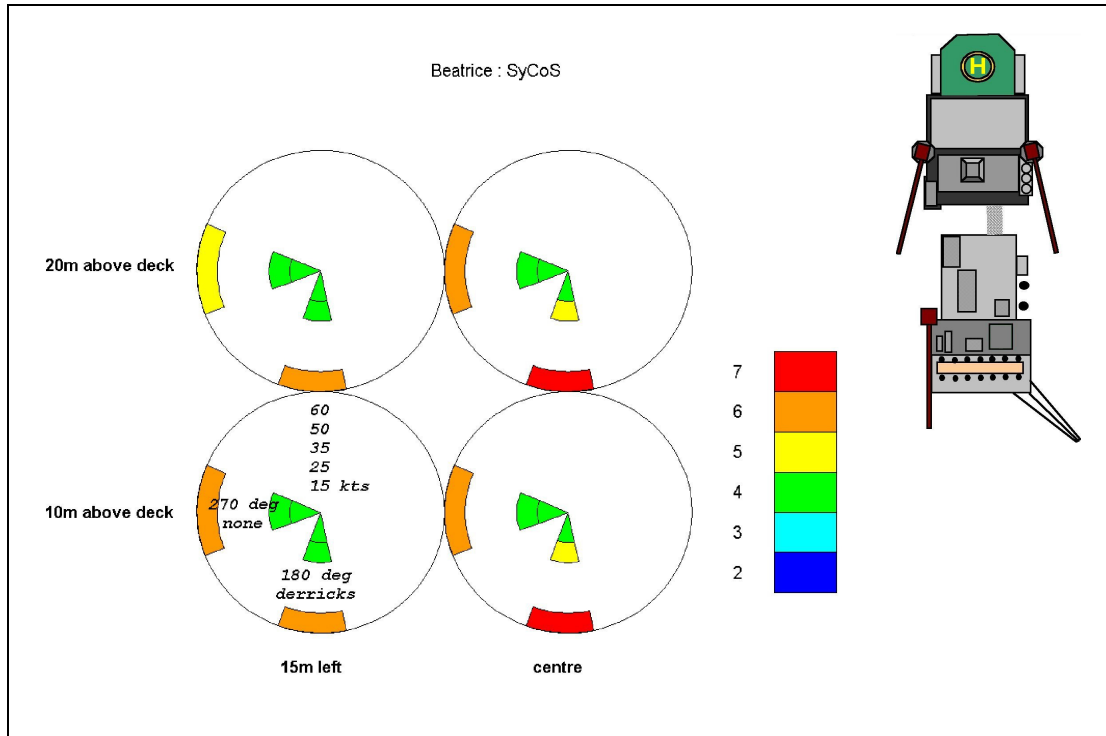


Figure 7.1 Workload Predictions for Beatrice Based on SyCoS Control Responses

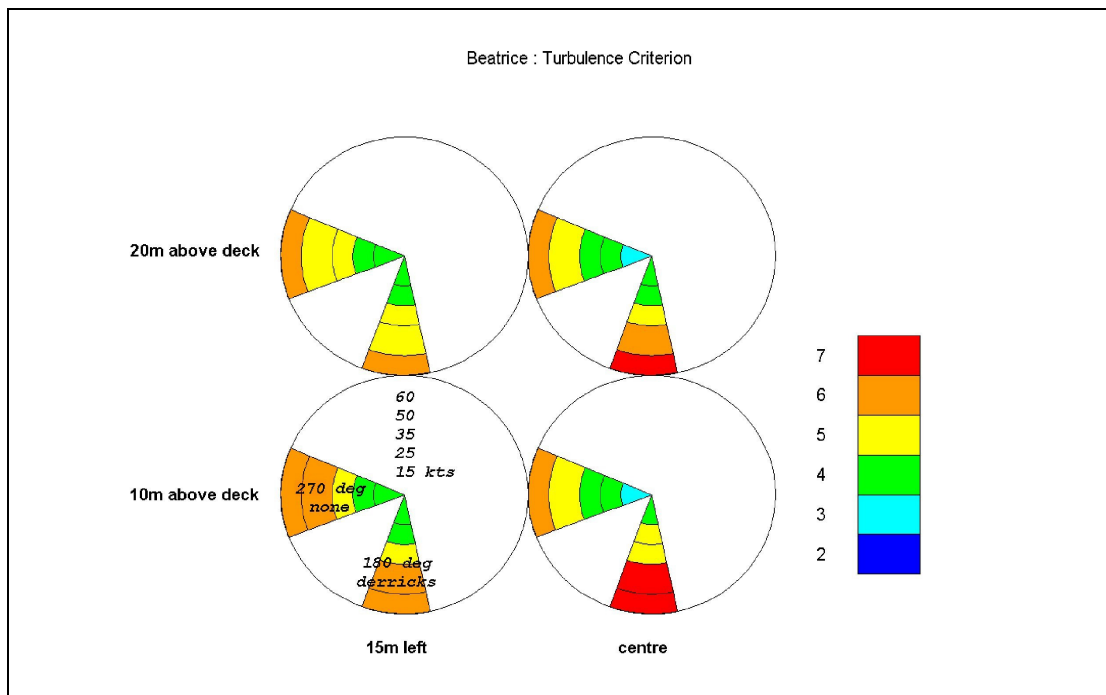


Figure 7.2 Workload Predictions for Beatrice Based on Turbulence Criterion

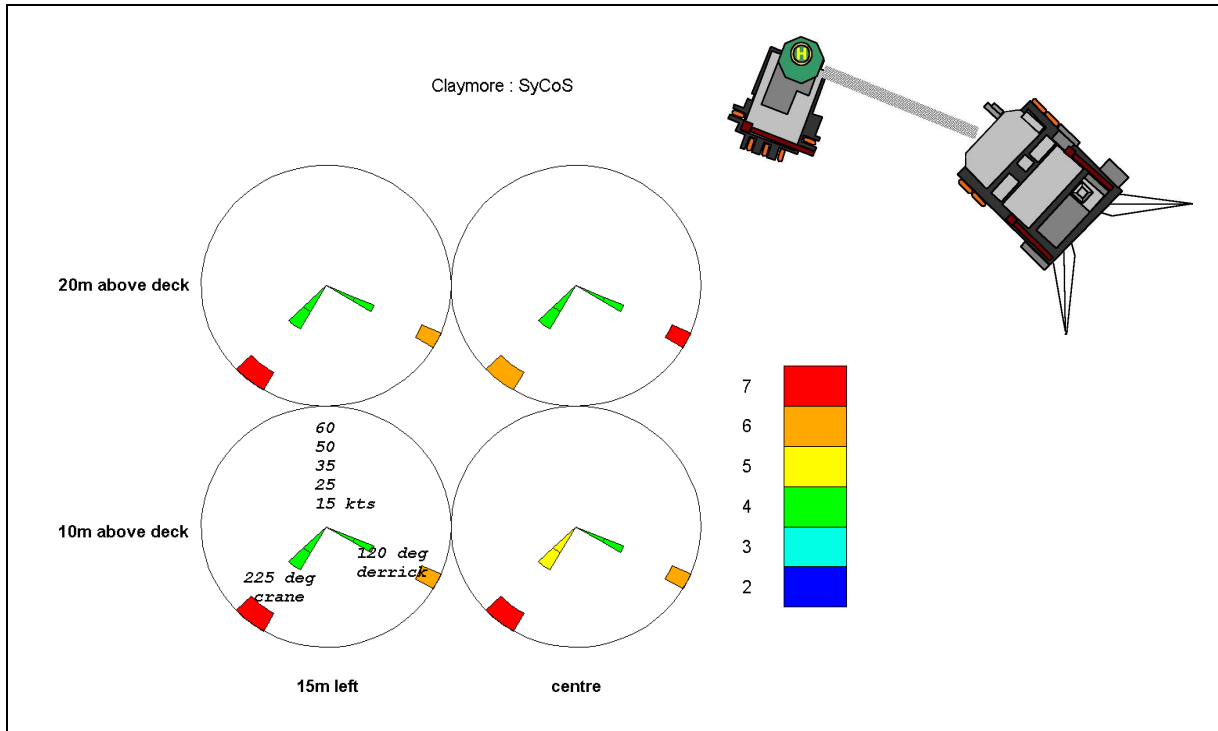


Figure 7.3 Workload Predictions for Claymore Based on SyCoS Control Responses

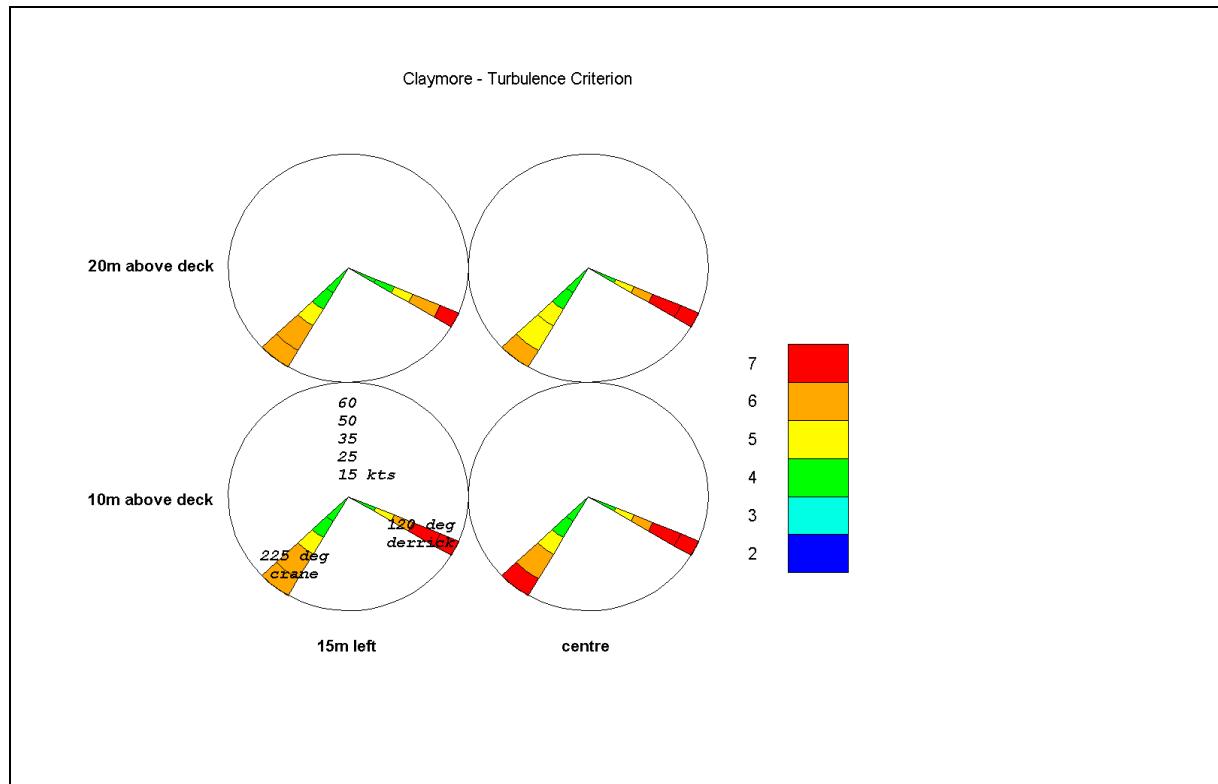


Figure 7.4 Workload Predictions for Claymore Based on Turbulence Criterion

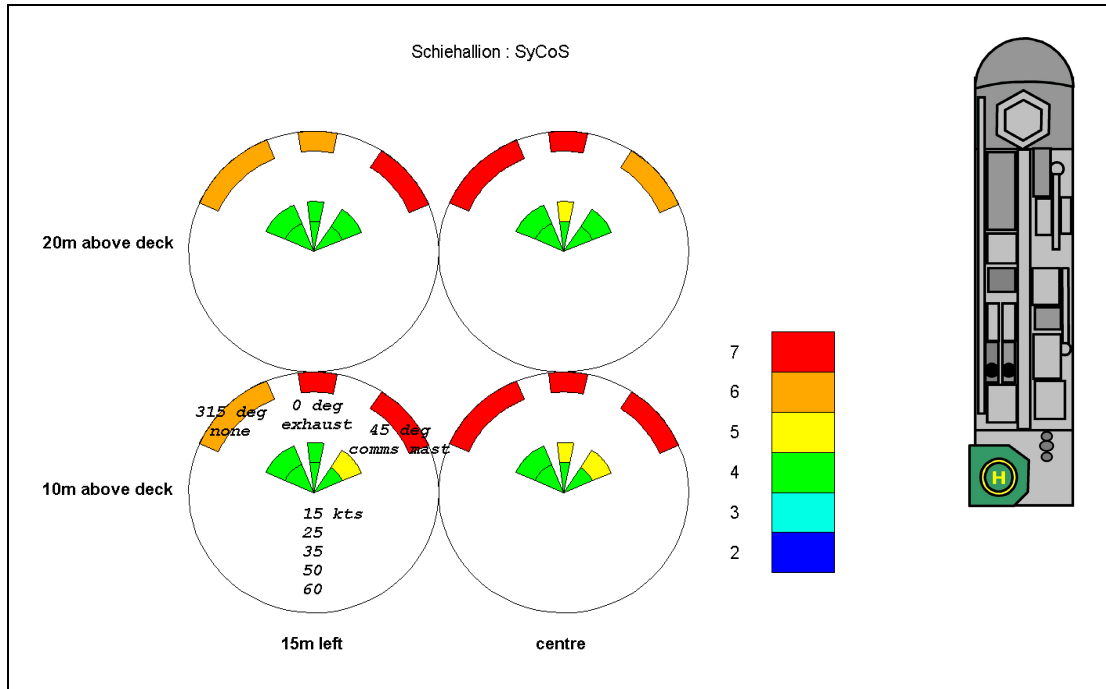


Figure 7.5 Workload Predictions for Schiehallion Based on Sycos Control Responses

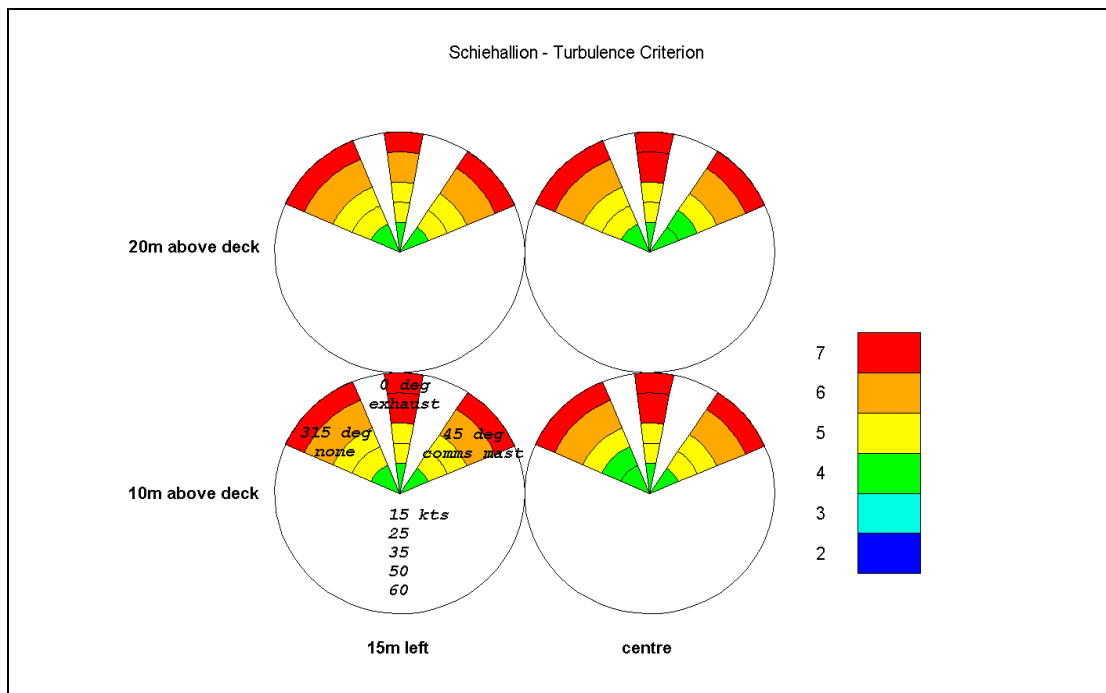


Figure 7.6 Workload Predictions for Schiehallion Based on Turbulence Criterion

Section 8 Summary and Discussion

Earlier Sections have contained discussions of various aspects of the modelling and results. This Section summarises the main issues, and draws together the discussion, with particular emphasis on the extent to which the method and turbulence criterion have been adequately validated.

8.1 Wind Tunnel Data and Desktop Modelling

This project has developed a technique for the estimation of pilot workload using desktop computer simulation of helicopter and pilot response to turbulence measured in a wind tunnel.

It is believed that this work is novel, and now offers a rational scientific method for interpreting the turbulence levels experienced around a specific offshore platform helideck, in terms of the response of a specific helicopter type, the pilot control activity required to stabilise the helicopter, the resulting pilot workload and the margin of safety.

Parts of the method have also been validated using piloted flight simulation (see sub-section 8.2), but potential further validation is discussed in sub-sections 8.5 and 8.6 below.

8.2 Piloted Flight Simulation

Piloted flight simulation in the QinetiQ AFS has been used to:

- a) Provide a direct relationship between turbulence and pilot workload (see sub-section 8.3 below).
- b) Calibrate the workload predictors used to estimate pilot workload in the desktop simulation (using the data from trial BRAE01).
- c) Validate the SyCoS pilot model and desktop workload predictions (using the independent data set from trial BRAE02).

Common elements in the desktop and piloted flight simulation are the wind tunnel modelling of the offshore platform wake flows, and the numerical model of the helicopter aerodynamics and response, and these are discussed further in sub-section 8.5 below.

8.3 Turbulence Criterion

A limiting criterion for safe flight in turbulence has been arrived at by direct comparison of the test pilot-awarded HQR values with the flow turbulence properties measured in the wind tunnel.

It was found that the standard deviation of the vertical component of the wake flow exhibited the best correlation, and that a value of 2.4 m/s corresponded to the average boundary between HQR = 6 and HQR = 7 (see sub-section 6.2). This boundary was selected as the boundary between safe and unsafe flight on the basis of the test pilot subjective HQR questionnaire (Figure 4.2).

The criterion has been demonstrated to show good correspondence with predictions from the full desktop simulation method not only for Brae A, but also using data from the Beatrice, Claymore and Schiehallion platforms.

It is important to note that the 2.4 m/s criterion is an average value, and takes no account of a) the scatter experienced in the HQRs awarded by the three test pilots, nor b) the variation in skill and experience that might be expected to exist in the larger population of operational line pilots. Furthermore it cannot be assumed that the scatter in a) is at all representative of the scatter in b). This issue is discussed further in sub-section 8.5 below.

8.4 **Application to Different Helicopter Types**

As noted above, the method developed by this project can be used for any specific offshore platform and any specific helicopter type. However, the desktop simulations and piloted flight simulations used to derive the turbulence criterion have all been performed using a single helicopter simulation model intended to approximate to a Sikorsky S-76. It was important therefore to attempt to determine the sensitivity of the criterion to differences between helicopter types. Clearly it would be convenient if the same limiting turbulence criterion could be applied to all helicopter types.

This sensitivity to helicopter type was investigated through desktop simulation of a number of different helicopters by varying four key helicopter design parameters (see Section 5). The key design parameters considered were; helicopter size (represented by weight class), helicopter weight, blade hinge offset and blade loading.

The design properties for this parametric variation were selected on the basis of average lines drawn through data available in the public domain for a wide population of helicopters. This process did, however, present some difficulties in creating a family of helicopter designs that differed simply in these three parameters, and this for example resulted in the 'light' helicopter in the family deviating somewhat from the S-76 used in the main part of the study.

The main conclusion from the results of this part of the work (see sub-section 5.2) was that changes to the selected parameters did not cause large variations in the pilot workload in turbulence. This was because in most cases there were balancing factors (e.g. increasing blade hinge offset increases the helicopter response to the turbulence, but it also increases the effectiveness of the control activity to stabilise the helicopter, and so the net effect is a small change in pilot workload). On the face of it, this would therefore suggest that the same limiting turbulence criterion can indeed be used for all helicopter types.

There is the potential for particular helicopter designs to exhibit quite large variations in pilot workload in turbulence if they happened to be designed with particular combinations of parameters. It was therefore not possible to conclude from the simulation study alone that the same limiting value of turbulence could be applied to all types.

Following consultations with pilots it would seem that there isn't any one helicopter currently operating offshore on the European continental shelf that is commonly recognised as generating significantly higher workload in turbulence relative to the fleet in general. Nevertheless it is accepted that the feel and ride offered by different aircraft types does vary significantly. This anecdotal evidence would seem to support the notion that a single turbulence criterion is appropriate for all aircraft types.

This issue is the subject of potential further validations considered below in sub-section 8.6.

8.5 **Validation**

There are many facets to the validation of the modelling methods used in this project and the turbulence criterion that has been derived, and Figure 8.1 illustrates the main elements linking turbulence with pilot workload and flight safety.

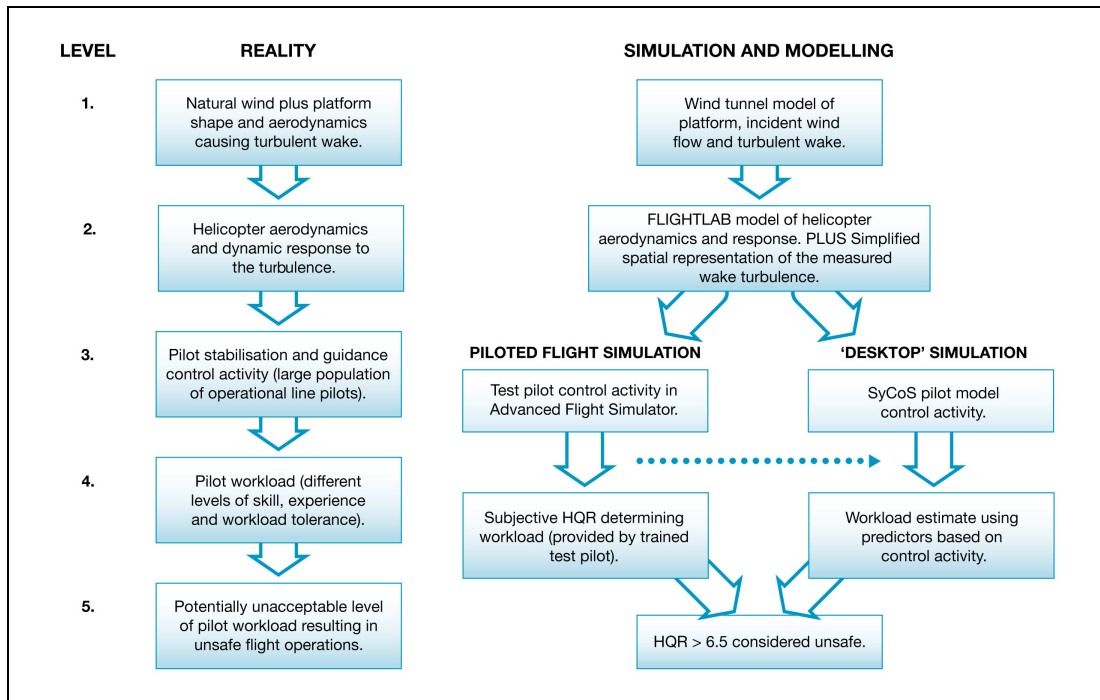


Figure 8.1 Reality Versus Modelling and Simulation

The boxes on the left illustrate the reality of operational flights to offshore platforms. At the top (level 1) is the natural wind and the turbulent flow around the obstruction caused by the bulk of the offshore platform. This translates into a dynamic response of the helicopter (level 2), which in turn requires the pilot to make stabilising control actions (level 3) resulting in a level of workload (level 4). For the purposes of this project it has been assumed that the safety of the flight in turbulence depends on the acceptability, or otherwise, of this level of pilot workload (level 5).

On the right hand side of the figure the equivalent steps in simulation and modelling performed in this research project are represented. In the lower half these split into two branches depending on whether 'desktop' simulation or piloted flight simulation are being used. It can be seen that the top two boxes are common. Both the piloted flight simulation and the desktop simulation depend on the wind tunnel adequately modelling the turbulent flow around the offshore platform. They both also depend on the *FLIGHTLAB* simulation software being an adequate representation of the aerodynamic properties and dynamic response of the helicopter.

So far as is known there have been no direct field measurements of turbulence in the wake of offshore platforms that have been compared with equivalent wind tunnel measurements of turbulence to provide a direct validation of the turbulence measured in the wind tunnel model. It would be quite difficult and expensive to perform such a validation¹. The key potential scale effect that could cause the model to differ from reality is that due to viscosity, and represented by Reynolds Number.

1. Although it would not be particularly difficult to make a measurement of turbulence in the wake of an offshore installation, and make a similar measurement on a wind tunnel model, it would be much more difficult to measure the onset incident wind profile and turbulence at the time of the full-scale measurements to a sufficient degree of accuracy.

The Reynolds Number is much lower in the wind tunnel than on the full-scale platform. However, classical fluid mechanics tells us that the flow around bluff sharp-edged bodies is not much influenced by Reynolds number¹, and all the circumstantial evidence (e.g. the independence of drag force on Reynolds number for such shapes) indicates that, provided the natural wind is well represented in the wind tunnel², we can expect the wake flows around the platform to be well represented also.

The *FLIGHTLAB* helicopter simulation model is an industry standard model that has been used in many industry applications, and so can be used in this research project with some confidence. However, clearly such a model is only as good as the data entered into it to describe the particular helicopter type being simulated. In this case the project created an approximation to a Sikorsky S-76 type (see sub-section 3.3.2 and Appendix D). The project has gathered a certain amount of qualitative validation of this model from the test pilots that flew this simulation in the AFS. They noted that, apart from the roll axis being too well damped and responsive, and the attitude-hold function being too efficient, the simulation seemed to be a realistic representation of an S-76 (see sub-section 4.2.5).

Another important element in the numerical simulation of the helicopter was the way in which the wake turbulence measured in the wind tunnel was modelled (see sub-section 4.2.4 and Appendix I). The measurements of the turbulence made in the wind tunnel were processed and presented to the *FLIGHTLAB* model in terms of the three axis components of wind speed and gradients of speed experienced at the rotor hub (see Figure 3.2 in sub-section 3.3.4). This is clearly a simplification of a complicated flow field that will, in reality, vary across the whole rotor disk, but again a degree of qualitative validation was obtained from the test pilots, who stated that the effect of the turbulence on the helicopter felt realistic. The exception of the lack of realistic yaw response was noted (neither the helicopter tail rotor nor the fuselage in the *FLIGHTLAB* model were made subject to the turbulence), but this was not considered to be material in the test pilot control activity, or their subjective estimates of workload.

The two branches of the modelling performed in the project at the pilot control activity (level 3) and workload (level 4) enable a substantial degree of validation. Firstly there is the direct comparison between the HQRs awarded by the test pilots and those predicted from SyCoS (see sub-section 4.4 and Appendix O). The subjective HQR values produced by the test pilot in the BRAE01 trial were used to tune and improve the workload predictors based on SyCoS control activity (represented by the dotted line in Figure 8.1), but these were then compared with the subjective HQRs from the independent BRAE02 data set (using three pilots). This can therefore be regarded as a quantitative validation of the step between levels 3 and 4 in the modelling process.

All the desktop, and most of the piloted flight simulation performed during the project have, for convenience, used a hover task that is not realistic in terms of normal flight operations. The steady state nature of the hover task makes it easier to simulate the control activity and to determine the workload from the model. This issue was recognised from the outset, and a set of realistic approach and landing tasks were

-
1. The shape of the superstructure of an offshore platform is mostly characterised by sharp-edged boxes and angular shapes. The sharp edges fix the point of flow separation. In the context of the consideration of the potential scale effect it is worth noting that, if offshore platform superstructures were more streamlined, and were characterised by smooth curves and shape transitions, then the wake flows experienced by the helicopter might be quite sensitive to viscous scale effects. In these circumstances both the size of the wake and the intensity of the turbulence might be incorrectly represented on a scale model in a wind tunnel.
 2. It is essential that such tests be performed in a wind tunnel designed to simulate the key properties of the offshore atmospheric boundary layer. Wind tunnel tests performed in a conventional (aerospace type) wind tunnel are likely to fail to correctly represent the shape of the boundary layer and the turbulence inherent in the natural wind, and are thus likely to give misleading results.

performed by one of the test pilots in order to provide a basis of comparison (see sub-section 4.2.5). The subjective HQRs from these tasks when compared with their equivalent hover tasks showed very close agreement, and therefore validated the use of this hover task in the simulations.

A simplification in the simulation model was the use of an idealised engine power/torque model and, in the case of the SyCoS pilot model, no torque limits. As was stated in sub-section 4.6, this was not considered to be a significant factor in the simulation and in the determination of pilot workload because, for all the cases where the helicopter experienced high levels of turbulence, there was also significant mean wind speed, meaning that the helicopter was never short of lift or power. It is possible that helicopters might experience conditions with a combination of high turbulence combined with high levels of downdraft and limited horizontal wind component. These would be unusual conditions with current offshore installation designs, but in these circumstances the power and torque limits might become an important factor. If it were intended to follow the proposal made in [1], and consider the relaxation of the 0.9 m/s downdraft criterion following the establishment of a validated turbulence criterion, then it would be particularly important to ensure that the role torque and power limits play in helicopter response to combined downdraft and turbulence is fully understood.

An aspect not explicitly covered in the present project concerns flight in degraded visual conditions. Such circumstances may arise due to meteorological conditions such as rain, sleet, hail, snow or fog or routinely due to helicopter operations being conducted at night. Although the importance of these factors on pilot workload is not in question, the flight simulation validation tasks performed during the project used only a daytime visual representation of the platform. The SyCoS pilot model used in the desktop simulation does not currently have the ability to modify its guidance or stabilisation references in such a way as to represent the degraded visual cues experienced by a real pilot.

There seems to be a general recognition and agreement that flying to offshore platforms at night involves higher levels of workload, and so presumably a limiting turbulence criterion should in principle be set at a lower level for night time operations (see sub-section 4.6). This contrasts with the operational flight experience of turbulent sectors as documented in the IVLL, which does not distinguish between night and day operations when imposing flight restrictions¹. From this it might be inferred that the difference between night time and daytime operations is not very great, or is perhaps overshadowed by other factors (such as differences in controllability or performance characteristics of different helicopter types). It might also be that the IVLL is assuming a level of common understanding amongst pilots regarding the greater difficulty of operations to fixed platform helidecks at night or in any other degraded visual environment. This aspect clearly deserves further attention in relation to the setting of a quantitative turbulence criterion.

An important issue in applying the results of the project to flight operations is variability in individual pilot skill and experience, and their possibly varying tolerance to high workload levels. In the piloted flight simulation part of the project, three test pilots were used and their control activity and subjective HQRs exhibited quite significant scatter (see sub-section 4.6).

Some of the reasons behind the bias of one pilot's HQR levels when compared with another were understood from pilots' comments, but it has not been possible to use

1. The IVLL **does** distinguish between day and night when imposing restrictions related to vessel helideck wave motions, and thus explicitly recognises the greater difficulty of landing on a moving deck as a result of degraded visual cues at night.

this information to numerically adjust the HQR results to reduce the general scatter. Likewise, the analysis of actual task performance in Appendix M cannot be used to adjust the HQR data as the pilot's perception of his performance during the task will drive the level of mental and physical effort devoted to controlling the vehicle. The pilot will not expend unnecessary effort if he believes the performance is within desired limits.

Furthermore, the scatter exhibited by the three test pilots cannot be assumed to be representative of the scatter in workload level in the much larger population of line pilots. When a turbulence criterion is applied that has been derived either from the desktop simulation or, in the case of Figure 6.1, directly from subjective assessments of the three test pilots, there is no rational way of applying a safety margin that will account for the variation in skill and experience of line pilots. This emphasises the need for validation of the criterion against operational experience that can be used to factor-in the normal variability in the line pilot population.

8.6 Further Possibilities for Validation

It has been seen from the above that, whilst the project has achieved a great deal in validating the steps in the simulation method, and in determining a rational turbulence criterion for safe flight in turbulence, there are a number of issues that could benefit from further validation.

There are two main possible directions for further validation, the first concerning the further analysis of existing offshore platform wind tunnel data and comparison with operational experience (as expressed in the IVLL), and the second using data from the Helicopter Operations Monitoring Programme (HOMP) [14].

8.6.1 Further Analysis of Existing Platform Wind Tunnel Data

Now that a quantitative turbulence criterion has been derived, it is possible to extend the initial relatively simple examination of existing wind tunnel data performed in the first phase of this project (see Section 2 and Appendix A). The new criterion can be applied to all the wind direction and speed combinations available for the 16 offshore installations in the database. It can be applied alone, and in combination with the existing 0.9 m/s downdraft criterion to develop new turbulent sectors based on the new criterion. Sensitivity variations in the precise level of the criterion could also be included in this analysis. The resulting turbulent sector plots would then be compared with the turbulent sectors contained in the IVLL with the objective of seeking overall validation of the criterion against the operational experience encapsulated in the IVLL.

8.6.2 Comparisons with Operational FDR Data

The routine analysis and archiving of Flight Data Recorder records from operational offshore helicopters as initiated under the HOMP trial, and now being extended to the entire offshore fleet, offers a number of possibilities for further validation of the method and the derived limiting turbulence criterion.

Some of these are possible to perform today with the FDR data already archived by HOMP, whilst others may need to await future data from the extended full fleet programme. The various possibilities are summarised in the following:

Using existing data in the HOMP archive:

- a) Compare the 'turbulence mapping' around offshore platforms obtained from HOMP, and as characterised using the Bristow HOMP Turbulence Parameter, with the turbulence sectors derived using the new turbulence criterion in sub-section 8.6.1 above.¹

1. Note that this depends on there being a reasonable overlap in the offshore installations flown to in the HOMP project with the 16 installations listed in Appendix A.

- b) Apply the workload predictor developed in the current project to the HOMP data¹, and thus provide the capability to derive quantitative HQRs for all HOMP flights. This might use the BRAE01 workload predictor, but as suggested in sub-section 4.6.8, would better employ new predictors derived from the entire BRAE02 trials database.
- c) Specific undesirable or unacceptable turbulence events reported by pilots flying within the HOMP project can be individually selected and investigated. If wind tunnel data exists for the installation concerned, then the results for the wind conditions at the time can be directly compared with the turbulence criterion.
- d) Analyse the population of HOMP data to derive workload estimates (as a) above), selecting the more severe wind conditions for a selected number of platforms. Use the variability in the data to estimate the normal variability in control activity for a large population of different pilots.
- e) Separate the HOMP data into daylight and night time populations. Compare the two data populations to seek a systematic difference in control activity, and hence workload for night versus day.²

With future (whole fleet) HOMP data:

Apart from future data offering a larger database for comparisons and validation as above, the new data may offer additional possibilities such as:

- f) Make use of data that will become available for a number of helicopter types³ to compare the workload populations for each type and draw conclusions about systematic variation between types⁴.

1. Note that the HQR prediction method used in this project has to-date only been applied to steady state hover data, and requires some further development (in terms of time-windowing) before it can be applied to FDR data captured in normal flight.

2. Care would need to be taken to eliminate any bias introduced by flight schedules to particular installations, which might mean that a given installation experiences a higher proportion of day or night flights than is the norm.

3. To-date HOMP data has only been gathered from Bristow Super Puma helicopters.

4. Note such analysis needs to be performed on a large quantity of data, and care needs to be taken to remove bias potentially caused by particular helicopter types tending to be used for particular offshore installations.

Section 9 Conclusions

The main conclusions from the work are summarised in the following sub-sections.

9.1 Turbulence Criterion

The overall objective of the project was to develop an easy-to-use maximum safe turbulence criterion for all helicopter operations to offshore helidecks. It is considered that this has been achieved, subject to certain caveats.

9.1.1 Main Conclusions

- a) Piloted flight simulation trials using three test pilots have been used to provide a relationship between turbulence (measured in terms of the standard deviation of the vertical velocity) and pilot workload (defined in terms of HQR) (sub-section 8.2).
- b) On the assumption that workload is excessive for cases where $HQR > 6.5$, the turbulence criterion based on the HQR ratings from all three test pilots is: **the standard deviation of vertical airflow velocity must be less than 2.4 m/s** (sub-sections 6.2 and 8.3).

9.1.2 Caveats

- a) Scatter or variability in excess of the 1 HQR point, normally considered acceptable, was seen in the test pilot HQRs. The available evidence suggests that this was due to bias in the way the different pilots assessed their performance, but no justifiable analysis could be found to reduce or remove it. Furthermore, the variability in the test pilot HQRs cannot be assumed to be representative of variability of pilot workload in the population of line pilots due to their varying levels of skill and experience (sub-sections 4.6.4 and 8.5).
- b) The project has not addressed the effect that operations in degraded visual conditions have in increasing pilot workload, and the possibility that a lower limiting turbulence criterion should therefore be defined for such operations. It is noted, however, that limitations contained in the IVLL make no distinction between good and degraded visual conditions (sub-sections 4.6.7 and 8.5).
- c) The piloted simulation trials were performed using a model representing a single helicopter type. Studies performed using desktop simulation and the opinions of the three test pilots, however, suggest that helicopter type is not a key parameter in determining workload generated by turbulence (sub-sections 5.2 and 8.4).
- d) No validation of the wind tunnel modelling employed to provide the data for the piloted simulation was performed. However, the techniques employed followed standard industry practice which is considered to be reliable (sub-section 8.5).
- e) No quantitative validation of the helicopter model used for the piloted simulation was performed. The *FLIGHTLAB* model employed, however, is widely used in industry and, as configured, was considered adequately representative of the S76 for the purposes of the piloted simulation by the three test pilots who took part (sub-section 8.5).

9.2 Pilot Workload Prediction Method

9.2.1 General

A detailed objective of the project was to develop and validate a helicopter pilot workload prediction method. It is considered that this objective has been achieved, and the following conclusions are drawn.

- a) A method has been developed for deriving the pilot workload required to operate a helicopter in a turbulent environment using wind tunnel test data and a desktop simulation of the helicopter and pilot response (sub-sections 1.2 and 8.1).
- b) The desktop workload predictions were demonstrated to be statistically within the same region defined by the subjective test pilot data, although tending towards the low side. It is considered that, overall, the desktop simulation using the SyCoS numerical pilot model under-predicts workload by 1-2 HQR points (sub-sections 4.6.2 and 8.5).
- c) The piloted simulation cannot be considered to have validated every step in the prediction method because the aerodynamic data produced from wind tunnel modelling, and the *FLIGHTLAB* helicopter model, were common to both the desktop and the piloted simulation. However, both the aerodynamic data and the helicopter model are considered sufficiently reliable for the purposes of this work (sub-section 8.5).
- d) The *FLIGHTLAB* helicopter model and the SyCoS pilot model are unable to recognise or respect torque and power limitations. However, as turbulence is primarily a problem in high winds when the available lift and power margin is increased, it is considered that torque and power limits are unlikely to influence workload due to turbulence. This assumption may not be valid in cases where there is either a large downdraft, or the rotor is shielded from the free stream flow by superstructure. If it were intended to consider the relaxation of the 0.9 m/s downdraft criterion following the establishment of a validated turbulence criterion, then it would be particularly important to ensure that the role torque and power limits play in helicopter response to combined downdraft and turbulence is fully understood (sub-sections 4.6.6, 5.2 and 8.5).
- e) The addition of lateral wind velocity measurements (to longitudinal and vertical measurements), and the introduction of spatial variation of vertical wind velocity over the rotor disc of the helicopter model did not improve the accuracy of the desktop workload predictions. They did, however, significantly enhance the realism of the piloted simulation (sub-section 4.2.5 and Appendix P).
- f) Following calibration using data from the initial BRAE01 trial, the desktop simulation workload predictor was validated using BRAE02 trial data and was seen to over-predict by 0.5 to 1 HQR points. This was considered to be an acceptable variation in the context of the overall programme (Appendix O).
- g) Comparison of test pilot workload ratings for the full approaches with those for the hover task indicated that the use of the hover task for both the desktop and piloted simulation was a valid simplification (sub-section 4.2.5).

9.2.2 Extension to Other Helicopter Types

A detailed objective of the project was to extend the applicability of the method so that it can be used for a number of different helicopter types. The following conclusions are drawn in this respect.

- a) The sensitivity analysis of the effect of varying certain helicopter design parameters on pilot workload tended to suggest that the overall effect on pilot workload was small, but it also recognised the possibility that a particular combination of design parameters might result in a significant difference (Section 5 and sub-section 8.4).
- b) Of the helicopter design parameters investigated, only aircraft weight and size had any discernable effect on workload. Increasing weight from the lower end of the S76 operating range to the upper end reduced the workload, and increasing size

from a 9,900 lb aircraft to a 32,000 lb example increased the workload (sub-section 5.1).

- c) Although adequate for the purposes of predicting the overall effect of turbulence on pilot workload, the level of fidelity of the desktop simulation is considered insufficient to enable clear distinctions to be made between the helicopter configurations modelled (sub-section 5.2).

9.3 Other Conclusions

9.3.1 Applicability of Results to Other Offshore Platforms

Since all validation was performed using wind tunnel data from only one platform, Brae A, efforts were made to assess how representative these data are of other platforms. The following conclusions are drawn:

- a) Neither the spectral characteristics nor length scales of turbulence have a significant effect on pilot workload predicted using the desktop simulation, indicating that the Brae A wind tunnel data used are representative of platform turbulence in general (Appendix E).
- b) Comparison of the predictions derived from applying the workload predictor to SyCoS control responses and the turbulence criterion to wind tunnel data for Beatrice, Claymore and Schiehallion platforms has shown that both methods produce similar results giving some confidence that both methods are applicable for platforms other than Brae A (Section 7).

9.3.2 Turbulence Generated by Offshore Platforms

The following conclusions are drawn:

- a) Turbulence levels vary greatly with wind direction, the highest levels being associated with the helideck being downstream of major items of superstructure (sub-section 2.1).
- b) Maximum turbulence levels vary significantly between individual installations, but not necessarily between different types of installation (sub-section 2.1).
- c) For the 16 platforms studied, the wind tunnel tests predicted high levels of turbulence for those having a turbulence limitation in the IVLL. The converse was not found to be true, but it is thought that this is likely due to helicopters not being exposed to the turbulence in-service (sub-section 2.2).

9.3.3 Calibration of Bristow Helicopters HOMP Turbulence Parameter

The data collected during the piloted simulation trials has been used to 'calibrate' the turbulence parameter currently being used in the Bristow Helicopters HOMP FDR data analysis. The following conclusions are drawn:

- a) An average value of 90 for the HOMP Turbulence Parameter was found to correspond with the HQR=6.5 boundary, however the calibration was found to be very sensitive (more so than the workload predictor) to the data set used. The standards applied by each of the three test pilots to assess task performance appears to be a major factor (sub-section 4.5 and Appendix R).
- b) The squaring operation used in the calculation of the Bristow HOMP Turbulence Parameter accentuates the differences in collective activity between pilots in a way that the workload predictor does not (sub-section 4.5 and Appendix R).
- c) There is some evidence that the cut-off frequency of the high-pass filter used in the HOMP Turbulence Parameter may be set too high (sub-section 4.5 and Appendix R).

Section 10 Recommendations

Based on the conclusions of this report the following recommendations are made:

- 1 Use the criterion that the standard deviation of vertical velocity must not exceed 2.4 m/s as a working limiting turbulence criterion subject to further validation (sub-section 9.1).
- 2 Reanalyse the predictors used to estimate HQR from pilot control activity using all the data available from the BRAE02 trial in order to derive coefficients of improved reliability for future general use (sub-section 4.6.8).
- 3 Seek validation of the entire modelling process and the limiting turbulence criterion against operational experience by means of:
 - a) Analysis of existing wind tunnel data using the new turbulence and existing vertical wind speed component criteria to predict the safe flight envelope for a number of offshore installations. Compare the results with the Installation/Vessel Limitation List (IVLL) for the installations concerned (sub-sections 8.6.1 and 9.1.2).
 - b) Implement the optimised HQR predictors (see recommendation 2 above) in the Helicopter Operations Monitoring Programme (HOMP) analysis, apply the analysis to the HOMP data archive and compare the resulting turbulence mapped around offshore installations with turbulent sectors as derived in a) above (sub-sections 8.6.2 and 9.1.2).
 - c) Use the analysis performed in b) above to identify specific severe turbulence events in the HOMP data archive, establish the turbulence levels likely to have been experienced from the associated wind conditions and wind tunnel data for the platforms concerned, and correlate this with the workload values obtained from the HOMP analysis (sub-sections 8.6.2 and 9.1.2).
- 4 Investigate the operational experience regarding the perceived increase in workload due to degraded visual conditions, and consider conducting further simulator trials to capture equivalent flight in turbulence data at night and in degraded meteorological conditions (sub-sections 4.6.7 and 9.1.2).
- 5 In the longer term, use data collected from the full-scale implementation of HOMP and optimised HQR predictors (see recommendation 2 above) to routinely map HQR around offshore installations, and make this information available to BHAB Helidecks to help improve and maintain the quality of the IVLL (sub-section 4.6.11).
- 6 Use data collected from the full-scale implementation of HOMP and optimised HQR predictors (see recommendation 2 above) to obtain evidence of any variation of turbulence induced pilot workload in different helicopter types. If it is apparent that significant differences are experienced across the offshore helicopter types in the fleet, consider extending the desktop simulation study to encompass selected types identified as particularly good or bad in this context (sub-section 5.2).
- 7 Consider re-assessing the 0.9 m/s vertical wind speed component criterion in the light of the new turbulence criterion (as proposed by [1]). However, note that this will require an improvement to the level of fidelity of the SyCoS model by implementing recent enhancements to produce more authentic control responses and consequently the ability to recognise and respect torque and power limits.

Section 11 Abbreviations

AFS	Advanced Flight Simulator, QinetiQ, Bedford
BHAB	British Helicopter Advisory Board
BMT	BMT Fluid Mechanics Limited
BHTP	Bristow HOMP Turbulence Parameter
CAA	Civil Aviation Authority
DERA	Defence Evaluation Research Agency (now QinetiQ)
FCCM	Fully Compensating Crossover Model
FDR	Flight Data Recorder
FPSO	Floating Production and Storage and Offloading vessel
GCU	Glasgow Caledonian University
HLG	Helicopter Liaison Group of the Offshore Industry Advisory Committee
HLL	Helideck Limitation List (was IVLL)
HOMP	Helicopter Operations Monitoring Programme
HQR	Handling Qualities Rating (Cooper-Harper Scale)
HSE	Health & Safety Executive
IVLL	Installation/Vessel Limitation List (now HLL)
OIAC	Offshore Industry Advisory Committee
PIO	Pilot Induced Oscillations
rms	root mean square
S-76	Sikorsky type S-76 helicopter
S-76X	The approximate numerical model of the S-76 used in the simulations.
SDG	Statistical Discrete Gust
SHOL	Ship Helicopter Operating Limits
SyCoS	GCU developed helicopter pilot model (Synthesis through Constrained Simulation)
UKOOA	United Kingdom Offshore Operators Association

Section 12 Acknowledgements

Particular thanks are due to the test pilots who performed the flight simulator trials in the QinetiQ Advanced Flight Simulator. Their patience and professionalism played a key role in the success of the project.

Thanks are also due to the CAA and HSE representatives on the project steering committee who helped guide the work.

This was a major programme of work conducted by a large team over several years, and the authors acknowledge the hard work of their colleagues at BMT, QinetiQ and GCU.

Section 13 References

- [1] Whitbread R E, Coleman, S A, *Research on Offshore Helideck Environmental Issues*, CAA Paper 99004, August 2000.
- [2] Civil Aviation Authority Contract No. 555/SRG/R&AD, commencement date 1st June 2001.
- [3] BMT Fluid Mechanics Limited Proposal Ref Q93514 *Offshore Helideck Environmental Issues: Development of a Turbulence Criterion*, dated 24th September 1998.
- [4] BMT Fluid Mechanics Limited Proposal Ref Q93836 Rel 2 *Helideck Environment - Turbulence Criterion Flight Simulator Trials Validation*, dated 6th April 2001.
- [5] *Installation/Vessel Limitation Lists (IVLLs)*, Issued by the British Helicopter Advisory Board, Helideck Sub Committee. Issue no.10 August 1999. (More recent updates have now been published, and are now referred to as the *Helicopter Limitations List* or *HLL*.)
- [6] *Offshore Helicopter Landing Areas - Guidance on Standards*. CAP 437 published by the CAA, October 1998 (revised Jan 2001).
- [7] *Offshore Helideck Design Guidelines (Chapter 10 – Helideck Environmental Effects)*, Health & Safety Commission, Issue 1 June 2004.
- [8] BMT Fluid Mechanics Limited, *Research on Helideck Environment Issues: Development of a Turbulence Criterion – Phase 1 Analysis of Existing Wind Tunnel Data and the IVLL*, Report No 43185Rep1v4, 3rd December 2001.
- [9] BMT Fluid Mechanics Limited, *Wind Tunnel Facilities*, datasheet, June 2003.
- [10] Cooper G E, Harper R P, *The use of pilot rating in the evaluation of aircraft handling qualities*. Report NASA-TN-D-5153, April 1969.
- [11] AAIB Bulletin No. 3/96 - Heavy landing on Claymore Accommodation Platform, 18 August, 1995.
- [12] McRuer D, Krendel E S, *Mathematical models of human pilot behaviour*. AGARDograph No. 188, January 1974.
- [13] Manning A P, *Prediction of pilot workload to offshore helidecks using desktop simulation*. DERA Customer Report DERA/AS/FMC/CR010236, April 2001.
- [14] Larder, B. D., *Final Report on the Helicopter Operations Monitoring Programme (HOMP) Trial*, CAA Paper 2002/02, 25th September 2002.
- [15] Turner G P, Bradley R, Brindley G, *Simulation of pilot control activity for the prediction of workload ratings in helicopter/ship operations*. Paper 91, presented at the 26th European Rotorcraft Forum, The Hague, September 2000.

Appendix A Existing Wind Tunnel Data and the IVLL

A.1 Introduction

The principal objective of this work was to assess the existing wind tunnel data held by BMT and the Installation and Vessel Limitation List (IVLL) [1]¹ for existing installations.

Data available from previous wind tunnel testing was assessed in terms of its usefulness to the project. In addition, the analysis considered the nature and magnitude of the turbulence experienced in the vicinity of offshore helidecks, and the variation of the key turbulence properties with platform or vessel type and wind direction.

A review of existing IVLL entries for a range of installations was undertaken. Where possible the data from the IVLL was compared with the turbulence measurements from the wind tunnel data. This review also assisted the selection of installations to be modelled in the wind tunnel to provide specific turbulence data for the helicopter handling analysis.

A.2 Existing Wind Tunnel Data and IVLL

A.2.1 Wind Tunnel Data

Existing wind tunnel turbulence data from previous projects were collated and assessed. In total, 16 offshore installations (incorporating a wide variety of types of structure) had been tested to determine rms (with respect to time) turbulence levels over the helideck.

In order to summarise this vast quantity of data, the worst-case rms turbulence values have been extracted for each installation. This simplification clearly does not take any account for wind direction weighting, so high worst-case rms turbulence values may only occur for a very narrow band of wind direction.

One set of spectral data was identified. This was for the Dunbar fixed platform, which was tested in September 1991. Apart from reflecting the rms turbulence values, the spectra did not reveal any additional features that could be correlated with the IVLL. On this basis it was judged that an adequate assessment of the turbulence was provided by the rms. The results of the analysis of the wind tunnel data are summarised in Table A-4, and inspection of the data resulted in the following observations:

- a) Longitudinal and vertical rms turbulence levels vary greatly with wind direction as shown in Figure A-1, which uses the measurements of turbulence for a semi-submersible platform as an example. The helideck is located on the northwest corner of the platform. From 0° to 90° and from 180° to 360° the measurements are consistent with levels of turbulence in the on-coming flow. From 90° to 180°, there is marked increase in the turbulence levels as a result of the upwind topside obstructions.
- b) It can be concluded that the highest rms turbulence levels for this platform are associated with the helideck being downstream of major items of superstructure such as the drilling derrick and, particularly, the gas turbine exhaust stacks. This observation is consistent with data from turbulence measurements from wind tunnel tests for other installations.

1. References for this Appendix are listed in Section A4.

- c) The worst-case rms turbulence levels vary significantly (approximately 30% to 50%) from installation to installation. From Table A-1 and Figures A-2 and A-3, the worst-case longitudinal rms components range between 3.8 and 6.1 m/s (in a 25 m/s wind) and the worst-case vertical rms components range between 2.1 and 4.0 m/s.

These worst-case rms turbulence levels were then grouped together into types of offshore installation to assess whether they have characteristic turbulence levels. Table A-2 and Figure A-4 show the results of this analysis. The worst-case rms values do not vary greatly between installation type. The only type of installation which has a worst-case value significantly different is the 'Jack-up' design with worst-case values of 4 m/s (longitudinal component) and 2 m/s (vertical component). The typical worst-case value for other installation types was approximately 6 m/s (longitudinal component) and 4 m/s (vertical component). It can be concluded, on the basis of the data reviewed, that there is not a significant variation in maximum rms turbulence levels between different types of offshore installation.

The analysis shows that the level of turbulence over the helideck is more likely to be installation-specific rather than installation-type-specific. In fact, testing different wind directions on certain installations will result in a greater range of turbulence levels over the helideck than for worst-case wind directions on different platforms.

The selection of offshore installations for the remainder of the study and to be wind tunnel tested should therefore concentrate on those installations with well-known turbulence characteristics over the helideck (both high and low turbulence levels) and concentrate on the variation with wind direction.

A.2.2 Installation and Vessel Limitation List (IVLL)

A copy of the IVLL [1] was obtained from the British Helicopter Advisory Board (BHAB), and was used as the basis for selecting the offshore installations for the wind tunnel turbulence measurements. The results of the review are summarised in Table A-3.

The approach was to select installations that are known for having high turbulence levels, low turbulence levels and typical turbulence levels. Where possible, installations of various types were selected. The selections were as follows:

- a) **Brae A fixed platform.** This was selected for its high turbulence levels over the helideck. In the IVLL entry, 'Extreme Caution' is recommended when the superstructure is upstream of the helideck.¹
- b) **Beatrice A fixed platform.** This was selected as it has a 'nil' entry in the IVLL for turbulence, and was not recommended for wind tunnel testing at the design stage by inspection.
- c) **Schiehallion FPSO.** Provides a different type of installation to be tested and is believed to produce a medium level of turbulence. The IVLL entry for October 1998 states 'Possible turbulence from turbine exhausts' as a limitation/comment.
- d) **Claymore fixed platforms.** At the request of the CAA, these two platforms were added because they represented a different 'combined operations' scenario, where an accommodation platform is bridge-linked to an adjacent production platform. The models of the production and accommodation platforms already existed, having been tested on behalf of the CAA to define the environmental conditions that occurred at the time of a helicopter accident [2].

1. A copy of the latest entry in the HLL for Brae A is included at Table T-4.

The wind tunnel turbulence measurements for the 16 installations, referred to in sub-section A.2.1, were compared with the corresponding IVLL entries. These comments are listed in Table A-3.

The most cautious IVLL report was for the East Brae platform, which stated that 'extreme caution' was required. This platform also gave the highest rms turbulence levels of those tested which also had an IVLL entry (5.5 m/s for the longitudinal component and 3.6 m/s for the vertical component). However, there are also high rms values measured on other platforms but no corresponding reference to high levels of turbulence in the IVLL. For example, on the Dunbar fixed platform, rms turbulence measurements of 5.4 m/s (longitudinal component) and 3.5 m/s (vertical component) were recorded. Also, the caution required when operating to the MacCulloch FPSO as recommended in the IVLL does not correlate with relatively low rms turbulence conditions measured over the helideck (4.6 m/s for the longitudinal component and 2.1 m/s for the vertical component).

This could possibly be explained by the helicopters not encountering these high turbulence levels due to operational or meteorological reasons. For instance, the platform may be orientated such that the prevailing wind direction does not produce the high turbulence levels over the helideck that occur for other less frequent wind directions.

A.3 Conclusions and Recommendations

The assessment of the existing wind tunnel data led to the following conclusions:

- a) rms turbulence levels vary greatly with wind direction.
- b) The highest rms turbulence levels are associated with the helideck being downstream of major items of superstructure such as the drilling derrick and, particularly, the gas turbine exhaust stacks.
- c) The worst case rms turbulence levels vary significantly from installation to installation.
- d) There does not appear to be a significant variation in maximum rms turbulence levels between different types of offshore installation.

The recommendation for 4 offshore installations for wind tunnel testing is as follows:

- a) Brae A fixed platform, selected for its expected high turbulence levels over the helideck.
- b) Beatrice A fixed platform, selected for its expected low turbulence levels over the helideck.
- c) Schiehallion FPSO, selected as a different type of installation to be tested and should produce a medium level of turbulence.
- d) Claymore fixed platforms, selected to represent a combined operations scenario.

Comparing the rms turbulence measurements with the IVLL entries shows that, in a number of cases, high levels of rms turbulence measured in the wind tunnel can be correlated with warnings of high turbulence in the IVLL. There are also a number of platforms where high rms values are measured in the wind tunnel and there is no corresponding reference to high levels of turbulence in the IVLL. It is postulated that these turbulent conditions are not being encountered by the helicopters due to operational or meteorological reasons.

More importantly perhaps, in three out of the four cases of Table A-3, the comparison shows that where platforms do have a turbulence limitation in the IVLL, the wind tunnel tests did predict high levels of turbulence.

A.4 References

- [1] *Installation/Vessel Limitation List*, British Helicopter Advisory Board, Issue 10, August 1999. (More recent updates have now been published, and are now referred to as the *Helicopter Limitations List* or *HLL*.)
- [2] *Claymore Platform: Wind Tunnel Test Programme*, BMT Fluid Mechanics Report No 43184, Rel 4, dated 2nd September 1999.

Table A-1 Worst Case rms Turbulence Values for each Offshore Installation Tested (full scale wind speed of 25 m/s)

Installation Name	Installation Type	Longitudinal rms	Vertical rms
Elgin PUQ	Jack-up	4.4	2.7
Cormorant Alpha	Fixed	3.9	2.3
Markham J6A	Fixed	4.9	3.7
Britannia	Fixed	3.8	3.2
Andrew	Fixed	4.7	2.9
Dunbar II	Fixed	4.4	2.6
Dunbar	Fixed	5.4	3.5
East Brae	Fixed	5.5	3.6
Goodwyn	Fixed	6.0	3.2
Scott	Fixed	4.4	3.4
Ekofisk Hotel	Fixed	5.7	3.9
Malampaya	Fixed	5.5	4.0
Njord	Floating	6.1	4.0
Janice	Floating	5.3	2.6
MacCulloch	FPSO	4.6	2.1
Schiehallion	FPSO	6.1	3.2

Table A-2 Worst Case rms Turbulence Values for each Offshore Installation Type (full scale wind speed of 25 m/s)

Installation Type	Longitudinal rms	Vertical rms
Jack-up	4.4	2.7
Fixed	6.0	4.0
Floating	6.1	4.0
FPSO	6.1	3.2

Table A-3 Turbulence Limitation or Comment in the IVLL Report for Installations Reviewed

Installation Name	Turbulence limitation in IVLL Report	Longitudinal rms	Vertical rms
Elgin PUQ	-	4.4	2.7
Cormorant Alpha	-	3.9	2.3
Markham J6A	-	4.9	3.7
Britannia	Nil	3.8	3.2
Andrew	Possible Turbulence (turbine exhausts close to helideck)	4.7	2.9
Dunbar II	Nil	4.4	2.6
Dunbar	Nil	5.4	3.5
East Brae	Extreme Caution. Turbulence reports required.	5.5	3.6
Goodwyn	-	6.0	3.2
Scott	-	4.4	3.4
Ekofisk Hotel	-	5.7	3.9
Malampaya	-	5.5	4.0
Njord	-	6.1	4.0
Janice	Nil	5.3	2.6
MacCulloch	Turbulence and temperature rise can be expected due to funnel exhausts (directly forward of helideck) and turbine exhausts (starboard/forward). Caution to be exercised. Turbulence reports must be submitted.	4.6	2.1
Schiehallion	Possible turbulence from turbine exhausts.	6.1	3.2

NOTE: '-' indicates that the installation does not appear in the recent IVLL.

Table A-4 Summary of Results from Various Previous Wind Tunnel Tests

Wind angles selected correspond to maximum wake effect from upstream structures. rms values scaled for a longitudinal wind speed of 25 m/s.

Installation Name	Installation Type	Wind angle (deg)	Height above h/d (m)	Longitudinal rms (m/s)	Vertical rms (m/s)
Elgin h/d elevated by 3m	Jack-up	90	5	2.07	0.92
			10	2.02	1.10
			15	2.32	1.32
			20	4.30	2.68
		90	5	1.99	0.90
			10	2.09	1.14
			15	2.43	1.44
			20	4.42	2.67
Cormorant Alpha	Fixed	195	5	3.14	1.96
			10	3.60	2.16
			15	3.88	2.26
Markham J6A	Fixed	15	5	4.20	2.45
			10	4.30	2.75
			15	4.90	3.10
			20	4.80	3.70
Britannia 23m h/d 27m h/d	Fixed	105	5	3.82	2.05
			10	3.35	2.21
			15	3.26	2.69
			20	3.80	3.23
		105	5	3.65	2.00
			10	3.09	2.00
			15	3.20	2.54
			20	3.51	2.94
Njord h/d elevated by 1 m h/d elevated by 2 m h/d elevated by 3 m h/d elevated by 5 m h/d elevated by 1 m Stair tower removed h/d widened by 5.5m Stair tower removed h/d widened by 3 m Stair tower removed h/d moved .45m S.	Floater	75	5	5.76	2.29
			10	5.44	2.73
			15	5.69	3.38
			20	5.93	3.92
		75	10	5.51	2.79
			15	5.72	3.41
		75	10	5.60	2.94
			15	5.71	3.44
		75	10	5.66	3.00
			15	5.71	3.72
		75	10	5.48	3.26
			75	10	5.67
		15		5.61	3.44
		5		5.71	2.27
		10		5.46	2.79
		75	15	5.59	3.37
			20	5.85	3.90
			5	5.70	2.37
			10	5.60	2.80
		75	15	5.91	3.44
20	6.13		3.98		

Table A-4 Summary of Results from Various Previous Wind Tunnel Tests

Wind angles selected correspond to maximum wake effect from upstream structures. rms values scaled for a longitudinal wind speed of 25 m/s.

Installation Name	Installation Type	Wind angle (deg)	Height above h/d (m)	Longitudinal rms (m/s)	Vertical rms (m/s)
Andrew Air gap 6m Air gap 4m	Fixed	90	5	4.27	2.54
			10	3.82	2.02
			15	3.67	2.14
		90	20	3.79	2.70
			5	4.65	2.89
			10	4.16	2.31
			15	3.90	2.10
20	3.99	2.59			
Dunbar II	Fixed	90	5	4.00	2.00
			10	4.14	2.50
			15	4.40	2.60
Dunbar Idealised 30m h/d	Fixed	90	5	3.51	2.47
			10	3.47	2.70
			15	3.27	2.63
		75	5	5.38	2.76
			10	5.03	3.34
			15	5.16	3.47
East Brae	Fixed	75	5	5.53	2.78
			10	5.22	3.36
			15	5.33	3.55
Janice	Floater	120	5	4.97	2.38
			10	5.25	2.58
			15	4.30	2.51
			20	3.80	2.19
Goodwyn Air gap 3m Air gap 3m Increased spacing and ht of exhausts Air gap 5m Increased spacing and ht of exhausts	Fixed	60	5	6.00	3.00
			10	5.90	3.20
			15	3.50	1.80
			20	3.10	2.20
		60	5	4.64	3.04
			10	3.85	2.93
			15	3.52	2.99
			20	3.73	2.19
		60	5	4.79	3.07
			10	3.61	2.89
			15	4.00	3.02
			20	3.18	2.11
Scott 3m air gap 5m air gap 8m air gap h/d elevated by 5 m 5m air gap h/d elevated by 2.5 m 5m air gap	Fixed	90	5	3.84	2.25
			10	4.00	2.76
			15	4.23	3.18
		90	5	3.85	2.29
			10	3.93	2.91
			15	4.40	3.25
		90	5	3.94	2.43
			10	4.22	3.00
			15	4.43	3.31
		90	5	4.00	2.33
			10	4.08	2.89
			15	4.41	3.16
		90	5	3.76	2.08
			10	3.91	2.65
			15	4.32	3.13

Table A-4 Summary of Results from Various Previous Wind Tunnel Tests

Wind angles selected correspond to maximum wake effect from upstream structures. rms values scaled for a longitudinal wind speed of 25 m/s.

Installation Name	Installation Type	Wind angle (deg)	Height above h/d (m)	Longitudinal rms (m/s)	Vertical rms (m/s)
MacCullouch	FPSO	150	5	4.62	2.08
			10	3.59	1.89
			15	3.20	1.88
			20	3.02	1.99
Schiehallion	FPSO	180	5	6.06	3.25
			10	2.87	1.96
			15	2.91	2.09
			20	2.93	2.17
Ekofisk Hotel Option 1	Fixed	0	5	5.04	2.37
			10	4.42	2.81
			15	4.40	2.63
			20	4.37	2.53
Ekofisk Hotel Option 2a	Fixed	200	5	5.65	2.99
			10	5.26	3.19
			15	4.78	2.85
			20	4.54	2.82
Ekofisk Hotel Option 2b	Fixed	0	5	5.74	2.95
			10	5.50	3.52
			15	5.53	3.34
			20	5.53	3.44
Ekofisk Hotel Option 2c	Fixed	330	5	5.65	3.28
			10	5.17	3.83
			15	4.96	3.91
			20	4.59	3.64
Malampaya	Fixed	0	5	5.49	4.00
			10	4.70	3.24
			15	3.76	2.43
			20	3.65	2.40

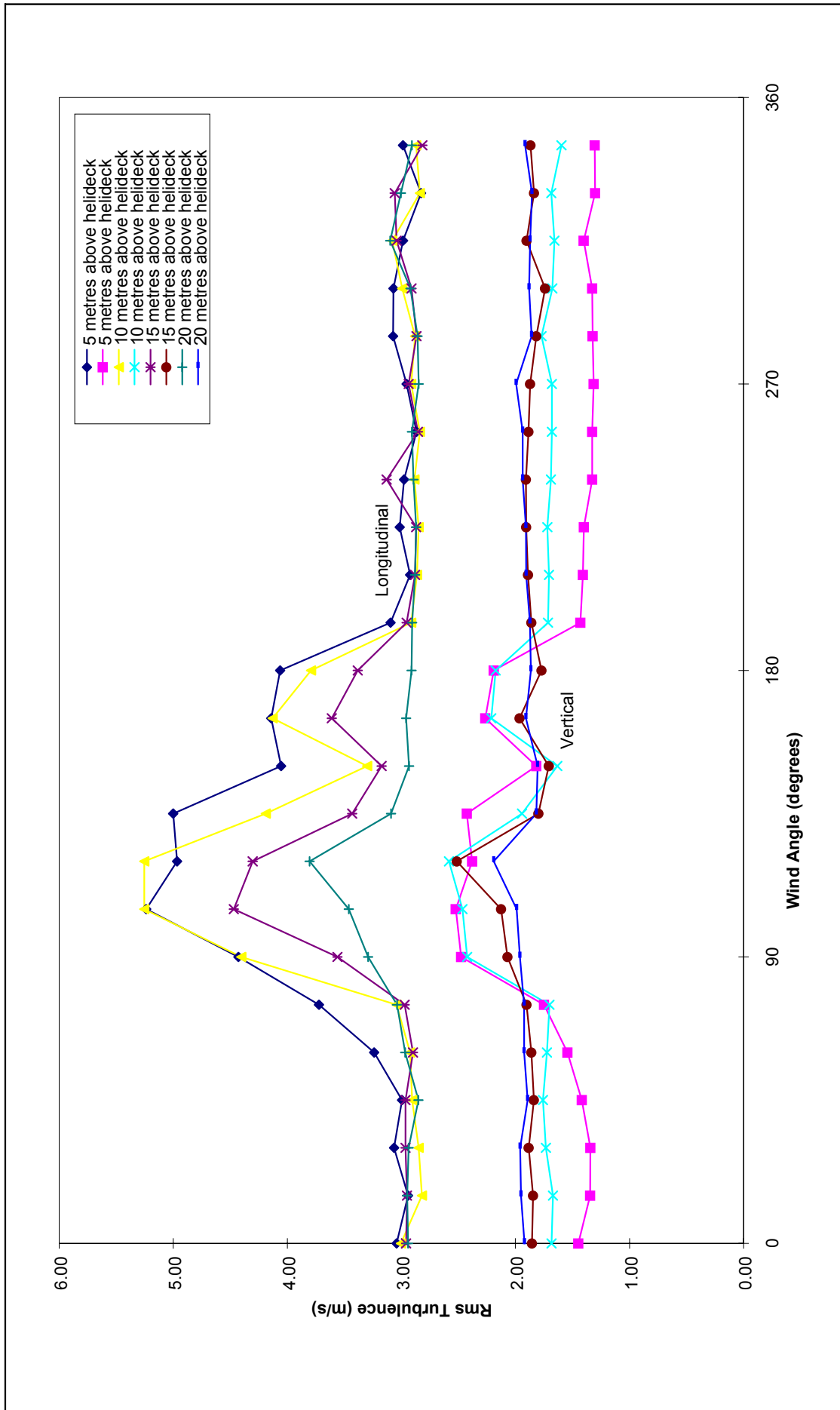


Figure A-1 Example of Variation of rms Turbulence with Wind Angle: Janice Semi-submersible (full scale wind speed of 25 m/s)

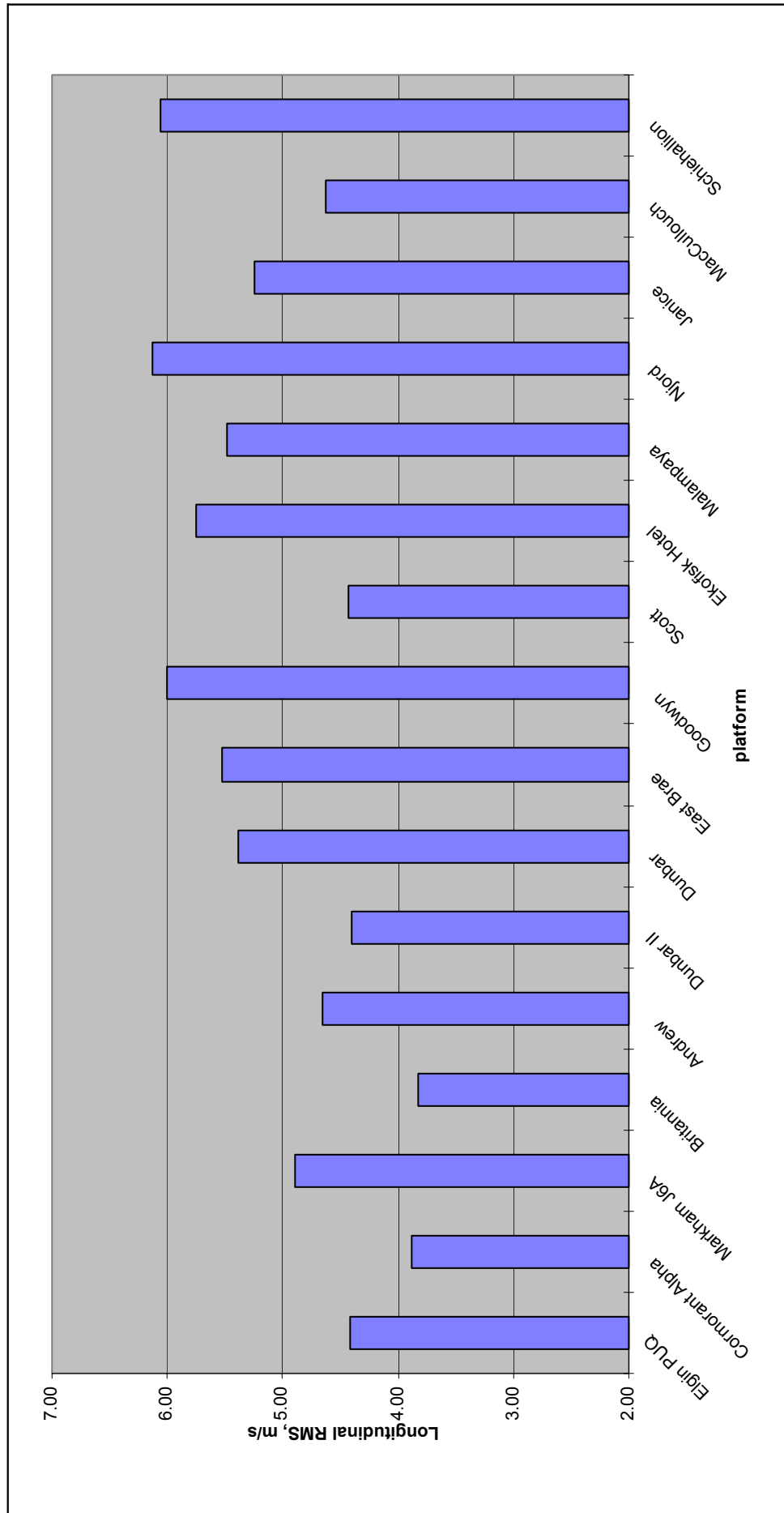


Figure A-2 Variation in Worst Case (Highest Magnitude) Longitudinal rms Turbulence with Installation (full scale wind speed of 25 m/s)

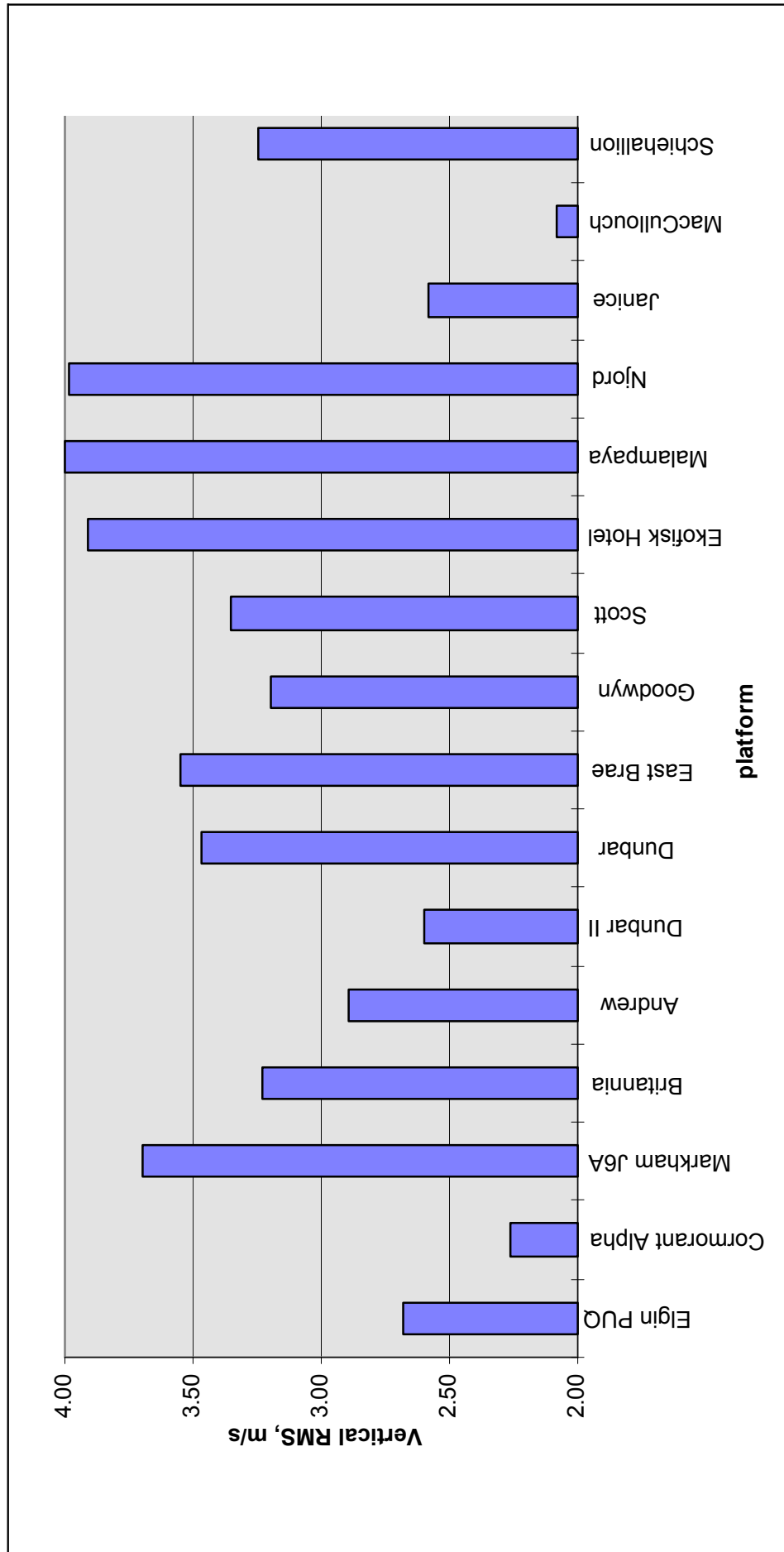


Figure A-3 Variation in Worst Case (Highest Magnitude) Vertical rms Turbulence with Installation (full scale wind speed of 25 m/s)

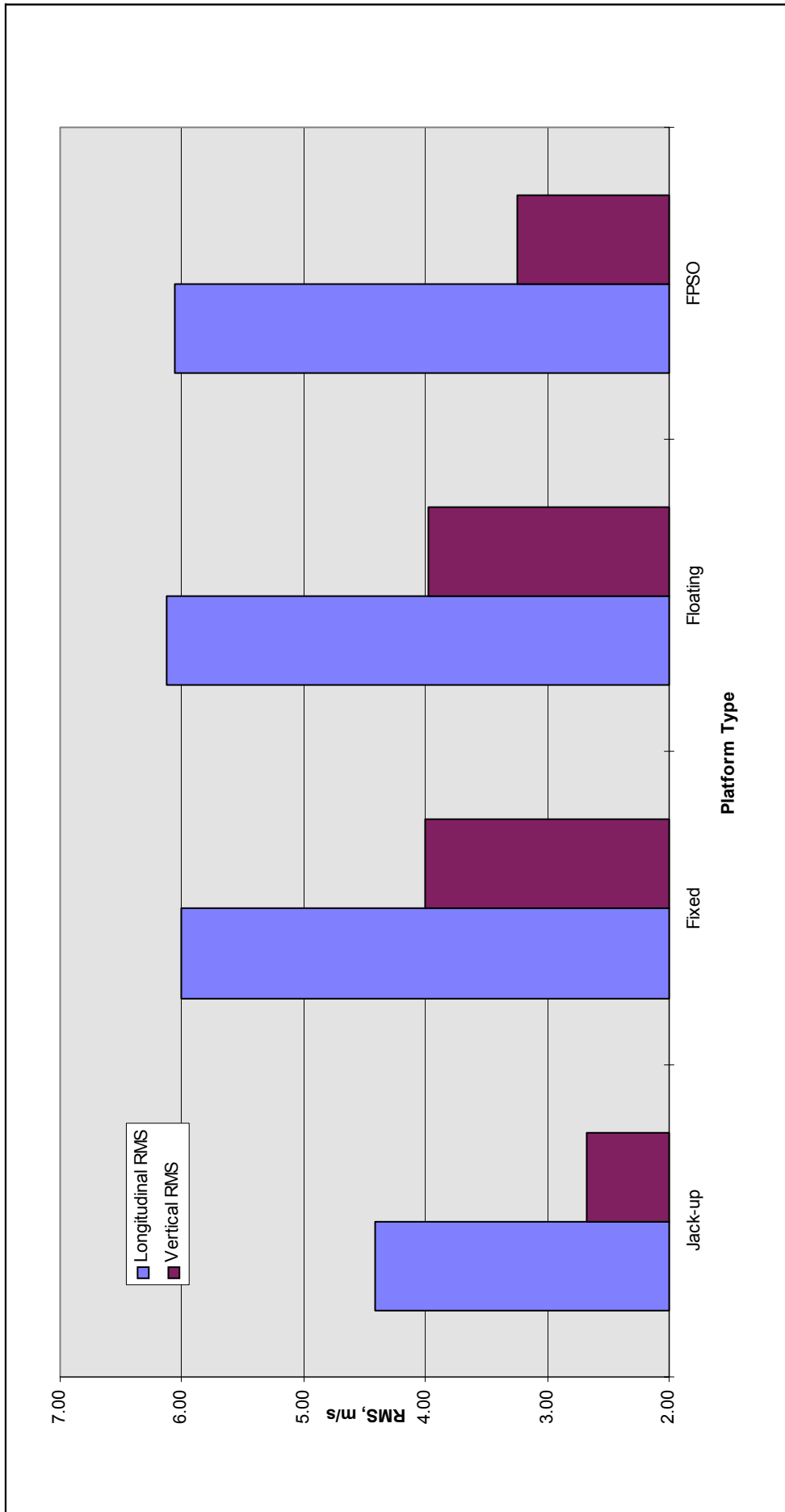


Figure A-4 Variation in Worst Case (Highest Magnitude) rms Turbulence with Installation Type (full scale wind speed of 25 m/s)

Appendix B Wind Tunnel Tests – Part 1

B.1 Introduction

The wind tunnel study was required to extend the initial appraisal of turbulence in the first phase of the project (see Appendix A) to enable the simulation of helicopter response in turbulence conditions typical of the offshore environment. It was also essential for the validation exercise.

The objectives of the test were to provide realistic time-series turbulence data for input to the helicopter performance analysis and to provide turbulence data for validation of the criterion against the IVLLs.

Wind tunnel tests were performed on four representative offshore installations in order to obtain turbulence data for modelling and validation purposes. The offshore platforms selected for this phase of the project were defined in the interim report submitted for phase 1 of the project [3]¹. These were as follows:

- a) Brae A fixed platform.
- b) Beatrice A fixed platform.
- c) Schiehallion FPSO.
- d) The Claymore complex.

B.2 Approach to Modelling and Measurement

B.2.1 Wind Tunnel

The test programme was carried out in the BMT Boundary Layer Wind Tunnel. This has a working section of 4.8 m wide by 2.4 m high and is large enough to accommodate 1:100 scale models without undue blockage effects. The latter is caused by the constraint applied by the walls of a wind tunnel and limits the size of model to no more than about 5% of the cross sectional area of the working section.

B.2.2 Boundary Layer Simulation

A marine boundary layer was generated using a barrier across the entry to the working section. The function of this is to induce an initial turbulent shear into the flow and promote effective mixing. The final conditioning of the boundary layer was achieved by a specific roughness covering the floor of the working section and extending across the test section.

Profiles of mean wind speed and turbulence are given in Figures B-1 and B-2. The mean wind speed profile follows a power law of 0.14. This is consistent with full-scale marine wind characteristics. The turbulence profiles are compared with a standard logarithmic profile for a roughness length of 0.001 m (typical moderate sea conditions).

B.2.3 Wind Tunnel Models

The three fixed platform models were constructed to a scale of 1:100 and the Schiehallion FPSO was constructed to a scale of 1:125. This allowed the models to have sufficient detail represented for accurate measurements of the turbulence conditions in the vicinity of the helideck.

1. References for this Appendix are listed in Section B5.

Photographs of all the models are shown in Figures B-9 to B-17. The models were generally 'block' type structures designed to simulate the overall blockage caused by the installations. A higher level of detail was included around the helideck particularly for structures likely to affect the wind flow conditions over the helideck. The various elements of the hardware can also be seen in the photographs.

B.2.4 **Scale Effects**

Modelling of the wind flow around small-scale models requires careful consideration of the likely effects of Reynolds number. To achieve correct scaling requires the tests to be run at a higher wind speed i.e. for a 1:100 model, the wind speed would have to be 100 times full scale to simulate full scale Reynolds Number. This is clearly impracticable and in fact not necessary, because bluff sharp-edged shapes such as those found on offshore installations show little variation in wind flow over a wide range of Reynolds number. Such tests are therefore conducted at a wind speed appropriate for testing.

B.3 Test Programme

B.3.1 **Hot-wire Anemometer Measurements**

In order to provide representative time-series turbulence data for input to the helicopter performance analysis and to provide turbulence data for validation of the criterion against the IVLLs, time-varying measurements in a plane representative of the helicopter rotor disc were required for a range of wind angles that bracketed all likely turbulence conditions.

One of the assumptions of the helicopter performance analysis phase of the project, into which these measurements are fed, is Taylor's frozen turbulence field assumption. This assumes that the turbulence is fixed in space and is convected downstream by the mean flow. In order to validate this assumption, the wind tunnel tests were required to provide a multi-station distribution of turbulence. Simultaneous time-series measurements were therefore required across the helicopter rotor disc. Three hot-wire anemometers were positioned across the disc, from upstream to downstream, with the forward anemometer at the upstream edge of the rotor disc, the middle anemometer at the rotor centre and the rear anemometer at the downstream edge of the rotor. The rotor disc was taken to be 20 metres in diameter.

In order to take simultaneous hot wire anemometer measurements in a line downstream of one another, a system of probe supports was designed to minimise interference effects. All three hot-wire anemometers were fixed to right-angle probe supports suspended from a computer controlled traverse gear. Initial calibrations were performed with the upstream supports removed to show that these interference effects were minimal.

The hot-wire anemometers used in these tests were capable of measuring only two of the three components of wind speed at one time (either lateral and longitudinal or vertical and longitudinal)¹. Given the choice between the vertical and lateral components of turbulence, the vertical component was considered to be the more important component. The measurements were therefore taken for the longitudinal and vertical components of turbulence (u and w).

Different wind directions were selected for each installation to enable measurements to be taken with different obstructions upwind of the helideck. A wind direction was also selected to represent free-stream conditions to give a full range of possible

1. A second phase of wind tunnel tests performed later on Brae A utilised 3-axis hot wire anemometry (see Appendix I).

turbulence conditions. With the models mounted on a large diameter turntable (4.4m), it was possible to represent changes in wind direction by a rotation of the turntable.

In order to obtain a range of turbulence conditions experienced by a helicopter during take-off and landing, simultaneous measurements were taken at four separate locations for each wind direction. These were at equivalent full-scale heights of 10 and 20 metres above the centre of helideck and at a distance of 15 metres to the port side of the helideck. The port side measurements were taken to demonstrate the difference in turbulence levels out of the wake region of the obstruction. It is understood that if a straight ahead landing is not desirable, then an approach which puts the structure on the starboard side of the helicopter is preferred, as it is normally the captain who occupies the right hand seat.

It is recognised that cross-wire probes are limited to measuring wind direction up to 30° from the normal axis (defined as parallel to the along wind direction). Beyond 30°, measurements will therefore not fully represent the precise flow conditions and beyond 45° the probes will not be able to determine the correct flow direction (see Figure B-3). In conditions where flow of this kind exists (highly disturbed, re-circulating flows), the turbulence level would be severe and further classification is assumed to be unnecessary.

B.3.2 Flow Visualisation

A limited programme of flow visualisation was conducted using smoke streamers positioned upwind of the helideck to indicate the extent of flow disturbance. These sequences were filmed to form an integral part of the records of the study.

B.4 Presentation of Results

The results of these tests, in the form of wind speed time series and measurements of mean and rms wind speed, form an extensive database which has been supplied on CD-ROM to DERA for use in the helicopter performance analysis phase of the project.

Examples of measured wind speed time histories recorded above the centre of the helideck of each platform are shown in Figures B-4 and B-5. The mean and rms wind speeds and turbulence intensity for each signal are shown in Table B-1 below together with the obstruction to which they relate.

Table B-1 Mean, Turbulence rms Wind Speeds and Turbulence Intensity

	obstruction	mean (m/s)	rms (m/s)	turbulence intensity (%)
Brae A	Derricks	19.60	4.68	23.86
Beatrice	Derrick	23.88	3.37	14.13
Claymore	Crane	24.28	2.93	12.07
Schiehallion	Exhausts	21.90	4.35	19.86

In Table B-1 turbulence intensity is defined as the $100 \cdot (\text{rms}/\text{mean})$.

The higher turbulence intensities for Brae A and Schiehallion are demonstrated clearly in Figures B-4 and B-5. For Brae A, the wind speed fluctuates between 5 and 30 m/s. In contrast, for Beatrice and Claymore, the variation is mostly between 20 and 30 m/s.

A visual indication of the turbulence created by large items of superstructure is shown in Figures B-6, B-7 and B-8. Figures B-6 and B-7 show the relatively modest disturbance created by the lattice drilling derrick on Beatrice. The main source of turbulence is clearly the solid wall around the monkey platform. Figure B-8 shows a far greater level of disturbance created by a more solid obstacle, in this case the array of exhaust stacks on Brae A.

B.5 References

- [1] Whitbread R E, Coleman, S A, *Research on Offshore Helideck Environmental Issues*, CAA Paper 99004, August 2000.
- [2] *Research on Offshore Helideck Environmental Issues, Development of a Turbulence Criterion*, BMT Fluid Mechanics Limited Proposal No. 93514, September 1998.
- [3] *Research on Offshore Helideck Environmental Issues: Development of a Turbulence Criterion. Phase 1: Analysis of existing wind tunnel data and the IVLL*. BMT Fluid Mechanics Limited Report 1 Version 3, August 1999.

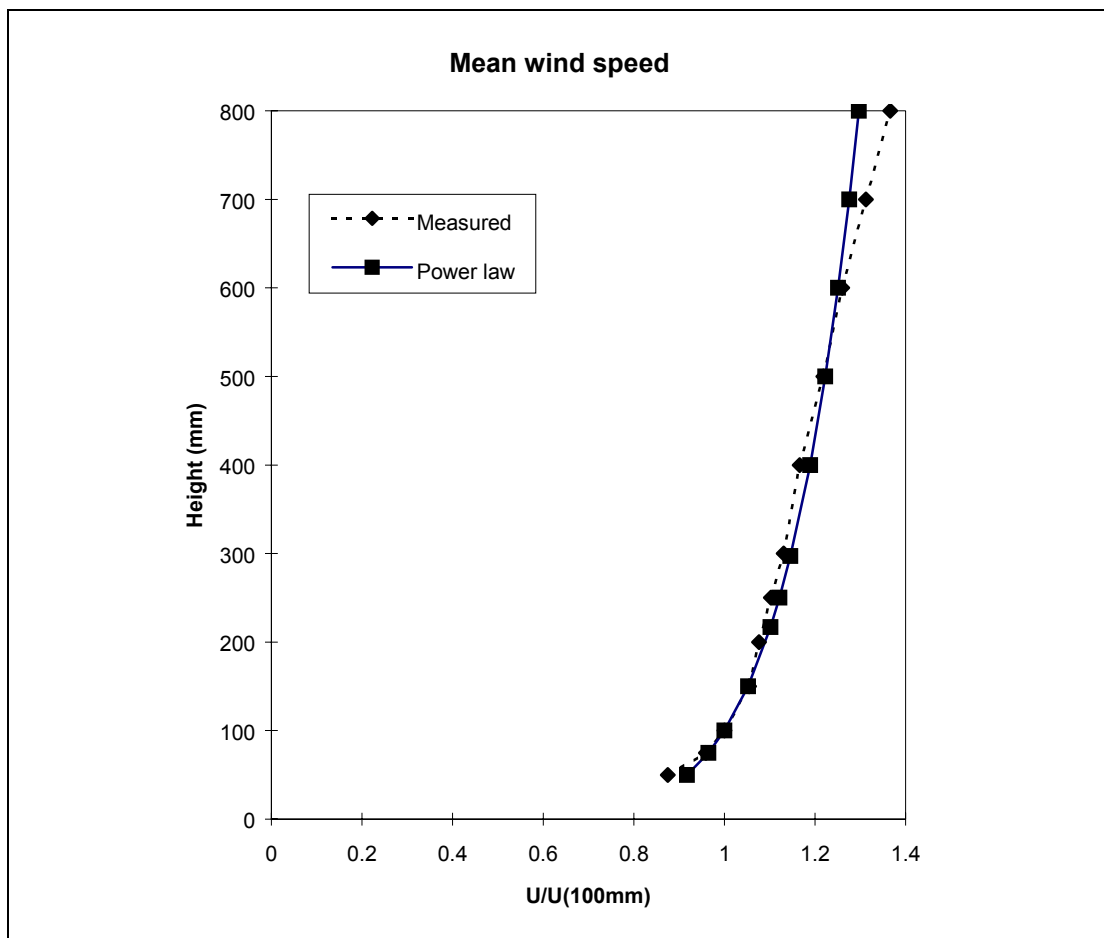


Figure B-1 Mean Velocity Profile (solid line represents power law profiles with an exponent of $1/8$)

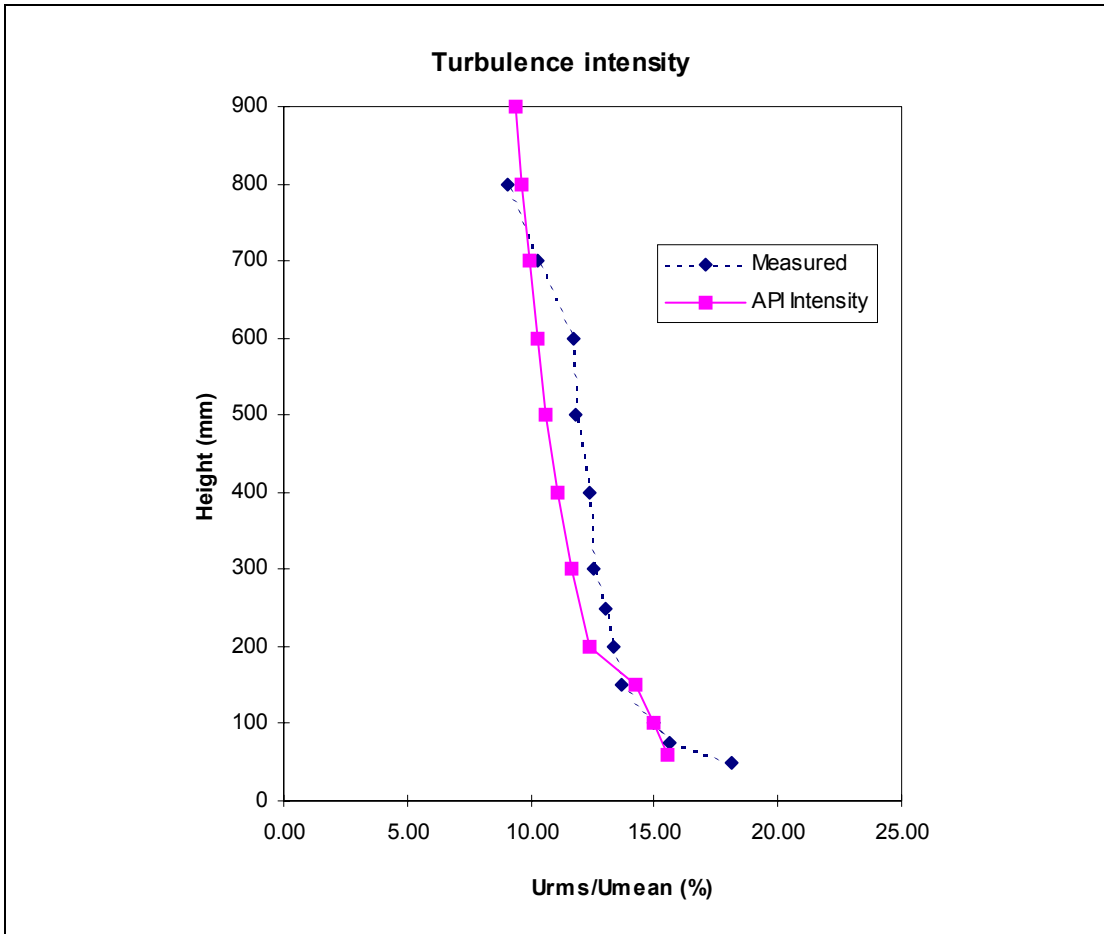


Figure B-2 Turbulence Intensity Profile (solid lines show ESDU empirical values for $Z_0=.001$ m)

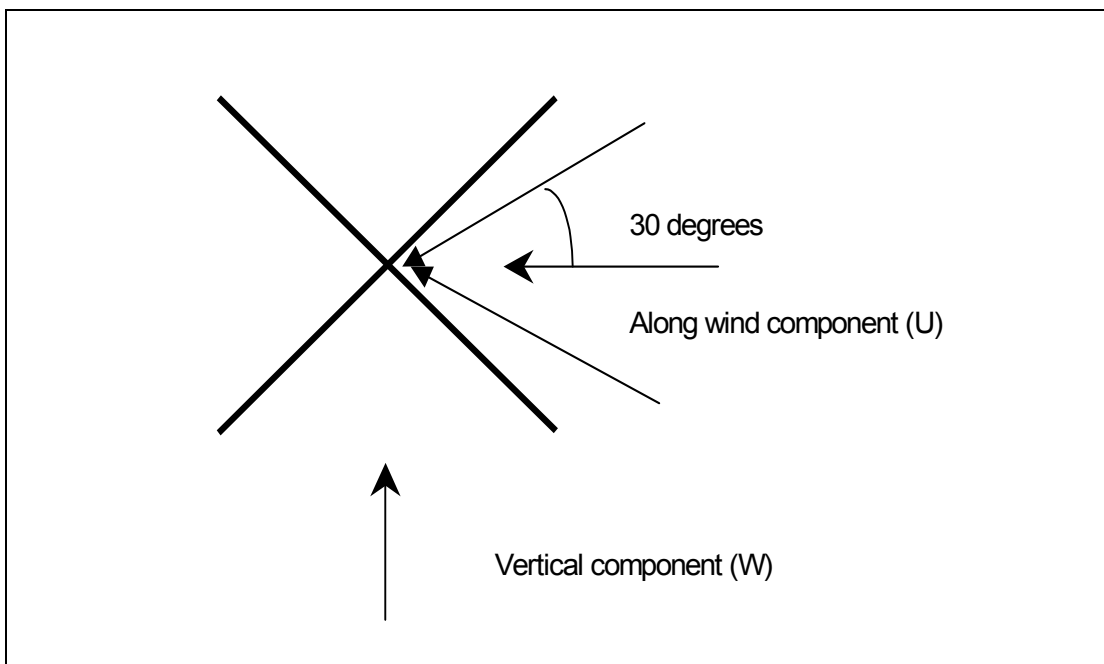


Figure B-3 Angle Limitations on Crossed Hot Wire Probes

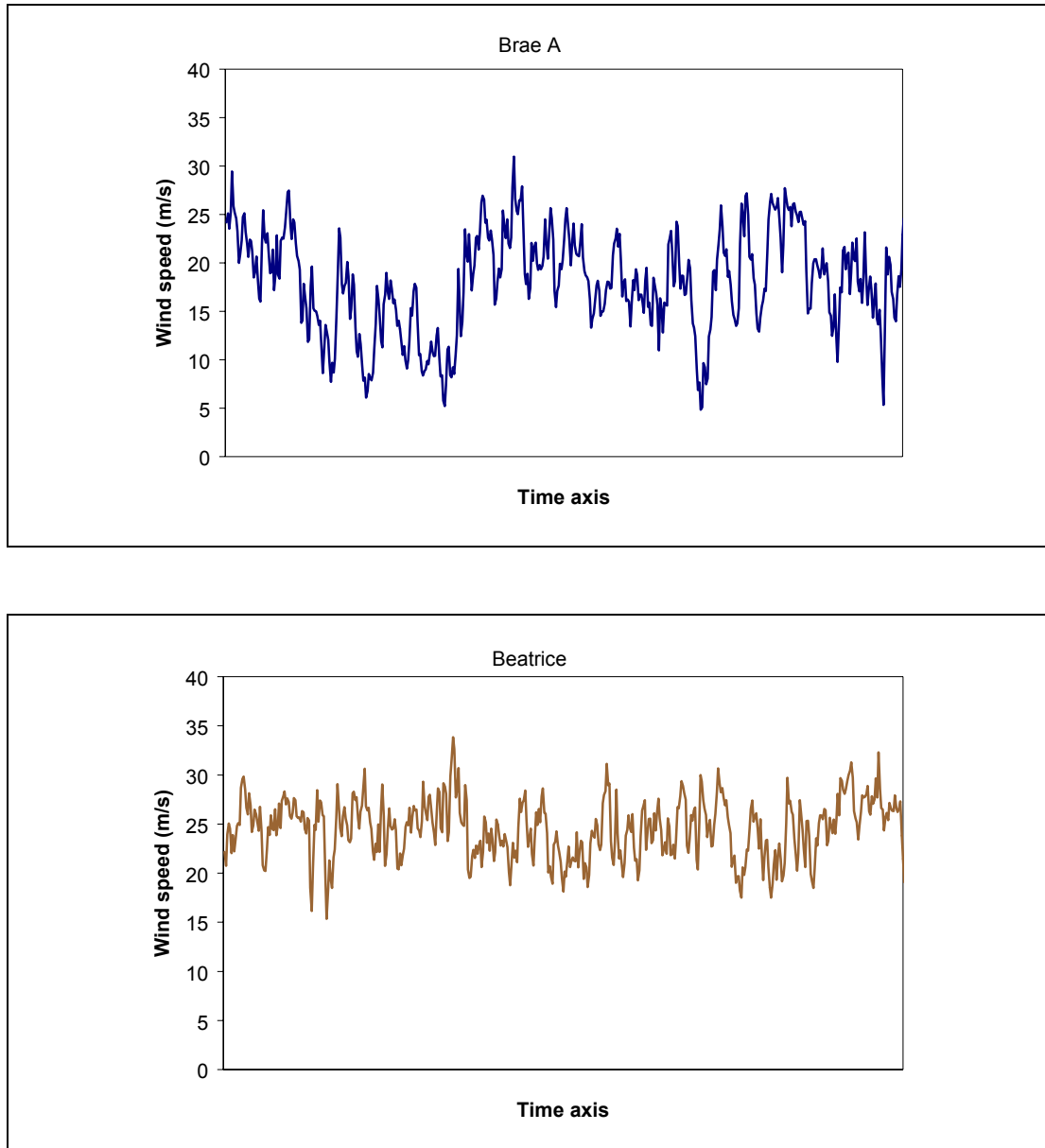


Figure B-4 Examples of Time Histories Measured above the Centre of the Helideck Brae A and Beatrice (free stream wind speed at helideck height = 25 m/s)

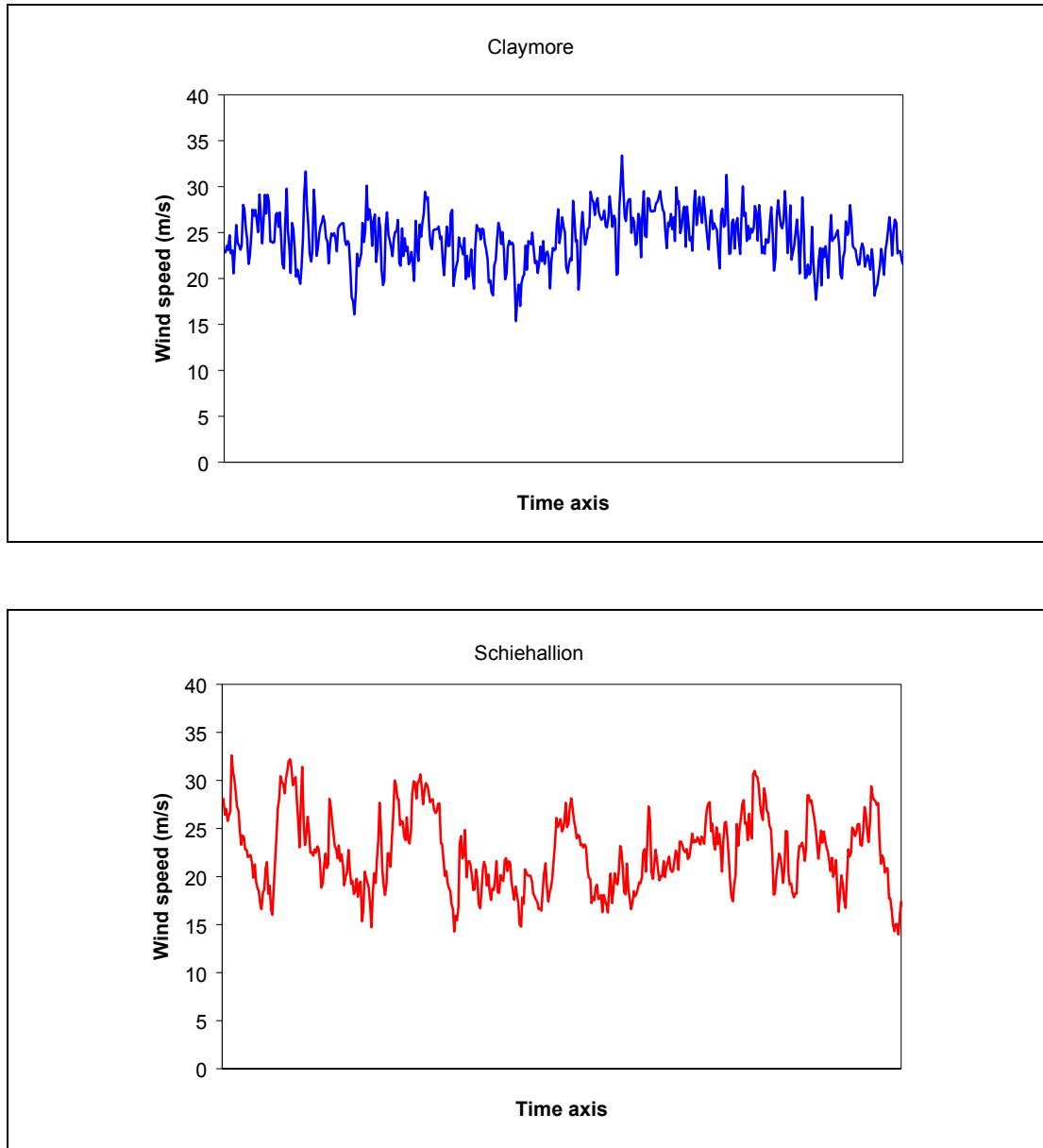


Figure B-5 Examples of Time Histories Measured above the Centre of the Helideck Claymore and Schiehallion (free stream wind speed at helideck height = 25 m/s)

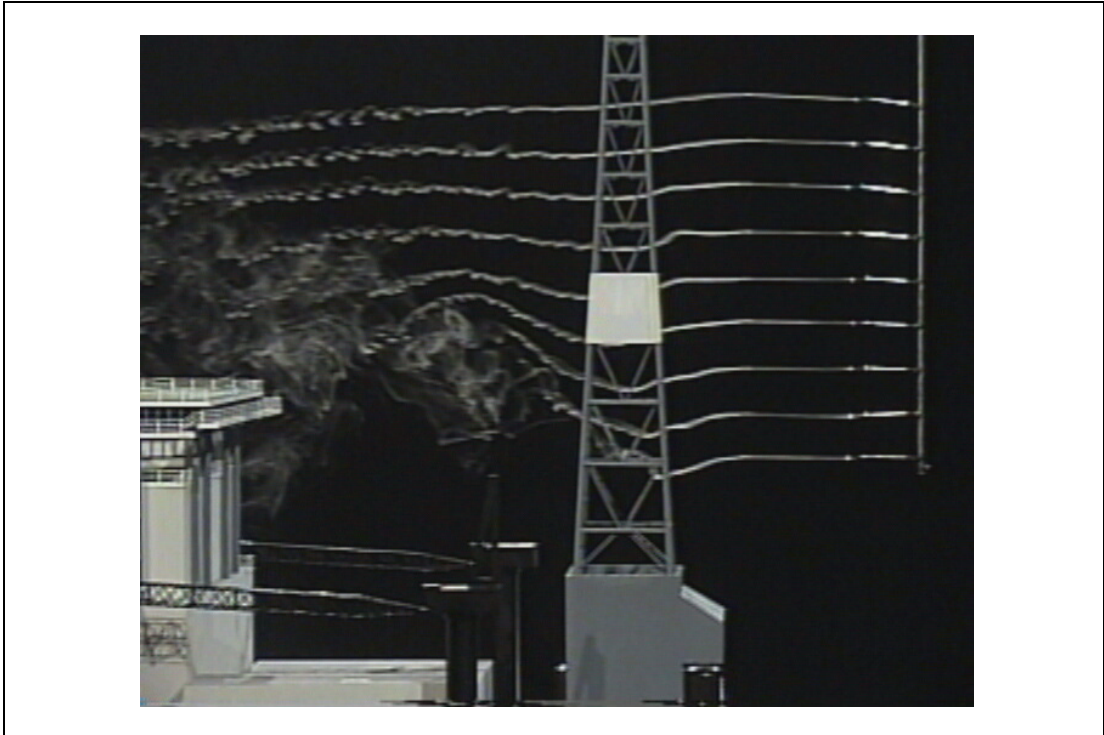


Figure B-6 Turbulence Created by an Open Lattice Derrick. (Smoke released off-centre. Streamers pass freely alongside the upper half. Slight distortion evident near the base where the streamers pass close to the derrick.)



Figure B-7 Turbulence Created by an Open Lattice Derrick. (Streamers released on the centre of the derrick. Turbulence created by the monkey platform is evident.)

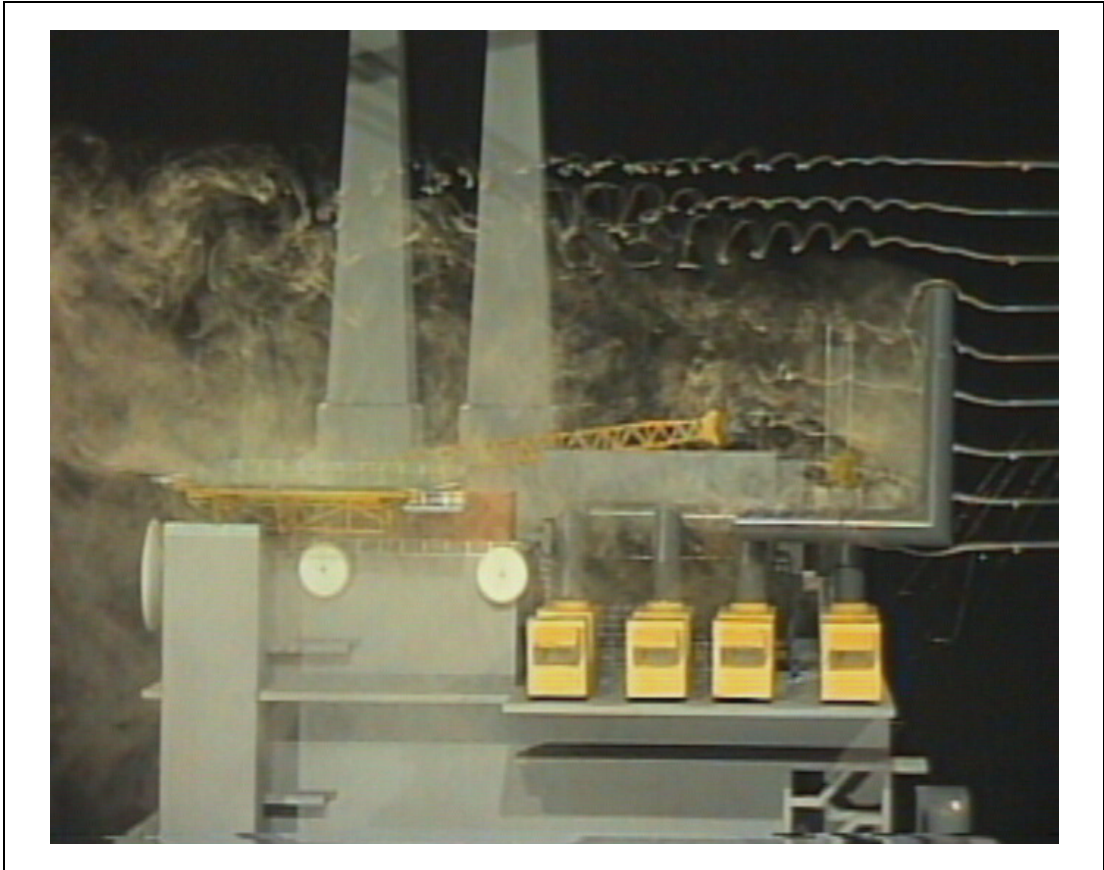


Figure B-8 Turbulence Created by a Solid Obstacle (in this case the exhaust stacks). Significant turbulence in the wake of the obstacle.

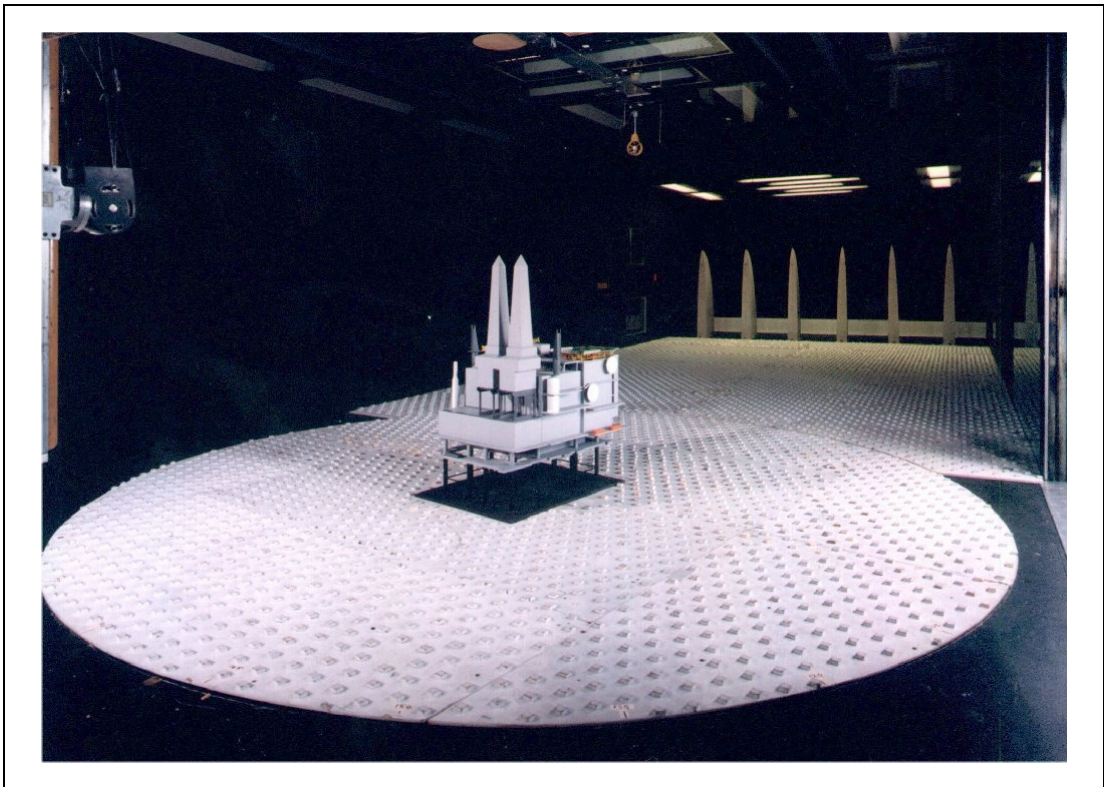


Figure B-9 Brae Alpha 1:100 Model in the Wind Tunnel. View looking upwind.

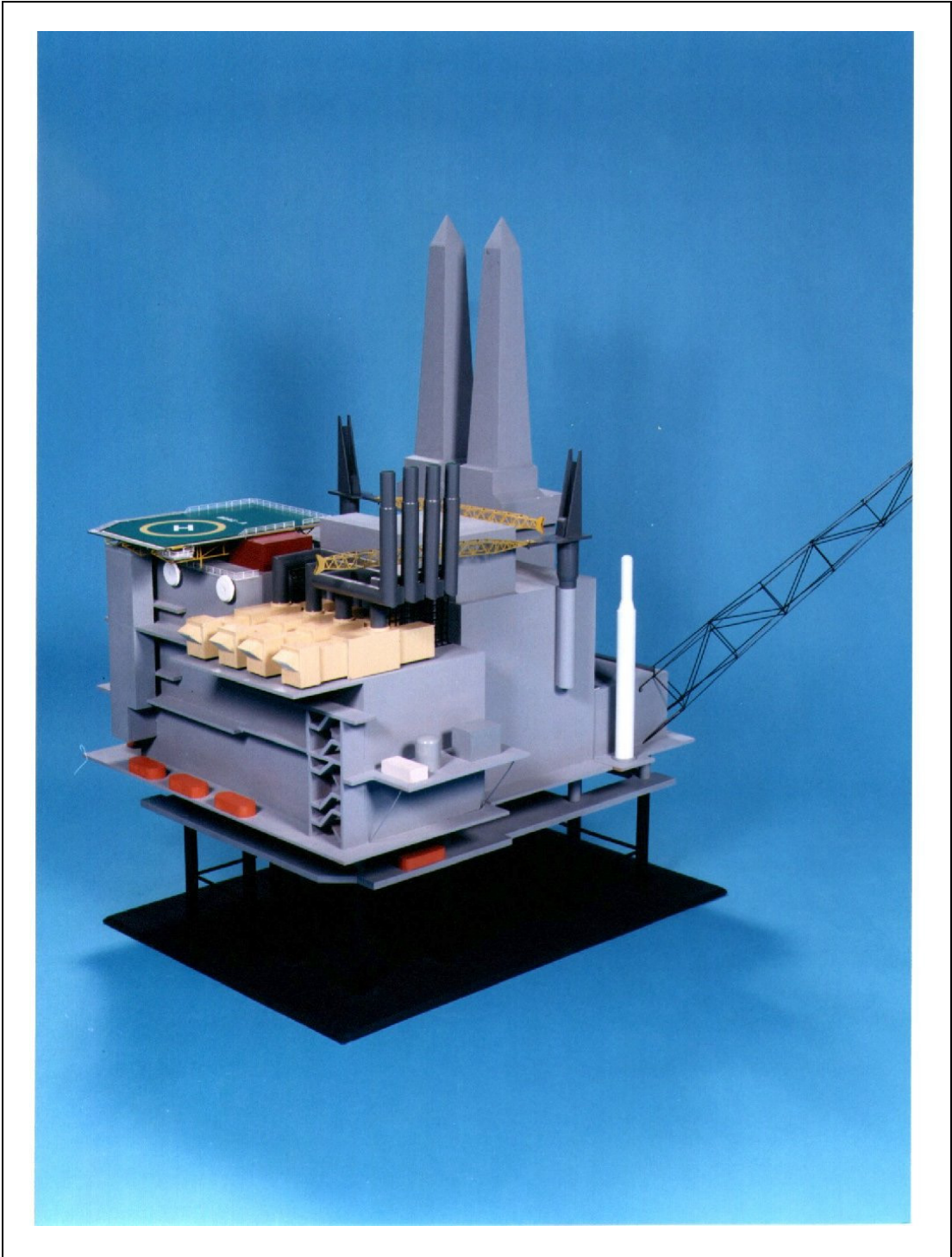


Figure B-10 Brae Alpha 1:100 Model. Close up showing general level of detail.

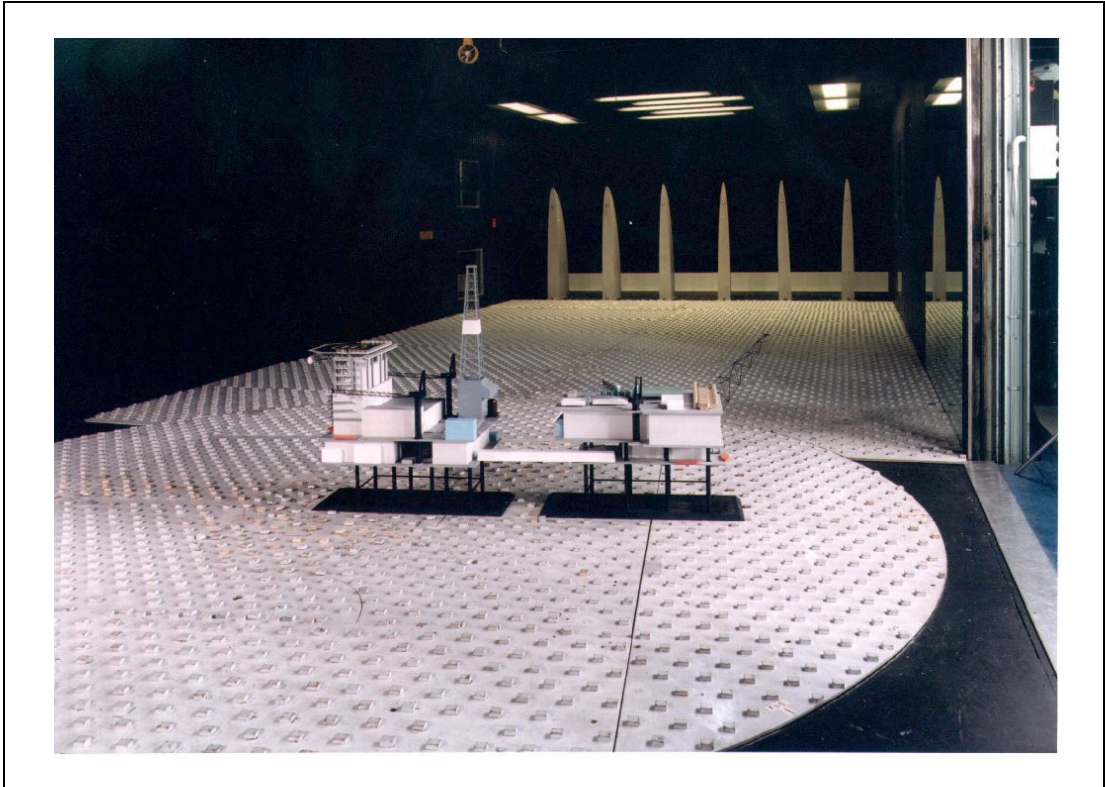


Figure B-11 BEATRICE Alpha 1:100 Model in the Wind Tunnel. View looking upwind.

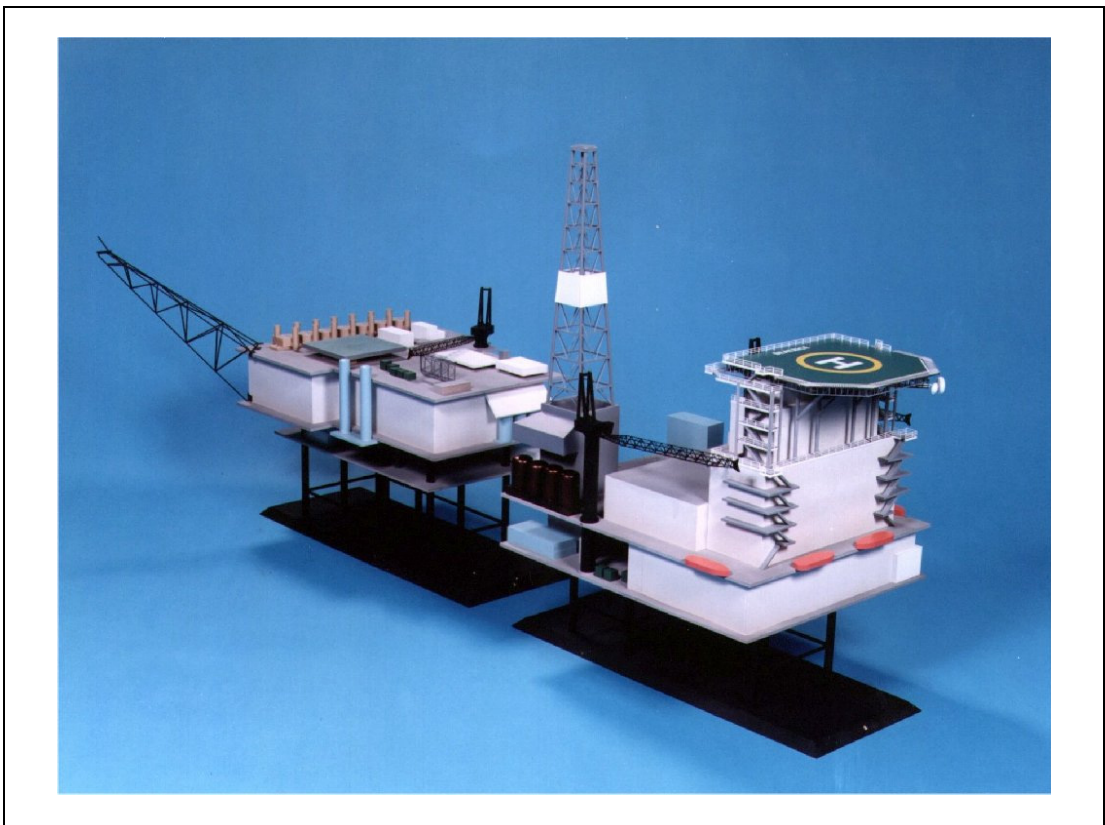


Figure B-12 BEATRICE Alpha 1:100 Model. Close up showing general level of detail.

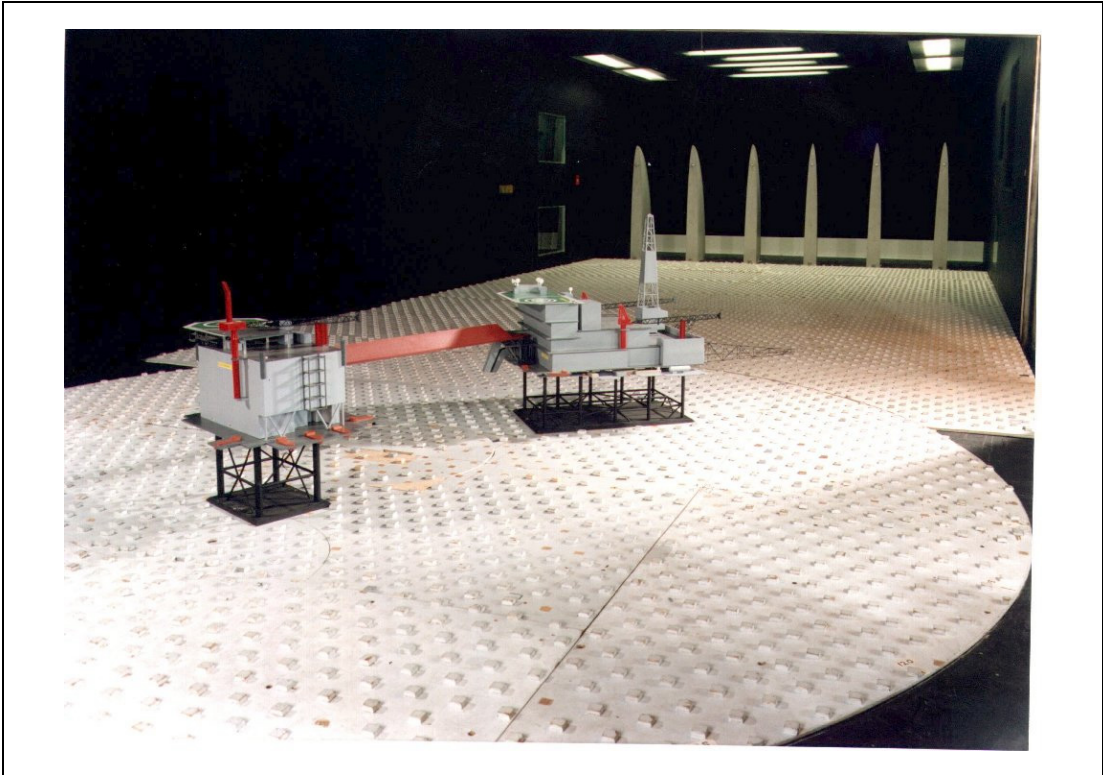


Figure B-13 Claymore Complex 1:100 Model in the Wind Tunnel. View looking upwind.

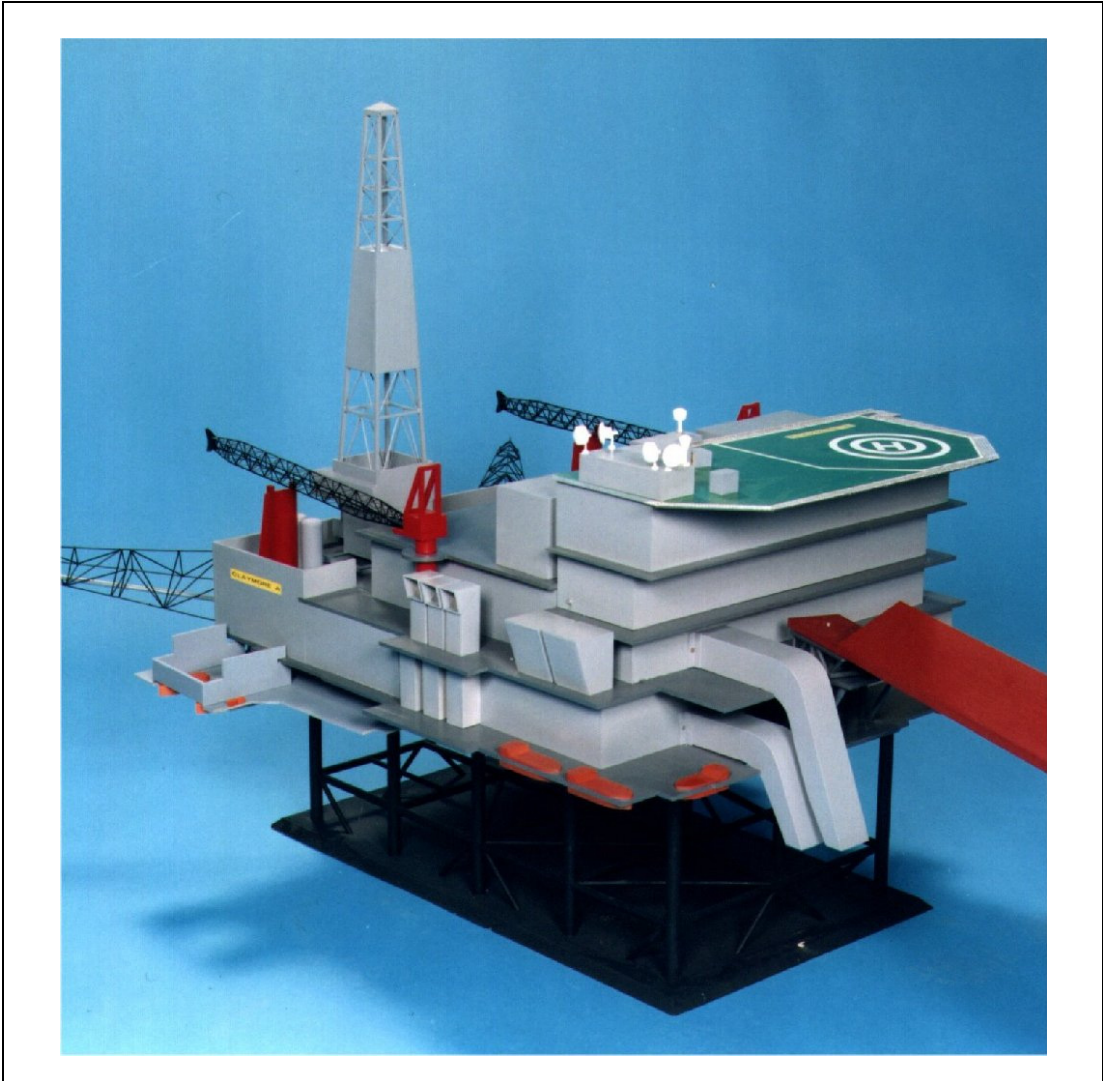


Figure B-14 Claymore Complex 1:100. Close up showing general level of detail of Claymore A.



Figure B-15 Claymore Complex 1:100. Close up showing general level of detail of Claymore CAP.

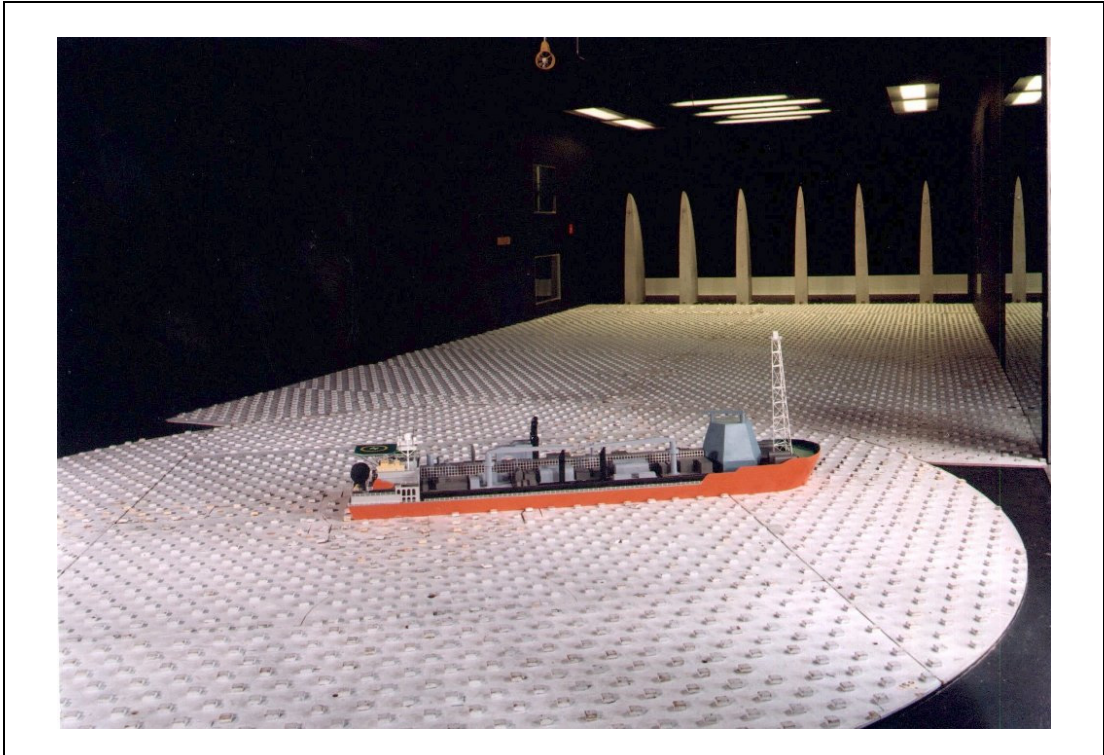


Figure B-16 Schiehallion FPSO 1:125 Model in the Wind Tunnel. View looking upwind.

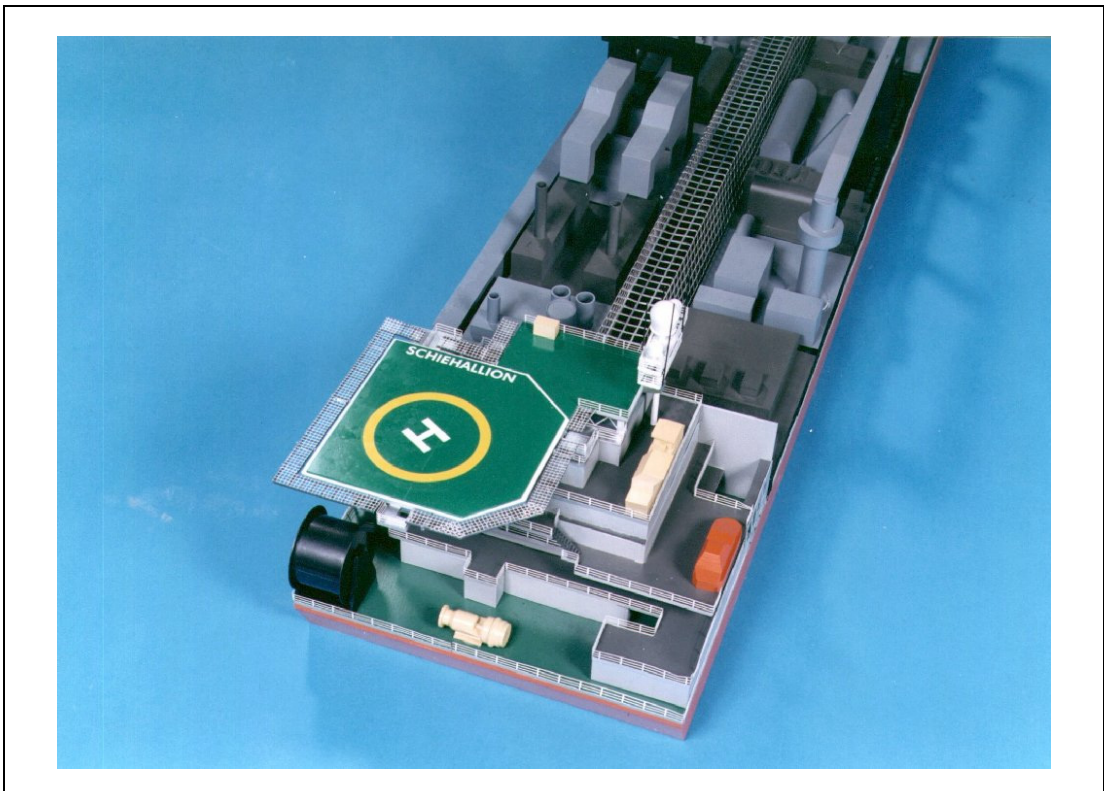


Figure B-17 Schiehallion FPSO 1:125 Model in the Wind Tunnel. Close-up showing general level of detail around the helideck.

Appendix C Exceedances and the Discrete Gust Model

C.1 Discrete Gusts

In the Statistical Discrete Gust method (SDG) of Jones [1] ¹ a discrete gust is taken as the basic element from which atmospheric turbulence is made up. For a gust rising to its maximum intensity w over a distance (ramp-length) H , the SDG model of turbulence considers an aggregation of such gusts in the following way. The number of discrete gusts per unit distance in the ramp length range $(H, H+dH)$ with gust intensity greater than w is taken to be $N_{H,w} dH$ where

$$N_{H,w} = (\alpha / H^2) \exp(-w/(\beta H^k)).$$

Jones notes several important features that this relationship incorporates:

- a) The distribution for fixed H is exponential and therefore non-Gaussian.
- b) The H^{-2} factor gives self similarity.
- c) α is a constant defining the mean rate of occurrence of gusts.
- d) The H^k factor is related to the exponent of the power spectrum, and β measures the overall amplitude of the gusts.

The second element of the SDG approach is the powerful result, which follows from the application of the turbulence model to the response of a linear system. It has been shown by Jones that the number, n_y , of peaks of the response whose magnitude exceeds y is given, asymptotically for large y , by

$$n_y = (\alpha / \lambda H^*) \exp(-y/(\beta \gamma^*))$$

where the 'tuning' parameters H^* , γ^* , and λ are derived from the response of the linear system to a family of discrete gusts of intensity w and ramp-lengths H . That is, once the tuning parameters have been found for a system, the exceedances in the response are easily predicted from the statistical properties of the turbulence. What has been established, however, by both Turner [Appendix C2] and MacDonald [Appendix C3] is the connection between discrete control actions in the form of ramps (in the latter case and decaying ramps in the former) and the pilot workload. The correlation is made via binary decision trees by MacDonald, and via exceedances by Turner, and therefore this strand of the methodology has already been established.

In the current study the system being investigated is, in the first place, the helicopter but can, via the SyCoS model, be extended to the helicopter/pilot combination so that the exceedance response of the control activity can be directly related to the measured turbulence. The exceedance response approach therefore offers an efficient implementation of the predictive framework - in that it is used simply to establish a correlation of exceedances, which can be easily applied to a wide range of platforms and helicopter types. Therefore although the method is more technically challenging to analyse, apply and communicate, it is potentially a robust and efficient way of delivering the guidance for platform design.

1. References for this Appendix are listed in Section C2.

There is, of course, a connection between the SDG approach and that based on the power spectrum density (PSD) since the parameter k is chosen to capture the correct PSD via

$$B = 2k+1$$

where the PSD has asymptotic behaviour $(frequency)^{-b}$. Well known spectra for atmospheric turbulence are the Von Karman ($k = 1/3$, $b = 5/3$) and Dryden ($k = 1/2$, $b = 2$). The particular benefit that is conveyed by the SDG representation is that it properly captures the occurrence of gusts of large amplitude whereas the PSD, by omitting the phase information in a signal, can fail to concentrate the energy necessary to form them. If responses of very large amplitude are important to an application then this property of the SDG can be crucial. The value of k is important in the tuning process which determines the values of H^* , γ^* , and λ for a given system since it determines the shape of the discrete gust which is input to the system. The value $k = 1/2$, for example, is associated with smooth ramp gusts and $k = 1/3$ gives a ramp with a subsequent decay or wash out. In practice, $1/3$ is sufficiently close to $1/2$ to allow the use of the simpler ramp profile even for turbulence with a Von Karman spectrum. Other values of k can demand complex profiles for the tuning process and their generation requires methods that are not widely available. For this reason, the SDG approach can only be considered for investigation within the current work if the measured turbulence has properties that allowed a value of k close to $1/2$, that is, a spectrum close to $b = -2$. Some examples of the spectra of measured atmospheric turbulence are shown in Figures C-1 and C-2.

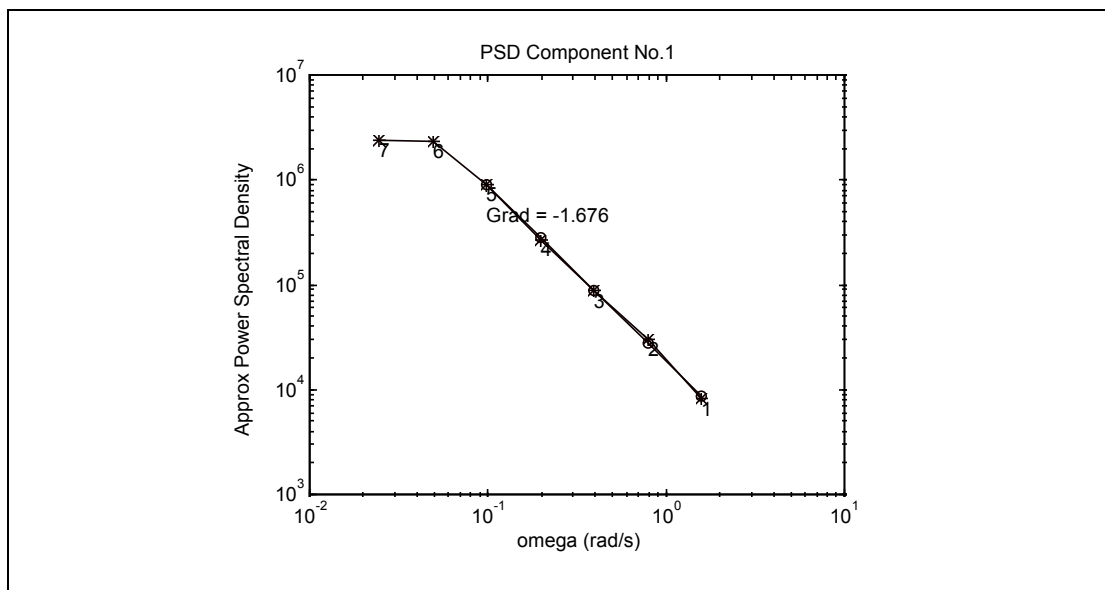


Figure C-1 Atmospheric Turbulence with a Typical Von Karman PSD

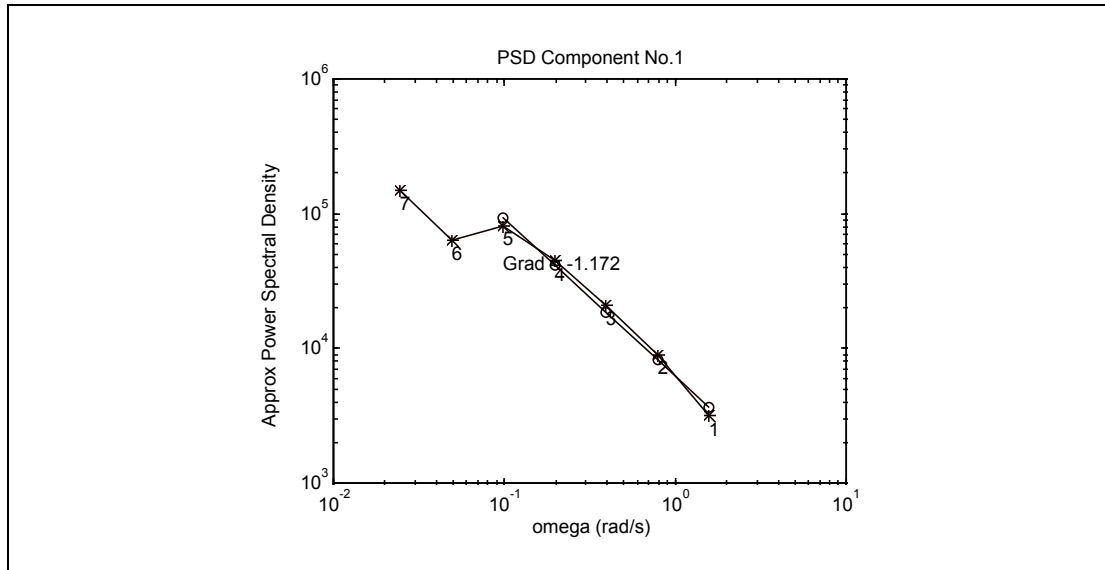


Figure C-2 Atmospheric Turbulence with a Non-standard PSD

In each case the time has been normalised to the sampling rate. It is clear, since the fitted gradient is close to -1.67 that the turbulence in Figure C-1 has a spectrum close to the Von Karman and that the use of ramp gusts in order to derive the tuning parameters would be appropriate, allowing the response exceedances to be predicted. The spectrum of the turbulence sample in Figure C-2 has a spectrum with a gradient that is not close to -1.67 and, further, has no clear asymptotic profile and an unusual shape at low frequency. Therefore it is not a straightforward matter to apply the SDG theory.

Samples of the measured turbulence from the wind tunnel tests were analysed and many of them were found to have spectra to which the SDG method could not be directly applied. Therefore, there was no encouragement to pursue SDG analysis within the scope of the current investigation and it was not pursued.

C.2 References

- [1] Jones J. G. *Statistical Discrete Gust Method for Predicting Aircraft Loads and Dynamic Response*, J Aircraft, April 1989, 2, (4), 382-392.
- [2] Turner G P, Bradley R, and Brindley G. *Simulation of Pilot Control Activity for the Prediction of Workload Ratings in Helicopter/Ship Operations*. 26th European Rotorcraft Forum, The Hague, September 2000, Paper 91.
- [3] MacDonald C. *The Development of an Objective Methodology for the Prediction of Helicopter Pilot Workload*, PhD Thesis, Department of Mathematics, Glasgow Caledonian University, 2001.

Appendix D Configuration Data for the S-76 Main Rotor

D.1 FLIGHTLAB Configuration Data

The data for the *FLIGHTLAB* model are modified using the Model Editor facility. The modifications were based upon the configuration parameters described by Thomson and Bradley [1]¹ and Prouty [2]. The data is entered using a series of input windows the contents of which are displayed in the following tables. The tables contain a description of the variable, the default value or the value used in the Lynx model and the value used in the S-76X model (if changes were necessary).

Table D-1 Data Displayed in the Rotor 1 Input Window

Description	Lynx Value	'S-76X' value
Fuselage station of Rotor1	0	
Buttline station of Rotor1	0	
Waterline station of Rotor1	4.1706	
Number of Rotor1 blades	4	
Rotor1 blade tip loss factor	0.97	
Rotor hub frame orientation	0 176 0	5° shaft tilt angle, i.e. 0 175 0
Axis about which the shaft tilts	2	
Rotor1 nominal speed	34.2	32.83
Rotor1 radius	21.0	22.00
Number of azimuth step/rev	24	
Swash plate phase angle	-15	

A generic articulated rotor model was then used to replace the Lynx hingeless rotor. The data shown in Table D-2 illustrates that a 3.8% hinge offset was used for flap, lag and feathering hinges.

Table D-2 Data Displayed in the Articulated Input Window

Description	Default Value	'S-76X' value
lag hinge option	1	
flap hinge offset	1.0	0.836ft (= 0.038R)
lag hinge offset	1.0	0.836ft (= 0.038R)
feathering hinge offset	1.0	0.836ft (= 0.038R)
delta 3	0	
spring stiffness of flap hinge	0	
damping coefficient of flap hinge	0	
flap hinge spring undeformed angle	0	

1. References for this Appendix are listed in Section D2.

The blade used in the rotor is defined in *FLIGHTLAB* using a series of look-up tables. From Thomson and Bradley [1] some of the blade parameters were known, i.e. blade chord, twist, mass distribution and structural root cut-out. The other data were estimated as being similar to that used in the UH60 model which was available in *FLIGHTLAB*. The values used for the 'S-76X' model are shown in Table D-3.

Table D-3 Data Displayed in the Blade Input Window

Description	Default Value	'S-76X' value
Blade structural root cut-out	0	3.531ft (= 0.1605R)
Blade structural grid generation opt	0	
Blade section chordwise c.g. offset	l_bcgoff.tab	Offset is zero in UH60 model
Blade chord	l_bchord.tab	Constant chord: 1.291'
Blade segment rotary mass	l_brotary_mass.tab	
Blade twist variation	l_btwtist.tab	Linear twist 0 to 10°
Blade Mass distribution	l_bmpl.tab	Constant mass per length: 0.2107 slugs/ft except first 16% of blade
Blade structural segment end nodes	l_bstruct_xnode.tab	
Offset of midchord from e.a	l_bsege0.tab	Offset is zero in UH60 model

The aerodynamics root cut-out was defined to be the same as the structural root cut-out in the airloads input window, see Table D-4.

Table D-4 Data Displayed in the Airloads Input Window

Description	Default Value	'S-76X' value
Number of blade aero segments	5	
Blade aerodynamic root cut-out	5.25	3.531ft (= 0.1605R)

The aerodynamic properties of the 'S-76X' were assumed to be the same as those of the UH60, as the same blade types were used in both vehicles. Thus the data in Table D-5 were used in the Quasi-Steady input window.

Table D-5 Data Displayed in the Quasi-Steady Input Window

Description	Default Value	'S-76X' value
number of airfoil	1	
airfoil boundary	afoilboundary1.tab	afoilboundary.tab for UH60
1st airfoil cl for low angle	l_cll1.sav	cll1.sav for UH60
1st airfoil cl for high angle	l_clh1.sav	clh1.sav for UH60
1st airfoil cm for low angle	l_cml1.sav	cml1.sav for UH60

Table D-5 Data Displayed in the Quasi-Steady Input Window

Description	Default Value	'S-76X' value
1st airfoil cm for high angle	l_cmh1.sav	cmh1.sav for UH60
1st airfoil cd for low angle	l_cdl1.sav	cdl1.sav for UH60
1st airfoil cd for high angle	l_cdh1.sav	cdh1.sav for UH60
1st airfoil low angle tab arguments	-20 20 0.5 81	-32 32 2 33
1st airfoil high angle tab arguments	-180 180 5 73	-180 180 2 181
1st airfoil Mach number arguments	0.3 0.95 0.05 14	0 1.0 0.1 11

D.2 References

- [1] Thomson D G, Bradley R., *Review of Falling 5-in-1 Gradient Criteria for Offshore Platform Operations*. Final Report, Annex to CAA Contract No. 7D/S/960
- [2] Prouty, R. W., *Helicopter Performance, Stability and Design*, R. E. Kreiger, 1995.

Appendix E Review of General Applicability of Turbulence Data

E.1 Introduction

Only wind tunnel data obtained on Brae A were used for the validation of the turbulence criterion. The decision to do so was based on the rationale that by varying the wind direction all turbulent conditions could be covered, ranging from high turbulence in the wake of the clad derricks to relatively low turbulence for undisturbed flow. This avoided the expense of setting up flight simulator trials for more than one platform.

This approach does, however, raise the question of how representative the Brae A data are of turbulence on other platforms. For example, if two turbulence signals have similar intensities or standard deviations but different spectral properties or length scales (for example turbulence generated by a drilling derrick compared with that generated by an exhaust stack), then the impact on helicopter performance might be expected to be different as the helicopter and pilot are likely to react differently to different time scales of turbulent disturbances.

To examine this in more detail, the spectral properties of selected time histories measured during the first phase of the wind tunnel tests (Appendix B) have been analysed.

The objective of the analysis was to determine if there was evidence to support the underlying premise that turbulence signals with similar turbulence intensities but generated from different sources (and potentially with different spectral properties) could lead to similar pilot workload ratings. To meet this objective, the criteria for choosing the time histories were required to be as follows:

- a) generated by different upstream obstructions;
- b) similar SyCoS predictions of pilot workload;
- c) similar turbulence intensities; and
- d) dissimilar spectra.

These criteria proved difficult to meet with the data available and only four time histories were identified.

E.2 Turbulence Spectra

For turbulence signals, the variance of a time history corresponds to the kinetic energy of the turbulence. The integral of the spectral density between any two frequencies therefore represents the kinetic energy of the turbulence within those frequencies i.e.

$$KE = \int S(n)dn \quad \text{for } n = n1 \text{ to } n2$$

where:

n = frequency (Hz)

$S(n)$ = spectral density

This is alternatively expressed as:

$$KE = \int nS(n)d(\log(n)) \quad \text{for } n=n_1 \text{ to } n_2$$

Therefore, in a plot of $nS(n)$ against $\log(n)$ the area under the curve is proportional to the kinetic energy, and so the frequency at which the peak value occurs indicates where the peak concentration of turbulent energy lies. In terms of length scale, low frequencies correspond to large turbulent eddies being transported at the mean wind speed and high frequencies correspond to small eddies. So low frequencies correspond to large length scales and high frequencies to small length scales.

E.3 Analysis

The four time histories selected are listed in Table E-1. The table shows that the mean wind speeds, standard deviations and the turbulence intensities are reasonably similar with turbulence intensity varying from 14.1% to 14.5%. The time histories were recorded above the centre of the helideck at a sample rate of 512 Hz for a sample time of 128 seconds.

The spectra for these runs are shown in Figures E-1 to E-4. Plotted in the form $nS(n)$ versus $\log(n)$. Plotted in this way, the peaks of the graphs correspond to frequencies of maximum energy. From these figures, the peak frequencies shown in Table E-2 are obtained. Also shown in Table E-2 are the SyCoS predictions of pilot workload obtained by GCU for each of the runs.

The estimated peak frequencies shown in Table E-2 vary from approximately 3 to 60 Hz with the Brae A crane obstruction producing the highest frequency and the Brae A exhausts and the Claymore derrick producing the lowest. Despite this large range of frequency, the SyCoS predictions remain relatively constant with a value of 4, increasing to 5 for the Beatrice case.

E.4 Conclusions

The results support the premise that neither the spectral characteristics nor the length scales of turbulence have a significant effect on predicted pilot workload. This indicates that, in terms of pilot workload, the Brae A data are representative of platform turbulence in general.

The present findings are, however, based wholly on the SyCoS predictions of pilot workload and single point turbulence measurements. Further piloted simulator trials on different platforms would have to be carried out to confirm the conclusions.

E.5 References

- [1] Manning, A P, *Prediction of Pilot Workload During Approaches to Offshore Helidecks using Desk Top Simulation*; DERA/AS/FMC/CR01236; October 2001.

Table E-1 Turbulence Records Selected for Analysis

Platform (BMT Run reference)	Obstruction	Height above helideck¹ (metres full scale)	Mean Wind Speed² (m/s)	Turbulence Standard Deviation² (m/s)	Turbulence Intensity (%)
Brae A (BR30)	Exhaust	20	7.815	1.134	14.5
Brae A (BR108)	Crane	10	8.397	1.204	14.3
Beatrice (BE45)	Derrick	10	7.249	1.044	14.4
Claymore (CL19)	Derrick	20	8.052	1.132	14.1

1. all records relate to the centre of the helideck
2. model test values

Table E-2 Estimated Values of Peak Spectral Frequency

Platform (BMT Run reference)	Obstruction	Peak Spectral Frequency (Hz)	SyCoS Rating at 60 kt¹
Brae A (BR30)	Exhaust	3 to 5	4
Brae A (BR108)	Crane	50 to 60	4
Beatrice (BE45)	Derrick	7 to 10	5
Claymore (CL19)	Derrick	3 to 5	4

1. The peak value at 60 kt was chosen on the basis that it is likely to reflect the impact of different turbulence levels more so than ratings at low wind speed.

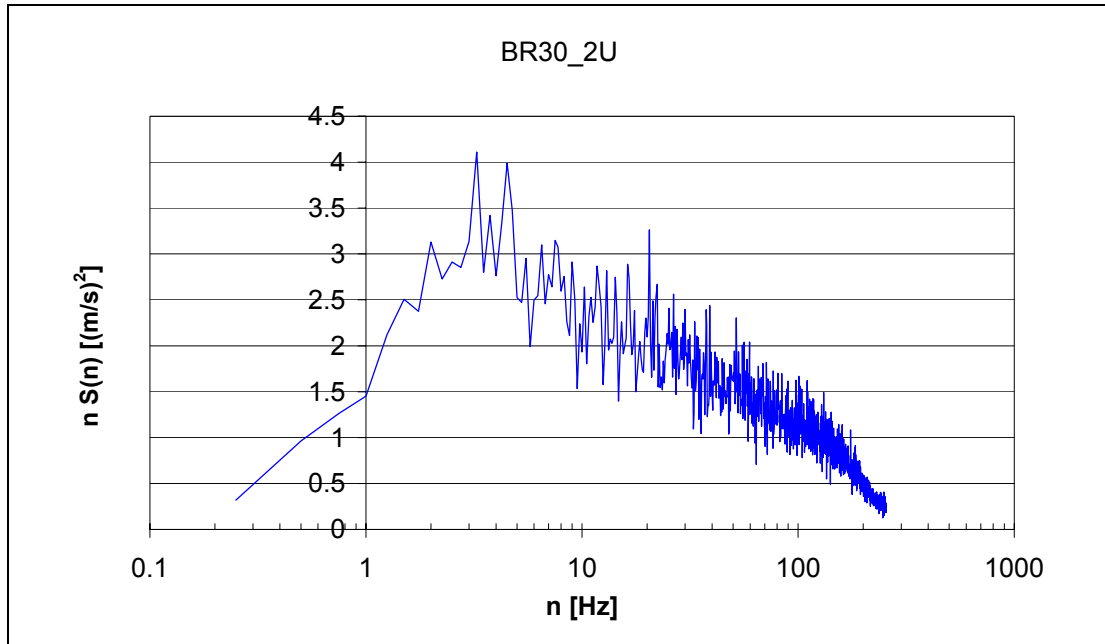


Figure E-1 Turbulence Spectra for Brae A Run 30 (exhausts upwind)

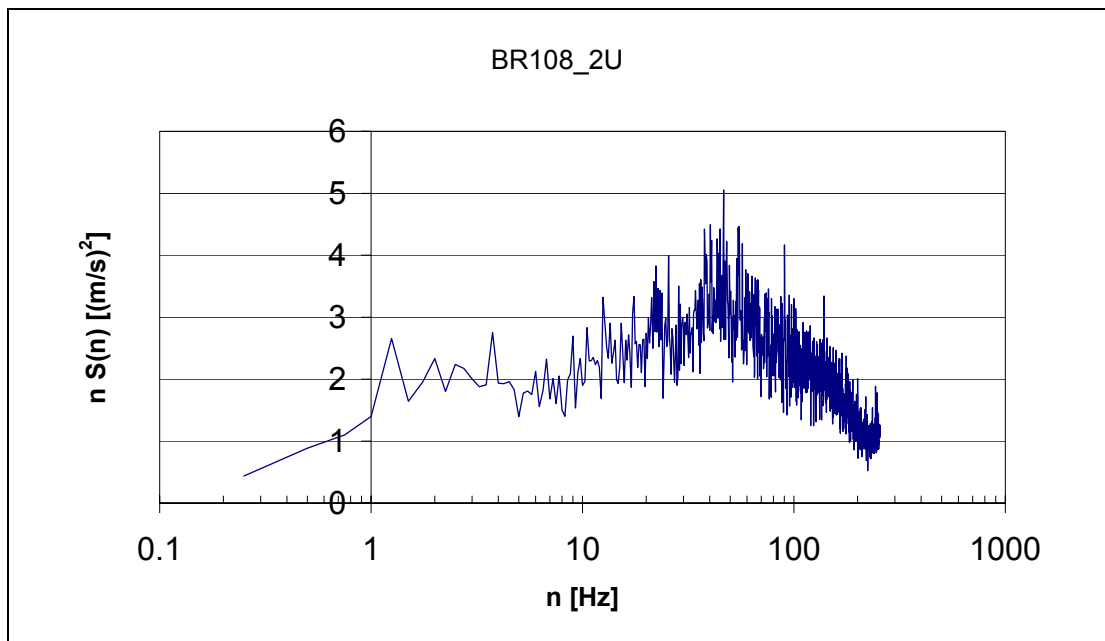


Figure E-2 Turbulence Spectra for Brae A Run 108 (crane upwind)

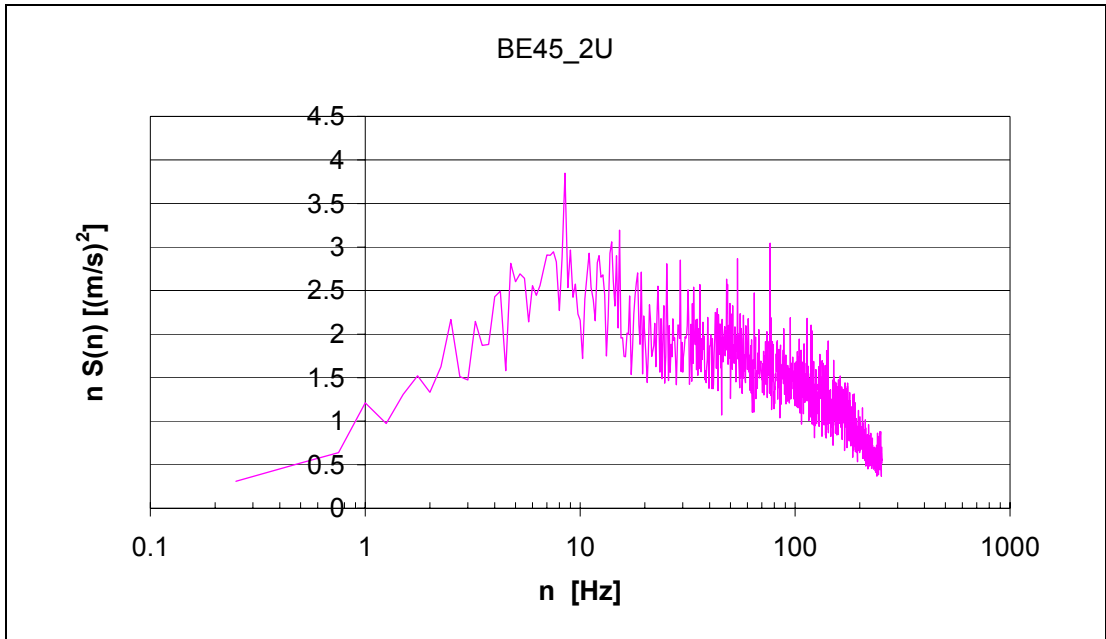


Figure E-3 Turbulence Spectra for Beatrice Run 45 (derrick upwind)

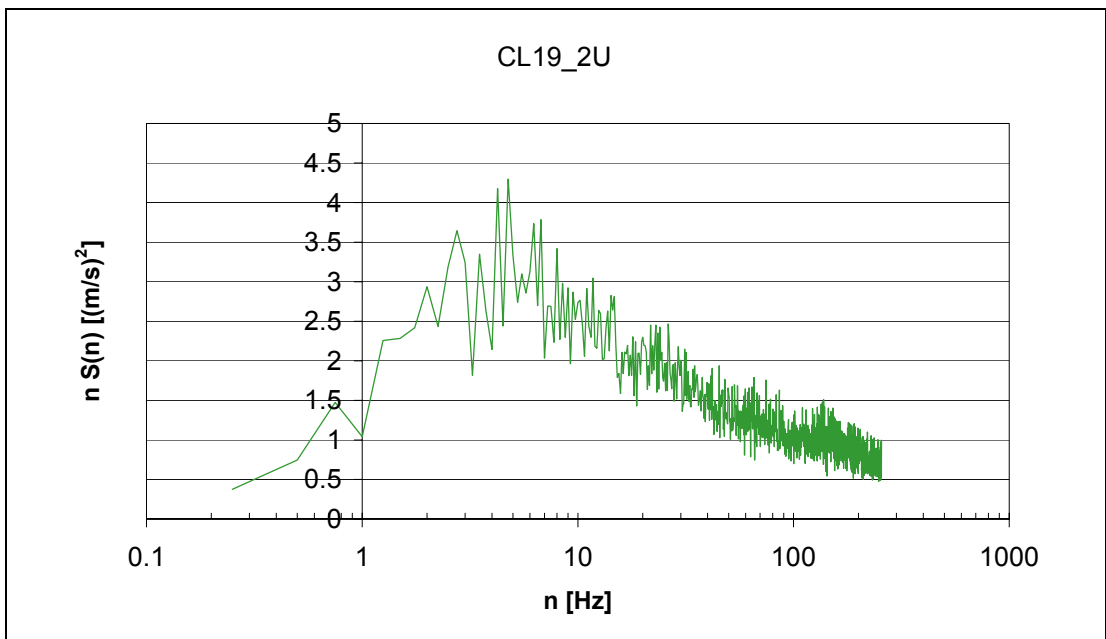


Figure E-4 Turbulence Spectra for Claymore Run 19 (derrick upwind)

Appendix F Transformation of Turbulence

The wind tunnel tests were carried out with the assumption that the recorded data could be scaled up to full-scale measurements (Table F-1). The assumption is that the quantity $\frac{UT}{L}$ must remain constant, where L , T and U are length, time and velocity, respectively, at a particular scale. Thus we must have:

$$\frac{U_{ms} T_{ms}}{L_{ms}} = \frac{U_{fs} T_{fs}}{L_{fs}}$$

where $\frac{L_{fs}}{L_{ms}}$ is the model scale (7th column in Table F-1),

U_{ms} is the measured wind speed (5th column in Table F-1),

U_{fs} is the target full scale wind speed,

T_{ms} is the sampling time interval (the reciprocal of the sampling frequency: 8th column in Table F-1),

T_{fs} is the corresponding full scale time interval.

Thus, knowing the target wind speed, measured wind speed and model scale, the equivalent sampling frequency of the data at full scale can be found from:

$$\frac{1}{T_{fs}} = \frac{U_{fs}}{U_{ms}} \cdot \frac{L_{ms}}{L_{fs}} \cdot \frac{1}{T_{ms}}$$

The supplied wind tunnel data was pre-scaled to a target wind speed of 25 m/s although analysis of the data for consistency revealed that the requisite scaling had, in fact, only been applied to the horizontal component. This omission was confirmed by BMT, and was easily corrected, but it should be noted for any subsequent use of the wind tunnel data.

In summary, the data is directly scaled to achieve the required wind speed it is then interpreted as being sampled at a frequency $1/T_{fs}$ given by the formula above. For its application within a simulation it will normally need to be interpolated in order to match the simulation frame rate.

Table F-1 Scaling Parameters used in Wind Tunnel Simulations

	Reference Height ms mm	U ref height ms (m/s)	Ratio U hd : Uref height	U hd ms (m/s)	U target hd fs (m/s)	Model Scale	Sample Frequency ms (Hz)	Sample Frequency Achieved fs (Hz)	Time Interval Achieved fs (seconds)
Schiehallion	hd + 80	4	0.992	3.968	5	125	512	5.161	0.194
Schiehallion	hd + 80	8	0.9857	7.8856	10	125	512	5.194	0.193
Schiehallion	hd + 80	12	0.9575	11.49	15	125	512	5.347	0.187
Brae_A	hd + 100	4	1	4	5	100	512	6.4	0.156
Brae_A	hd + 100	8	1	8	10	100	512	6.4	0.156
Brae_A	hd + 100	12	1	12	15	100	512	6.4	0.156
Beatrice	hd + 100	4	1	4	5	100	512	6.4	0.156
Beatrice	hd + 100	8	0.9825	7.86	10	100	512	6.514	0.154
Beatrice	hd + 100	12	0.9525	11.43	15	100	512	6.719	0.149
Claymore	hd	4	1	4	5	100	512	6.4	0.156
Claymore	hd	8	1	8	10	100	512	6.4	0.156
Claymore	hd	12	1	12	15	100	512	6.4	0.156

Appendix G Fully Compensated Crossover Model

G.1 The Fully Compensated Crossover Model

The implementation of the Fully Compensated Crossover Model (FCCM) for this study is shown in Figure G-1, and the matrix elements occurring in the inverse are readily obtained by standard methods [1]¹ summarised below.

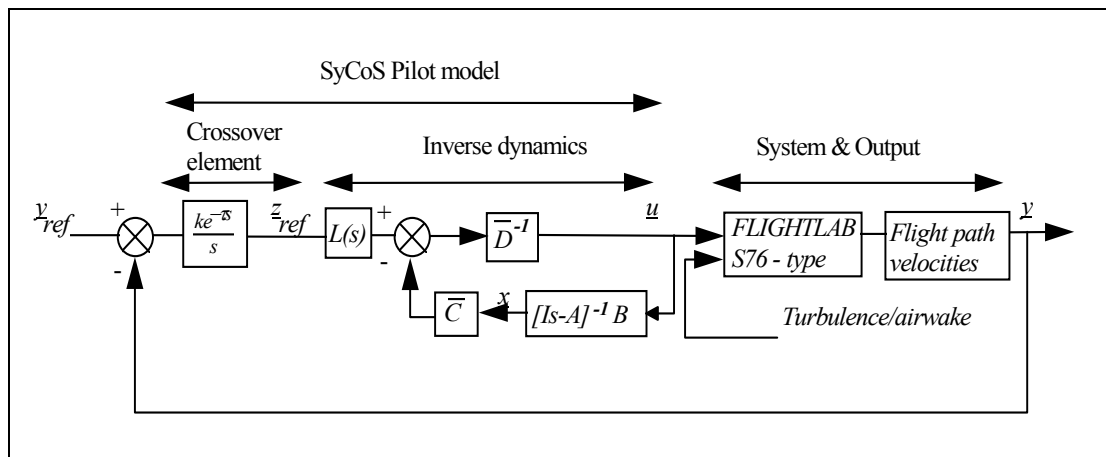


Figure G-1 Implementation of the SyCoS FCCM Pilot Model

A linear, time invariant, model of a helicopter is written:

$$\dot{x} = Ax + Bu$$

where x is the vector of the helicopter state variables (velocity components, attitudes and rates), and u is the vector of controls (collective lever, cyclic stick and pedal). The values of the variables and controls are measured relative to a reference flight condition - which is hover with prescribed sideslip in the current context. The elements of the matrices A and B are the constants that define the model. Similarly, there is a linear form of the relationship between the helicopter variables and the output quantities, y , which is written:

$$y = Cx \quad \text{G.1}$$

where C is the output matrix. Differentiating this equation with respect to time and using the model equation gives:

$$\dot{y} = CAx + CBu \quad \text{G.2}$$

However, CB is not invertible since $\det(CB)=0$ so it is necessary to repeat the differentiation to get:

$$\ddot{y} = CA^2x + CABu + CB\dot{u} \quad \text{G.3}$$

1. References for this Appendix are listed in Section G2.

By combining these two last equations, G.2 and G.3, it is possible to arrive at the equation:

$$\bar{y} = \bar{C}x + \bar{D}u \quad G.4$$

where the matrices \bar{C} and \bar{D} are obtained from the original A , B , and C and $\det(\bar{D}) \neq 0$. Equation G.4 can be solved to obtain, for a given x , the control u which will result in the specified output \bar{y} .

$$u = \bar{D}^{-1}(\bar{y} - \bar{C}x) \quad G.5$$

Finally, the transfer function $L(s)$ represents the differentiations etc. required to obtain \bar{y} from y . The inverting feedback specified by Equation G.5 can be identified in the pilot model in Figure G-1.

In the context of the present study, for each specified flight condition a trim state is established and the corresponding linear model obtained using the standard *FLIGHTLAB* facilities. The pilot model is then implemented using the matrix operations available in the *FLIGHTLAB* environment.

G.2 Reference

- [1] Bradley R, Brindley G. 'Synthesis through Constrained Simulation (SyCoS): Phase 1', Final Report ASF/3391, Glasgow Caledonian University, Department of Mathematics, FR/MAT/RB-GB/98-104.

Appendix H Workload Prediction: Wavelets, Spectra and Variances

H.1 Wavelet Analysis

A decomposition of stick, or lever, activity into smooth ramps is used for the current study. A typical control response is shown in Figure H-1. In this case it is the lateral cyclic stick displacement, scaled to the interval $[-1,1]$, during a slalom manoeuvre. Three relatively long scale ramp features in the response are identified on the figure as an illustration. They have approximate amplitude 1 and are centred at times 12, 31 and 35 seconds. The whole manoeuvre takes about 38 seconds and the response contains many ramps of different amplitudes and scales.

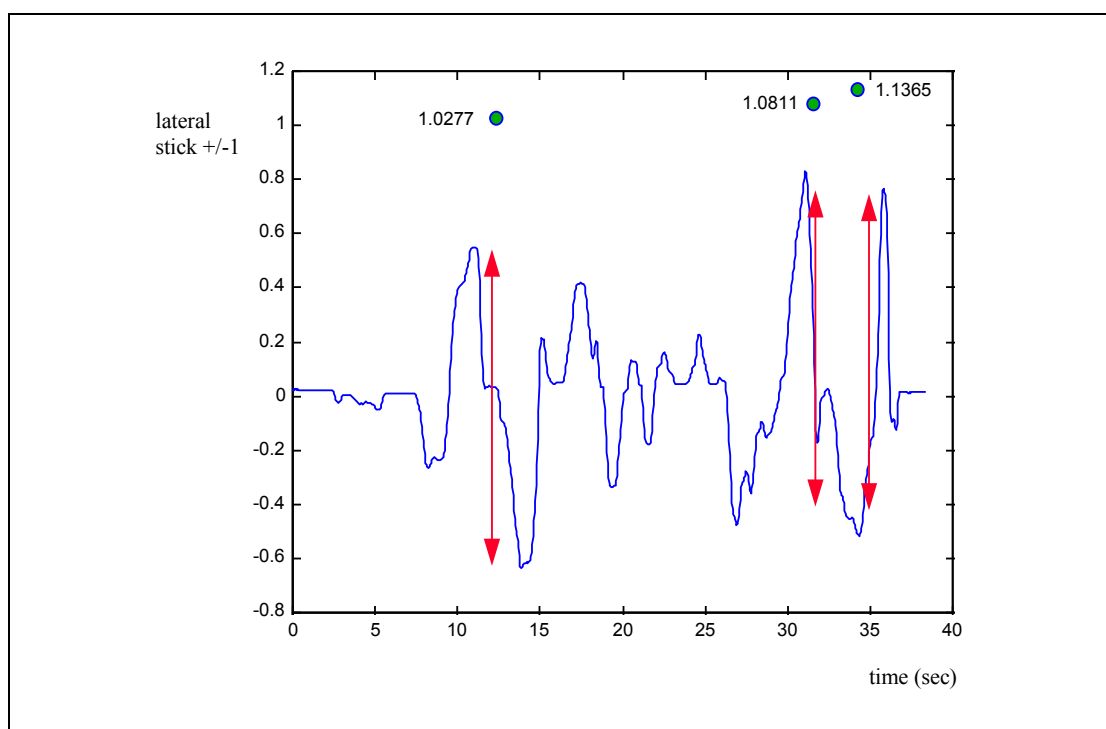


Figure H-1 Lateral Cyclic Stick during Slalom Manoeuvre showing Ramp Features

The results from the decomposition into ramps are presented by plotting the time-scale, l , of each ramp against its amplitude. In fact, the quickness ($2/l$), proportional to the reciprocal of the time-scale is conventionally used since it is a discrete measure of frequency. The complete plot of the ramps in this way is called an attack chart of the control response. The attack chart for the lateral response shown in Figure H-1 is given in Figure H-2.

Each cross on the chart shown in Figure H-2 represents a discrete movement of the lateral cyclic and the three features whose amplitude exceeds 1, marked on Figure H-1, can be identified. Some recent work by MacDonald [1]¹ and Turner [2] have attempted to correlate the distribution of points on this chart with workload by identifying specific quickness intervals with different types of activity. For example, guidance activity (those actions concerned with steering a particular path) are situated in the band of quickness values $[0,2]$ and stabilisation activity lies in the interval $[4,6]$.

1. References for this Appendix are listed in Section H4.

The additional bands [2,4] and [6,10] make four bands in all. Macdonald has employed rule induction with some success and Turner employs an exceedance gradient for each band coupled with special wavelets to detect sequences of actions characterising PIO (pilot induced oscillations) in order to capture accurately high values of workload rating. In the context of the present work, the relevance of bands of quickness values is not justified since the manoeuvring activity should be minimal. Therefore in order to characterise an attack chart such as Figure H-2, a single exceedance chart is derived, showing for every amplitude the logarithm of the number of events which exceed. The exceedance chart corresponding to Figure H-2 is shown in Figure H-3.

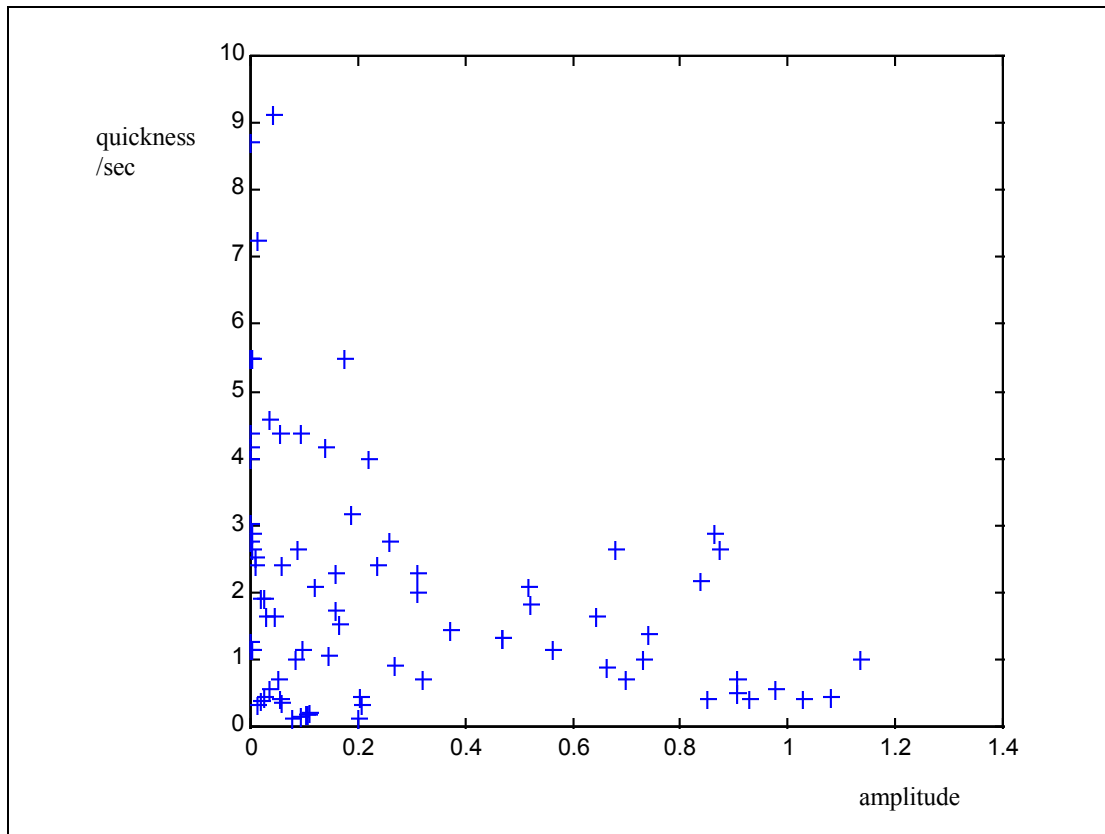


Figure H-2 Attack Chart for Lateral Cyclic Response

The number of actions is normalised to one minute in order to standardise comparisons. The exceedance charts are parameterised by means of the intercept and slope of a straight line fits to the exceedance plot and a sample of sets of values are correlated with the corresponding workload rating to get a best fit of the form:

$$rating = A*m+B*c+C$$

where m and c are the gradient and intercept of the straight line fit. The parameters A, B and C are then available to predict workload ratings from lateral stick control responses from other sources and, in particular, the output of the SyCoS pilot in response to turbulence. The straight-line fits are taken over the amplitude range [0.2,0.8] which was found to give the best results. Also derived, were predictors based on $1/m$, the reciprocal of the gradient but the accuracy of the resulting predictors was little improved.

It should also be noted that the wavelet analysis algorithm is computationally intensive to such an extent that the elapsed time for processing the anticipated programme of simulations would appear to be prohibitive without recourse to developing a more efficient algorithm or investment in superior hardware.

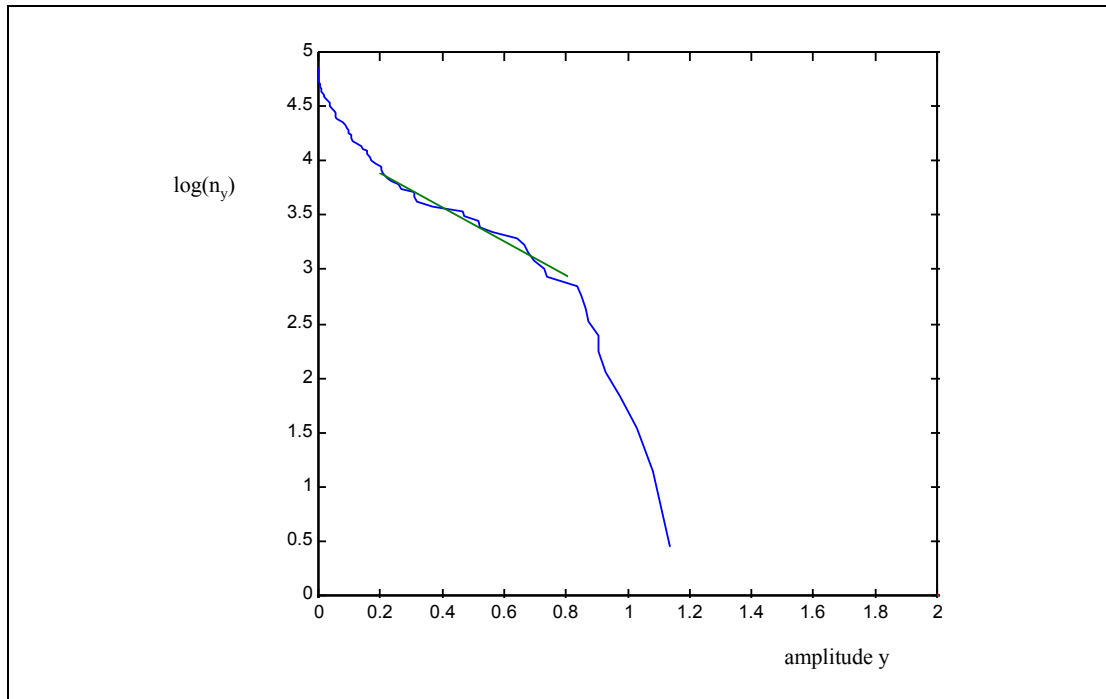


Figure H-3 Exceedance Chart for Lateral Cyclic Stick

H.2 Cut off Frequency

The underlying belief is that as workload increases the pilot is moving the stick at higher frequencies so that a correlation can be established between cut off frequency, f_c and workload. That is, a predictive model of the form:

$$\text{rating} = A f_c + B$$

for constants A and B that give the best fit for the training data.

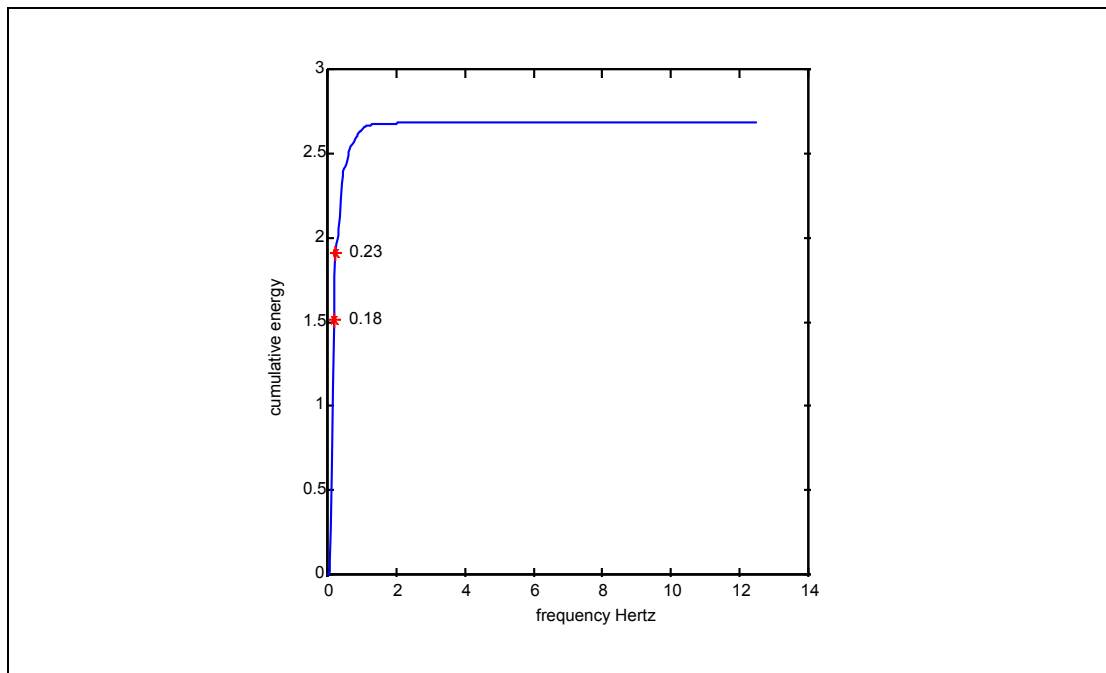


Figure H-4 Spectrum and Cut Off Frequency for Lateral Cyclic Stick

Figure H-4 shows the cut-off frequencies corresponding to both 50% and 70% of the total energy. The frequencies are both low: 0.18 and 0.23 Hertz respectively indicating that a significant proportion of the energy of the stick movement is related to guidance inputs.

H.3 Variance

Another simple metric that can be used to compare energy in a signal, $\eta(t)$, is the standard deviation, $\sigma(\eta)$. Here it was found beneficial to add an additional term $\sigma(\dot{\eta})$, the standard deviation of the time derivative of the signal. The signal mean, $\mu(\eta)$, was also added so that the prediction model took the form:

$$\text{rate} = A\mu(\eta) + B\sigma(\eta) + C\sigma(\dot{\eta}) + D$$

Two versions of this model were investigated. Type 1 set A to zero and looked for best, least squares, fits with only positive constants. Type 2 retained A but used singular value decomposition to eliminate noise caused by overfitting. For a stick response $\eta(t)$, the vector:

$$\underline{x} = \text{row}(1, \text{mean}(\eta), \text{variance}(\eta), \text{variance}(\dot{\eta}))$$

is calculated. The assumed regression, with parameter vector $\underline{\theta}$ has the form:

$$\underline{x} \cdot \underline{\theta} = w$$

where w is the workload rating. Taken over all the associated sample runs - such as all of the slalom data for the lateral stick - gives the matrix equation to be solved for the vector $\underline{\theta}$:

$$X\underline{\theta} = \underline{w}$$

where each row corresponds to a single run. Since there are many more sets of responses than the number of parameters, these equations are typically solved by a least squares approximation. Further, it is not unexpected that the elements of \underline{x} display some inter-dependence and the ratio of the largest and smallest singular values forming the diagonals of S in the decomposition:

$$USV'\underline{\theta} = \underline{w}$$

being typically 10^5 confirms that this is so. Consequently, for each axis, a reduction in the dimension of the parameter space is made and the approximate solution, $\underline{\theta}^*$, is obtained by

$$\underline{\theta}^* = V S^+ U' \underline{w}$$

where

$$S^+ = \begin{bmatrix} 1/s_{11} & 0 & 0 & 0 \\ 0 & 1/s_{22} & 0 & 0 \\ 0 & 0 & 1/s_{33} & 0 \\ 0 & 0 & 0 & 0 \end{bmatrix}$$

This value of $\underline{\theta}^*$ is then used to predict workload ratings on the basis of the vector \underline{x} calculated from the measured control response $\eta(t)$:

$$\underline{x} \cdot \underline{\theta}^* = w.$$

This process is intended to 'clean up' the predictions and eliminate fitting to random errors in the data.

H.4 References

- [1] MacDonald C. *A Methodology for the Prediction of Pilot Workload in Helicopter Manoeuvring Flight*, PhD Thesis, Department of Mathematics, Glasgow Caledonian University, 2001.
- [2] Turner G P, Bradley R, and Brindley G. *Simulation of Pilot Control Activity for the Prediction of Workload Ratings in Helicopter/Ship Operations*. 26th European Rotorcraft Forum, The Hague, September 2000, Paper 91.

Appendix I Wind Tunnel Tests – Part 2 (Brae A)

I.1 Objectives

The objectives of the work were as follows:

- a) To measure simultaneous time histories of the three components of wind velocity on Brae A for the four wind directions studied in Part 1. The directions corresponding to the following obstructions upwind:
 - i) drilling derricks;
 - ii) crane;
 - iii) exhaust stacks; and
 - iv) none.
- b) To ensure that the data collected captured the spatial variations of the turbulence in the wakes of the obstructions.
- c) To ensure that the data collected could be used to represent, as realistically as possible, the variation of wind fluctuations throughout the helicopter rotor disc.
- d) To analyse and present the data in a format suitable for input to the flight simulator.

I.2 Measurement Strategy

I.2.1 Data Acquisition

Simultaneous time histories of the three components of wind velocity were measured using 3 triple hot wire anemometers arranged in an upwind pointing horizontal triangular array. The arrangement is shown in Figure I-1. The radius of the out-scribed circle was set to 5.8m full scale.

The probe triplet was mounted on the computer controlled traverse gear and traversed to prescribed locations at which longitudinal, transverse and vertical components of wind velocity were simultaneously recorded at each probe position. Figure I-2 shows the probes in position.

Time histories of velocity were recorded at a sample rate of 512 Hz for a sampling time of 64 seconds.

I.2.2 Definition of Measurement Arrays

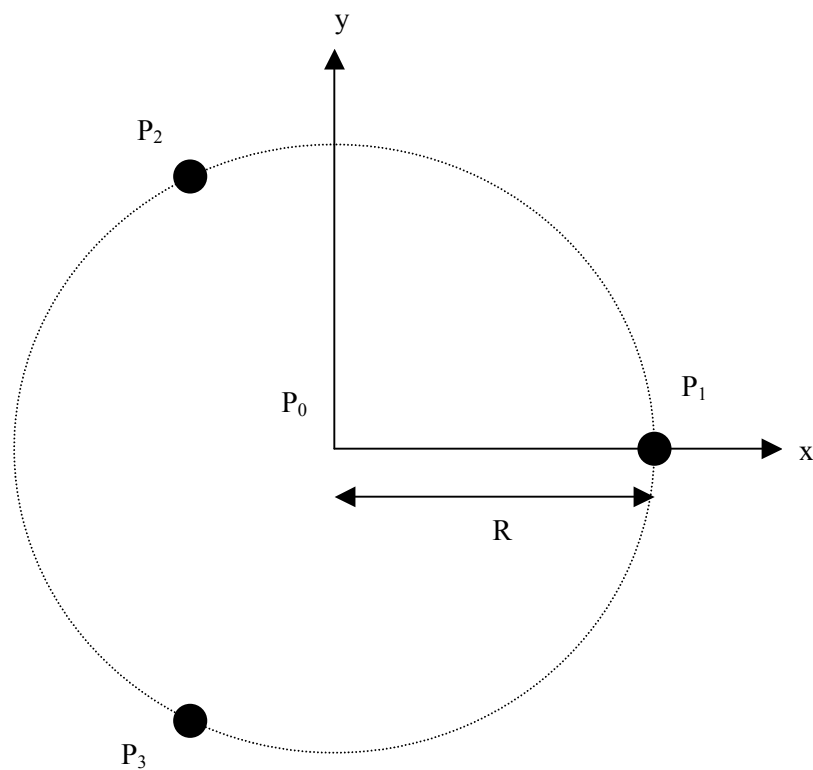
Measurements were taken at locations distributed in arrays extending crosswind in 5m intervals, along wind in 10 m intervals and at heights above the helideck of 5, 10, 20 and 30 m. The disposition of the array varied according to the wind direction under test and which obstruction was upwind. The measurement locations are shown in Figures I-3 to I-6 where the dots denote the position of the centre of the probe array.

Plan view details of the arrays are summarised in the following table.

Obstruction	Outboard	Inboard	Interval	Figure
Derricks	25 m	10 m	5 m	Figure I-3
Exhausts	25 m	10 m	5 m	Figure I-4
Crane	15 m	15 m	5 m	Figure I-5
None	20 m	5 m	5 m	Figure I-6

I.3 Analysis Procedure

I.3.1 Measurement Geometry



The measurement probes are arranged in an equilateral triangle, of radius R , with the first probe in the positive X direction with respect to the centre of the circle.

The coordinates of the probe with respect to the circle centre are therefore given by:

$$P_1 = (R, 0)$$

$$P_2 = \left(-\frac{R}{2}, \frac{\sqrt{3}R}{2} \right)$$

$$P_3 = \left(-\frac{R}{2}, -\frac{\sqrt{3}R}{2} \right)$$

1.3.2 Calculation of Gradients

Suppose that the three probes are used to measure a property α , that has a linear gradient, so that:

$$\alpha(x, y) = \alpha_0 + \beta x + \gamma y$$

Then the measurements at the three probe locations are:

$$\alpha_1 = \alpha_0 + R\beta$$

$$\alpha_2 = \alpha_0 - \frac{1}{2}R\beta + \frac{1}{2}\sqrt{3}R\gamma$$

$$\alpha_3 = \alpha_0 - \frac{1}{2}R\beta - \frac{1}{2}\sqrt{3}R\gamma$$

These three measurements can be used to determine the value and gradient of α at the centre of the measurement circle:

$$\alpha_0 = \frac{1}{3}(\alpha_1 + \alpha_2 + \alpha_3)$$

$$\beta = \frac{1}{3R}(2\alpha_1 - \alpha_2 - \alpha_3)$$

$$\gamma = \frac{1}{\sqrt{3}R}(\alpha_2 - \alpha_3)$$

1.3.3 Wind Velocity and Wind Shear

The above expressions are true irrespective of what parameter is being measured. In particular, they are applicable to the (U , V , W) components of flow velocity, and their corresponding shears in the x and y directions. The corresponding expressions are:

$$U_0 = \frac{1}{3}(U_1 + U_2 + U_3)$$

$$A = \frac{\partial U}{\partial x} = \frac{1}{3a}(2U_1 - U_2 - U_3)$$

$$B = \frac{\partial U}{\partial y} = \frac{1}{\sqrt{3}a}(U_2 - U_3)$$

$$V_0 = \frac{1}{3}(V_1 + V_2 + V_3)$$

$$C = \frac{\partial V}{\partial x} = \frac{1}{3a}(2V_1 - V_2 - V_3)$$

$$D = \frac{\partial V}{\partial y} = \frac{1}{\sqrt{3}a}(V_2 - V_3)$$

$$W_0 = \frac{1}{3}(W_1 + W_2 + W_3)$$

$$E = \frac{\partial W}{\partial x} = \frac{1}{3a}(2W_1 - W_2 - W_3)$$

$$F = \frac{\partial W}{\partial y} = \frac{1}{\sqrt{3}a}(W_2 - W_3)$$

In practice the flow over the measured region will be more complex than the assumed linear shear. However, the above expressions will give a reasonable approximation, averaged over the measurement area.

The results of this analysis should be considered to be point measurements of the flow velocity and flow shear at the centre of the probe array.

I.4 Helicopter Loading

I.4.1 Calculations of loads on Helicopter Rotor

If the wind velocity and wind shear at the centre of the rotor are known, then the velocity at any point on the rotor disc can be estimated as follows (in Cartesian coordinates centred on the rotor hub):

$$U = U_0 + Ax + By$$

$$V = V_0 + Cx + Dy$$

$$W = W_0 + Ex + Fy$$

Or in polar coordinates:

$$U = U_0 + Ar \cos(\theta) + Br \sin(\theta)$$

$$V = V_0 + Cr \cos(\theta) + Dr \sin(\theta)$$

$$W = W_0 + Er \cos(\theta) + Fr \sin(\theta)$$

If it is required to have radial and axial velocities:

$$U_r = U_0 \cos(\theta) + V_0 \sin(\theta) + Ar \cos^2(\theta) + (B + C)r \sin(\theta)\cos(\theta) + Dr \sin^2(\theta)$$

$$U_\theta = -U_0 \sin(\theta) + V_0 \cos(\theta) - Br \sin^2(\theta) + (D - A)r \sin(\theta)\cos(\theta) + Cr \cos^2(\theta)$$

$$W = W_0 + Er \cos(\theta) + Fr \sin(\theta)$$

It should be noted that each of the flow components (velocity or shear) are assumed to be perfectly correlated across the area of the rotor blade, and will result in a force and/or moment. There will be no force cancellation due to uncorrelated flow at different locations on the rotor. However, the velocity and shear measurements will represent an average over the area of the measurement array.

I.4.2 Interpolation for Helicopter Position

During the free flight simulations (as opposed to hover simulations), the position of the rotor hub will not in general correspond to a measurement position. In this case it is necessary to interpolate the wind velocity and wind shear for locations between the measurement grid points.

The interpolation should correctly represent the variation of both mean flow and of turbulence intensity with location. This requires different interpolation for the mean flow, and for the velocity fluctuations.

The wind velocity (and wind shear) at any location is assumed to consist of two components, a mean flow, and a fluctuating component. For example:

$$U(t) = \bar{U} + u(t)$$

It is assumed that the fluctuating components at two adjacent locations are uncorrelated. It is believed that the grid spacing is sufficiently large that there is no

actual correlation in the air flow over this distance. Even if there should be some correlation between adjacent points, the measurement system is not capable of measuring it.

Between grid points, the mean flow is estimated by simple linear interpolation. Suppose that the fluctuating velocity is also calculated as a linear combination of the velocities at the two grid points:

$$u = \lambda_1 u_1 + \lambda_2 u_2$$

Then the turbulence intensity at the intermediate point is given by:

$$\begin{aligned} E[u^2] &= E[\lambda_1^2 u_1^2 + 2\lambda_1 \lambda_2 u_1 u_2 + \lambda_2^2 u_2^2] \\ &= \lambda_1^2 E[u_1^2] + 2\lambda_1 \lambda_2 E[u_1 u_2] + \lambda_2^2 E[u_2^2] \\ &= \lambda_1^2 E[u_1^2] + \lambda_2^2 E[u_2^2] \end{aligned}$$

Thus in order to prevent a dip in turbulence intensity between the grid points it is necessary that:

$$\lambda_1^2 + \lambda_2^2 = 1$$

And in order to provide a linear interpolation in turbulence intensity for a position that is a fraction ξ from point 1 to point 2:

$$\begin{aligned} \lambda_1^2 &= 1 - \xi \\ \lambda_2^2 &= \xi \end{aligned}$$

These expressions apply in three dimensions, and for each component of the flow velocity and flow shear: Thus for a point (x, y, z) within the grid, such that:

$$x_i \leq x \leq x_{i+1}$$

$$y_j \leq y \leq y_{j+1}$$

$$z_k \leq z \leq z_{k+1}$$

The linear interpolation factors are given by:

$$\xi = \frac{x - x_i}{x_{i+1} - x_i}$$

$$\eta = \frac{y - y_j}{y_{j+1} - y_j}$$

$$\zeta = \frac{z - z_k}{z_{k+1} - z_k}$$

And then the interpolated U component of velocity at the point is given by:

$$\begin{aligned}
U(x, y, z, t) = & (1-\xi)(1-\eta)(1-\zeta)\bar{U}_{i,j,k} + \sqrt{(1-\xi)(1-\eta)(1-\zeta)} u_{i,j,k}(t) \\
& + (1-\xi)(1-\eta)\zeta\bar{U}_{i,j,k+1} + \sqrt{(1-\xi)(1-\eta)\zeta} u_{i,j,k+1}(t) \\
& + (1-\xi)\eta(1-\zeta)\bar{U}_{i,j+1,k} + \sqrt{(1-\xi)\eta(1-\zeta)} u_{i,j+1,k}(t) \\
& + (1-\xi)\eta\zeta\bar{U}_{i,j+1,k+1} + \sqrt{(1-\xi)\eta\zeta} u_{i,j+1,k+1}(t) \\
& + \xi(1-\eta)(1-\zeta)\bar{U}_{i+1,j,k} + \sqrt{\xi(1-\eta)(1-\zeta)} u_{i+1,j,k}(t) \\
& + \xi(1-\eta)\zeta\bar{U}_{i+1,j,k+1} + \sqrt{\xi(1-\eta)\zeta} u_{i+1,j,k+1}(t) \\
& + \xi\eta(1-\zeta)\bar{U}_{i+1,j+1,k} + \sqrt{\xi\eta(1-\zeta)} u_{i+1,j+1,k}(t) \\
& + \xi\eta\zeta\bar{U}_{i+1,j+1,k+1} + \sqrt{\xi\eta\zeta} u_{i+1,j+1,k+1}(t)
\end{aligned}$$

Similar expressions apply to the V and W velocity components, and the shear terms (A-F).

I.5 Output Format of Results

Results were formatted into single column ASCII data files containing simultaneous time histories of the following parameters:

- a) Longitudinal velocity.
- b) Lateral velocity.
- c) Vertical velocity.
- d) Along wind gradient of longitudinal velocity.
- e) Along wind gradient of lateral velocity.
- f) Along wind gradient of vertical velocity.
- g) Crosswind gradient of longitudinal velocity.
- h) Crosswind gradient of lateral velocity.
- i) Crosswind gradient of vertical velocity.

Individual files were generated for each parameter and for each measurement location resulting in 4,356 files and a total of approximately 740 Mb of data.

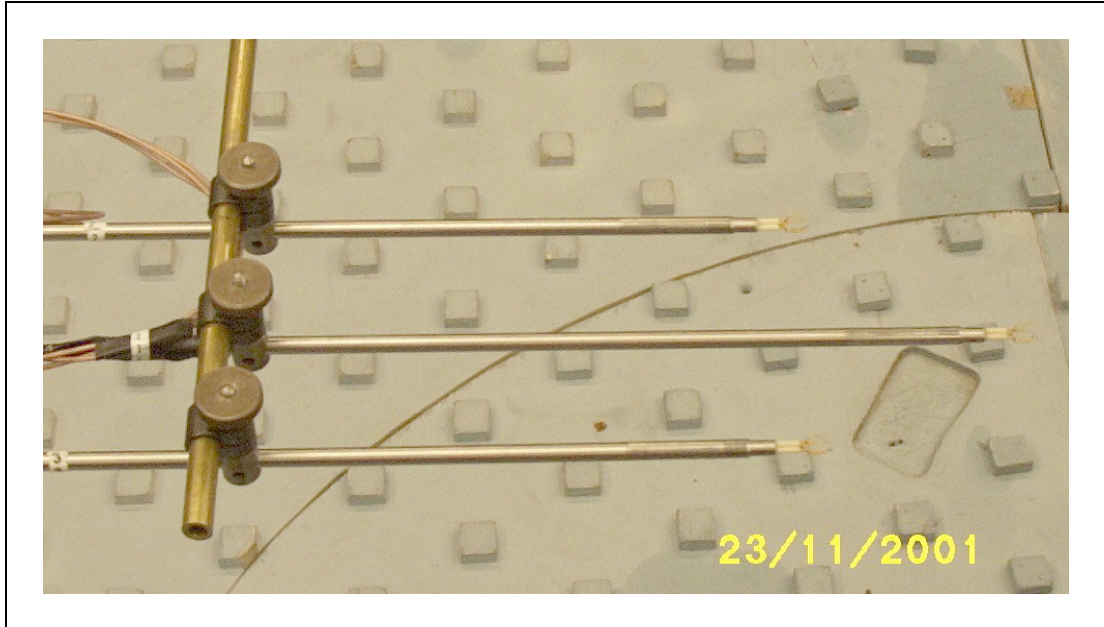


Figure I-1 Close up View of the Triplet of Three Component Hot Wire Probes (Wind Blowing from Right to Left)

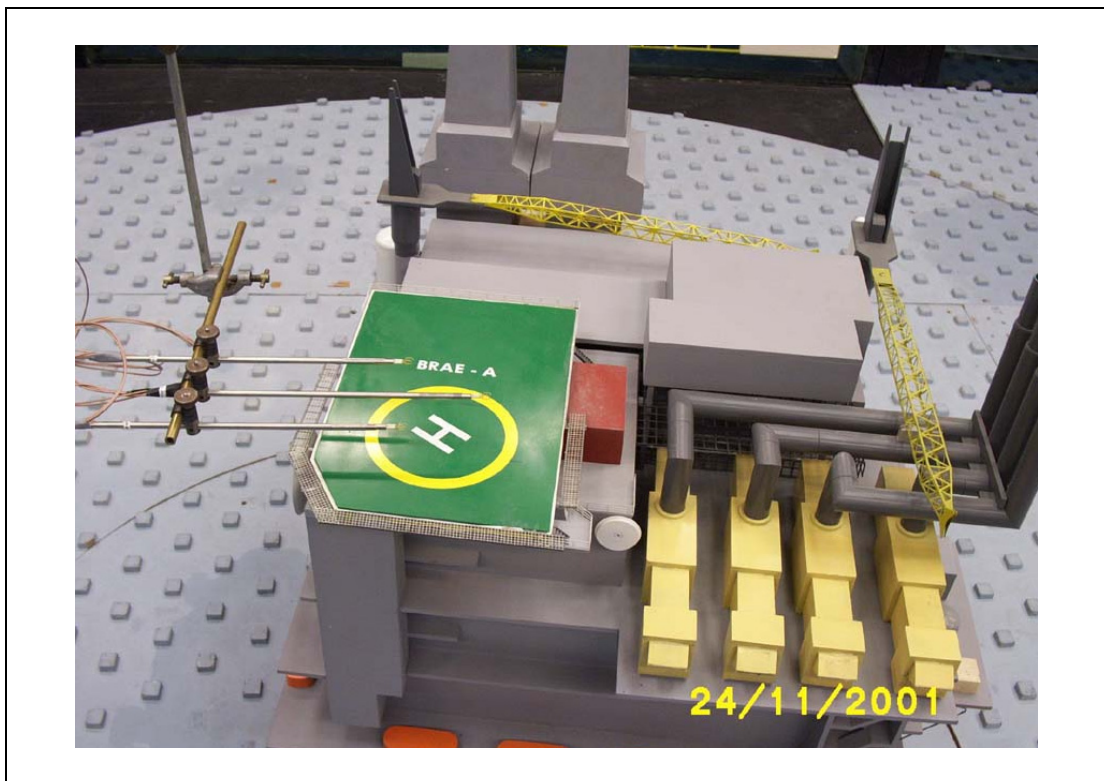


Figure I-2 Hot Wire Probes Located Above the Helideck for Exhaust Obstruction Configuration (Wind Blowing from Right to Left)

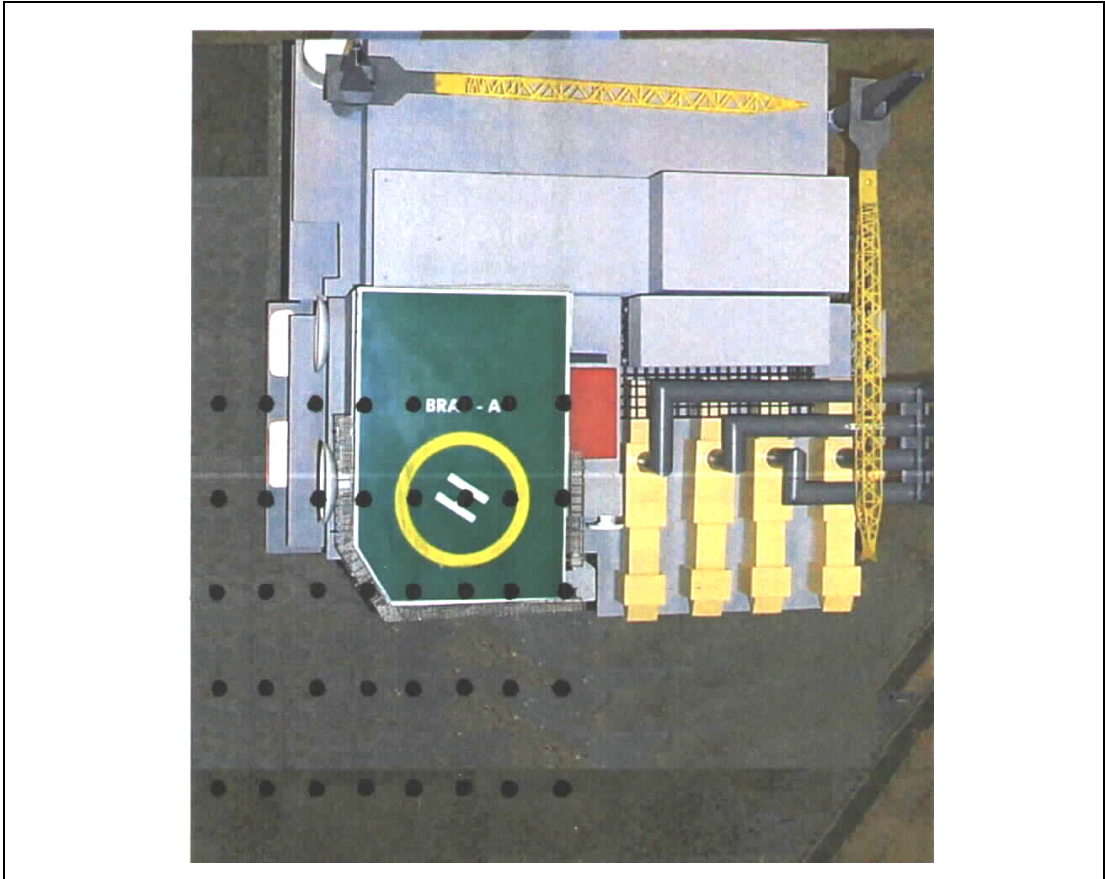


Figure I-3 Measurement Locations with Drilling Derricks Upwind

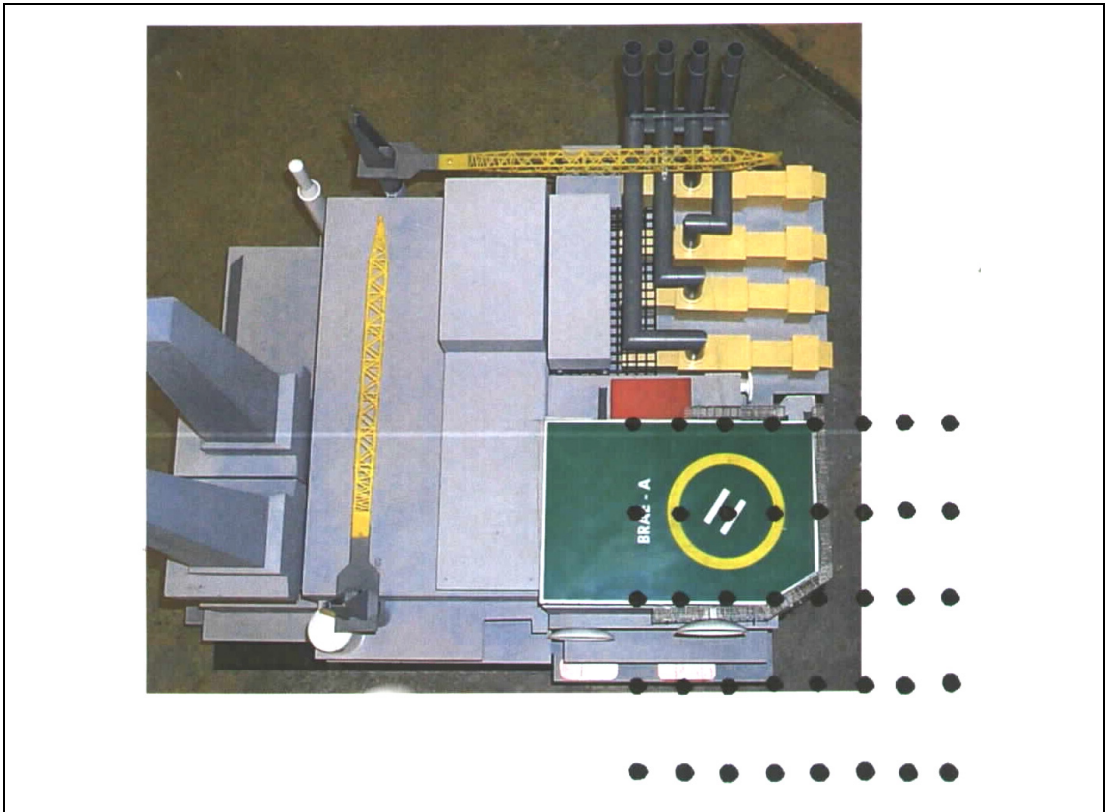


Figure I-4 Measurement Locations with Gas Turbine Exhausts Upwind

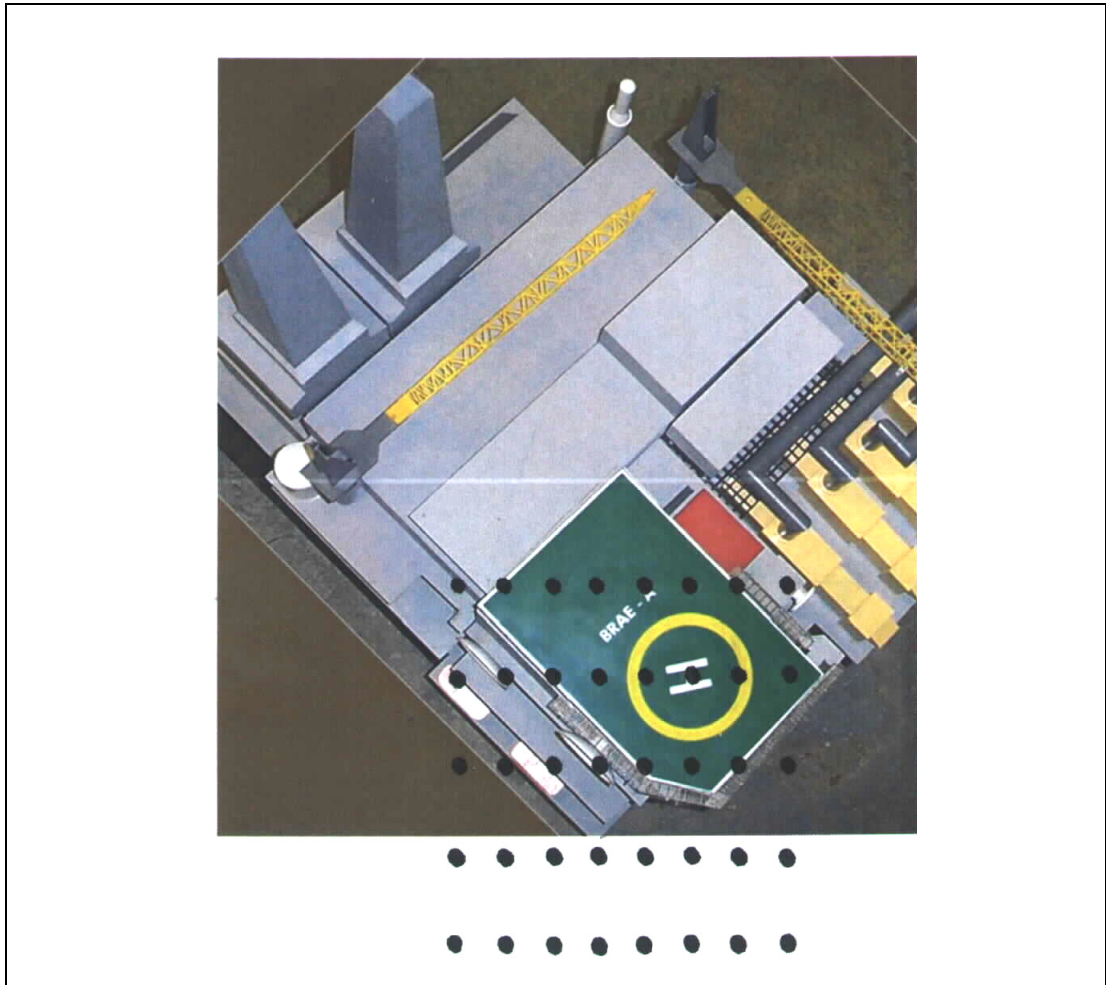


Figure I-5 Measurement Locations with Crane Upwind



Figure I-6 Measurement Locations with No Obstructions Upwind

Appendix J Derivation of HQR Predictors from BRAE01 Trial

This appendix describes the calculation of Handling Qualities Rating (HQR) predictors from the pilot awarded ratings and measured control activity during the BRAE01 trial.

BRAE01 provided 29 runs where control activity could be correlated with the HQRs awarded by the pilot over a realistic range of wind speeds and turbulence levels induced by platform obstructions. The trial covered a realistic range of turbulent conditions to give a spread of HQRs in the range 3-7.

J.1 Metrics

The metrics calculated from the responses were:

metric	symbol	calculation	rationale
mean	μ	MATLAB function <i>mean</i>	The mean position measures the offset of the control from a null position and implicitly contains control margin information
standard deviation	σ	MATLAB function <i>std</i>	The standard deviation is a measure of the general level of activity from the mean position
standard deviation of stick/lever rate	σ^*	MATLAB function <i>std(diff)</i> divided by sample time	The standard deviation of the rate is a measure of the overall speed of activity

These were calculated for:

Control	Range	Symbol
Lateral stick	[-1,1]	ξ
Longitudinal stick	[-1,1]	η
Collective lever	[0,1]	θ_0

Metrics for the pedal activity were not calculated because they were not employed in the original HQR predictions derived from Mission Task Element data.

J.2 Predictors

A predictor is a coefficient vector \underline{c} that relates the metrics above to the HQR awarded by the pilot: that is:

$$r = c_1 + c_2 \sigma(\xi) + c_3 \sigma^*(\xi) + c_4 \sigma(\eta) + c_5 \sigma^*(\eta) + c_6 \sigma(\theta_0) + c_7 \sigma^*(\theta_0).$$

where the mean, μ , is omitted from this representation because investigations have shown that its contribution was not significant.

The data from the BRAE01 trial leads to the matrix equation of the form:

$$X\mathbf{c}=\mathbf{r}+\mathbf{e},$$

where X is the m by n matrix of the n metrics from the m runs, \mathbf{r} is the vector of ratings and \mathbf{e} is an error vector. The matrix X is factored in singular value decomposition into:

$$X=USV'$$

where U and V are orthogonal matrices and S is m by n and non-zero only in the diagonal elements which contain the singular values s_i . The decomposition algorithm produces singular values that are ordered in reducing magnitude. Small values indicate a rank deficiency in the original data, and a need to avoid over-fitting to supplied data.

The error is minimised in the least square sense by writing:

$$\mathbf{c}=VS^+U'\mathbf{r}$$

where S^+ is n by m with diagonal elements $1/s_i$.

If s_i is zero or small then $1/s_i$ is replaced by zero. This removal of small singular values eliminates noise from the process and allows a more generalised fit. In practice, a sudden change from large to small singular values is not often observed and some judgement must take place about how many to retain.

In the present work a full set of coefficients was calculated corresponding to retaining 1 to 7 singular values. Each singular value represents a linear combination of the raw variables ($\sigma(\xi)$, $\sigma^*(\xi)$, $\sigma(\eta)$, $\sigma^*(\eta)$, $\sigma(\theta_0)$ and $\sigma^*(\theta_0)$) that is independent from other singular values providing orthogonality. For each increase in the order of the solution the number of retained singular values is increased by one. However, the composition of each singular value in terms of the raw variables will change with each successive change to the solution order and hence the coefficients can not be expected to be similar for different orders of solution. The trade off is that a better fit to the BRAE01 data brings in smaller singular values which compromise the future use of the coefficients as predictors. Having determined a predictor vector \mathbf{c} , a vector of control activity metrics \mathbf{m} is converted into the predicted HQR, r^* , by the product:

$$r^*=\mathbf{c}'\mathbf{m}$$

For the present work Table J-1 shows the full set of predictors obtained for the BRAE01 data and highlights the order 5 set which was used for subsequent work, the BRAE02 trial in particular. The final choice was between the order 4 and 5 sets that provide a similar quality of fit to the BRAE01 data as indicated by the correlation coefficients of 0.8808 and 0.8849 respectively. It was also noted that the order 3 set had entirely positive values which may be beneficial for wider application. Here the choice to opt for a higher order was made in order to better fit the higher rated cases. The negative entries in Table J-1 can legitimately arise from fitting the data within the range of HQRs and control activity metrics in the BRAE01 training set. Essentially the process is interpolation and consequently needs to be used with care outside the range of interpolation (for example in higher turbulence levels or a significantly different helicopter type). Fitting to random variations in the data (over-fitting) may also lead to negative values and that is why the full order predictor is seldom used.

Table J-1 Full predictor set for trial BRAE01

Order	1	2	3	4	5	6	7
c ₁	4.1832	1.8924	1.8978	2.0971	2.1238	1.3434	0.7878
c ₂	0.2434	1.0325	1.4531	1.5840	0.6240	9.7234	46.5698
c ₃	1.1954	6.0130	7.4460	7.5999	7.2237	5.9211	-2.3776
c ₄	0.1961	0.7600	0.3611	0.3568	-.7879	65.4232	60.3412
c ₅	0.9879	4.4560	2.5453	2.2804	0.8214	-12.4400	-9.6098
c ₆	0.3168	-.3030	0.1992	-1.4695	- 4.7042	-5.2539	-5.1046
c ₇	0.3875	1.1395	1.0590	0.3926	8.8116	16.2860	19.9755

Table J-1 is full, i.e. there are non-zero entries for the predictor vector \underline{c} for all orders because of the way the singular value decomposition approach works. It takes the best linear combination of the metrics for each order of approximation.

The initial equation:

$$X\underline{c} = \underline{r} + \underline{e}$$

is written as:

$$USV'\underline{c} = \underline{r} + \underline{e}$$

or:

$$SV'\underline{c} = U'(\underline{r} + \underline{e})$$

(Since U and V are orthogonal, the inverse is simply the transpose.) The equations are orthogonalised by writing:

$$\underline{c}^* = V'\underline{c}$$

so that:

$$S\underline{c}^* = U'(\underline{r} + \underline{e})$$

Since S is diagonal (non-zero elements only on the diagonal - the singular values) this system is easily solved, setting \underline{e} to zero, for each number of singular values retained. For example, if only the first is retained then c^*_1 can be found and the rest of the elements are zero; if two then c^*_2 can also be found. Because:

$$\underline{c} = V\underline{c}^*,$$

the vector \underline{c} is potentially full at each stage even though \underline{c}^* is filled with values only incrementally.

J.3 Comparison of Predicted and Awarded HQRs

Figure J-1 shows the relationship between the actual HQRs and those calculated from the selected predictors. The figure plots $X\underline{c}$ against \underline{r} .

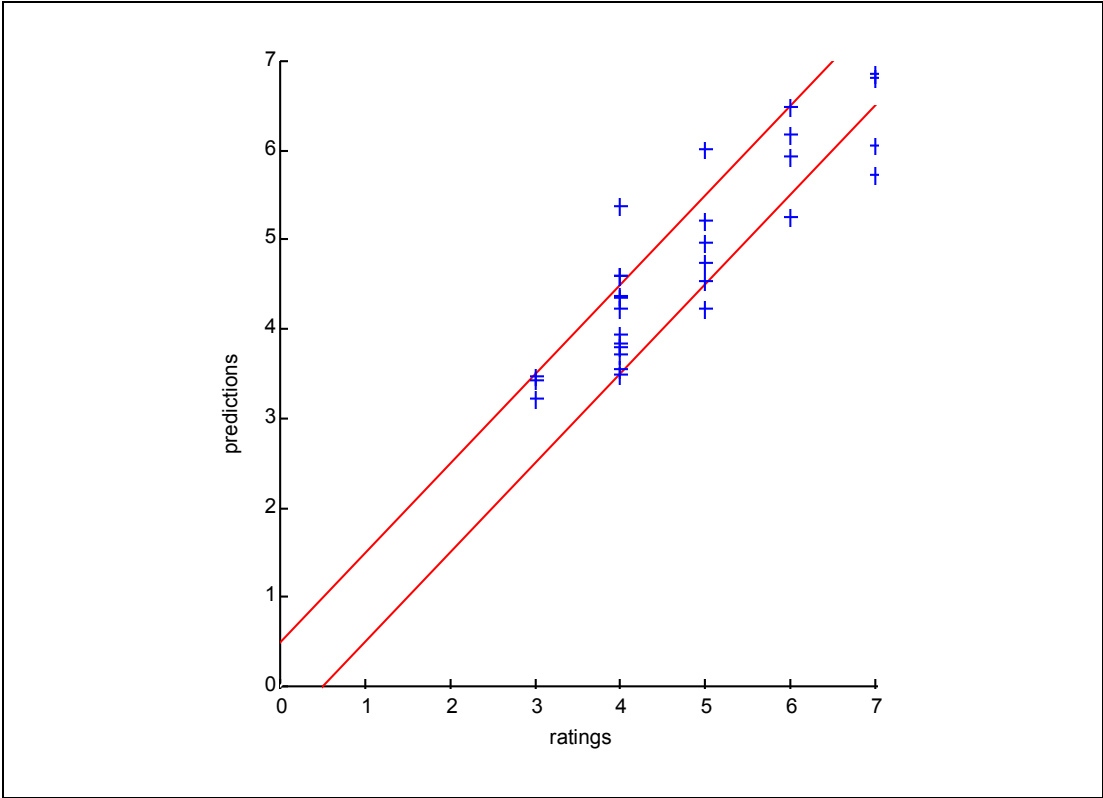


Figure J-1 Comparison of Predictors against Ratings for 5 Retained Singular Values

Appendix K Simulator Test Schedule

K.1 BRAE01 and BRAE02

	Weight (lb)	Obstruction	Wind	Task
1	10,510	None	272°/15 kt	Hover
2	10,510	None	272°/25 kt	Hover
3	10,510	None	272°/35 kt	Hover
4	10,510	None	272°/50 kt	Hover
5	10,510	None	272°/60 kt	Hover
6	10,510	Cranes	050°/15 kt	Hover
7	10,510	Cranes	050°/25 kt	Hover
8	10,510	Cranes	050°/35 kt	Hover
9	10,510	Cranes	050°/50 kt	Hover
10	10,510	Cranes	050°/60 kt	Hover
11	10,510	Exhaust stacks	088°/15 kt	Hover
12	10,510	Exhaust stacks	088°/25 kt	Hover
13	10,510	Exhaust stacks	088°/35 kt	Hover
14	10,510	Exhaust stacks	088°/50 kt	Hover
15	10,510	Exhaust stacks	088°/60 kt	Hover
16	10,510	Derricks	001°/15 kt	Hover
17	10,510	Derricks	001°/25 kt	Hover
18	10,510	Derricks	001°/35 kt	Hover
19	10,510	Derricks	001°/50 kt	Hover
20	10,510	Derricks	001°/60 kt	Hover
21	9,510	Derricks	001°/15 kt	Hover
22	9,510	Derricks	001°/25 kt	Hover
23	9,510	Derricks	001°/35 kt	Hover
24	9,510	Derricks	001°/50 kt	Hover
25	9,510	Derricks	001°/60 kt	Hover
26	9,910	Exhaust stacks	088°/15 kt	Hover
27	9,910	Exhaust stacks	088°/25 kt	Hover
28	9,910	Exhaust stacks	088°/35 kt	Hover
29	9,910	Exhaust stacks	088°/50 kt	Hover
30	9,910	Exhaust stacks	088°/60 kt	Hover
31	10,510	Derricks	001°/15 kt	Hover 329°
32	10,510	Derricks	001°/25 kt	Hover 336°
33	10,510	Derricks	001°/35 kt	Hover 338°
34	10,510	Derricks	001°/50 kt	Hover 341°
35	10,510	Derricks	001°/60 kt	Hover 341°
36	9,510	Derricks	001°/15 kt	Hover 329°
37	9,510	Derricks	001°/35 kt	Hover 338°
38	9,510	Derricks	001°/60 kt	Hover 341°

K.2 BRAE02 only

Case	Weight (lb)	Obstruction	Wind	Task
39	10,510	Derricks	001°/15 kt	Approach
40	10,510	Derricks	001°/25 kt	Approach
41	10,510	Derricks	001°/35 kt	Approach
42	10,510	Derricks	001°/50 kt	Approach
43	10,510	Derricks	001°/60 kt	Approach

Appendix L Wind Tunnel Measurement Grid

CAA

BRAE A

Wind angle = derricks

Z=100

+ve X = downwind

+ve Y = to the left looking downwind

all dimensions in model mm (model scale = 100)

	towards console		Y			away from console			
X	-100	-50	0	50	100	150	200	250	
-100	17	16	15	18	19	20	21	22	
0	9	8	7	10	11	12	13	14	
100	25	24	23	28	29	30	31	32	
200	35	34	33	36	37	38	39	40	
300	43	42	41	44	45	46	47	48	

Z=200

	towards console		Y			away from console			
X	-100	-50	0	50	100	150	200	250	
-100	59	58	57	60	61	62	63	64	
0	51	50	49	52	53	54	55	56	
100	68	67	66	69	70	71	72	73	
200	76	75	74	77	78	79	80	81	
300	84	83	82	85	86	87	88	89	

Z=300

	towards console		Y			away from console			
X	-100	-50	0	50	100	150	200	250	
-100	100	99	98	101	102	103	104	105	
0	92	91	90	93	94	95	96	97	
100	108	107	106	109	110	111	112	113	
200	116	115	114	117	118	119	120	121	
300	124	123	122	125	126	127	128	129	

Z=50

	towards console		Y			away from console			
X	-100	-50	0	50	100	150	200	250	
-100	140	139	138	141	142	143	144	145	
0	132	131	130	133	134	135	136	137	
100	148	147	146	149	150	151	152	153	
200	156	155	154	157	158	159	160	161	
300	164	163	162	165	166	167	168	169	

CAA
BRAE A
Wind angle = exhausts

Z=100

	towards console		Y			away from console			
X	-250	-200	-150	-100	-50	0	50	100	
-100	216	217	218	219	220	221	222	223	
0	215	214	213	212	211	210	225	224	
100	233	232	231	230	229	228	227	226	
200	234	235	236	237	238	239	240	241	
300	249	248	247	246	245	244	243	242	

Z=200

	towards console		Y			away from console			
X	-250	-200	-150	-100	-50	0	50	100	
-100	261	260	259	258	259	254	253	252	
0	262	263	264	265	266	267	268	269	
100	277	276	275	274	273	272	271	270	
200	278	279	280	281	282	283	284	285	
300	293	292	291	290	289	288	287	286	

Z=300

	towards console		Y			away from console			
X	-250	-200	-150	-100	-50	0	50	100	
-100	302	301	300	299	298	297	296	295	
0	303	304	305	306	307	308	309	310	
100	318	317	316	315	314	313	312	311	
200	319	320	321	322	323	324	325	326	
300	334	333	332	331	330	329	328	327	

Z=50

	towards console		Y			away from console			
X	-250	-200	-150	-100	-50	0	50	100	
-100	183	182	181	180	179	178	184	185	
0	175	174	173	172	171	250	176	177	
100	191	190	189	188	187	186	192	193	
200	199	198	197	196	195	194	200	201	
300	207	206	205	204	203	202	208	209	

CAA
BRAE A
Wind angle = crane

Z=100

	towards console		Y		away from console		
X	-150	-100	-50	0	50	100	150
-100	445	444	443	442	446	447	448
0	438	437	436	435	439	440	441
100	452	451	450	449	453	454	455
200	459	458	457	456	460	461	462
300	466	465	464	463	467	468	469

Z=200

	towards console		Y		away from console		
X	-150	-100	-50	0	50	100	150
-100	481	480	479	478	482	483	484
0	474	473	472	471	475	476	477
100	488	487	486	485	489	490	491
200	495	494	493	492	496	497	498
300	502	501	500	499	503	504	505

Z=300

	towards console		Y		away from console		
X	-150	-100	-50	0	50	100	150
-100	517	516	515	514	518	519	520
0	510	509	508	507	511	512	513
100	527	526	525	524	528	529	530
200	534	533	532	531	535	536	537
300	541	540	539	538	542	543	544

Z=50

	towards console		Y		away from console		
X	-150	-100	-50	0	50	100	150
-100	343	344	345	346	347	348	349
0	342	341	340	339	338	337	336
100	356	355	354	353	352	351	350
200	357	358	359	360	361	362	363
300	370	369	368	367	366	365	364

CAA
BRAE A
Wind angle = unobstructed

Z=100

	towards console		Y		away from console	
X	-50	0	50	100	150	200
-100						
0	567	554	553	552	551	550
100						
200						
300						

Z=200

	towards console		Y		away from console	
X	-50	0	50	100	150	200
-100						
0	566	555	556	557	558	559
100						
200						
300						

Z=300

	towards console		Y		away from console	
X	-50	0	50	100	150	200
-100						
0	565	564	563	562	561	560
100						
200						
300						

Z=50

	towards console		Y		away from console	
X	-50	0	50	100	150	200
-100						
0	568	545	546	547	548	549
100						
200						
300						

Appendix M Simulator Trial Results – BRAE01 and BRAE02

Table M-1 Results from BRAE01

Case	Weight (lb)	Obstruction	Wind	Task	Pilot Ratings		
					Pilot A	Pilot B	Pilot C
1	10,510	None	272°/15 kt	Hover	4		
2	10,510	None	272°/25 kt	Hover	4		
3	10,510	None	272°/35 kt	Hover	5		
4	10,510	None	272°/50 kt	Hover	5		
5	10,510	None	272°/60 kt	Hover	4		
6	10,510	Cranes	050°/15 kt	Hover	3		
7	10,510	Cranes	050°/25 kt	Hover	4		
8	10,510	Cranes	050°/35 kt	Hover	5		
9	10,510	Cranes	050°/50 kt	Hover	5		
10	10,510	Cranes	050°/60 kt	Hover	7		
11	10,510	Exhausts	088°/15 kt	Hover	3		
12	10,510	Exhausts	088°/25 kt	Hover	4		
13	10,510	Exhausts	088°/35 kt	Hover	4		
14	10,510	Exhausts	088°/50 kt	Hover	5		
15	10,510	Exhausts	088°/60 kt	Hover	6		
16	10,510	Derricks	001°/15 kt	Hover	3		
17	10,510	Derricks	001°/25 kt	Hover	not run		
18	10,510	Derricks	001°/35 kt	Hover	4		
19	10,510	Derricks	001°/50 kt	Hover	6		
20	10,510	Derricks	001°/60 kt	Hover	6		
21	9,510	Derricks	001°/15 kt	Hover	not run		
22	9,510	Derricks	001°/25 kt	Hover	not run		
23	9,510	Derricks	001°/35 kt	Hover	not run		
24	9,510	Derricks	001°/50 kt	Hover	not run		
25	9,510	Derricks	001°/60 kt	Hover	7		
26	9,910	Exhausts	088°/15 kt	Hover	not run		
27	9,910	Exhausts	088°/25 kt	Hover	4		
28	9,910	Exhausts	088°/35 kt	Hover	not run		
29	9,910	Exhausts	088°/50 kt	Hover	not run		
30	9,910	Exhausts	088°/60 kt	Hover	5		
31	10,510	Derricks	001°/15 kt	Hover 329°	6		
31 rpt	10,510	Derricks	001°/15 kt	Hover 329°	4		
32	10,510	Derricks	001°/25 kt	Hover 336°	4		
33	10,510	Derricks	001°/35 kt	Hover 338°	4		
34	10,510	Derricks	001°/50 kt	Hover 341°	7		
35	10,510	Derricks	001°/60 kt	Hover 341°	7		
36	9,510	Derricks	001°/15 kt	Hover 329°	not run		
37	9,510	Derricks	001°/35 kt	Hover 338°	not run		
38	9,510	Derricks	001°/60 kt	Hover 341°	4		

Table M-2 Results from BRAE02 - Hover Task

Case	Weight (lb)	Obstruction	Wind	Task	Pilot Ratings		
					Pilot A	Pilot B	Pilot C
1	10,510	None	272°/15 kt	Hover	4	3	4
2	10,510	None	272°/25 kt	Hover	4	not run	5
3	10,510	None	272°/35 kt	Hover	5	4	6
4	10,510	None	272°/50 kt	Hover	not run	not run	not run
5	10,510	None	272°/60 kt	Hover	6	not run	7
6	10,510	Cranes	050°/15 kt	Hover	4	not run	4
7	10,510	Cranes	050°/25 kt	Hover	5	4	4
8	10,510	Cranes	050°/35 kt	Hover	5	4	4
9	10,510	Cranes	050°/50 kt	Hover	6	5	6
10	10,510	Cranes	050°/60 kt	Hover	8	5	7
11	10,510	Exhausts	088°/15 kt	Hover	4	3	4
12	10,510	Exhausts	088°/25 kt	Hover	5	3	5
13	10,510	Exhausts	088°/35 kt	Hover	6	4	6
14	10,510	Exhausts	088°/50 kt	Hover	7	5	5
15	10,510	Exhausts	088°/60 kt	Hover	not run	5	6
16	10,510	Derricks	001°/15 kt	Hover	4	3	4
17	10,510	Derricks	001°/25 kt	Hover	6	4	5
18	10,510	Derricks	001°/35 kt	Hover	6	4	6
19	10,510	Derricks	001°/50 kt	Hover	7	6	7
20	10,510	Derricks	001°/60 kt	Hover	9	7	7
21	9,510	Derricks	001°/15 kt	Hover	not run	not run	not run
22	9,510	Derricks	001°/25 kt	Hover	not run	not run	not run
23	9,510	Derricks	001°/35 kt	Hover	not run	not run	not run
24	9,510	Derricks	001°/50 kt	Hover	not run	not run	not run
25	9,510	Derricks	001°/60 kt	Hover	not run	not run	not run
26	9,910	Exhausts	088°/15 kt	Hover	not run	not run	not run
27	9,910	Exhausts	088°/25 kt	Hover	4	not run	not run
28	9,910	Exhausts	088°/35 kt	Hover	not run	not run	not run
29	9,910	Exhausts	088°/50 kt	Hover	not run	not run	not run
30	9,910	Exhausts	088°/60 kt	Hover	8	not run	not run
31	10,510	Derricks	001°/15 kt	Hover 329°	5	not run	4
32	10,510	Derricks	001°/25 kt	Hover 336°	5	5	6
33	10,510	Derricks	001°/35 kt	Hover 338°	5	not run	4
34	10,510	Derricks	001°/50 kt	Hover 341°	8	7	6
35	10,510	Derricks	001°/60 kt	Hover 341°	9	not run	not run
36	9,510	Derricks	001°/15 kt	Hover 329°	4	not run	not run
37	9,510	Derricks	001°/35 kt	Hover 338°	not run	not run	not run
38	9,510	Derricks	001°/60 kt	Hover 341°	not run	not run	not run

Table M-3 Results for BRAE02 - Approach Task

Case	Weight (lb)	Obstruction	Wind	Task	Pilot Ratings		
					Pilot A	Pilot B	Pilot C
39	10,510	Derricks	001°/15 kt	Approach	4		
40	10,510	Derricks	001°/25 kt	Approach	5		
41	10,510	Derricks	001°/35 kt	Approach	6		
42	10,510	Derricks	001°/50 kt	Approach	7		
43	10,510	Derricks	001°/60 kt	Approach	9		

Appendix N Analysis of Task Performance in Trial BRAE02

This appendix presents an analysis of the actual performance (normalised by the desired limit) achieved by pilots A, B and C during trial BRAE02. The position of the helicopter during the assessment runs was logged in terms of X-position, Y-position, height and heading. The time histories for each run have been examined to identify the largest deviation from the average value for each position parameter. These data have been used to construct the plots shown in this appendix.

The notes that accompanied pilot A's ratings also included an axis-by-axis breakdown of what level of performance was judged to have been achieved. This allowed the actual performance achieved for each run to be compared with the pilot's own assessment of desired, adequate or beyond adequate performance.

Figures N-1 to N-4 show the actual performance, sorted in order of pilot rating and then in order of size. For all axes it is clear that the spread of actual performance for each level of performance exhibit a large amount of overlap. This is consistent with pilot comment that expressed the difficulty of judging the performance accurately given the visual cues available.

Using the minimum, maximum and average values for each performance level and in each axis, a new set of performance limits based on observed levels has been estimated in Table N-1 alongside the limits used during the trial BRAE02. These may offer a more realistic set of limits to apply to future trials. Although the performance limits were not strictly adhered to by any of the pilots, the assessment of task performance appears to show a similar perception of desired and adequate limits was experienced by the three pilots. Hence, if the modified limits had been adopted then the ratings would not be expected to vary significantly. However, if the visual cueing was enhanced (perhaps artificially) to the point where the pilot could accurately assess the task performance then the scatter on the ratings may decrease but would also become more sensitive to the choosing of performance limits.

An axis-by-axis breakdown of the task performance was not available from all pilots, however, the assessment of overall task performance can be deduced from the HQR. Specifically the task performance rankings have been grouped in terms of desired (HQR 1 to 4), adequate (HQR 5 to 6) and not achieved (HQR 7 and above). Figures N-5 to N-9 show the pilot task performance (normalised to desired performance) grouped into desired, adequate and not achieved and colour-coded by pilot. If each pilot was generally performing with the same degree of accuracy then there should be an even distribution of colours in the bar chart. For the x-position task performance, and to a lesser extent the y-position and height, pilot A appears to generally outperform the other two pilots whereas for heading all pilots generally performed with a similar degree of accuracy and if anything pilots B and C obtained a tighter performance.

Figure N-9 shows histograms of task performance data for all pilots together. The first column of plots gives the task performance in terms of X-position, the second in terms of Y-position, the third in terms of height and the fourth in terms of heading. The rows of plots relate to desired, adequate and 'not achieved' task performance respectively. The x-axis in each case gives the task performance in units of feet or degrees as appropriate and the y-axis gives the number of occurrences in the normal way for a histogram. The non-shaded areas show the relevant range of task performance as per the amended task performance limits in Table N-1. The bulk of occurrences on each plot should appear in the non-shaded region. A limitation of plotting data in this way is that the overall task performance need only be reflected in one of the performance measures and not necessary all of them. However, making allowance for this and the experimental scatter, there is a reasonable agreement between the amalgamated task performance for all pilots and the proposed amended task performance limits.

Table N-1 Task Performance Limits - Used and Observed

Level of Performance	Mean	Minimum	Maximum	BRAE02 limit	Estimated Observed Limit
Longitudinal (all values in ft)					
Desired	4.2	2.5	7.9	± 3	± 5
Adequate	6.3	4.0	8.2	± 5	± 8
Not Achieved	10.6	7.4	15.6	--	--
Lateral (all values in ft)					
Desired	3.8	2.7	5.8	± 2	± 4
Adequate	5.6	3.9	8.4	± 4	± 7
Not Achieved	8.6	5.5	12.4	--	--
Height (all values in ft)					
Desired	3.8	2.9	5.7	± 3	± 4
Adequate	5.5	3.6	7.4	± 5	± 6
Not Achieved	6.3	5.5	7.5	--	--
Heading (all values in degrees)					
Desired	4.7	3.0	6.8	± 5	± 5
Adequate	5.9	4.6	7.3	± 10	± 7
Not Achieved	9.4	9.4	9.4	--	--

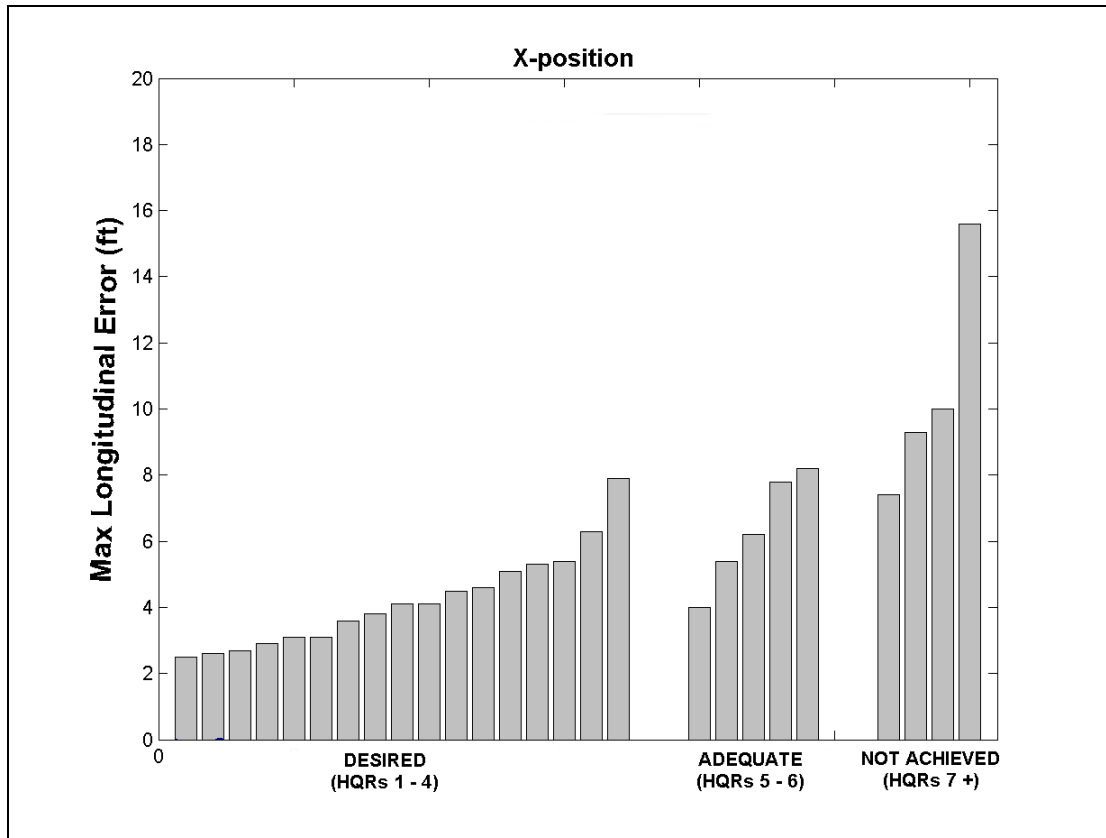


Figure N-1 Task Performance in Fore/Aft Axis for Pilot A only

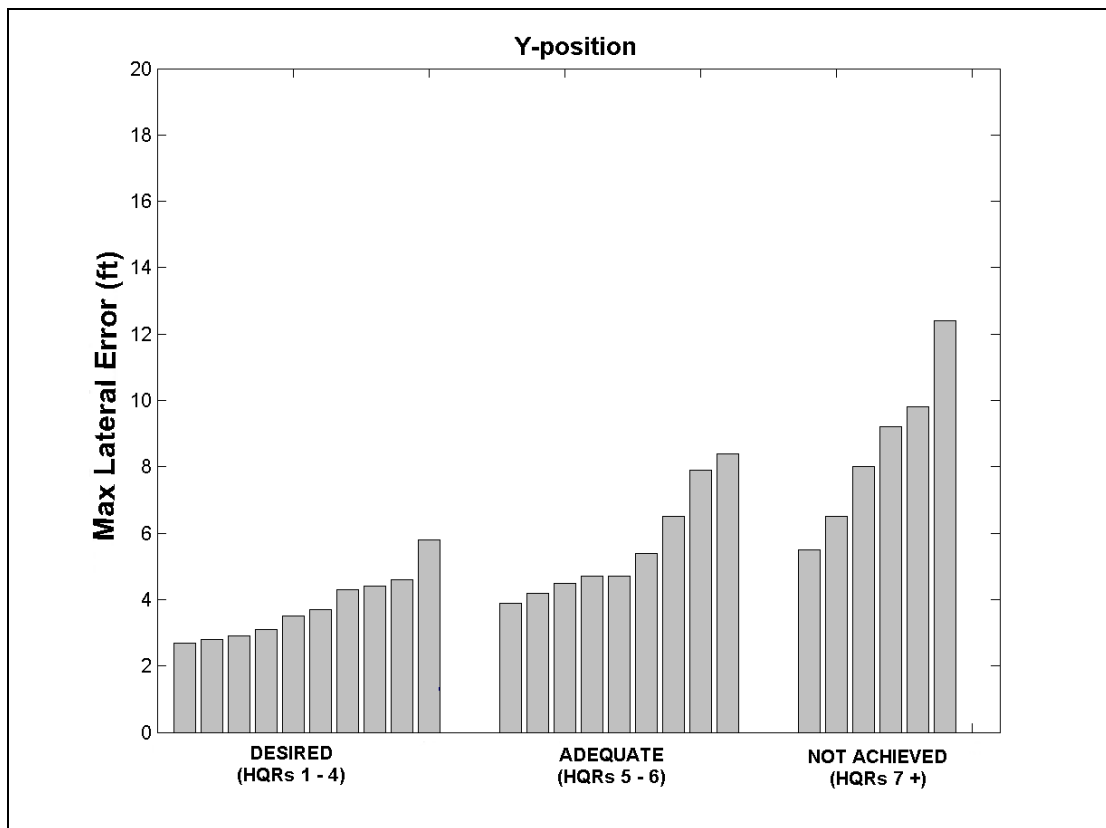


Figure N-2 Task Performance in Lateral Axis for Pilot A only

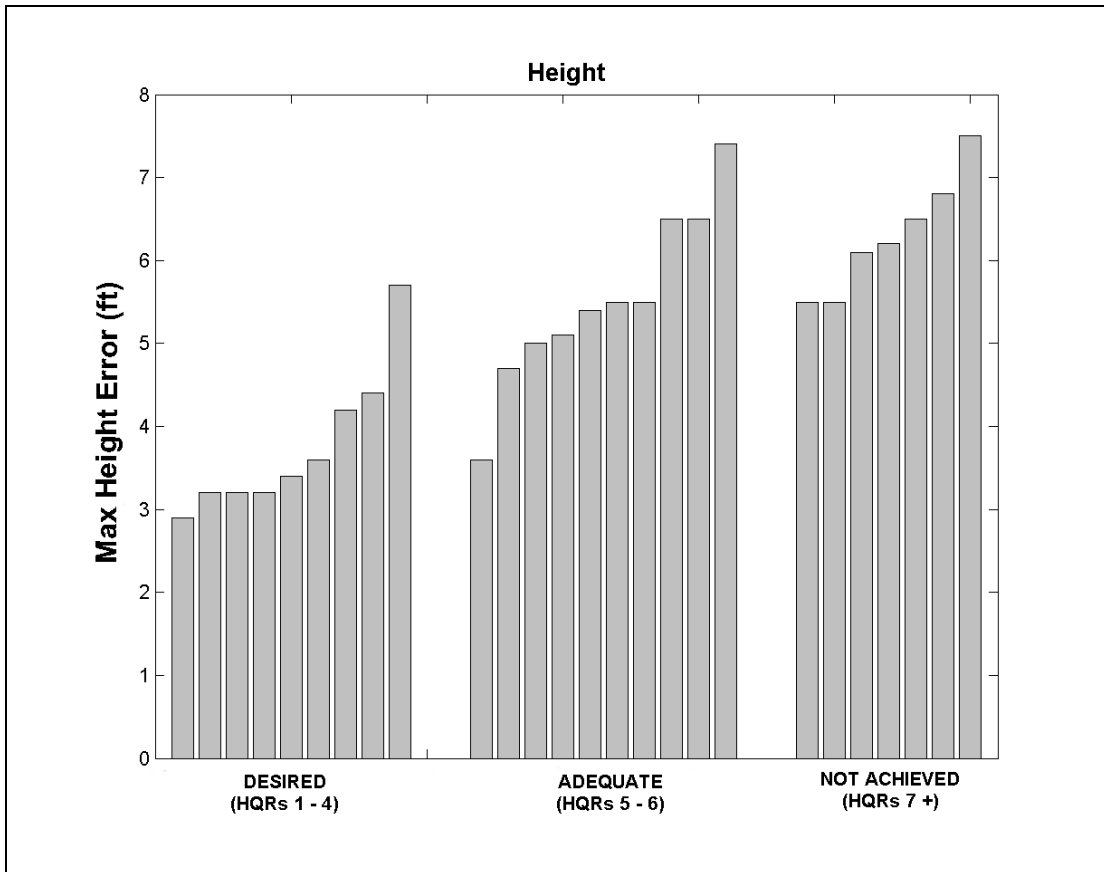


Figure N-3 Task Performance in Vertical Axis for Pilot A only

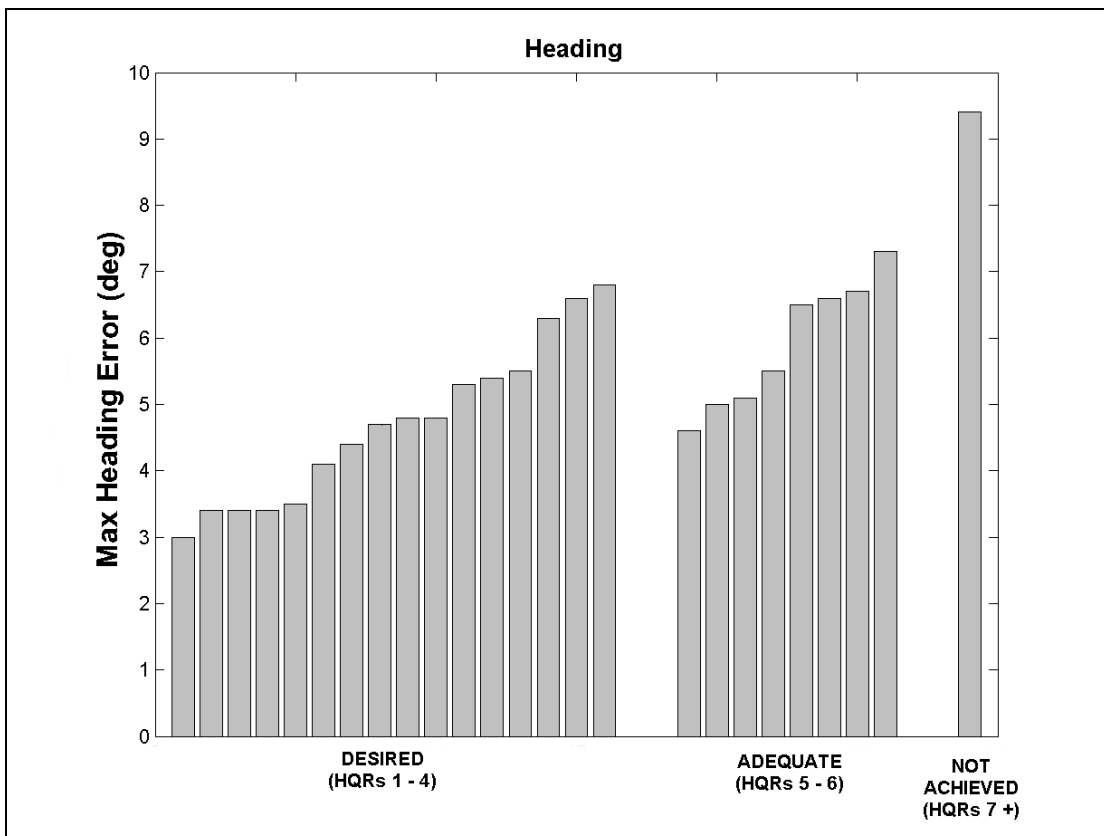


Figure N-4 Task Performance in Yaw Axis for Pilot A only

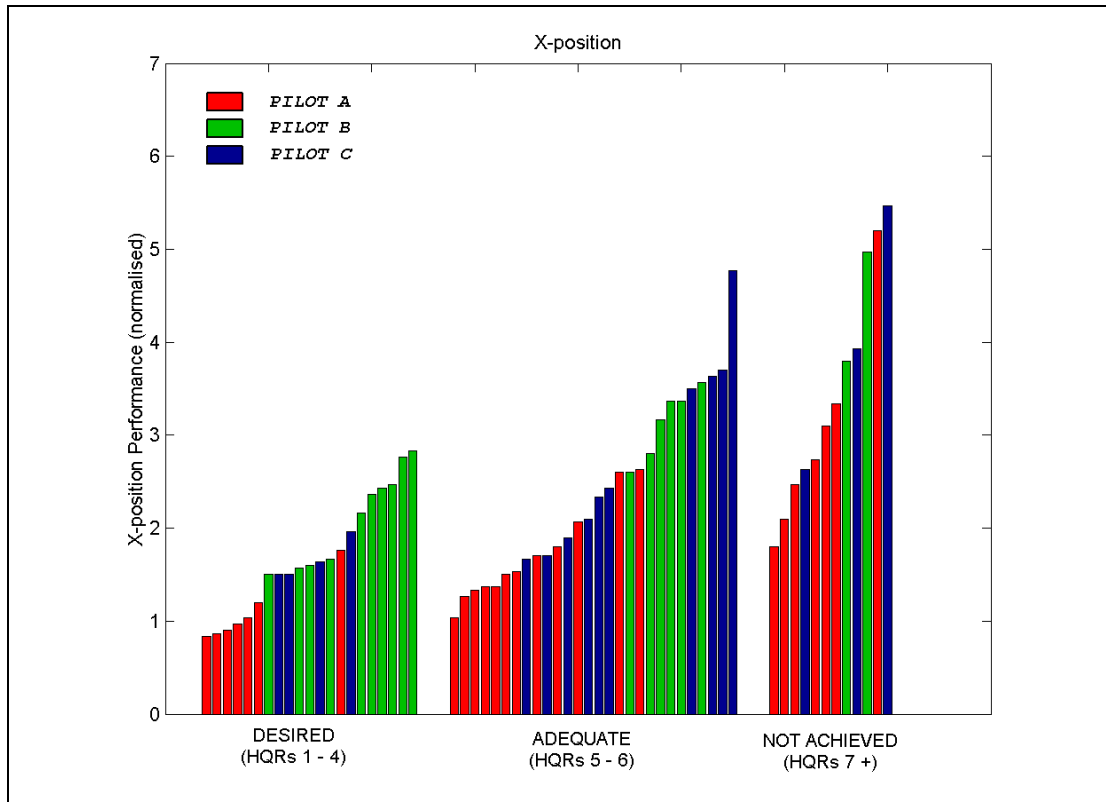


Figure N-5 Actual Task Performance in Fore/Aft Axis against Overall Performance Assessment

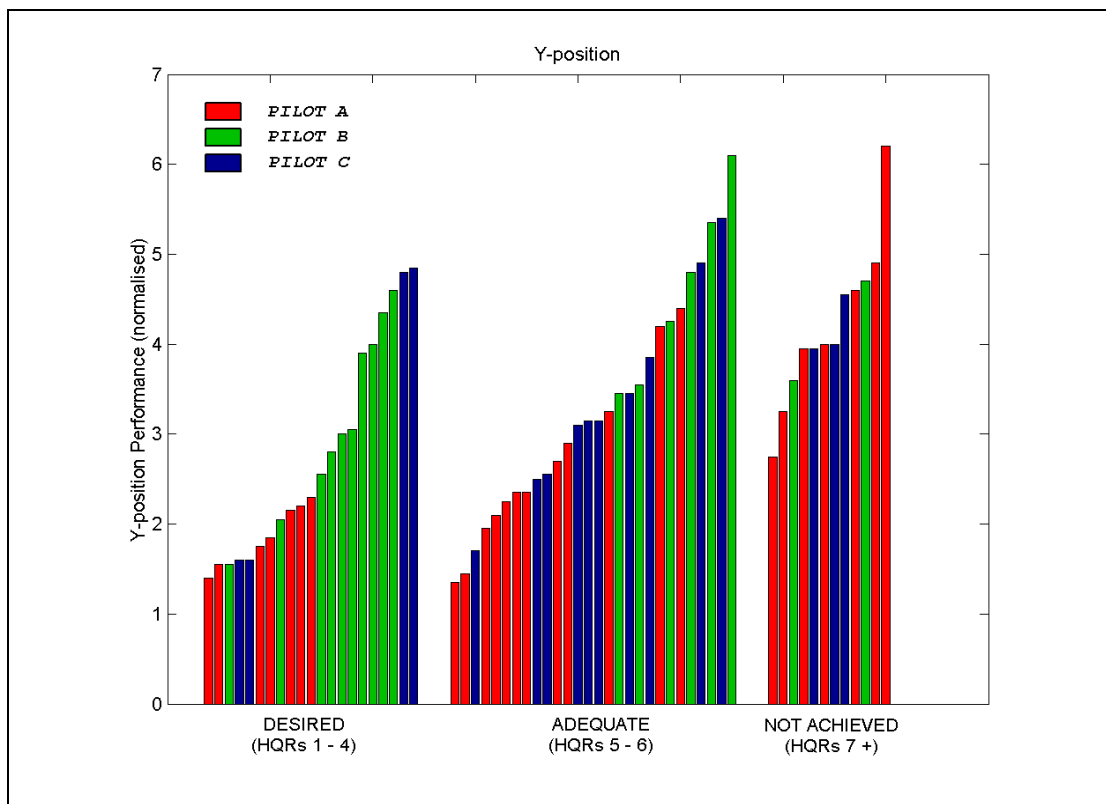


Figure N-6 Actual Task Performance in Lateral Axis against Overall Performance Assessment

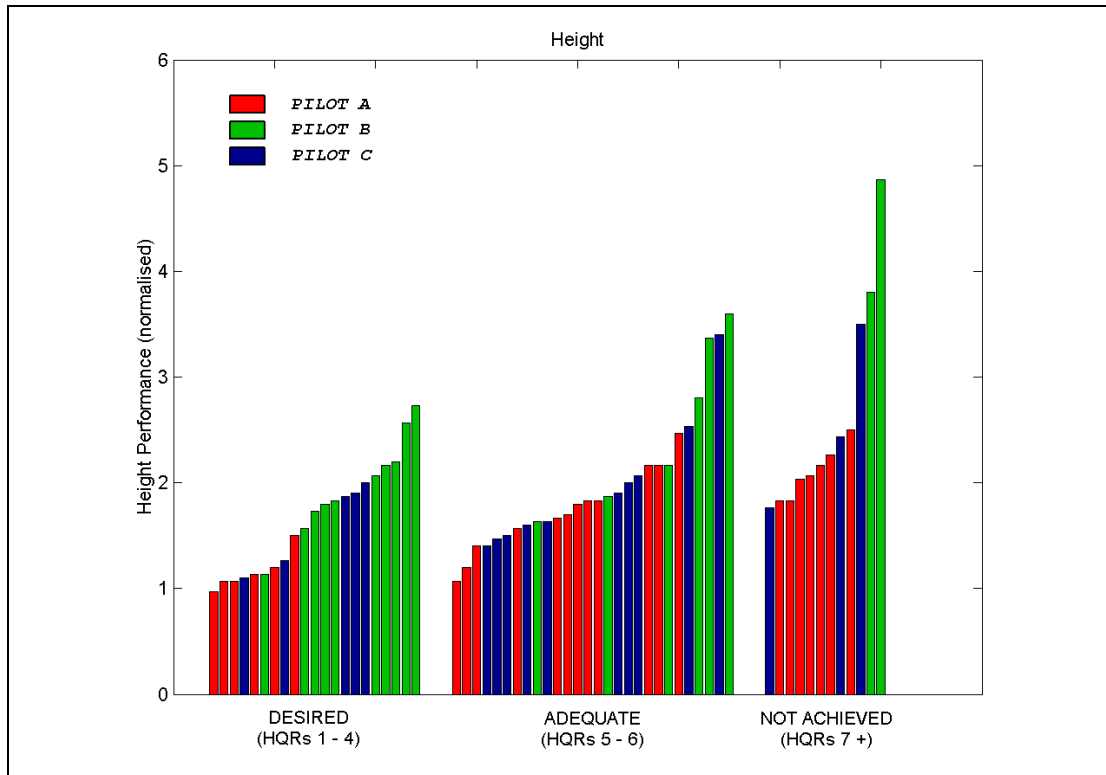


Figure N-7 Actual Task Performance in Vertical Axis against Overall Performance Assessment

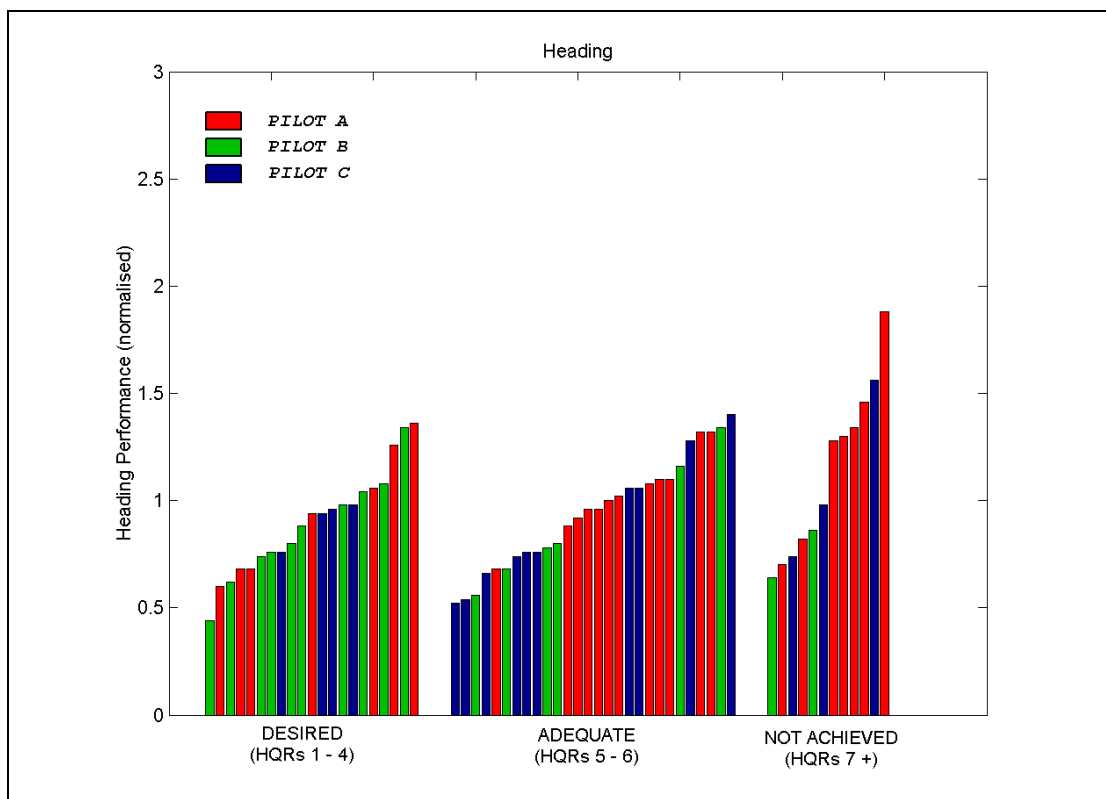


Figure N-8 Actual Task Performance in Yaw Axis against Overall Performance Assessment

Appendix O Results from the BRAE02 Trial

O.1 Validation of Predictors Derived in the BRAE01 Trial

This appendix validates the predictors which were derived from the BRAE01 trial by applying them to the control activity from the BRAE02 trial and comparing the calculated ratings with the HQRs awarded by the pilots. The BRAE02 trial involved three pilots each carrying out a significant proportion of the 38 scheduled cases:

Sortie Number	Pilot	Runs
15	A	26
16	B	18
18	C	23

Of the 38 cases, 17 were flown by all three pilots. A comparison of the HQRs awarded and those predicted from control activity metrics is shown in Table O-1. Figures O-1 to O-3 below show the same data plotted for each individual pilot. The combination of all the predictions is shown in Figure O-4, where the results from the three pilots are overlaid.

A general observation is that the predictions are higher than those awarded by the pilot by approximately 0.5 to 1.0 HQR. In the context of the overall programme this is taken to be an acceptable variation.

Table O-1 Awarded HQRs and Predictions for Trial BRAE02

Case No	Pilot A		Pilot B		Pilot C	
	HQR	Prediction	HQR	Prediction	HQR	Prediction
1	4	4.75	3	3.97	4	4.52
2	4	5.54	not run		5	5.14
3	5	5.54	4	5.16	6	5.85
4	not run		not run		not run	
5	6	7.64	not run		7	6.73
6	4	3.54	not run		4	3.12
7	5	5.54	4	4.60	4	4.68
8	5	5.77	4	4.91	4	4.70
9	6	8.27	5	6.52	6	7.02
10	8	10.68	5	6.74	7	6.11
11	4	3.19	3	3.66	4	5.13
12	5	5.85	3	3.84	5	5.91
13	6	6.85	4	5.69	6	6.41
14	7	7.93	5	5.90	5	7.77
15	not run		5	4.80	6	8.20
16	4	6.04	3	3.80	4	4.73
17	6	7.20	4	4.73	5	5.36
18	6	7.44	4	5.25	6	6.79
19	7	7.87	6	6.89	7	9.82
20	9	10.90	7	8.01	7	9.83
21	not run		not run		not run	
22	not run		not run		not run	
23	not run		not run		not run	
24	not run		not run		not run	
25	not run		not run		not run	
26	not run		not run		not run	
27	4	4.78	not run		not run	
28	not run		not run		not run	
29	not run		not run		not run	
30	8	10.13	not run		not run	
31	5	4.75	not run		4	4.13
32	5	5.72	5	5.26	6	8.31
33	5	6.52	not run		4	5.49
34	8	7.93	7	7.61	6	8.28
35	9	10.83	not run		not run	
36	4	4.53	not run		not run	
37	not run		not run		not run	
38	not run		not run		not run	

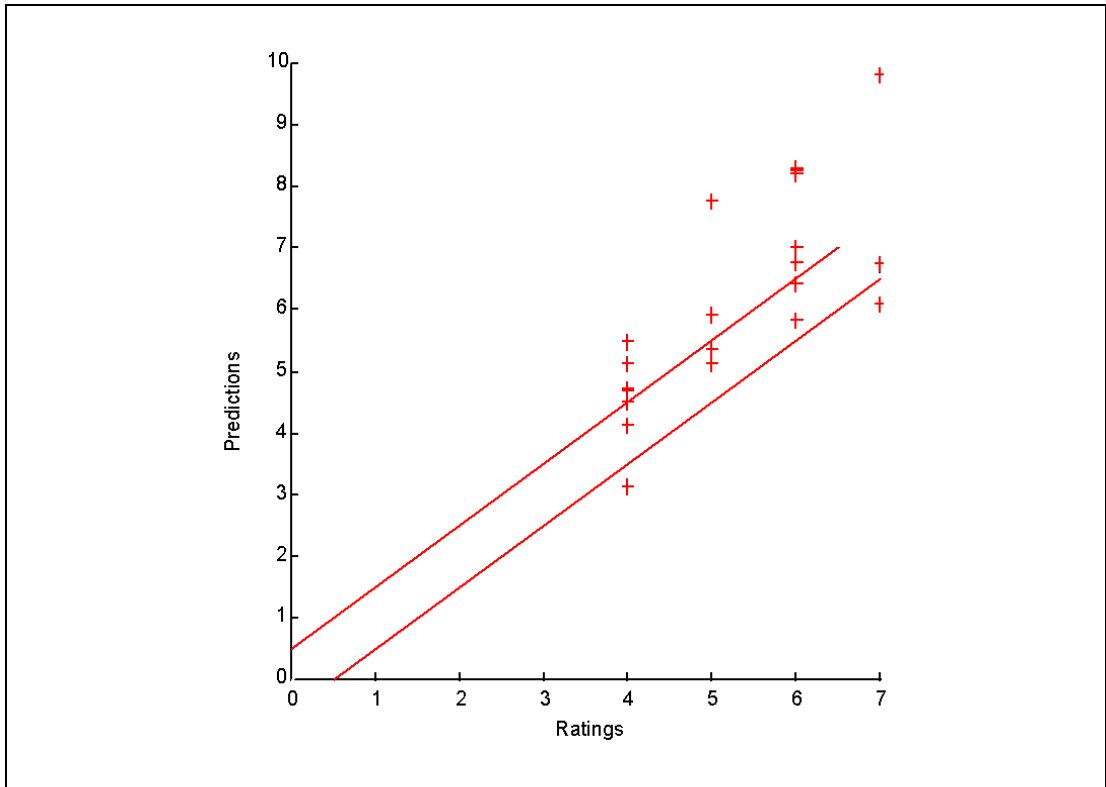


Figure O-1 Comparison of HQRs and Predictions for Pilot A

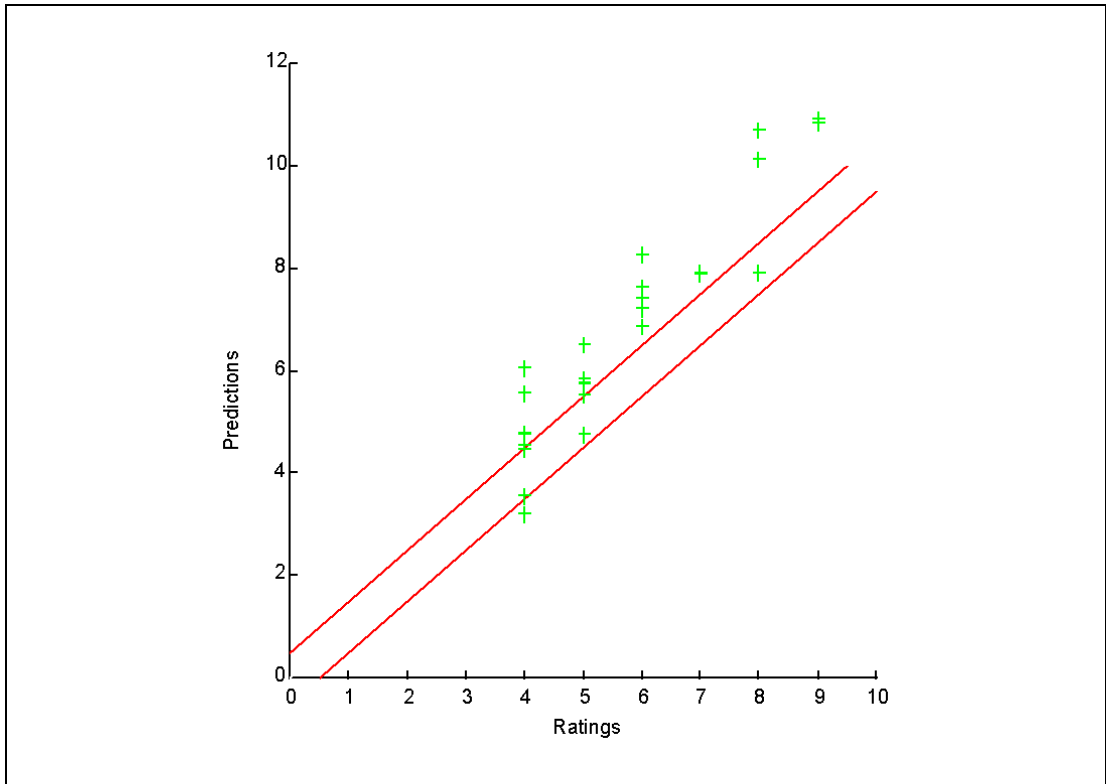


Figure O-2 Comparison of HQRs and Predictions for Pilot B

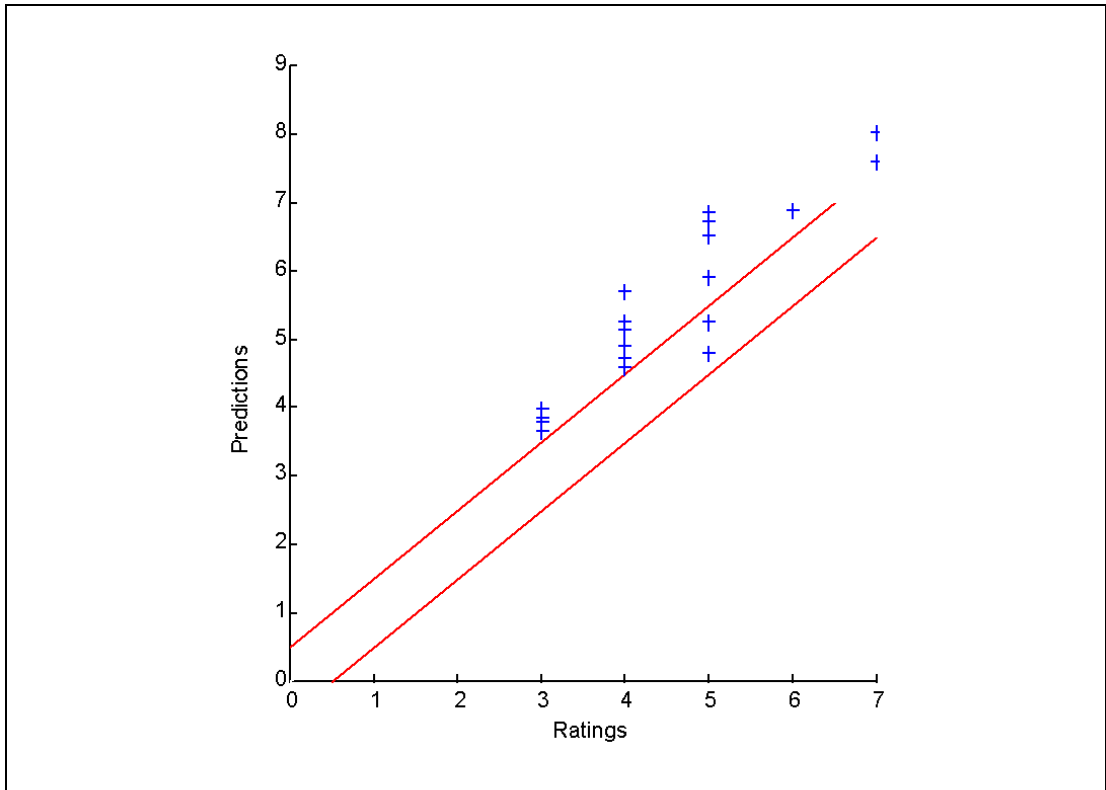


Figure O-3 Comparison of HQRs and Predictions for Pilot C

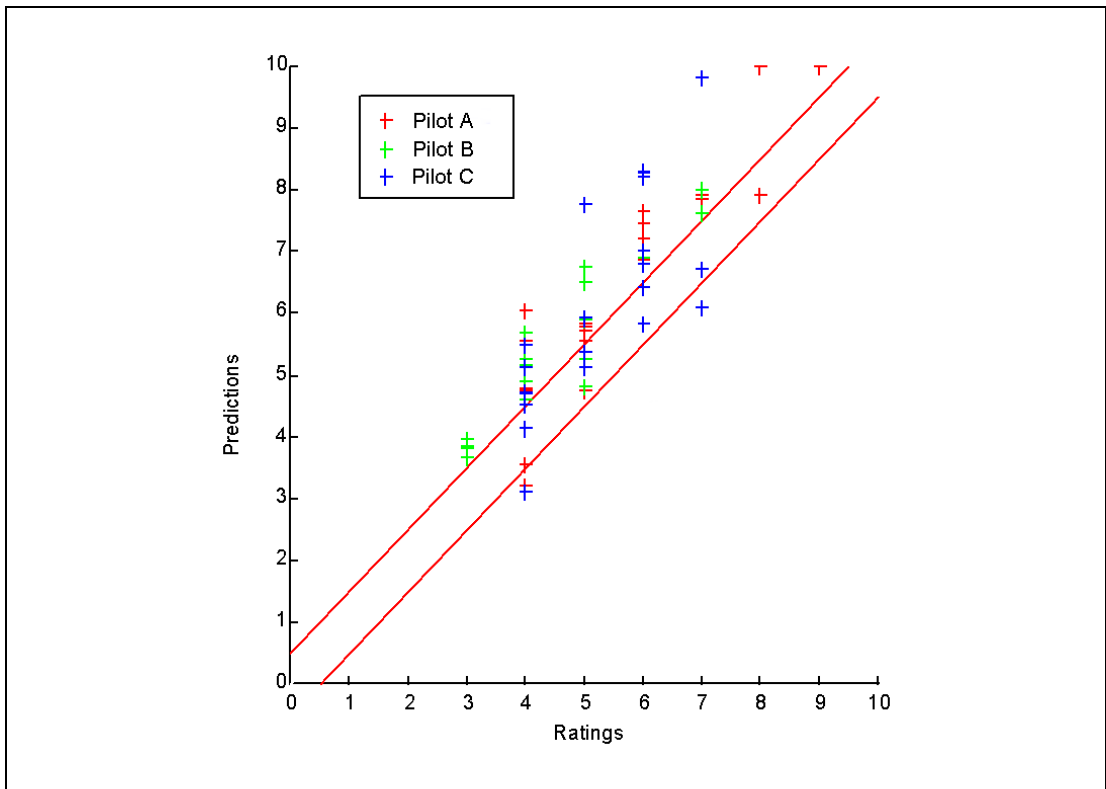


Figure O-4 Comparison of HQRs and Predictions for Pilots A, B and C

Appendix P Results from Validation of Desktop Simulation

This appendix compares the predictions calculated from the SyCoS pilot model with the HQRs awarded by the pilots. It therefore validates the process of desktop simulation for the prediction of handling qualities ratings.

Out of the 38 cases selected for the BRAE02, 34 were repeated by desktop simulation using the same turbulence data and simulation environment as those for the piloted trial. The helicopter model configured to resemble an S-76 type, was identical to that employed in the simulator trial BRAE02 including the implementation of the non-uniform turbulence field. However, in the desktop trial the helicopter was flown by the SyCoS pilot model rather than by a human pilot.

The usual set of metrics based on the standard deviations of stick and stick rate were calculated for the control activity produced by SyCoS and using the workload predictors described in Appendix J, HQRs were predicted for 34 of the 38 cases. The results are shown in Table P-1 (column SyCoS (new turb)) together with the HQRs awarded by the human pilots. It can immediately be seen that the SyCoS predictions are generally lower than the HQRs awarded by pilots A and C but are very close to those of pilot B. It may be concluded therefore that the SyCoS predictions fall within the range of HQRs awarded by human pilots.

Also included in Table P-1 are the HQRs predicted on the basis of control activity from the original desktop simulations where only two components of a uniform turbulence field provided the aerodynamic environment (column SyCoS (old turb)). Again the BRAE01 predictors were employed. Generally the predictions are very similar and to those with the full turbulence field. These results give some confidence in the validity of the original simulations.

The comparisons for the three pilots are depicted in Figures P-1 to P-3. The remarkable agreement for pilot B is clearly illustrated. Figure P-4 shows a comparison of the HQRs produced by the two turbulence representations.

Surprisingly, the full turbulence of the BRAE02 simulations does not have a significant effect although in the majority of cases the old turbulence has produced a slightly lower rating. The important point of these results, apart from completing the cross-referencing of the methodology, is that there are no serious anomalies to give concern. Based on this evidence alone it would seem the efforts to include lateral turbulence and estimates of the flow gradients across the rotor disc are not rewarded with more accurate predictions. However, the overall realism of the turbulence to the pilots flying the simulator had been significantly enhanced.

Table P-1 HQRs Desktop Simulation and BRAE02 Trials

Case	Pilot A	Pilot B	Pilot C	SyCoS (new turb)	SyCoS (old turb)
1	4	3	4	2.81	2.63
2	4	NA	5	3.51	2.64
3	5	4	6	4.38	2.99
4	NA	NA	NA	5.45	3.58
5	6	NA	7	6.08	4.09
6	4	NA	4	2.81	2.90
7	5	4	4	3.51	3.50
8	5	4	4	4.49	3.72
9	6	5	6	5.80	4.77
10	8	5	7	6.19	5.68
11	4	3	4	2.73	2.92
12	5	3	5	3.41	3.61
13	6	4	6	4.36	3.68
14	7	5	5	5.20	4.73
15	NA	5	6	6.10	5.59
16	4	3	4	2.61	2.80
17	6	4	5	3.51	3.67
18	6	4	6	4.20	4.01
19	7	6	7	5.52	5.36
20	9	7	7	6.66	6.17
21	4	NA	NA	NA	NA
22	8	NA	NA	NA	NA
23	5	NA	4	4.28	3.98
24	5	5	6	5.50	5.32
25	5	NA	4	6.81	6.16
26	8	7	6	NA	NA
27	9	NA	NA	3.44	3.62
28	4	NA	NA	4.29	3.69
29	NA	NA	NA	5.23	4.72
30	NA	NA	NA	6.25	6.19
31	NA	NA	NA	2.78	2.83
32	NA	NA	NA	3.57	3.77
33	NA	NA	NA	4.19	4.22
34	NA	NA	NA	5.96	6.52
35	NA	NA	NA	7.49	8.15
36	NA	NA	NA	NA	NA
37	NA	NA	NA	4.30	4.17
38	NA	NA	NA	7.66	7.97

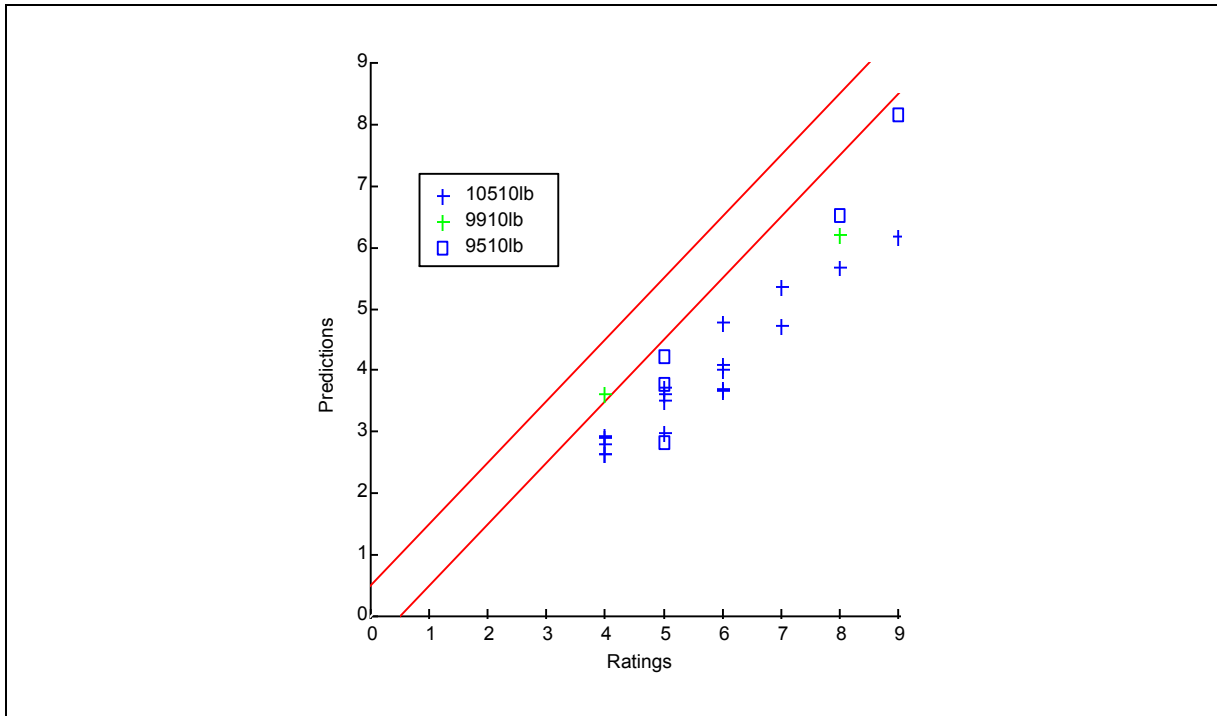


Figure P-1 Comparison of HQRs from Desktop Simulation with BRAE02, Pilot A

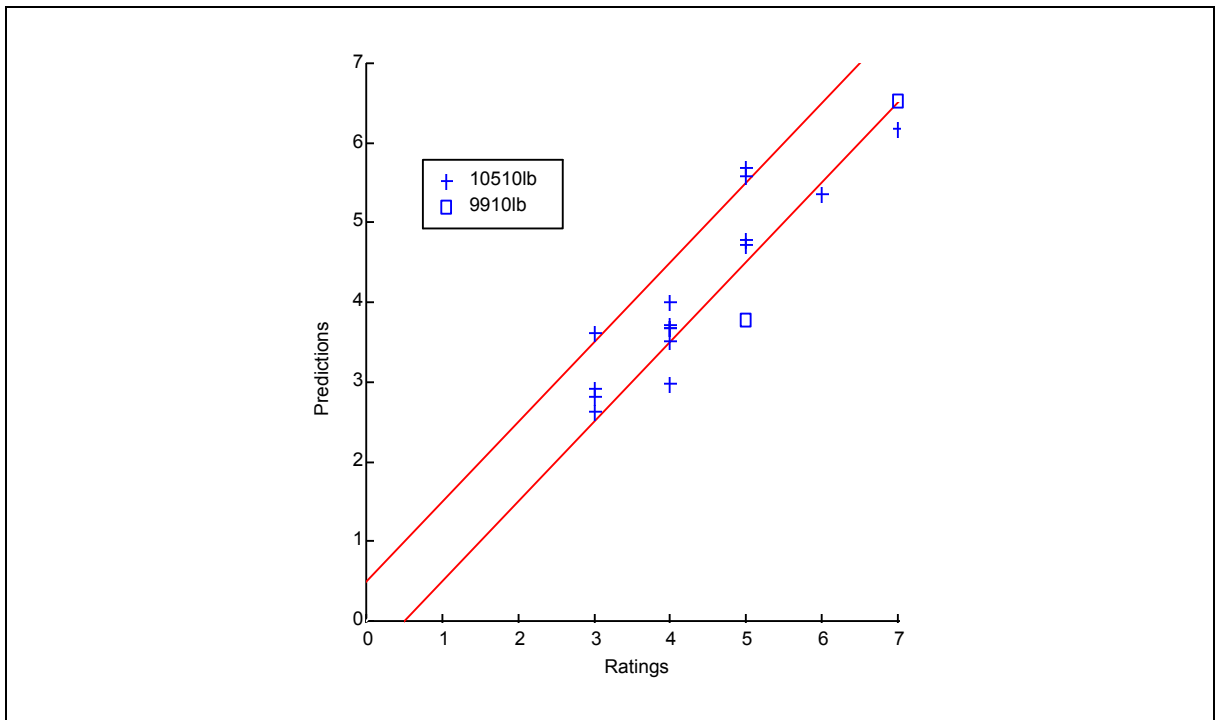


Figure P-2 Comparison of HQRs from Desktop Simulation with BRAE02, Pilot B

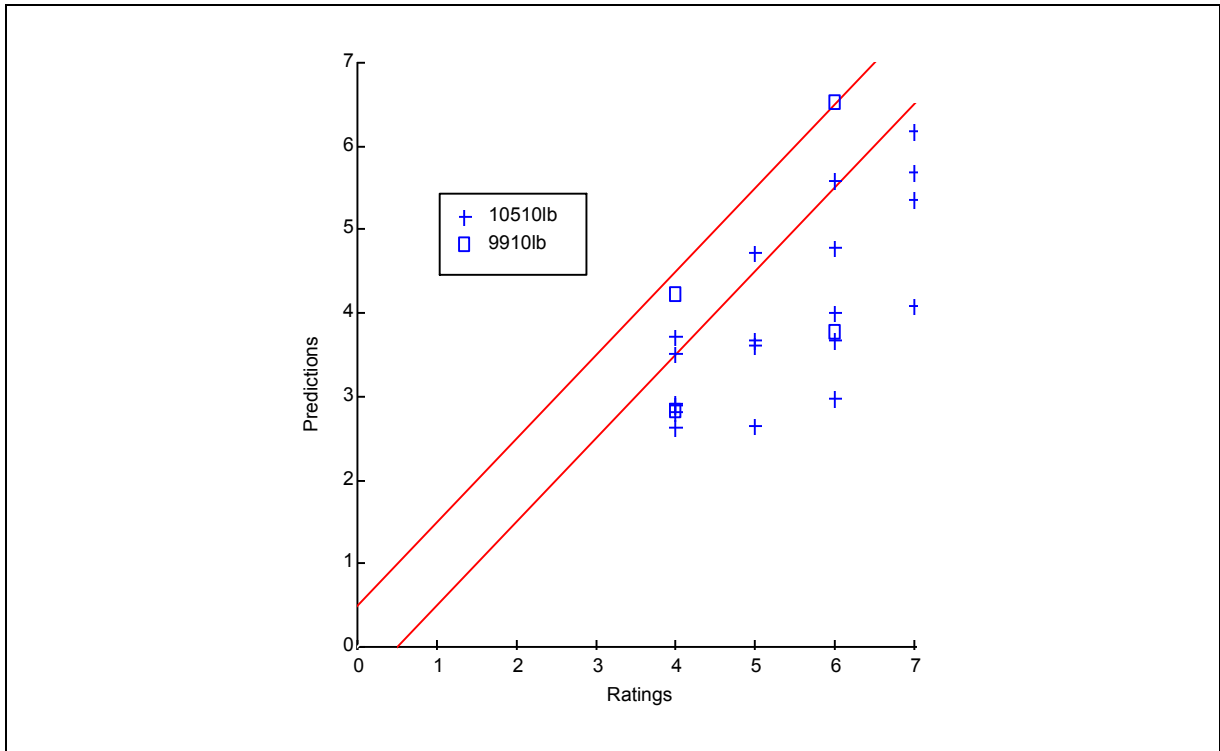


Figure P-3 Comparison of HQRs from Desktop Simulation with BRAE02, Pilot C

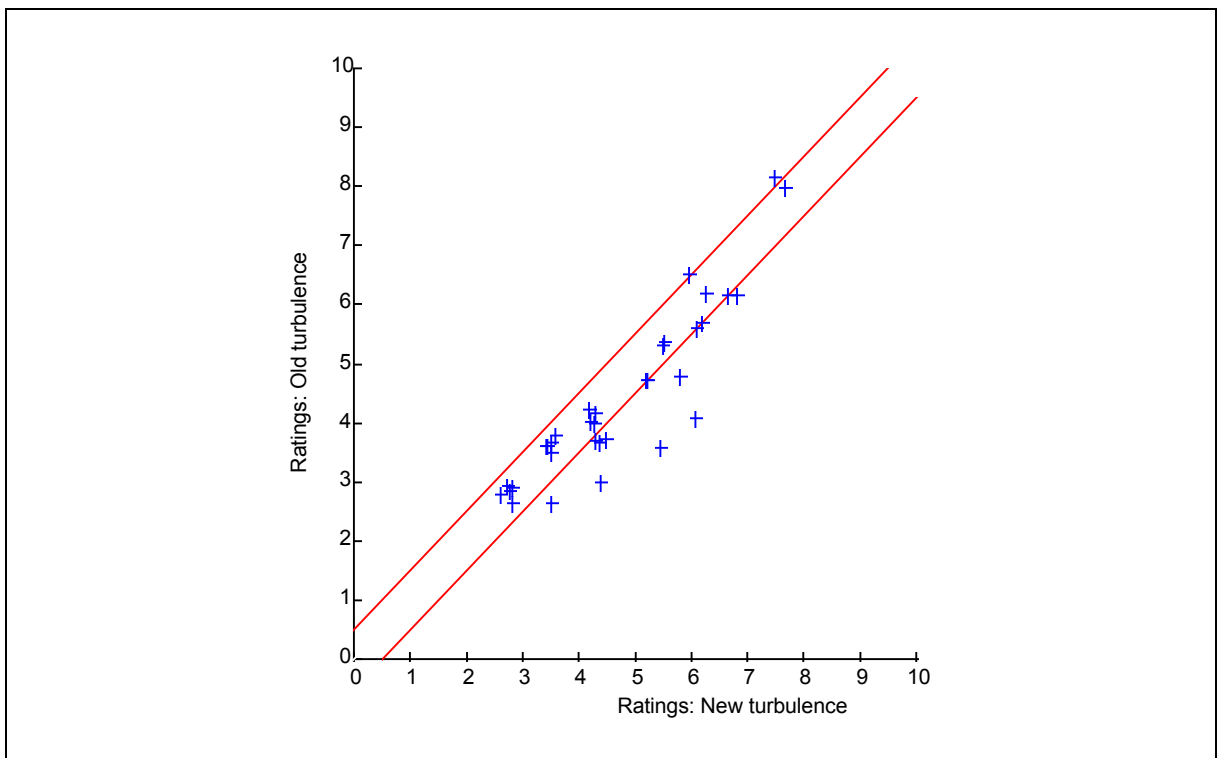


Figure P-4 Comparison of SyCoS Workload Ratings for New and Old Turbulence Models

Appendix Q Statistical Analysis of HQRs

The pilot ratings from the BRAE02 trial were analysed in detail using recently developed techniques for ordered categorical response data. The BRAE02 experimental situation where three pilots flew identical tasks provided a rare opportunity for using these new techniques to factor into a predictive process the explanatory variables of wind speed, pilot and wind direction – the last-mentioned referring to platform obstructions. A full and detailed account of the procedure is given in [1]¹ and it will be seen that the essence of the method is to model (and hence estimate) the ratio of the probability of a particular rating being the same as or below a given value to the probability of it being above. Hence it is probabilities that are being numerically estimated rather than actual ratings. The technique is called Ordinal Logistic Regression where the regression model takes the following form:

$$\begin{aligned} \log_e \left(\frac{\gamma_j}{1-\gamma_j} \right) = & \alpha_j + \beta_1 \times \text{Pilot A} + \beta_2 \times \text{Pilot C} \\ & + \beta_3 \times \text{Wind Speed 25} + \beta_4 \times \text{Wind Speed 35} \\ & + \beta_5 \times \text{Wind Speed 50} + \beta_6 \times \text{Wind Speed 60} \\ & + \beta_7 \times \text{Wind Direction } 001^\circ + \beta_8 \times \text{Wind Direction } 050^\circ \\ & + \beta_9 \times \text{Wind Direction } 088^\circ \end{aligned} \quad (j=1,\dots,9)$$

where γ_j is the probability that a run is rated j or less and the α_j and β_1, \dots, β_9 are regression coefficients. The quantities Pilot A, Pilot C, Wind Speed 25/35/50/60 and Wind Direction 001°/050°/088° are indicator variables taking the values 0 or 1 to indicate their presence in the regression equation. (In this method, no indicator variables are needed for the baseline levels: Pilot B, Wind Speed 15 kt and Wind Direction 272°). For example, consider the above equation for the case of a task flown by Pilot C, at a wind speed of 35 kt and a wind direction of 050°. The regression equation simplifies to:

$$\log_e \left(\frac{\gamma_j}{1-\gamma_j} \right) = \alpha_j + \beta_2 + \beta_4 + \beta_8$$

The quantity $\log_e \left(\frac{\gamma_j}{1-\gamma_j} \right)$ is the logistic function – that is the natural logarithm of the odds of rating $(j+1)$.

If π_j denotes the probability that a run is rated j ($j = 1, \dots, 10$), since γ_j denotes the probability that a run is rated Category j **or less** ($j = 1, \dots, 10$):

$$\gamma_j = \pi_1 + \pi_2 + \dots + \pi_j \quad (j = 1, \dots, 10),$$

with the particular cases $\gamma_1 = \pi_1$, $\gamma_{10} = 1$. Estimates of π_j can then be found from:

$$\pi_j = \gamma_j - \gamma_{j-1} \quad (j = 2, \dots, 10), \quad \pi_1 = \gamma_1$$

once estimates of the γ_j have been determined.

Tables Q-1 to Q-3 show the predicted probabilities and predicted ratings for three pilots.

1. References for this Appendix are listed in Section Q1.

Table Q-1 For Pilot A, Predicted Probabilities and Predicted Rating from the Regression Model including Wind Speed, Pilot and Wind Direction

Pilot	Task	Wind Direction	Wind Speed	Rating	Predicted probability of Rating π_j									Predicted Rating
					3	4	5	6	7	8	9			
A	1	272	15	4	0.08	0.88	0.04	0.00	0.00	0.00	0.00	0.00	0.00	4
A	2	272	25	4	0.00	0.28	0.60	0.11	0.01	0.01	0.00	0.00	0.00	5
A	3	272	35	5	0.00	0.12	0.60	0.26	0.02	0.02	0.00	0.00	0.00	5
A	5	272	60	6	0.00	0.00	0.01	0.12	0.50	0.00	0.28	0.10	0.00	7
A	6	050	15	4	0.10	0.87	0.03	0.00	0.00	0.00	0.00	0.00	0.00	4
A	7	050	25	5	0.00	0.34	0.57	0.09	0.00	0.00	0.00	0.00	0.00	5
A	8	050	35	5	0.00	0.15	0.62	0.21	0.01	0.01	0.00	0.00	0.00	5
A	9	050	50	6	0.00	0.00	0.05	0.52	0.36	0.05	0.05	0.01	0.00	6
A	10	050	60	8	0.00	0.00	0.01	0.15	0.53	0.24	0.00	0.07	0.00	7
A	11	088	15	4	0.08	0.88	0.04	0.00	0.00	0.00	0.00	0.00	0.00	4
A	12	088	25	5	0.00	0.29	0.60	0.11	0.01	0.01	0.00	0.00	0.00	5
A	13	088	35	6	0.00	0.12	0.61	0.25	0.01	0.01	0.00	0.00	0.00	5
A	14	088	50	7	0.00	0.00	0.04	0.47	0.41	0.06	0.01	0.01	0.00	6
A	16	001	15	4	0.01	0.67	0.29	0.02	0.00	0.00	0.00	0.00	0.00	4
A	17	001	25	6	0.00	0.03	0.38	0.53	0.05	0.00	0.00	0.00	0.00	6
A	18	001	35	6	0.00	0.01	0.18	0.65	0.14	0.01	0.01	0.00	0.00	6
A	19	001	50	7	0.00	0.00	0.00	0.08	0.44	0.34	0.13	0.13	0.00	7
A	20	001	60	9	0.00	0.00	0.00	0.01	0.12	0.33	0.53	0.00	0.00	9
A	27	088	25	4	0.00	0.29	0.60	0.11	0.01	0.01	0.00	0.00	0.00	5
A	30	088	60	8	0.00	0.00	0.01	0.12	0.50	0.28	0.09	0.09	0.00	7
A	31	001	15	5	0.01	0.67	0.29	0.02	0.00	0.00	0.00	0.00	0.00	4
A	32	001	25	5	0.00	0.03	0.38	0.53	0.05	0.00	0.00	0.00	0.00	6
A	33	001	35	5	0.00	0.01	0.18	0.65	0.14	0.01	0.01	0.00	0.00	6
A	34	001	50	8	0.00	0.00	0.00	0.08	0.44	0.34	0.13	0.13	0.00	7
A	35	001	60	9	0.00	0.00	0.00	0.01	0.12	0.33	0.53	0.00	0.00	9
A	36	001	15	4	0.01	0.67	0.29	0.02	0.00	0.00	0.00	0.00	0.00	4

Table Q-2 For Pilot B, Predicted Probabilities and Predicted Rating from the Regression Model including Wind Speed, Pilot and Wind Direction

Pilot	Task	Wind Direction	Wind Speed	Rating	Predicted probability of Rating (π_j)									Predicted Rating	
					3	4	5	6	7	8	9				
B	1	272	15	3	0.91	0.09	0.00	0.00	0.00	0.00	0.00	0.00	0.00	0.00	3
B	3	272	35	4	0.06	0.89	0.05	0.00	0.00	0.00	0.00	0.00	0.00	0.00	4
B	7	050	25	4	0.19	0.80	0.01	0.00	0.00	0.00	0.00	0.00	0.00	0.00	4
B	8	050	35	4	0.07	0.88	0.04	0.00	0.00	0.00	0.00	0.00	0.00	0.00	4
B	9	050	50	5	0.00	0.28	0.60	0.11	0.01	0.00	0.00	0.00	0.00	0.00	5
B	10	050	60	5	0.00	0.05	0.46	0.45	0.04	0.00	0.00	0.00	0.00	0.00	5
B	11	088	15	3	0.91	0.09	0.00	0.00	0.00	0.00	0.00	0.00	0.00	0.00	3
B	12	088	25	3	0.15	0.83	0.02	0.00	0.00	0.00	0.00	0.00	0.00	0.00	4
B	13	088	35	4	0.06	0.89	0.05	0.00	0.00	0.00	0.00	0.00	0.00	0.00	4
B	14	088	50	5	0.00	0.23	0.62	0.14	0.01	0.00	0.00	0.00	0.00	0.00	5
B	15	088	60	5	0.00	0.04	0.41	0.50	0.05	0.00	0.00	0.00	0.00	0.00	6
B	16	001	15	3	0.49	0.51	0.00	0.00	0.00	0.00	0.00	0.00	0.00	0.00	4
B	17	001	25	4	0.02	0.80	0.17	0.01	0.00	0.00	0.00	0.00	0.00	0.00	4
B	18	001	35	4	0.01	0.60	0.36	0.03	0.00	0.00	0.00	0.00	0.00	0.00	4
B	19	001	50	6	0.00	0.03	0.32	0.57	0.07	0.01	0.00	0.00	0.00	0.00	6
B	20	001	60	7	0.00	0.00	0.06	0.55	0.33	0.04	0.01	0.00	0.00	0.00	6
B	32	001	25	5	0.02	0.80	0.17	0.01	0.00	0.00	0.00	0.00	0.00	0.00	4
B	34	001	50	7	0.00	0.03	0.32	0.57	0.07	0.01	0.00	0.00	0.00	0.00	6

Table Q-3 For Pilot C, Predicted Probabilities and Predicted Rating from the Regression Model including Wind Speed, Pilot and Wind Direction

Pilot	Task	Wind Direction	Wind Speed	Rating	Predicted probability of Rating (π_j)									
					3	4	5	6	7	8	9			
C	1	272	15	4	0.22	0.77	0.01	0.00	0.00	0.00	0.00	0.00	0.00	4
C	2	272	25	5	0.00	0.57	0.39	0.04	0.00	0.00	0.00	0.00	0.00	4
C	3	272	35	6	0.00	0.31	0.58	0.10	0.00	0.00	0.00	0.00	0.00	5
C	5	272	60	7	0.00	0.00	0.02	0.30	0.53	0.12	0.03	0.00	0.00	7
C	6	050	15	4	0.28	0.72	0.01	0.00	0.00	0.00	0.00	0.00	0.00	4
C	7	050	25	4	0.01	0.64	0.33	0.03	0.00	0.00	0.00	0.00	0.00	4
C	8	050	35	4	0.00	0.38	0.54	0.07	0.00	0.00	0.00	0.00	0.00	5
C	9	050	50	6	0.00	0.01	0.16	0.65	0.16	0.01	0.00	0.00	0.00	6
C	10	050	60	7	0.00	0.00	0.03	0.36	0.49	0.09	0.02	0.00	0.00	7
C	11	088	15	4	0.23	0.76	0.01	0.00	0.00	0.00	0.00	0.00	0.00	4
C	12	088	25	5	0.00	0.58	0.38	0.03	0.00	0.00	0.00	0.00	0.00	4
C	13	088	35	6	0.00	0.32	0.58	0.09	0.00	0.00	0.00	0.00	0.00	5
C	14	088	50	5	0.00	0.01	0.13	0.64	0.19	0.02	0.00	0.00	0.00	6
C	15	088	60	6	0.00	0.00	0.02	0.31	0.52	0.12	0.03	0.00	0.00	7
C	16	001	15	4	0.03	0.86	0.11	0.01	0.00	0.00	0.00	0.00	0.00	4
C	17	001	25	5	0.00	0.11	0.60	0.27	0.02	0.00	0.00	0.00	0.00	5
C	18	001	35	6	0.00	0.04	0.41	0.49	0.05	0.00	0.00	0.00	0.00	6
C	19	001	50	7	0.00	0.00	0.01	0.23	0.55	0.16	0.04	0.00	0.00	7
C	20	001	60	7	0.00	0.00	0.00	0.04	0.30	0.41	0.25	0.00	0.00	8
C	31	001	15	4	0.03	0.86	0.11	0.01	0.00	0.00	0.00	0.00	0.00	4
C	32	001	25	6	0.00	0.11	0.60	0.27	0.02	0.00	0.00	0.00	0.00	5
C	33	001	35	4	0.00	0.04	0.41	0.49	0.05	0.00	0.00	0.00	0.00	6
C	34	001	50	6	0.00	0.00	0.01	0.23	0.55	0.16	0.04	0.00	0.00	7

The model fitting strategy progressively identifies the most significant explanatory variables by using sub-models of the complete model above. As might be expected, the best fit to the data using only one variable is achieved by using wind speed. More surprising is that the best fit using only two explanatory variables involves wind speed and pilot. That is, in determining the ratings, the pilot is a more significant factor than wind direction. However all three variables *are* significant in the final model which was subsequently verified by standard goodness of fit tests. In addition, the model provides predictions of the most probable ratings and inspection of these predictions shows that the agreement with pilot subjective ratings is very good. One may have some confidence, therefore, that conclusions drawn from the model are valid.

The model also indicates the effect on the ratings within each explanatory variable. As an example, for a given pilot and wind direction, the ratings are most strongly affected by changes of wind speed from 15 to 25 kt and from 35 to 50 kt. Further, for a given pilot and wind speed, the change in direction from 272° (no obstruction) to 001° (derricks) increased the ratings significantly but changes from 272° to 050° (cranes) and to 088° (exhaust stacks) caused no significant increase. Finally, variations in pilot were significant, for given wind speeds and directions. Pilot A rated higher than Pilot C who in turn rated higher than Pilot B. The work here therefore shows that the pilot effect is significant and that variation between pilots should not be regarded as an experimental aberration but treated as a genuine explanatory variable. Consequently there are good reasons in any criterion which involves, or is based on HQR ratings, for applying a margin. The analysis in [1] treats pilots as individuals, that is, they are not treated as samples from a population so a suitable margin cannot be statistically estimated by these techniques. The number of pilots being only three would, in any case, make it inadvisable to place much confidence in estimates of the statistical properties of such a population from the BRAE02 data.

In [1] the same procedure was also applied, as a separate exercise, to the ratings from the SyCoS pilot model with the conclusion that the difference between the ratings awarded by the pilot model are not significantly different from those from Pilot B – that is, the SyCoS pilot produces ratings that are not untypical of human pilots.

This investigation has shown that data of the type collected in the BRAE02 trial is well suited to analysis by the techniques of Ordinal Logistic Regression. It is possible to state this with confidence because of its verification by goodness of fit tests. The conclusions drawn from the model may also, therefore, be considered valid. For example, the wind from the direction of the derricks is the only direction that has a significant effect on increasing ratings. Also, individual pilots strongly affect the rating process. The former result is important from the design point of view, the latter is important from the evaluation and operational viewpoint.

Q.1 Reference

- [1] *Ordinal Logistic Regression Analysis of Flight Task Ratings*. Glasgow Caledonian University, School of Computing and Mathematical Sciences, Technical Report CMS-MAT-2003-1.

Appendix R Calibration of the Bristow HOMP Turbulence Parameter

R.1 Bristow HOMP Turbulence Parameter

R.1.1 General Description of Algorithm

The details of the Bristow algorithm for assessing workload was provided by CAA in an e-mail in May 2001 [1]¹, and originated from Captain Norman at Bristow Helicopters Limited. The algorithm is based solely on the recorded changes to the main rotor collective pitch to produce a turbulence parameter that has been implemented as part of the Helicopter Operations Monitoring Programme (HOMP) [2]. The processing of the collective pitch signal comprises the following steps:

- a) Apply a high pass filter to remove any trim changes and low frequency ('guidance') inputs.
- b) Square the result to accentuate the peaks.
- c) Multiply by 100 to give the final result a value to the order of 10.
- d) Apply a low pass filter to remove excessive noise from the metric.

The result of the processing is a time history that is intended to describe the level of turbulence throughout the period for which logged data are available. The severity of the turbulence during an approach to a particular platform is assessed by looking for the maximum value of the turbulence parameter. From Bristow's current experience of assessing data from North Sea operations on a Super Puma helicopter, a maximum value of more than approximately 10 is considered to relate to conditions of high turbulence.

R.1.2 High-pass Filtering

The purpose of the high-pass filtering is to remove any low frequency inputs from the collective signal. Such low frequency inputs may relate to the inevitable trim changes made during an approach as the aircraft descends and washes off speed, and to so-called guidance inputs intended to change the aircraft's direction e.g. the initiation of the descent or the flare to the hover. The filter is defined by a polynomial of the form given below where x_n is the collective pitch at time point n and y_n is the filtered signal.

$$y_n = (a_0 x_n + a_1 x_{n-1} + a_2 x_{n-2} + a_3 x_{n-3} + a_4 x_{n-4} - b_1 y_{n-1} - b_2 y_{n-2} - b_3 y_{n-3} - b_4 y_{n-4}) / b_0$$

where the coefficients are given by:

$$a_0 = 0.26419124$$

$$b_0 = 1$$

$$a_1 = -1.056765$$

$$b_1 = -1.5750506$$

$$a_2 = 1.5851474$$

$$b_2 = 1.4319522$$

$$a_3 = -1.056765$$

$$b_3 = -0.543089$$

$$a_4 = 0.26419124$$

$$b_4 = 0.1927239$$

1. References for this appendix are listed in Section R7.

From the filter utilities in Matlab it is possible to identify the filter as a Chebyshev Type I filter with a cut-off frequency of 0.5 Hz. The gain and phase characteristics for this filter are shown in Figure R-1. It is seen how the signal content with a frequency greater than 0.5 Hz is passed with no decrease in magnitude whereas at frequencies below 0.5 Hz the signal is attenuated. The filtered signal will exhibit a frequency-dependent phase delay in relation to the input signal, but this will not have an adverse effect in this application as all analysis is done using post-processing of logged data. Sharp changes in the input signal may result in the filtered output exhibiting transients commonly referred to as 'ringing'. The coefficients b_0 to b_4 can be used to identify the frequency of the transients, which in this case occur at 0.5 Hz and 0.803 Hz. The extent to which ringing occurs will depend on the nature of the input signal and the damping of each of the filter characteristic modes.

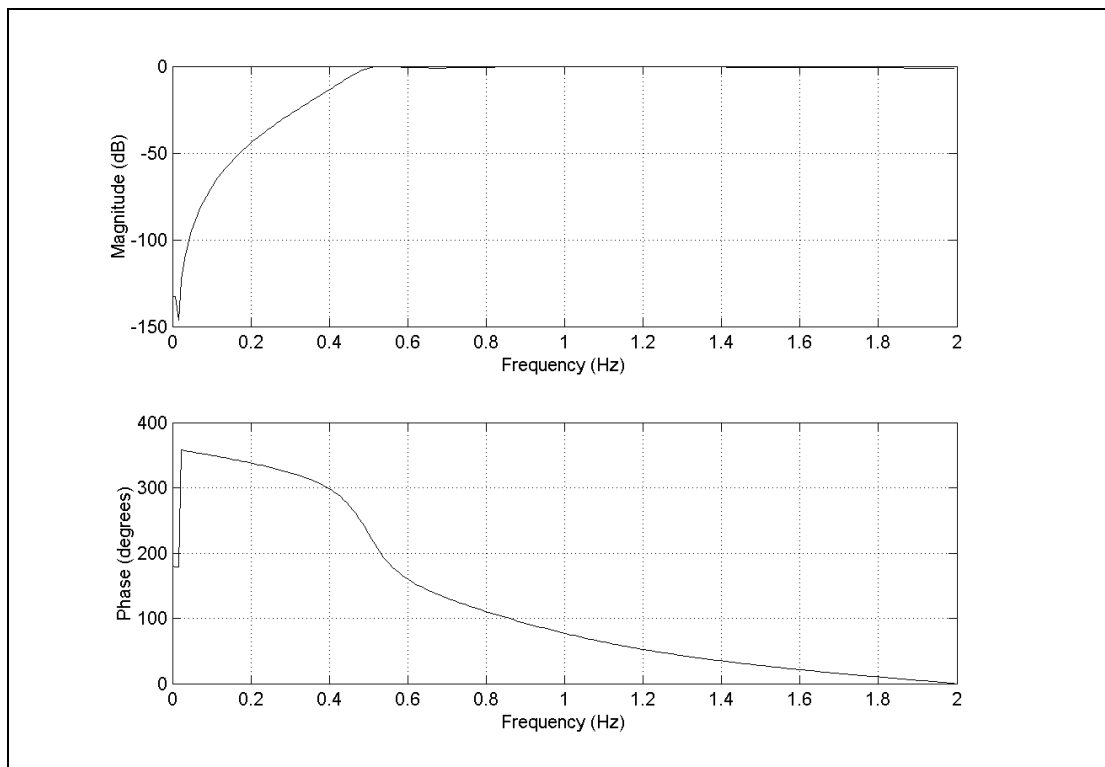


Figure R-1 Frequency Response for High-pass Filter

R.1.3 Low-pass Filtering

The low-pass filter is intended to remove the noise from the processed collective pitch prior to using the signal as a turbulence parameter. The form of the filter is identical to that given above for the high-pass filter, but the coefficients have changed to the following:

$$a_0 = 0.00003123898$$

$$b_0 = 1$$

$$a_1 = 0.00012495591$$

$$b_1 = -3.5897338$$

$$a_2 = 0.00018743388$$

$$b_2 = 4.851276$$

$$a_3 = 0.00012495591$$

$$b_3 = -2.9240527$$

$$a_4 = 0.00003123898$$

$$b_4 = 0.6630105$$

The design in this case is that of a Butterworth filter with a cut-off frequency of 0.1 Hz, as can be observed in the frequency response given in Figure R-2. The characteristic modes (as calculated from coefficients b_0 to b_4) occur at 0.092 Hz and 0.039 Hz. The experience from Bristow is that ringing can be a problem with the low-pass filter, and this may in some instances cause unwarranted fluctuations in the turbulence parameter.

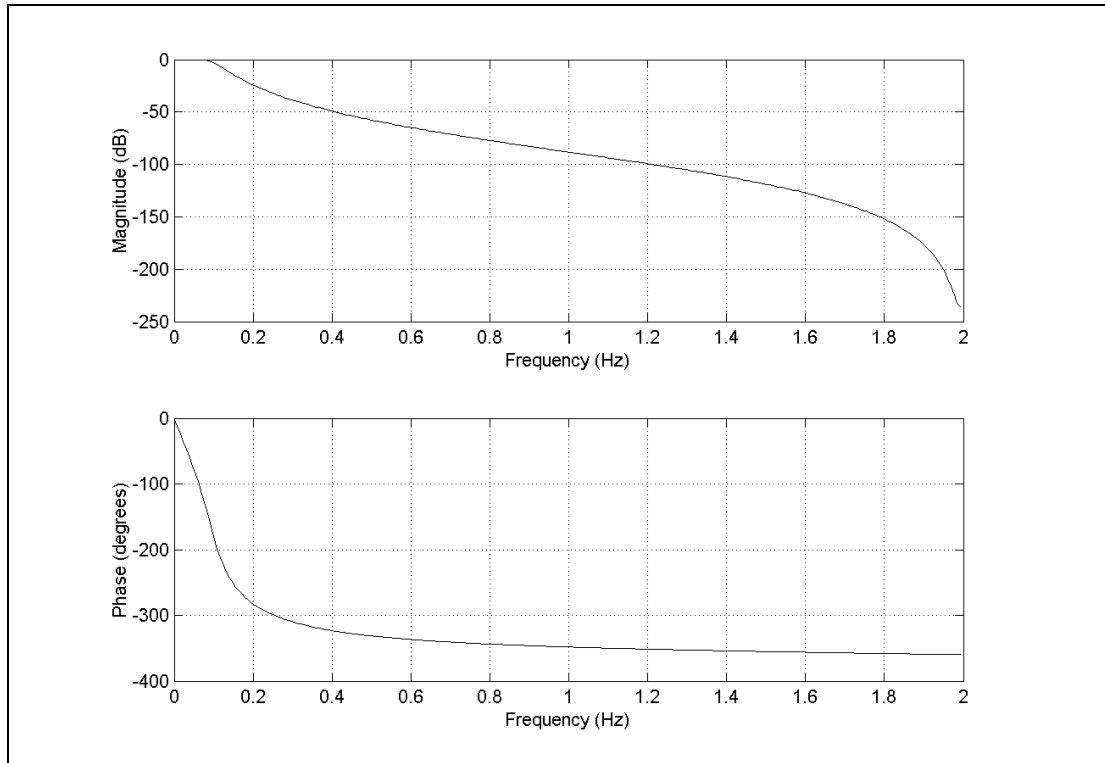


Figure R-2 Frequency Response for Low-pass Filter

R.1.4 Implementation in Matlab

The Bristow HOMP Turbulence Parameter algorithm has been implemented in Matlab in the exact form it was received in Ref [1], for application to pilot control responses recorded in the simulator during trials BRAE01 and BRAE02. There are several steps of pre-processing that were necessary before applying the algorithm. Firstly, the collective signal in the simulator was recorded on a scale of 0 to 1 relating to the overall collective blade angle range. As the relationship is linear, the collective pitch was reconstructed using the following expression:

$$\text{Collective pitch (degrees)} = 7 + 13.3 (\text{Col [0 to 1]})$$

Secondly, the simulator data were logged at 20 Hz whereas the filters have been designed for data at 4 Hz. The simulator data were therefore decimated before input to the high-pass filter by using every fifth point in sequence only.

R.1.5 Verification of Matlab Code

Verification data was available in [1]. The electronic version of the document contained embedded spreadsheets giving records of collective angle and turbulence parameter for three approach cases. The approaches were conducted to platforms Britannia (low turbulence), Brae A (high turbulence) and Brae B (high turbulence). Figure R-3 shows a comparison of the Bristow parameter with the calculations using Matlab for the three cases available. It is seen that all data gave the same answer.

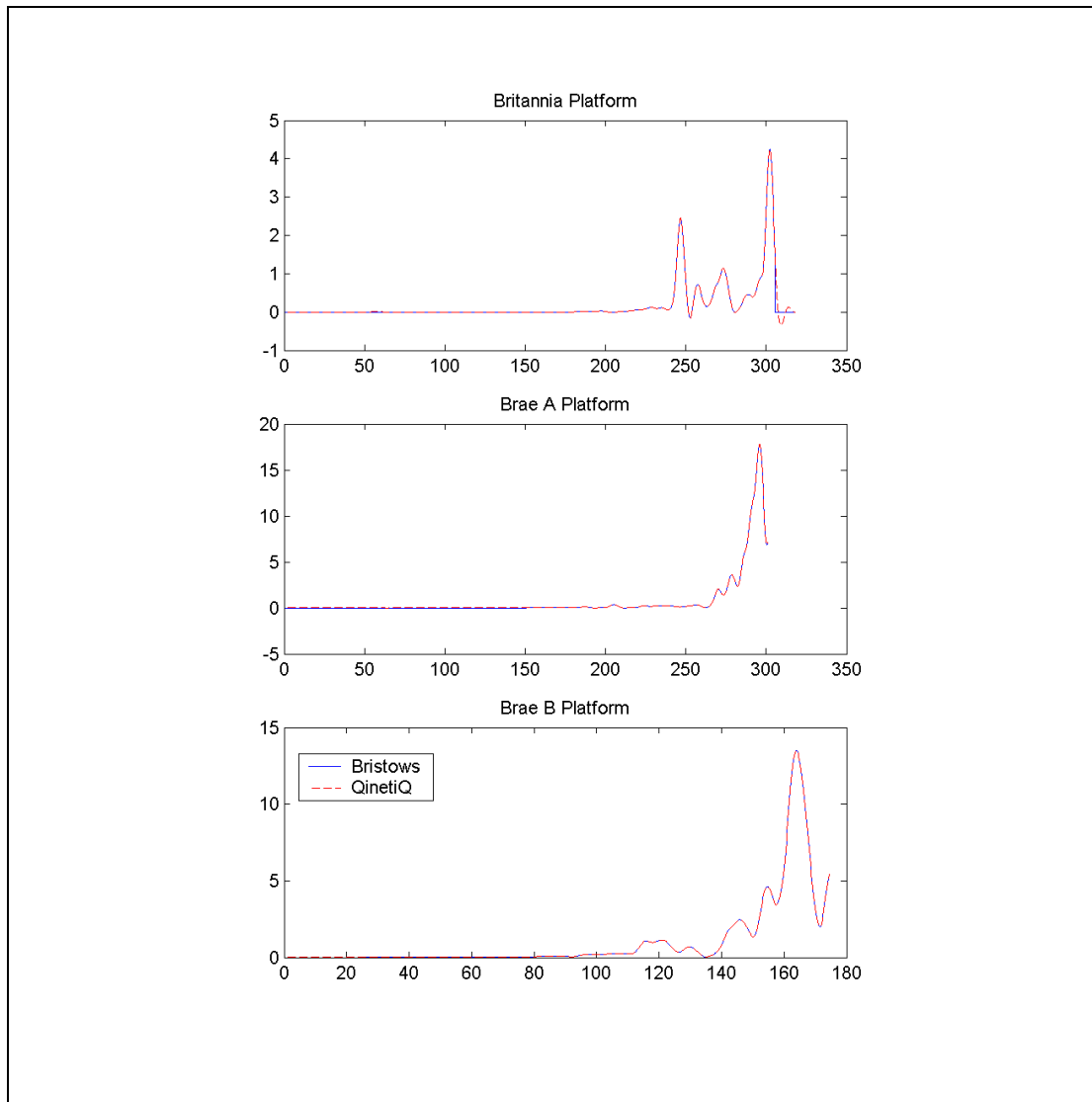


Figure R-3 Comparison of HOMP Data with those Calculated using Matlab

R.2 Simulator Approach Data (Trial BRAE02)

The Bristow algorithm has been applied to the approach data giving a maximum value of the turbulence parameter for each of the five approach cases available. Figure R-4 shows these data plotted against the Cooper-Harper Handling Quality Rating (HQR) awarded by the pilot during the simulator tests. A best-fit line has been identified, using the Matlab utility *polyfit*, and is also shown on the graph. The turbulence parameter corresponding to an HQR of 6.5 has then been calculated to indicate the approximate boundary between safe and unsafe flight. The value of 6.5 has been used previously in defining the turbulence criterion and was chosen by interpretation of the descriptive text relating to HQRs 6 and 7. From the BRAE02 approach data the critical value of turbulence parameter would appear to be about 18. This compares reasonably well with the working value of 10+ used by Bristow.

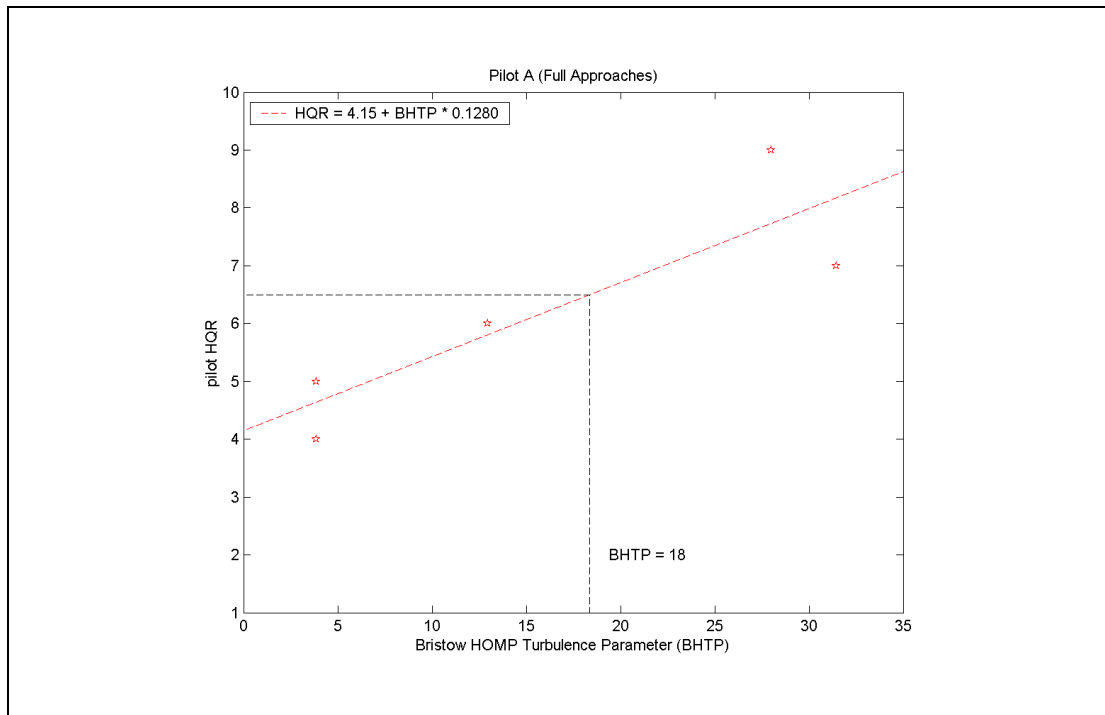


Figure R-4 Approach Data: Comparison of HQR with Bristow HOMP Turbulence Parameter

R.3 Simulator Hover Data (Trial BRAE02)

The hover data involved the aircraft hovering over a fixed point on the platform helideck whilst being buffeted by random turbulence measured in a wind tunnel and appropriate to the wind condition and strength being considered. A relatively large database was captured covering four wind directions, five wind speeds and were flown using three different pilots. A fuller description of the hover data is provided in Appendix M. Each run lasted for approximately one minute before the pilot awarded an HQR based on an assessment of task performance and pilot workload.

A plot of the power spectral density of a sample of hover data is shown in Figure R-5 compared with the spectra of the approach data provided by the simulator BRAE02 trial and HOMP. It is seen that despite the potential differences between wind condition, approach angle and the known difference in aircraft type there is greater similarity between the spectra of simulator and HOMP approach data than there is between simulator hover and approach data. In particular, the hover data has significantly more energy across the whole frequency range and there is a wide peak between 0.2 Hz and 0.9 Hz. As all the inputs in the hover task are associated in some way with compensating for turbulence this would suggest that the high-pass frequency of 0.5 Hz in the Bristow algorithm might be excluding some of the pilot response to turbulence.

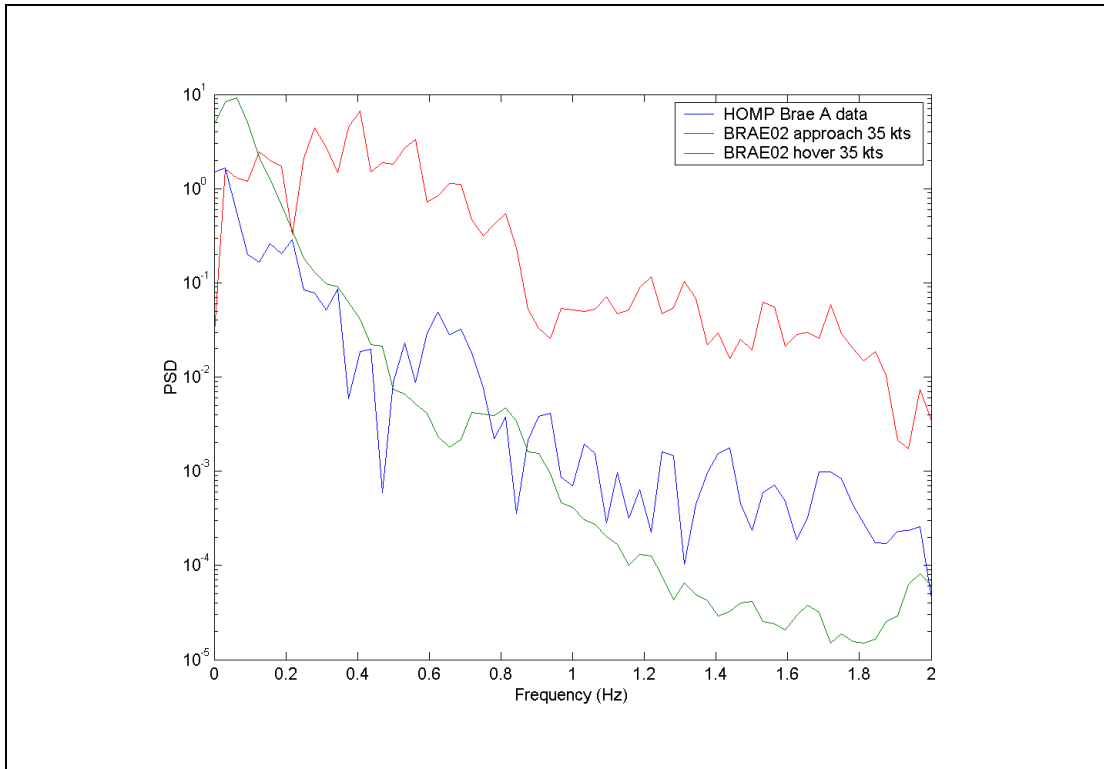


Figure R-5 Comparison of PSDs from HOMP, BRAE02 Approach and BRAE02 Hover Data

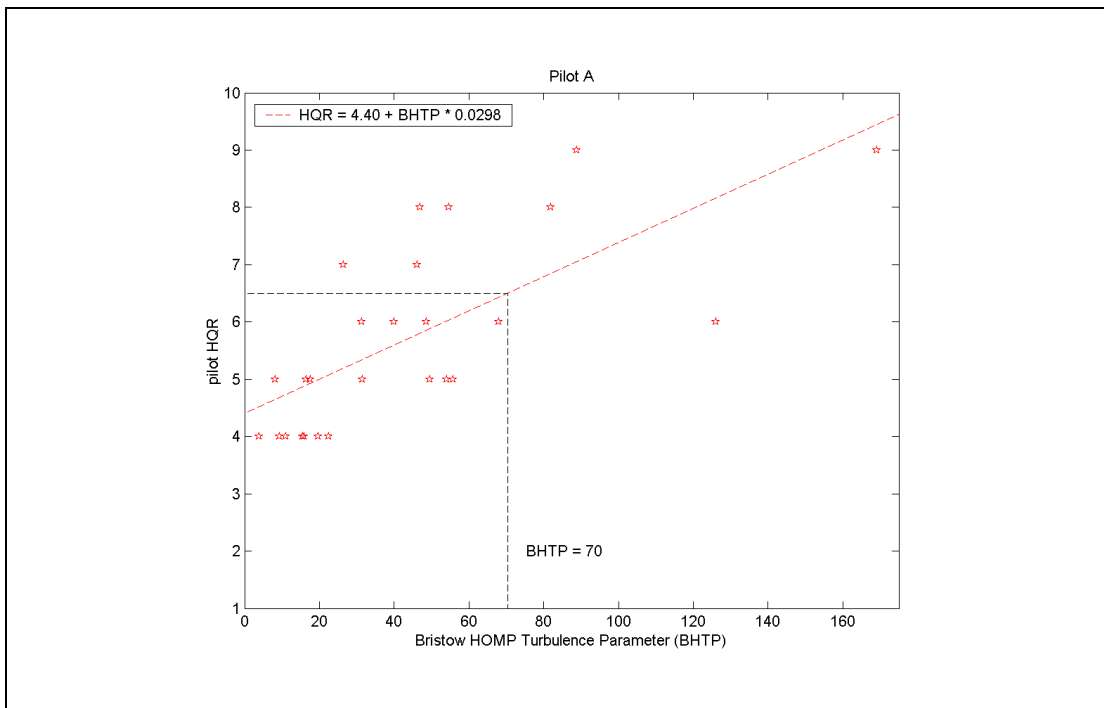


Figure R-6 Pilot A Data: Comparison of HQR with Bristow HOMP Turbulence Parameter

Figures R-6 to R-9 show comparisons and best fit lines for Bristow HOMP Turbulence Parameter and pilot HQR from pilot A, B, C and all pilots together. It is clear that there

are significant differences between the calibration from each data set and that the critical turbulence parameter, relating to HQR 6.5, varies considerably giving values of 70, 19 and 120 for pilots A, B and C respectively and an average value of 90 using data from all pilots simultaneously.

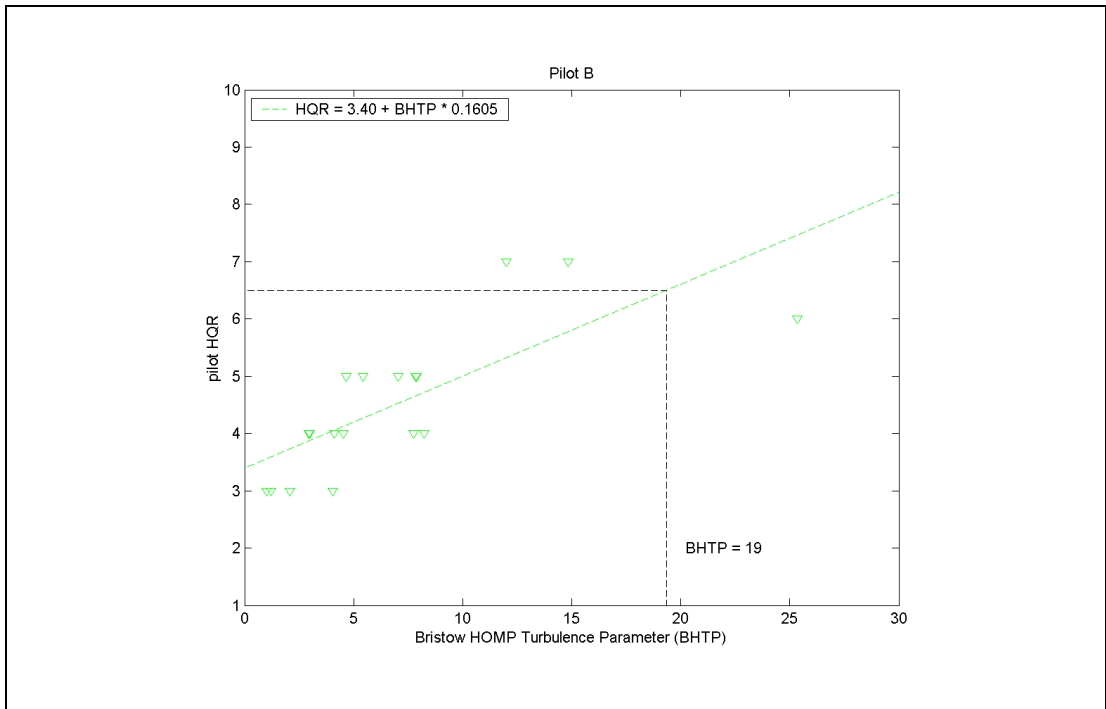


Figure R-7 Pilot B Data: Comparison of HQR with Bristow HOMP Turbulence Parameter

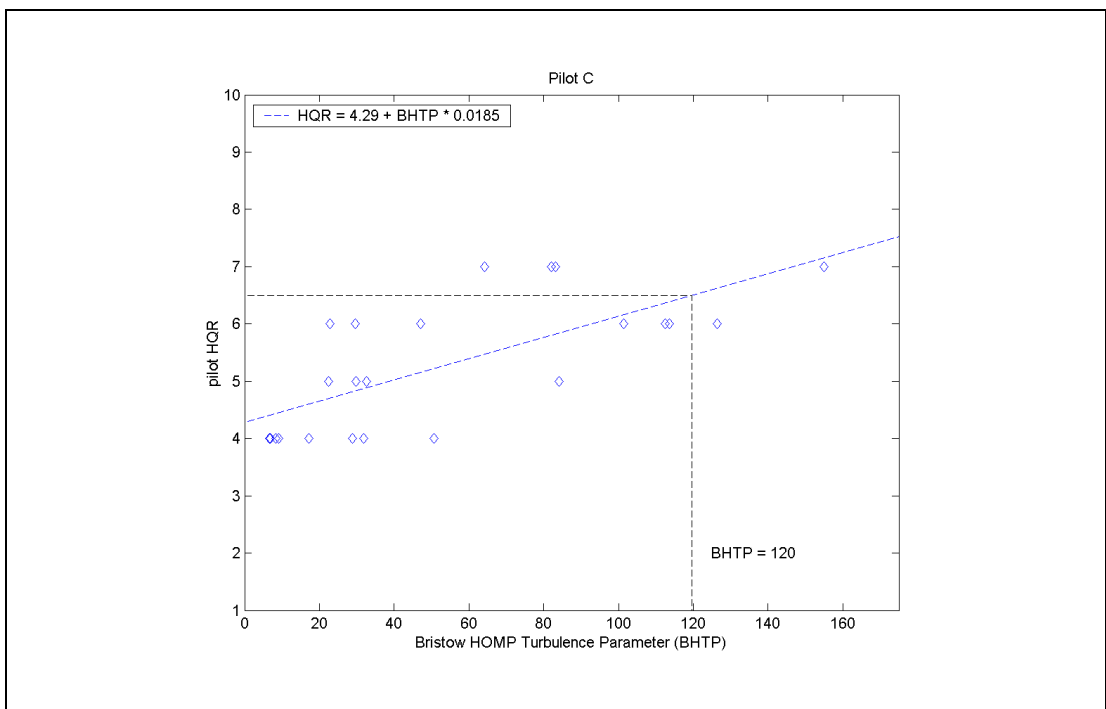


Figure R-8 Pilot C Data: Comparison of HQR with Bristow HOMP Turbulence Parameter

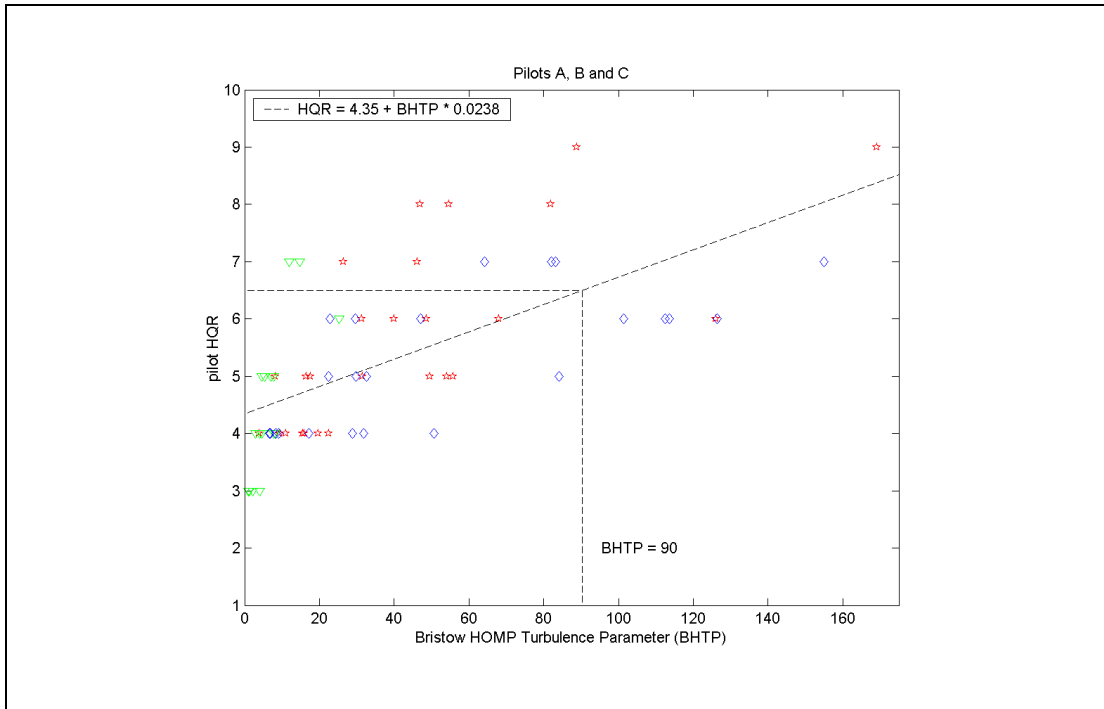


Figure R-9 Pilot A, B and C Data: Comparison of HQR with Bristow HOMP Turbulence Parameter

One of the main drivers for these differences is thought to be the assessment of task performance, and how this was interpreted by the pilots in the simulator. Sub-section 4.6 of the main report gives a full discussion of the issues observed, but suffice to say that overall it was considered that pilot B applied less stringent task performance limits than the other pilots due to particular difficulties in judging his actual task performance in relation to the task performance limits provided.

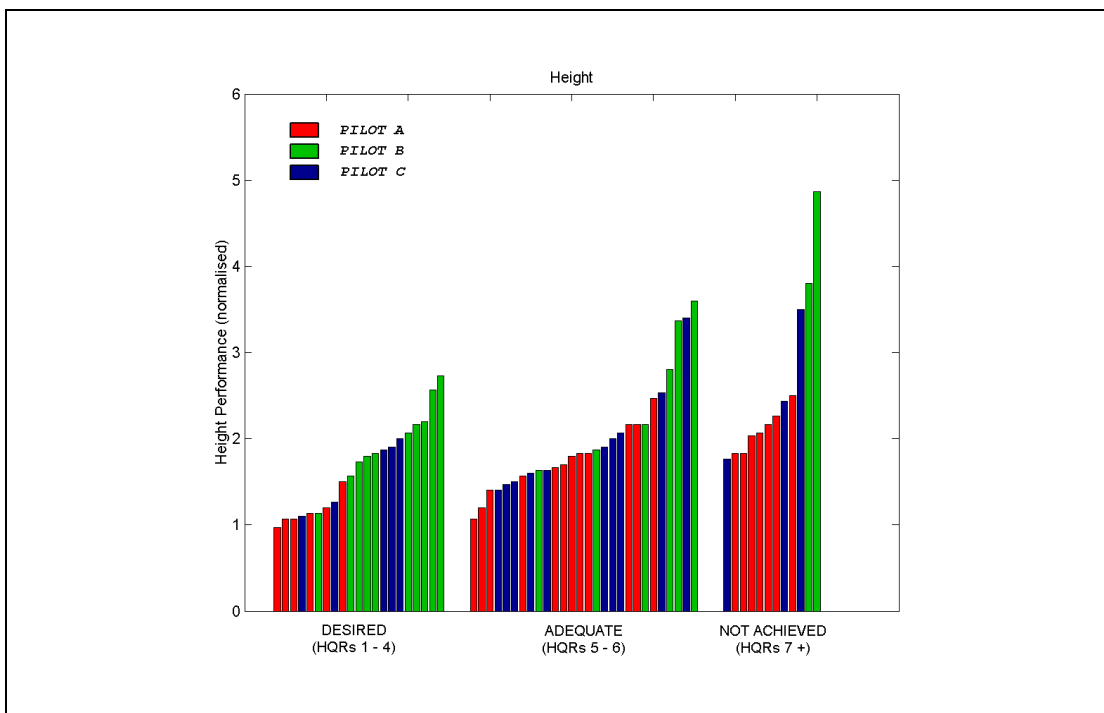


Figure R-10 Comparison of Height Hold Performance for Pilots A, B and C

This can be seen, in terms of the performance in holding height, by the bar graph in Figure R-10. The bars are grouped into desired, adequate and 'not achieved' performance and coloured coded according to pilot. The height of each bar represents the maximum deviation from the mean hover height normalised by the limit for desired performance. If each pilot was performing with the same level of accuracy then the coloured bars would, on average, be evenly distributed. In fact Figure R-10 shows that whereas pilots A and C performed about equally, pilot B gave ratings at each performance level with a larger maximum height deviation.

Figure R-11 shows the standard deviation of the collective control for the same cases, but grouped by pilot and ordered by HQR. The figure shows that the control activity used by pilots A and C were similar in amplitude whereas those used by pilot B were significantly lower. The combination of Figures R-10 and R-11 indicates that pilot B was not attempting to achieve the same level of performance as pilots A and C, and therefore was able to make generally smaller collective inputs in return for a less accurate control of height. The fact that the calibration of the Bristow HOMP Turbulence Parameter based on pilot B data alone, gives a critical value of turbulence parameter relatively close to that used by Bristow (at HQR 6.5, turbulence parameter is 19) would suggest that his appraisal of task performance was more consistent with the standards applied in actual offshore operations.

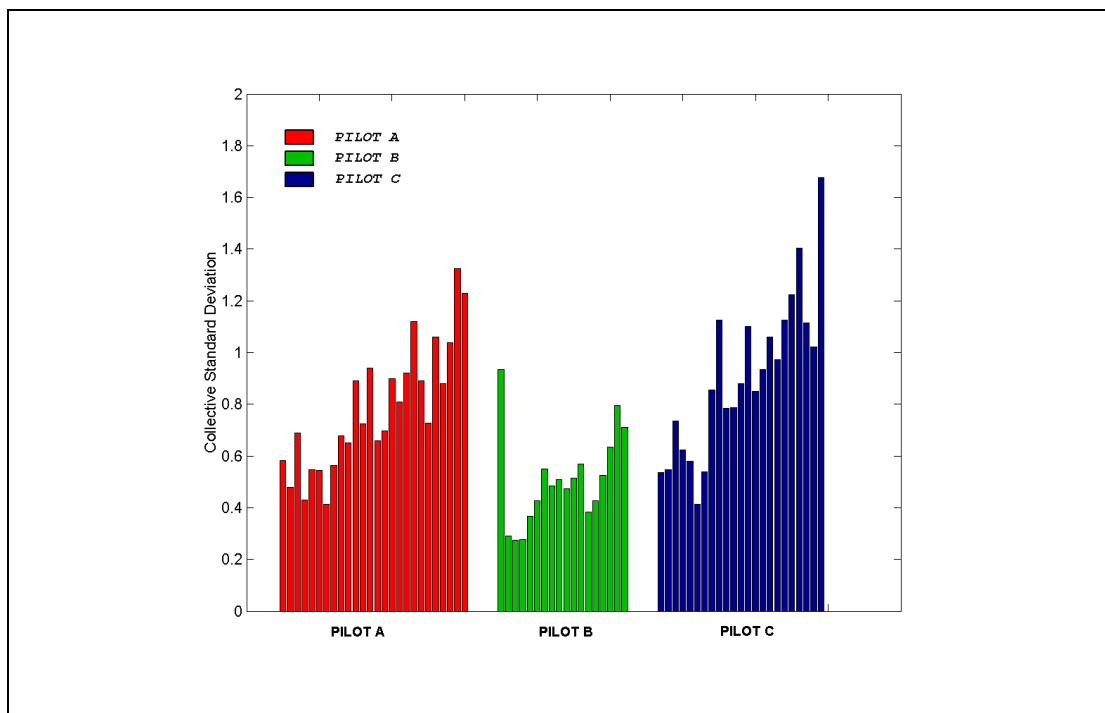


Figure R-11 Pilot A, B and C: Comparison of Collective Standard Deviation

R.4 Simulator Hover Data (Trial BRAE01)

One further source of data was the hover tests carried out in the initial simulator trial, BRAE01. These data were generated by pilot A for nominally the same conditions but, due to an oversight in the implementation of the turbulence model, the amplitudes of the time dependent turbulence were significantly lower. Additionally, other model changes were made prior to trial BRAE02 to introduce time-dependent flow gradients across the rotor disc as well as measurements of lateral velocity. The changes would

have modified the pilot workload for many conditions but should not have affected ability of the pilot to rate consistently against the HQR scale i.e. the changes would be perceived as a different range of environmental conditions for which control response and rating would also change. Therefore, despite these data not being valid for assessment of particular wind conditions they were still valuable as a further database of pilot control responses with associated pilot HQRs. Indeed these data were used to define the workload predictor prior to its validation using the BRAE02 data, as described in the main report.

Figure R-12 shows the comparison of Bristow HOMP Turbulence Parameter with pilot HQR with the resulting best-fit line. The turbulence parameter corresponding to an HQR of 6.5 is calculated as 28, much lower than the value of 70 calculated from the same pilot in BRAE02.

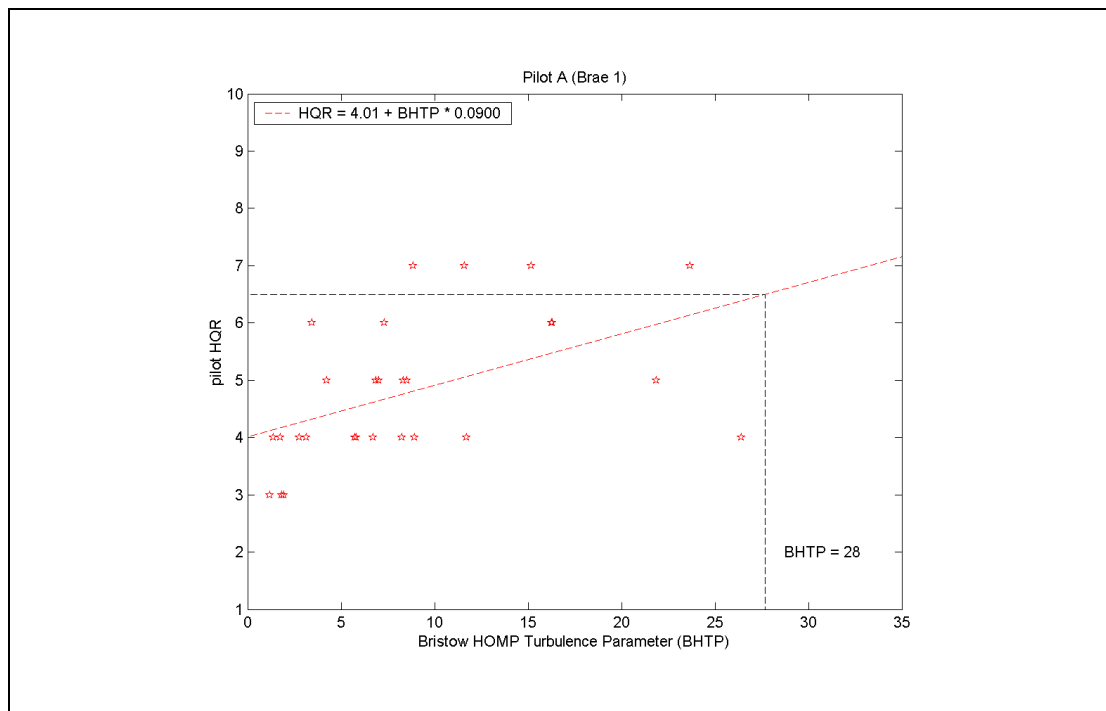


Figure R-12 Pilot A Data (BRAE01) : Comparison of HQR with Bristow HOMP Turbulence Parameter

Figure R-13 shows a comparison of actual task performance achieved by pilot A in trials BRAE01 and BRAE02. In a similar form to that used in Figure R-10, the bars have been grouped by the pilots assessment of the overall task performance and colour coded according to which trial pilot A awarded the rating. It is seen that the task performance was generally better in trial BRAE01 than in BRAE02, at all task performance levels.

Figure R-14 shows the standard deviation of the collective control for the two sets of data grouped by trial. The overall range of HQRs was different for the two trials being HQR 3 to 7 in BRAE01 and HQR 4 to 9 in BRAE02. This is indicated in Figure R-14 by blanking those bars relating to HQR 3, 8 and 9 leaving the red bars for both trials over the same range HQR 4 to 7. Further to this Figure R-15 shows the distribution of ratings for the two trials, which are generally similar, although the BRAE01 ratings do have a bias towards HQR 4.

It is considered that the sets of ratings are similar enough to compare the standard deviation of collective as indicated by the red bars in Figure R-14. It is seen that better task performance in BRAE01 is accompanied by lower control activity i.e. the pilot made smaller inputs but achieved more accurate height control. This is consistent with the lower turbulence values that were known to be present in trial BRAE01 and would be expected to produce ratings over a lower range than in the subsequent BRAE02 trial, a feature that is present in the results but perhaps not to the extent that could be expected given the degree to which BRAE01 turbulence was lower. A possible explanation for this behaviour is shown by the distribution of the actual task performances for BRAE01 and BRAE02 within each task performance category (see Figure R-14) which indicates that the standards used to assess task performance were slightly more stringent in BRAE01 making the awarded HQRs relatively high for the conditions flown. This is reflected in the validation of the BRAE01 workload predictor using the BRAE02 data, illustrated and discussed in Appendix O. The predictions based on applying the workload predictor to BRAE02 control activity were higher than the ratings awarded by the BRAE02 pilots by 0.5 to 1 HQR points.

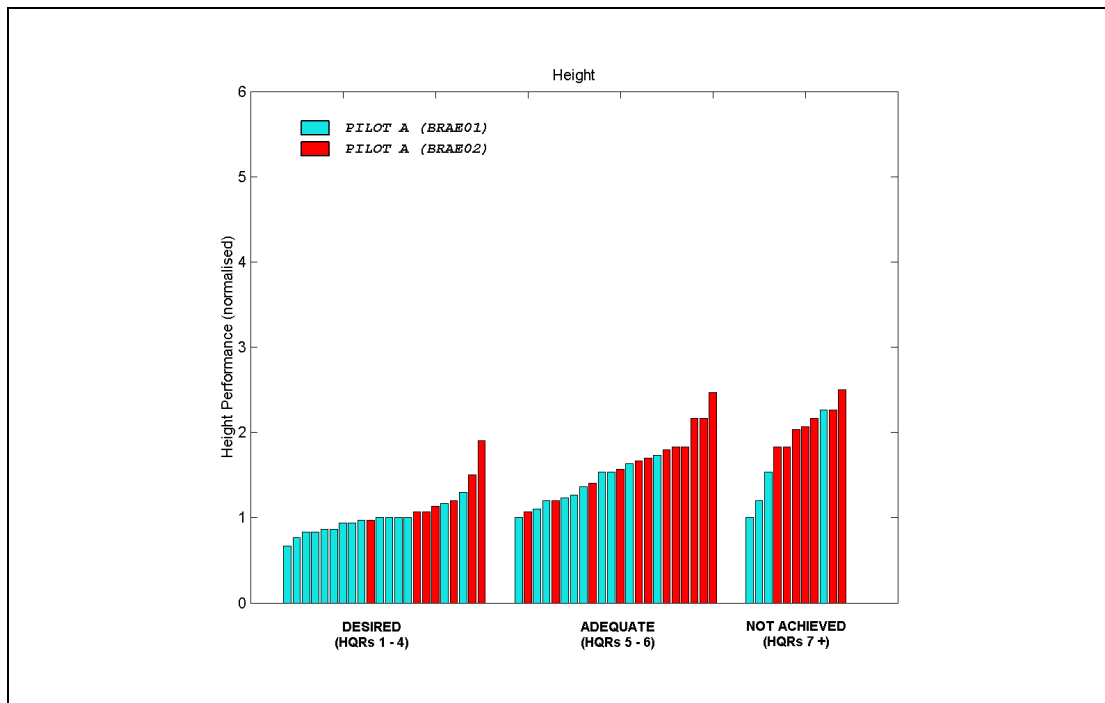


Figure R-13 Comparison of Height Hold Performance for Pilot A in Trial BRAE01 and BRAE02

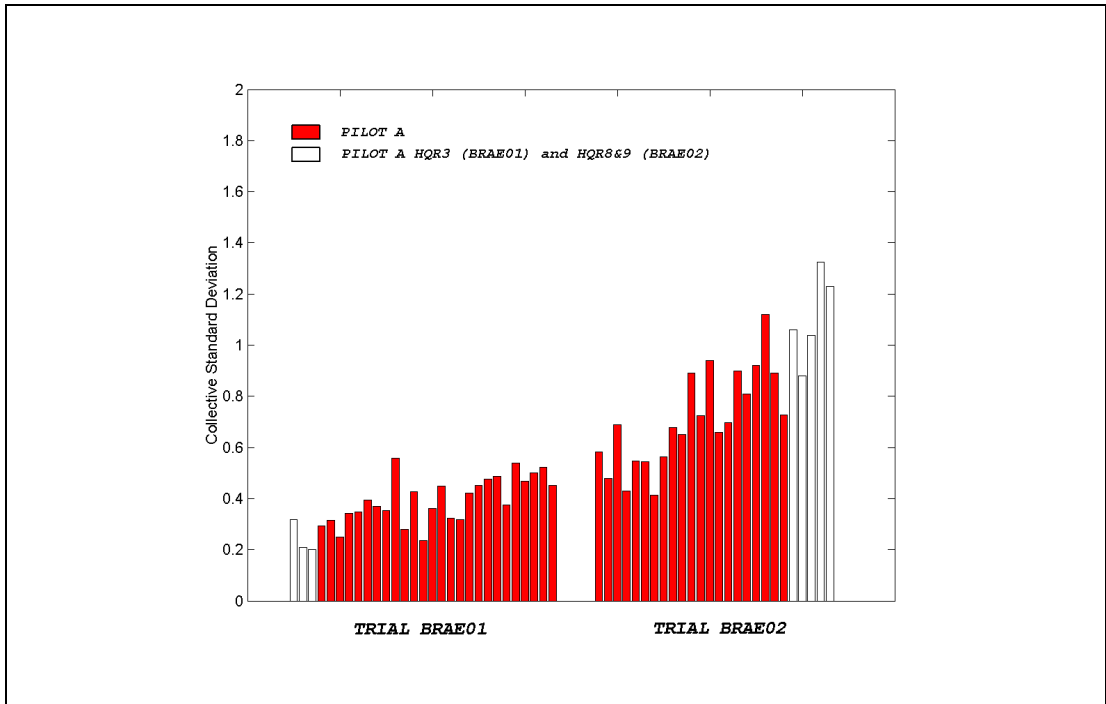


Figure R-14 Pilot A, BRAE01 and BRAE02: Comparison of Collective Standard Deviation

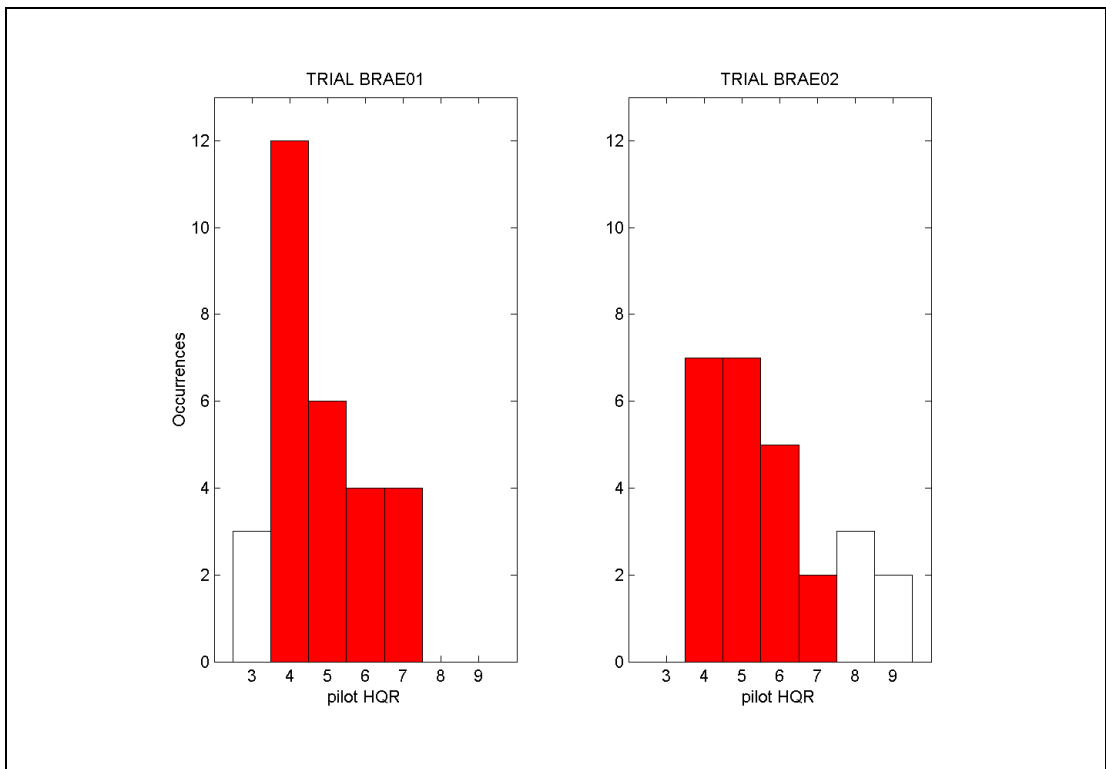


Figure R-15 Pilot A, BRAE01 and BRAE02: Distribution of Pilot HQRs

R.5 Discussion

Table R-1 summarises the calibration of the Bristow HOMP Turbulence Parameter for all the data sets considered. It is seen that there is a large variation in the results most visible by observing the turbulence parameter corresponding to HQR 6.5, given in the last column.

Table R-1 Summary of Calibrations of Bristow HOMP Turbulence Parameter (BHTP)

Data set	Calibration	Turbulence Parameter at HQR 6.5
Pilot A (BRAE02 Approaches)	$HQR = 4.15 + BHTP * 0.1280$	18
Pilot A (BRAE02 Hover)	$HQR = 4.40 + BHTP * 0.0298$	70
Pilot B (BRAE02)	$HQR = 3.40 + BHTP * 0.1605$	19
Pilot C (BRAE02)	$HQR = 4.29 + BHTP * 0.0185$	120
All pilots (BRAE02)	$HQR = 4.35 + BHTP * 0.0238$	90
Pilot A (BRAE01 Hover)	$HQR = 4.01 + BHTP * 0.0900$	28

It was anticipated that there might be differences between the critical value of turbulence parameter calculated here (equivalent to HQR 6.5) and the working value used by Bristow, due to the different aircraft used in the simulator (approximated S-76) and the HOMP project (Super Puma). However, it is clear that there is a far greater sensitivity between the simulator data sets, considered to be due to the exact standards from which task performance has been judged.

The interaction of the standard deviation of control movements with the task performance achieved has been shown to be consistent with the variation of the turbulence parameter. The high sensitivity of the Bristow HOMP Turbulence Parameter to relatively small variations in the assessment of task performance is considered to be exacerbated by the squaring operation of the processing to obtain the metric. These will act to accentuate the differences in overall collective movements whereas the BRAE01 workload predictor (see Appendix J) does not exhibit such sensitivity, as it is based on the standard deviations of stick position and stick rate. The overall quality of the HQR predictions from BRAE01 workload predictor and the Bristow HOMP Turbulence Parameter is illustrated in Figure R-16. The plot on the left shows the comparison of predicted HQR against the pilot HQR using the BRAE01 Workload Predictor (based on cyclic as well as collective activity). The right hand plot shows a similar comparison with pilot HQR where the predicted values are obtained by combining the Bristow algorithm (based on collective activity only) with the calibration to HQR defined using data from pilots A, B and C (and previously shown in Figure R-9). Figure R-16 shows that the overall quality of the predictions is similar although the dependence on the pilot awarding the ratings is clear when the Bristow metric is used, particularly for pilot B.

Interestingly, the two sets of data where there appears to be the greatest correspondence between the calibration and that expected from Bristow's experience in the HOMP project are the pilot A approaches and pilot B hover. In the former the pilot was not provided with any specific task performance limits but was asked to rate the approach task from general impression and in the latter the pilot felt

unable to judge his own task performance and instead reverted to a general impression based on his offshore experience. This may indicate that the simulator hover task was artificially difficult, although from the data available the evidence is rather speculative and inconclusive. The findings support the need for further validation of the workload predictor and turbulence criterion against operational data.

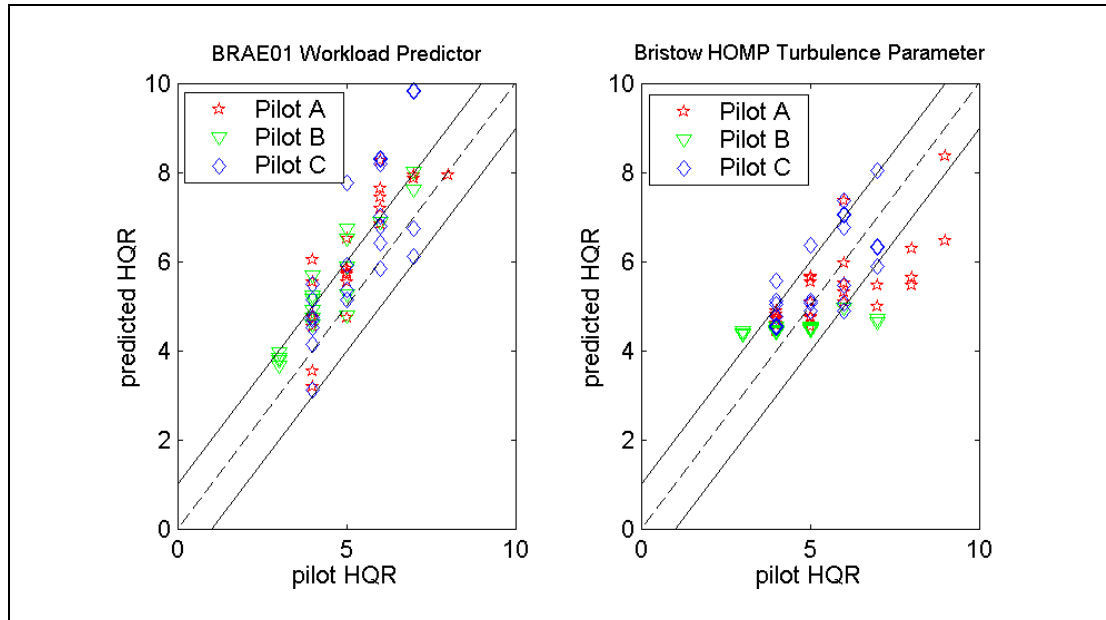


Figure R-16 Comparison of BRAE01 Workload Predictor and Bristow HOMP Turbulence Parameter

In the description of the filtering performed within the Bristow algorithm reference has been made to the possibility of ringing due to the natural modes of the filter itself. Owing to the volume of data analysed here, only spot checks have been made to check that this characteristic was not disrupting the analysis. For the cases considered this does not appear to be an issue. It was also highlighted that the frequency band over which compensation inputs were evident in the hover data, extended rather lower than the cut-off frequency of the Bristow HOMP Turbulence Parameter high-pass filter. If the cut-off frequency was lowered then this may make the metric a better indicator of workload due to turbulence albeit that during approach type tasks there will be a risk of not removing sufficient of the low frequency control inputs. Despite this misgiving, and notwithstanding the different calibrations obtained from each dataset, the Bristow HOMP Turbulence Parameter does appear to offer a reasonable indication of the workload as shown by its general correlation with pilot HQR.

R.6 Conclusions

From the study of the simulator data from trials BRAE01 and BRAE02 the following conclusions are drawn:

- The calibration of the turbulence parameter to pilot HQR is very sensitive to the data set used.
- The exact causes for the high sensitivity of the metric are not clear but the standards applied by each pilot to assess task performance would appear to be an important factor.

- c) The squaring operation used to form the turbulence parameter has accentuated the differences in collective activity in a way that the BRAE01 workload predictor did not.
- d) There is some evidence that the cut-off frequency of the high-pass filter may be slightly too high.
- e) Assessing each dataset individually, the turbulence parameter was shown to be a reasonable indicator of workload.

R.7 References

- [1] *HOMP Pilot Workload Rating: Initial Implementation and Analysis*, document with embedded spreadsheets e-mailed by D Howson (CAA) to S Rowe (BMT), May 2001.
- [2] Larder, B. D., *Final Report on the Helicopter Operations Monitoring Programme (HOMP) Trial*, CAA Paper 2002/02, 25th September 2002.

Appendix S Simulation of other Configurations

S.1 Introduction

In order to assess the sensitivity of the workload in turbulence to key helicopter parameters, some additional desktop simulations were run with modifications to the helicopter model. There were three sets of results that aimed to cover the following:

- a) Change of rotor hub design reflected in the modification to the flapping stiffness of the blade via the flapping hinge offset from the hub centre.
- b) Change to the blade loading defined as the weight of the aircraft divided by the total blade area. This property would be expected to influence the sensitivity to gusts in the heave axis.
- c) Change to the aircraft weight varied within the normal expected operating range of the S-76.
- d) Change to the overall size of the vehicle represented using three weight classes, accompanied with representative changes to other key parameters consistent with this modification.

In all cases the wind tunnel data used was the most severe, i.e. that measured in the lee of the derricks on the Brae A platform for wind speeds between 15 and 60 kt.

S.2 Hinge Offset

The hinge offset is given by the distance between the centre of the rotor hub and the flapping hinge. The greater the offset of the flapping hinge then the greater the transfer of pitching and rolling moments to the fuselage as the lift on each blade is cyclically varied. Cyclic variations in blade lift may occur due to application of cyclic pitch or due to the presence of a non-uniform flow field over the area of the rotor disc.

A range of hinge offsets were chosen to represent the values expected for a number of helicopter types currently operated in the North Sea and some expected to do so in the future, although no exact design data was available. The lowest value of 2% rotor radius would be typical of an articulated rotor type such as the Sikorsky S-61 and the highest of 5% would relate to more modern types such as the Eurocopter 225 and EH101.

Figure S-1 shows the workload ratings from desktop simulation for the basic S-76X model but with the hinge offset modified over the range 2% to 5% where it is clear that not much effect is predicted. The actual workload ratings are given in Table S-1 below.

Table S-1 Workload Ratings for Various Flapping Hinge Offsets

Windspeed	2% offset	3% offset	4% offset	5% offset
15 kt	2.92	2.90	2.87	2.86
25 kt	3.64	3.58	3.65	3.65
35 kt	4.32	4.21	4.33	4.33
50 kt	5.63	5.40	5.47	5.42
60 kt	7.20	6.54	6.63	6.55

There is little difference in the workload at each flight condition irrespective of the hinge offset. In most cases all the predictions are within 0.1 of an HQR point. The reason for such behaviour is due to the increase in hinge offset not only giving an increased transfer of pitching and rolling moments in response to turbulence but also a greater pitch and roll control effectiveness with which to compensate for the disturbance. It would appear that the net result of these effects is only a small change to the scale of control activity required and hence workload.

The exception is the slightly elevated workload for the 2% hinge offset at 50 kt and 60 kt. On examination of the dynamics of the combined pilot/vehicle system there was found to be a lower damping for these cases and in effect the computer pilot may have been exhibiting a small degree of over-controlling. With the present version of SyCoS there was no mechanism by which to modify the damping. However, this could be provided with some further development of the pilot model.

S.3 Blade Loading

The blade loading from a number of common types was assessed from [1]¹ and found to give values over the range 75 lb/ft² to 105 lb/ft², where no particular dependence on the weight or size of the aircraft was evident. This was the range applied to the S-76X model where changes were implemented via the blade chord, as this had no significant knock on effects on other key parameters.

Figure S-2 shows the results from desktop simulation where it is seen that there is an almost indistinguishable difference between the configurations. Table S-2 below shows the calculated workload ratings.

Table S-2 Workload Ratings for Various Blade Loadings

Windspeed	75 lb/ft ²	90 lb/ft ²	105 lb/ft ²
15 kt	2.90	2.88	2.87
25 kt	3.78	3.67	3.63
35 kt	4.45	4.40	4.32
50 kt	5.60	5.50	5.46
60 kt	7.07	6.88	6.62

S.4 Aircraft Weight (Within S-76 Operating Range)

The range of take-off weights assumed to be appropriate for the S-76 was 8,800 lbs to 11,700 lbs. The S-76X model was modified to take account of weight variations in this range using values of 8,800 lbs, 10,510 lbs and 11,700 lbs. The results are shown in Table S-3 below and plotted in Figure S-3. It is seen that the workload is lower for the heavy S-76 across the speed range with the maximum difference occurring at 50 kt. The trend is contrary to what would generally be expected in the HLL where in highly turbulent conditions the maximum allowable aircraft weight would be decreased to allow a landing to proceed. However, the assessment made here is based purely on workload related to aircraft handling whereas the HLL will be influenced by the amount of spare power available, a parameter that would be

1. References for this Appendix are listed in Section S6.

expected to increase as the aircraft weight is reduced. The pilot model being used in the study is not currently of sufficient fidelity to take account of limited power margins.

Table S-3 Workload ratings S-76 over the Weight Range 8,800 to 11,700 lbs

Windspeed	8,800 lbs	10,510 lbs	11,700 lbs
15 kt	2.69	2.61	2.72
25 kt	3.54	3.51	3.37
35 kt	4.44	4.20	4.03
50 kt	5.86	5.52	5.01
60 kt	6.82	6.66	6.38

S.5 Aircraft Size

The sensitivity of workload ratings to changes in aircraft size was assessed using three weight classes. The lightest was 9,900 lb (approximately equivalent to the S-76X) and the others were a medium weight class of 22,000 lb and a heavy weight class of 32,000 lb.

To create models in these weight classes required changes to the S-76X model that were far more extensive than for either the hinge offset or blade loading case studies. The list below shows the vehicle parameters that were modified to produce the configurations.

- Rolling, pitching and yawing inertias
- Number of main rotor blades
- Main rotor radius
- Main rotorspeed
- Main rotor chord
- Main rotor mass distribution
- Tail rotor moment arm
- Tail rotorspeed
- Tail rotor radius and chord
- Tail plane moment arm
- Tail plane area
- Fin moment arm
- Fin area

No changes were made to the automatic flight control system for any of the models. This remained as it was for the baseline S-76X model (which was originally copied from the QinetiQ model of the Lynx Mk 3). However, as the control authority and design of the control system has been kept constant for all three models, the performance of the system in the presence of the gusts would also be expected to be broadly the same. Changes to the fuselage inertias and rotor speed were

approximated using curves of known data from other types that defined the variation of these quantities as functions of aircraft weight. Both light and medium configurations were chosen to have 4 main rotor blades whereas for the heavy aircraft it was considered more representative to have 5 blades. All other parameters were adjusted using basic helicopter design rules of thumb and attempts to keep other key parameters constant where no variation was considered to be a generic feature of a heavier aircraft.

The results from desktop simulation are tabulated in Table S-4 and plotted in Figure S-4. It is seen that the differences are more significant than either of the previous cases but the largest difference between light and heavy classes is still less than a single HQR point. The workload predictor is only reliable over a range of HQR 3-7, corresponding to the range of experimental data used to identify the predictor coefficients. The HQR predictions at 60 kt for all weight classes are therefore significantly outside this range and have not been plotted in the Figure.

Perhaps surprisingly, the light weight class was in most cases slightly less difficult to handle in turbulence than medium and heavy classes. In fixed wing operations it is normal for aircraft in a light weight class to be grounded in gusty conditions whilst larger aircraft can continue to fly. The reasons for the light weight class in this study being less susceptible to the effects of wind were not clear, although it was the control activity in the roll and pitch axes that gave rise to the difference. A key parameter appeared to be the main rotor radius, and it is possible that the larger radii of the medium and heavy models may have led to a disproportionate generation of rolling and pitching moments due to the gradients of vertical flow that were imposed. The flow gradients were based on measurements over a distance representative of the S-76 rotor diameter (and similar to the rotor diameter of the light configuration) and will not be strictly applicable to rotors of larger size. Owing to the larger number of blades on the main rotor of the heavy model, the radii of medium and heavy rotors were about the same and approximately 50% higher than that of the light rotor.

Table S-4 Workload Ratings for Various Aircraft Weights

Windspeed	Light	Medium	Heavy
15 kt	3.24	3.21	3.28
25 kt	4.01	4.09	4.26
35 kt	4.61	4.88	5.20
50 kt	6.17	6.76	7.18
60 kt	8.67	8.31	8.75

Applying the criterion that an HQR of greater than 6.5 indicates a likelihood of excessive workload, then this would mean that the light class could fly in about 52 kt of wind (linear extrapolation from available data) whereas the heavy aircraft would be restricted to 45 kt.

It can also be seen that there is an increase of between 0.4 and 0.65 of an HQR point between the predicted ratings for the S-76X (given by cases 16-20 in column 5 of Table P-1) and the results for the light class given in the table above. As the weight of these models was similar it might be expected that the workload ratings would also be comparable. There are three contributory factors that have lead to these configurations being different:

- a) The roll and pitch inertias for the light class (and subsequently the medium and heavy classes) have been taken from a curve of these properties as a function of weight formed by known data of other conventional helicopter types. In the case of the light configuration both pitch and roll inertias were significantly less than the S-76X – meaning in effect that the inertias of the S-76 are relatively high compared to other types.
- b) The blade mass properties of the light, medium and heavy classes have been chosen to be equivalent to each other (allowing for scaling effects). Although these properties were initially taken from the S-76X, this produced a poor design for the rotor of the heavy model, necessitating the blade mass to be decreased. The effect of this change has been seen to increase the workload across the speed range by a small amount.
- c) Finally, as was seen for the 2% hinge offset configuration, there is evidence that the damping of the combined pilot/vehicle dynamics is low in most cases and this may have lead to increased control activity due to a small amount of over-controlling.

This feature of the results brings into focus an important issue regarding the three weight classes. Best attempts have been made to produce a well-designed configuration in each weight category using design rules of thumb. However, there is the possibility that a specific helicopter type used for operations offshore may exhibit a combination of design features that doesn't sit within the 'averaged' designs assumed here and could give workload predictions outside of the range predicted. If a particular aircraft type is known to exhibit notably poor (or good) response in turbulence, this may provide a good candidate for modelling using a more faithful set of configuration data if a suitable source of the data could be identified.

S.6 Reference

- [1] *Jane's All the Worlds Aircraft 2001-2002*, Jane's Information Group, 2002.

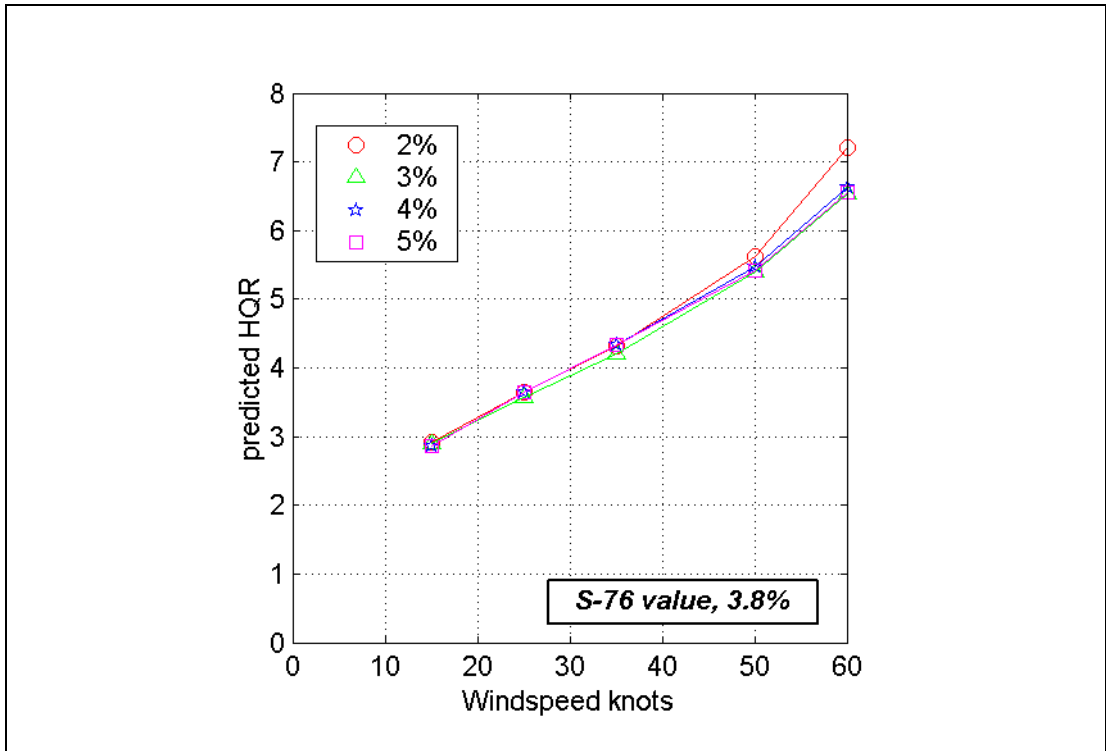


Figure S-1 Workload Ratings for Various Hinge Offsets

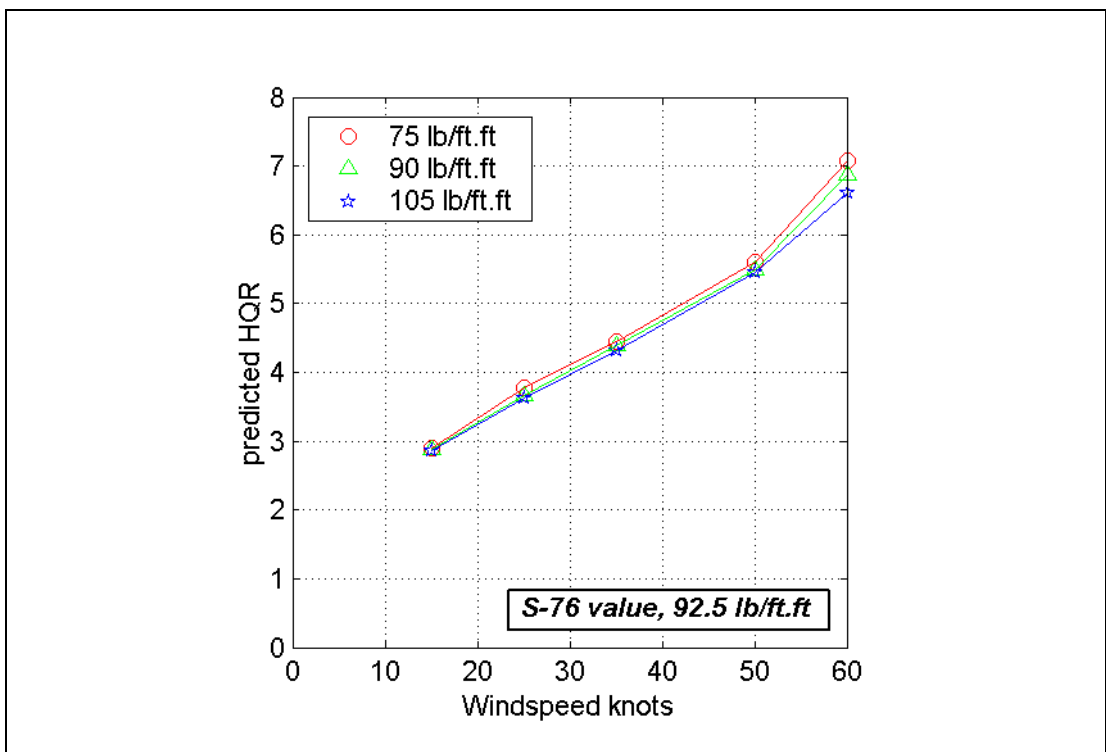


Figure S-2 Workload Ratings for Various Blade Loadings

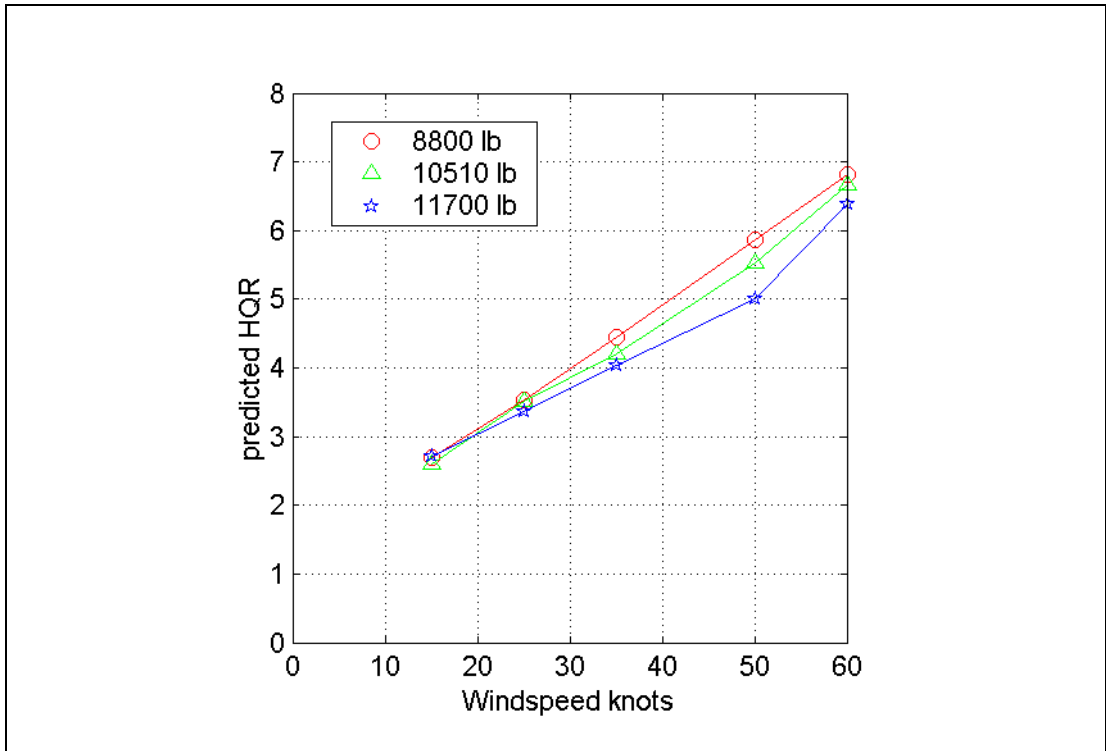


Figure S-3 Workload Ratings Varying Aircraft Weight

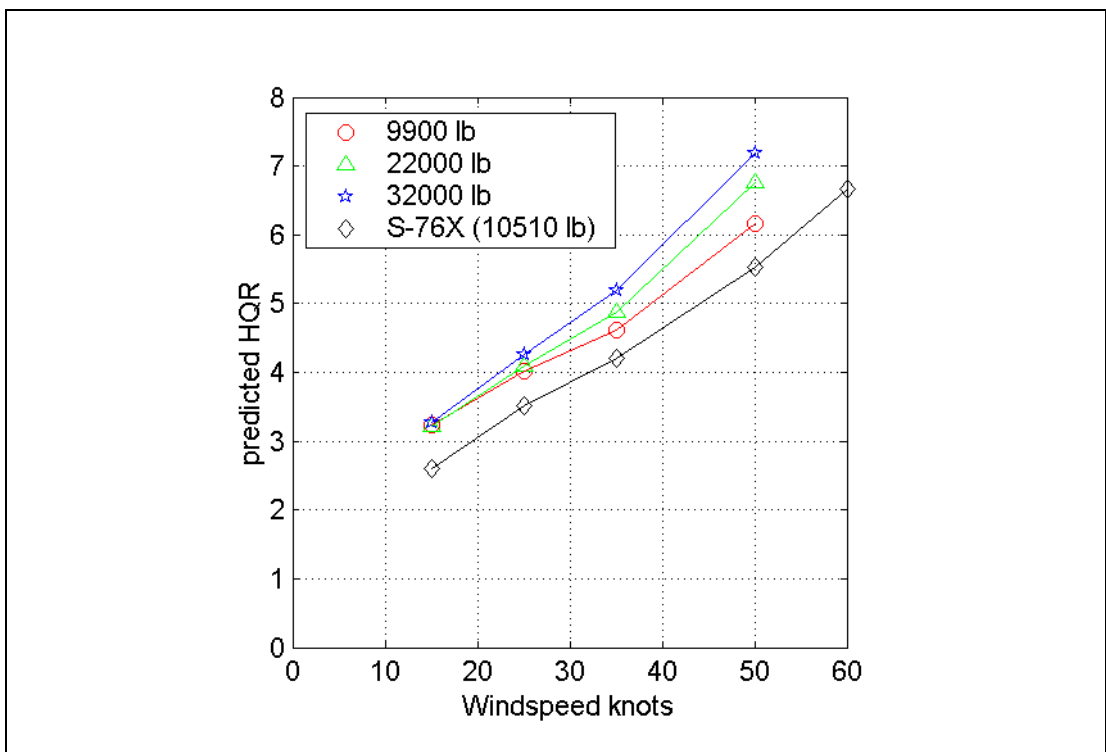


Figure S-4 Workload Ratings for Various Aircraft Weight Classes

Appendix T Analysis of Turbulence Standard Deviations and HQRs

Table T-1 gives the calculated values of standard deviation for each of the time histories of flow velocity and flow gradients that were implemented in the simulator for trial BRAE02.

Table T-1 Standard Deviations for BRAE02 Turbulence Time Histories

	St. Dev U_{turb} (m/s)	St. Dev V_{turb} (m/s)	St. Dev W_{turb} (m/s)	St. Dev $(dW/dx)_{\text{turb}}$ (/s)	St. Dev $(dW/dy)_{\text{turb}}$ (/s)
Derricks					
15 kt	0.9002	0.7355	0.6710	0.1700	0.1604
25 kt	1.6843	1.3457	1.1576	0.3076	0.2808
35 kt	2.3086	1.4190	1.5170	0.3789	0.3541
50 kt	3.2561	2.2824	2.2838	0.5410	0.5351
60 kt	3.9777	3.0005	2.7943	0.6882	0.6679
Cranes					
15 kt	0.5522	0.8433	0.5291	0.1367	0.1273
25 kt	1.2581	1.6703	0.9860	0.2404	0.2372
35 kt	1.8619	2.2373	1.3983	0.3337	0.3279
50 kt	2.6159	3.0978	1.9693	0.4810	0.4545
60 kt	2.9523	3.6408	2.3620	0.5842	0.5465
Unobstructed					
15 kt	0.6614	0.6686	0.6433	0.1427	0.1329
25 kt	1.0927	1.2319	1.1028	0.2375	0.2120
35 kt	1.5562	1.6067	1.5050	0.3110	0.2887
50 kt	2.1424	2.4244	2.1635	0.4602	0.4259
60 kt	2.9299	2.5719	2.4861	0.5542	0.5246
Exhausts					
15 kt	0.8745	0.6482	0.5947	0.1505	0.1317
25 kt	1.6483	1.1778	0.9323	0.2556	0.2100
35 kt	2.8178	1.6207	1.4581	0.3596	0.2805
50 kt	3.2111	2.1548	1.9858	0.4963	0.4202
60 kt	4.1077	2.6422	2.3820	0.6182	0.4875

Figure T-1 shows these standard deviations plotted against each other in a matrix of plots that should be interpreted as follows. The plots along the diagonal are $\text{std}(U)$ v's $\text{std}(U)$, $\text{std}(V)$ v's

std(V) etc. and are of no interest. All other plots show the variation of each pair of standard deviations i.e. the first row shows std(U) v std(U), std(U) v std(V), std(U) v std(W), std(U) v std(dW/dx) and finally std(U) v std(dW/dy). The purpose of the plot is to show the degree to which the standard deviation from a particular measurement is generally a linear function of those from any other measurements. It is concluded from the figure that if a function to predict the workload is to be constructed from the standard deviation, then as the measurements are not independent, a single parameter will accomplish just as much as a number of parameters combined.

The vertical velocity is selected as the single measurement to be correlated with HQR on the basis that it most closely relates to the others measurements. In fact the two gradient measurements are just as close, but these involve a far more complex wind tunnel experimental measurement and hence are less convenient to use.

Figure T-2 shows the variation of the standard deviation of vertical velocity with the HQRs of all three pilots awarded for the corresponding test points in trial BRAE02. Table T-2 shows the results from using the *polyfit* function in MATLAB to obtain the best fit lines defining the relationship between HQR and turbulence using the data from pilots A, B and C separately and then all pilots together. The line corresponding to use of all the available data is plotted in Figure T-2. The accuracy with which the HQR are estimated using the formula from the combined data set (all pilots) is shown in Figure T-3.

Table T-2 Best Fit Lines Relating HQR to Turbulence

Pilot	Best Fit Line	Lower std(W) for HQR>6.5
A	$HQR = 2.90 + 1.851 * std(W)$	1.94 m/s
B	$HQR = 1.94 + 1.543 * std(W)$	2.96 m/s
C	$HQR = 3.21 + 1.427 * std(W)$	2.31 m/s
All	$HQR = 2.77 + 1.571 * std(W)$	2.37 m/s

Unfortunately there is no independent trials data on which to validate this relationship. However, Figure T-3 shows the prediction of HQR from the standard deviation of vertical velocity using the same data as was used for curve fitting. The agreement is good although it is emphasised that validation of the relationship would require data from an independent source.

It is assumed that the workload has become excessive when the workload rating crosses the HQR 6/7 boundary. In experimentation an HQR should only ever take an integer value however the prediction of HQR produced by the formulae in Table R-2 will produce non-integer values. If each HQR prediction is rounded to the nearest integer (i.e. 6.49 becomes 6 and 6.50 becomes 7) then the value describing the boundary between safe and unsafe flight becomes an HQR of 6.5. Using the criteria for unsafe flight in turbulence is indicated by the condition $HQR > 6.5$, the relationship for predicting HQR (from all pilots combined) can be used to give the result that if the standard deviation of vertical velocity is greater than 2.37 m/s then the workload is likely to be excessive. The results for each set of Brae A tunnel data are given in Table T-3 where the conditions beyond the safe flight envelope are shaded.

Table T-3 Safe operating enveloped predicted for Brae A

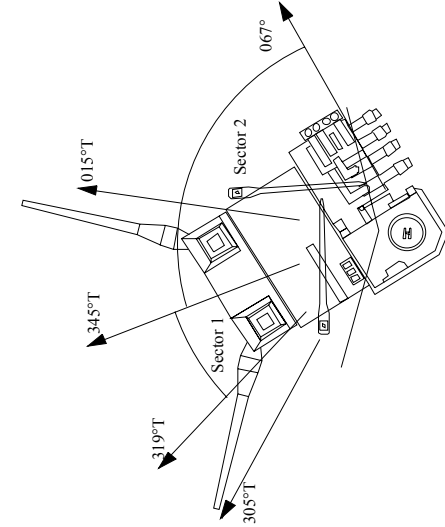
W/S	derricks	cranes	unobstructed	exhausts
15 kt	3.82	3.60	3.78	3.70
25 kt	4.59	4.32	4.50	4.23
35 kt	5.15	4.97	5.13	5.06
50 kt	6.36	5.86	6.17	5.89
60 kt	7.16	6.48	6.68	6.51

Using the data from each pilot separately gives estimates of the standard deviation limit as 1.94, 2.31 and 2.96 m/s. Since there was some evidence on debriefing that pilot B was under-rating, possibly leading to a high estimate of 2.96 m/s, it is considered most appropriate to use the criterion of 2.37 m/s, obtained from using all available data.

It is interesting to compare the HQR ratings of Table T-3 with the current entry in the Helicopter Limitations List for Brae A, which is reproduced here in Table T-4. Differences in the way the wind speed ranges and wind direction sectors have been defined make a precise comparison difficult, but the general trend is clearly similar. The HLL prohibits landings for S-76 types in wind speeds above 40 kt in the 345°-067° wind direction range, which interpolates to a limiting HQR \approx 5.4 in Table T-3. In the 319°-345° sector the >45 kt 'Commander Discretion' limit corresponds with a limiting HQR \approx 5.9 in Table T-3.

Table T-4 Brae A Platform Entry in Helideck Limitations List (HLL - Issue 01 Jan 2003) – Courtesy BHAB Helidecks

Restrictions for Brae A							
Flare sector 305°- 015°T If both flares flaring at full output.		Landings prohibited in this sector					
If wind from 305°- 345°T		Only eastern flare on full output					
If wind from 346°- 015°T		Only western flare on full output					
Crew should be aware of the effect of turbulence that can be caused by the difference in wind strengths between the top of the derrick and the helideck.							
	W/V	S61N	AS332L2	AS332L	B214ST	S76C	S76A+
SECTOR 1 319-345°T	30-45	Max. weight limited to 19000 lb	Extreme caution. * See note 1	Extreme caution. * See note 1	Extreme caution. * See note 1	Calculated weight reduced by 600 lb	Max. weight limited to 10000 lb 10200 lb (Scotia)
	>45	Commanders discretion to be exercised and voyage report submitted.					
SECTOR 2 345-067°T	20-30	Max. weight limited to 19000 lb or Restricted graph, nil wind (whichever is least)	Extreme caution. * See note 1	Extreme caution. * See note 1	Extreme caution. * See note 1	Calculated weight reduced by 600 lb	Max. weight limited to 10000 lb 10200 lb (Scotia)
	31-40	Nil landings	Max. weight limited to Helipad	Max. weight limited to Helipad	Max. weight limited to 15000 lb	Calculated weight reduced by 1000 lb	Max. weight limited to 9500 lb 9800 lb (Scotia)
	>40	Nil landings	Nil landings	Nil landings	Nil landings	Nil landings	Nil landings



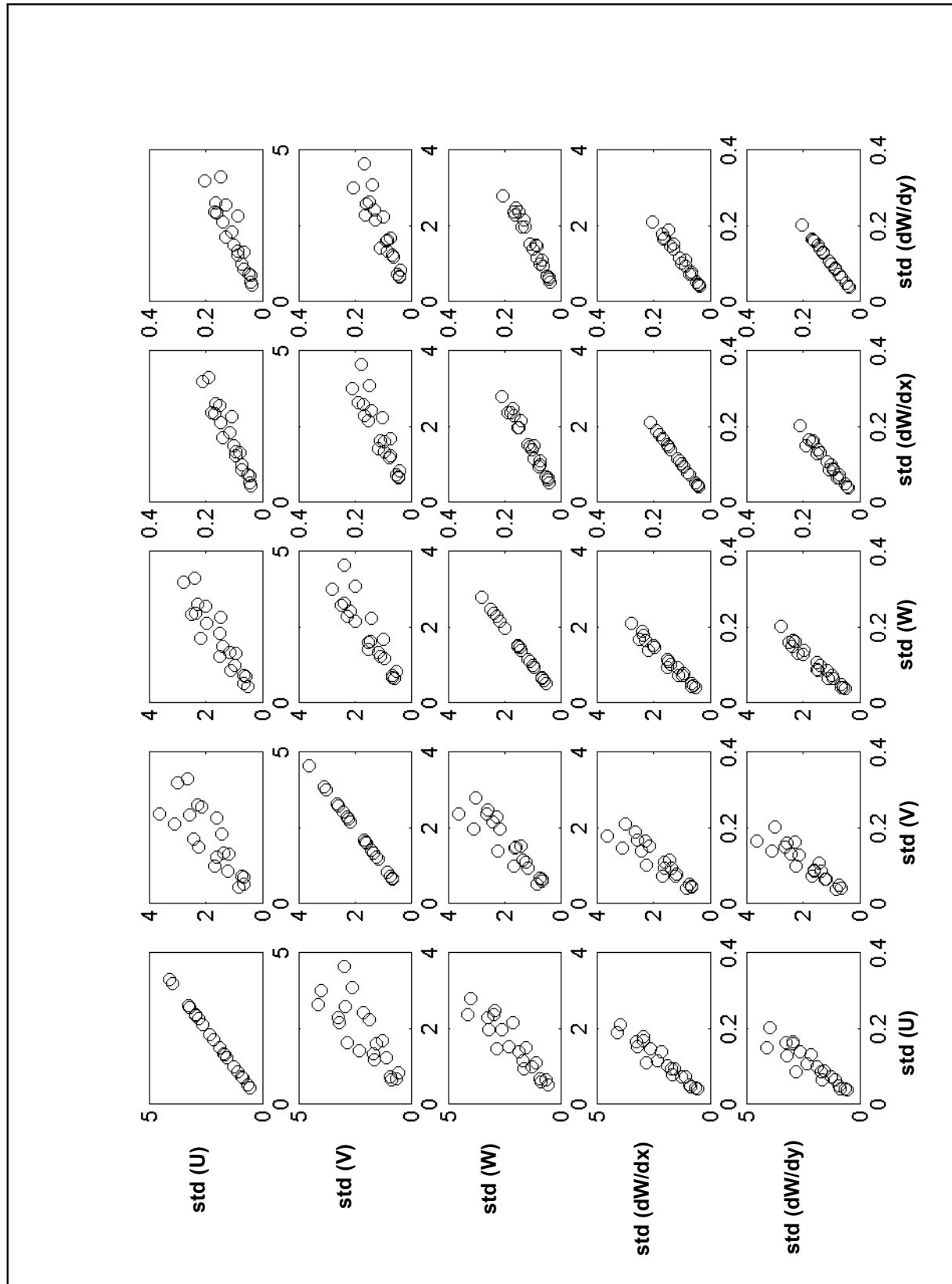


Figure T-1 Correlation of Standard Deviations from Different Measurements

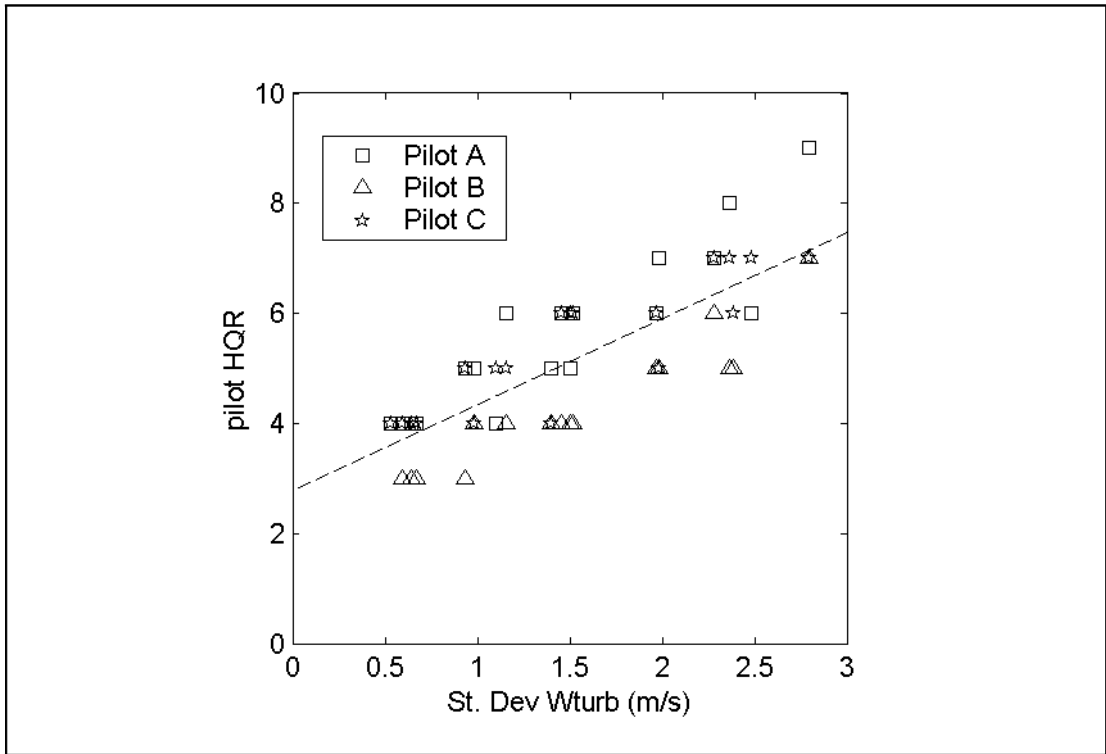


Figure T-2 Pilot HQR Plotted Against Standard Deviation of Vertical Flow

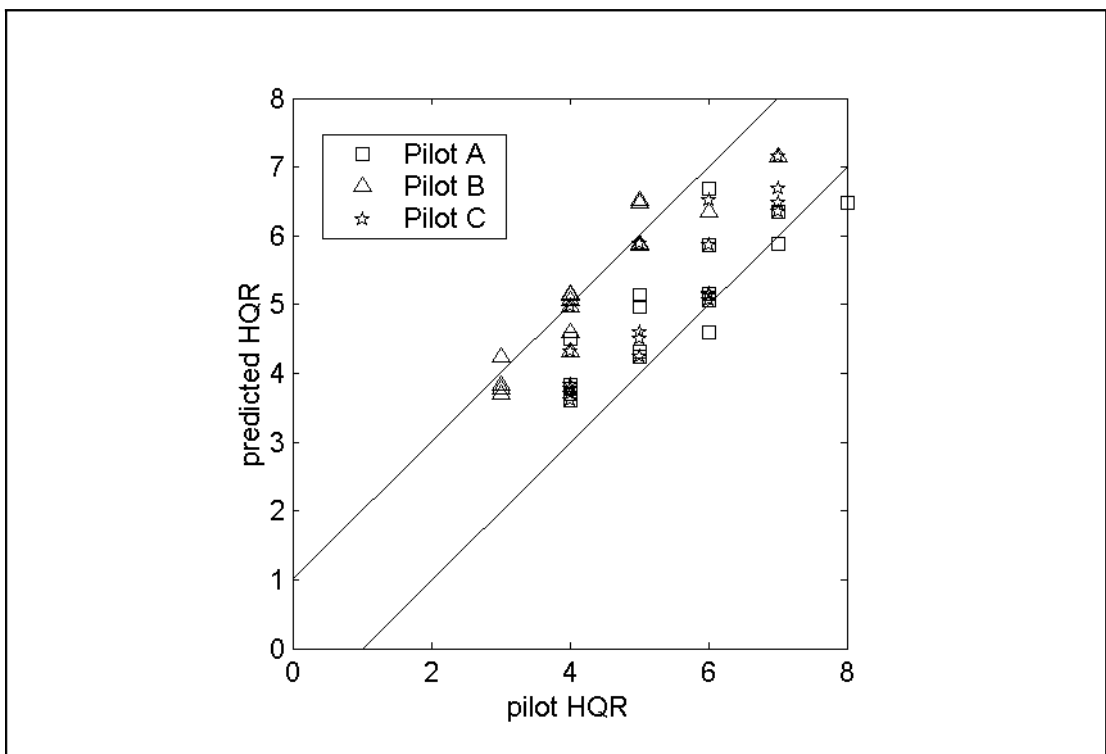


Figure T-3 Pilot HQR Against Prediction Based on Turbulence